CENTRO INTERNACIONAL DE ESTUDOS
DE DOUTORAMENTO E AVANZADOS
DA USC (CIEDUS)

DOCTORAL THESIS

NANOMEDICINES FOR CELL REPROGRAMMING IN TISSUE ENGINEERING AND IMMUNOMODULATION

Adriana Martínez Ledo

INTERNATIONAL DOCTORAL SCHOOL

DOCTORAL PROGRAM IN DRUG RESEARCH AND DEVELOPMENT

SANTIAGO DE COMPOSTELA

2018

USC
UNIVERSIDADE
DE SANTIAGO
DE COMPOSTELA

CENTRO INTERNACIONAL DE ESTUDOS
DE DOUTORAMENTO E AVANZADOS
DA USC (CIEDUS)

TESIS DOCTORAL

NANOMEDICINAS PARA LA REPROGRAMACIÓN CELULAR EN INGENIERÍA DE TEJIDOS E IMMUNOMODULACIÓN

Adriana Martínez Ledo

ESCUELA DE DOCTORADO INTERNACIONAL

PROGRAMA DE DOCTORADO EN I + D DE MEDICAMENTOS

SANTIAGO DE COMPOSTELA

2018

USC
UNIVERSIDADE
DE SANTIAGO
DE COMPOSTELA

AUTHORIZATION OF THE THESIS SUPERVISORS

Nanomedicines for cell reprogramming in tissue engineering and immunomodulation

Prof. María José Alonso, full Professor of the Department of Pharmacology, Pharmacy and Pharmaceutical Technology at the University of Santiago de Compostela,

Prof. Marcos García-Fuentes, Associate Professor at the Department of Pharmacology, Pharmacy and Pharmaceutical Technology at the University of Santiago de Compostela,

REPORT:

That the present thesis, corresponds to the work carried out by Ms. Adriana Martínez Ledo, under our supervision, and that we authorize its presentation considering it gathers the necessary requirements of article 34 of the USC Doctoral Studies regulation, and that as supervisors of this thesis, it does not incur in the abstention causes established by the law 40/2015.

At Santiago de Compostela, on April 2nd 2018

Prof. María José Alonso

Prof. Marcos García Fuentes

USC
UNIVERSIDADE
DE SANTIAGO
DE COMPOSTELA

AUTORIZACIÓN DEL DIRECTOR / TUTOR DE LA TESIS

Nanomedicinas para la reprogramación celular en ingeniería de tejidos e inmunomodulación

D./Dña. María José Alonso Fernández
D./Dña. Marcos García Fuentes

INFORMA/N:

Que la presente tesis, se corresponde con el trabajo realizado por D/Dña. Adriana Martínez Ledo, bajo mi dirección, y autorizo su presentación, considerando que reúne los requisitos exigidos en la Regulación de Estudios de Doctorado de la USC, y que como director de ésta no incurre en las causas de abstención establecidas en la Ley 40/2015.

En Santiago de Compostela a 2 de abril de 2018

Prof. María José Alonso

Prof. Marcos García Fuentes

USC
UNIVERSIDADE
DE SANTIAGO
DE COMPOSTELA

PhD CANDIDATE STATEMENT

Nanomedicines for cell reprogramming in tissue engineering and immunomodulation

Ms. Adriana Martínez Ledo

I submit my Doctoral thesis, following the procedure according to the Regulation, stating that:

1) This thesis gathers the results corresponding to my work.
2) When necessary, explicit mention is given to the collaborations the work may have had.
3) The present document is the final version submitted for its defense and coincide with the document sent in electronic format.
4) I confirm that this thesis does not incur in any plagiarism of any other authors or documents submitted by me for obtaining other degrees.

At Santiago de Compostela, April 2nd 2018

Sgd. Adriana Martínez Ledo

USC
UNIVERSIDADE
DE SANTIAGO
DE COMPOSTELA

DECLARACIÓN DEL AUTOR/A DE LA TESIS

Nanomedicinas para la reprogramación celular en ingeniería de tejidos e inmunomodulación

D./Dña. Adriana Martínez Ledo

Presento mi tesis, siguiendo el procedimiento adecuado a la Regulación, y declaro que:

1) La tesis abarca los resultados de la elaboración de mi trabajo.
2) De ser el caso, en la tesis se hace referencia a las colaboraciones que tuvo este trabajo.
3) La tesis es la versión definitiva presentada para su defensa y coincide con la versión enviada en formato electrónico.
4) Confirmo que la tesis no incurre en ningún tipo de plagio de otros autores ni de trabajos presentados por mí para la obtención de otros títulos.

En Santiago de Compostela a 2 de abril de 2018

Fdo. Adriana Martínez Ledo

USC
UNIVERSIDADE
DE SANTIAGO
DE COMPOSTELA

A mis padres

A mis familias

USC
UNIVERSIDADE
DE SANTIAGO
DE COMPOSTELA

“Destino y sentimiento son el nombre de un solo concepto”

Novalis

“Resistiré”

El Dúo Dinámico

“- ¡Burocracia! … … … … … … - Su lechuguita”

Mafalda

USC
UNIVERSIDADE
DE SANTIAGO
DE COMPOSTELA

ACKNOWLEDGEMENTS

A pesar de haber ensayado mentalmente este momento, al verme frente a frente con esta página en blanco, me invade el vértigo. Vértigo de lo que fui y lo que seré. De los que están y los que se irán. De los que ya se fueron.

Yo no sería sin vosotros. Por eso, GRACIAS a todos.

Pero centrémonos. Probablemente ésta sea la primera (y última?) página que consultaréis en esta tesis, así que procuremos que sea un poco alegre. Además, tengo que aprovechar para dar las gracias aquí porque dudo que algún día vaya a salir en la tele.

GRACIAS…

… a María José y Marcos. Por confiar en mí y concebir la línea temática de esta tesis. A María José, por ser siempre un ejemplo de trabajo duro y compromiso. Por tu pragmatismo y energía. A Marcos, por apoyar mis iniciativas y darme la libertad para aprender de mis propios errores.

A Carmen y Anxo, por tener siempre abierta la puerta de vuestro laboratorio para ayudarme con cualquier duda (incluso aunque hiciera algún que otro destrozo!).

A la Universidad de Santiago de Compostela, por proporcionarme las instalaciones y soporte técnico para realizar esta investigación. A la Xunta de Galicia y al programa de Formación de Profesorado Universitario del Gobierno de España por haberme concedido las becas de investigación que hicieron posible la realización de esta tesis. A todas las entidades financiadoras de los proyectos en los que he participado.

A Bruno de la unidad de cristalografía del CACTUS. Por todo tu apoyo y todo lo que me has enseñado. A Raquel, Albina, y Montse, por su asistencia con la microscopía. A Lucía, por su ayuda con el FACS y con el mantenimiento de la sala de cultivos. Gracias en especial a Ana Senra, por ayudarme con toda la histología.

A Sagrario, a Puri y a Rafa, por su trabajo para que el laboratorio funcione cada día mejor. A los profesores del Departamento de Farmacología, Farmacia y Tecnología Farmacéutica, en especial a Loli y Noemi, por ayudarme con las gestiones. A María, Abi, Sandra y la gente del hospital, por el “contrabando” de células y reactivos. A toda la gente, que a lo largo de todo el CIMUS, me ha dejado usar sus equipos o alguna vez me ha socorrido. En especial, al laboratorio de Carmen Rivas, Miguel Fidalgo, Rosa Señarís y Román Pérez.

To Maristella, Dr. Ilaria Marigo and Prof. Bronte, from the University of Padova, for your collaboration in this work and for giving me the chance to learn about the exciting world of cancer immunotherapy.

To Prof. Mooney at Harvard University, for giving me the opportunity to do an internship in your group and to live one of the biggest experiences in my life. Thank you for your mentoring and for stimulating me to think from new perspectives. To all the Mooney Lab, thank you for your warm welcome and for making me learn so much from your amazing work. Thank you Sandeep and Alex, for including me in your team and made me feel at home at the Wyss (also, for living there with me haha). Thank you for all the fun moments, you are great! Thank thank thank you Kyle, for having such a big heart. For your constant support, inside and outside of the lab. Thank you for your scientific guidance and for letting me be part of your life with Melissa and Nina. You are enormous.

Thank you to Aline, Vicente, Eddy, Carlos, Amina, Vadika, Bissrat… and all the people that helped me during the Boston experience. Especially to Matt and Amanda, for making Centre St. my home and help me adapt to the American way of living. For all the conversations, the songs and the drinks together. For all the Spanish and English lessons.

Thank you to all the Nanochachos that have constructed the lab family during all these years. This thesis wouldn't have been possible without your support. Thank you for all the moments we spent together and all the lessons I learned from each one of you.

Gracias a José Vicente, Ana, Giovanna y Raquel por haber sido mis veteranos y haberme enseñado que entre superhéroes, no nos pisamos las capas. Gracias a Adam, por ser mi primer mentor y enseñarme a pensar con originalidad. Gracias a Erea, por haberme introducido en el mundo de la biología y sus caprichosos misterios, que habitualmente demandan ser resueltos en fin de semana. Creo que por fin podemos decir que la maldición de SOX9 ha terminado! Jajaja. Gracias a Pinto, por tus enseñanzas de vida y tu sentido de la justicia. Y sobre todo, por la palabra F, que siempre ayuda a canalizar los momentos difíciles.

Gracias a Carmen, por tu bondad y la serenidad que me inspiras. Desde los tiempos del EuroFlorens hasta ahora. Porque contigo aprendí que el conceto, es el conceto.

Gracias a Sonia, por tu alegría a pesar del Juan Palomo del día a día. Por estar siempre dispuesta a ayudar con unas pipetas o unas cervezas. Gracias por luchar conmigo mano a mano todos estos años.

Gracias a Ana, torbellino de energía. De planes y de ideales. Gracias por hacer tambalear nuestra rutina y por ser mi punto de apoyo en mi aventura americana. Gracias por todos los bacallaus y los viajes. Y por todas las palabras inventadas jajaj

Os echo taaanto de menos! La sexta sin vosotras no es lo mismo.

Y gracias Jose, porque para mí también sigues siendo de la sexta. Gracias por aportarme ese contrapunto de templanza y diplomacia que tanto me hace falta. Gracias por tus bromas y por tus enseñanzas.

Gracias a Tania y a Marta, las primeras biólogas nanochachas. Gracias Tania por tu risa contagiosa. Por tu optimismo. Por las fiestas y por estar siempre dispuesta a echar una mano. Gracias Marta por las risas que nos echamos con las macgyveradas y por el troubleshooting de IPNs y todas esas cosas raras que sólo tú entiendes.

Hablando de nanochachas biólogas y de macgyveradas… gracias Belén! Porque sólo tú podrías ayudarme a diseñar el hydrogel pumping technique®. Gracias por tu energía y tu alegría. Gracias por tenernos la sexta planta bien recogidita :P

Y gracias Esther y Mariajo, por inspirarme con vuestra filosofía y ayudarme con dudas experimentales. Gracias a Patricia, por tu ilusión y cercanía y a Khair, por las conversaciones sobre la vida.

Pero habrá que bajarse a la quinta planta antes de escribir un testamento… Y aquí nos encontramos con las patronas. Gracias Desi, Balbi, Vanessa y Noelia por todas las comidas compartidas. Por poner un poco de cordura materna a nuestras vidas. Gracias a Belén, por siempre tener tiempo para escuchar mis problemas y por hacerme olvidarme de ellos con unas risas. ¿Qué sería de mis roñitas sin ti?

Gracias Sara, compañera de faenas desde el principio. Gracias por tu tranquilidad y optimismo. Gracias por mantener los pies en la tierra y recordarme que hay problemas más importantes que el trabajo. Gracias por tu poesía.

Gracias Inma, porque a pesar de haber estado menos tiempo en el laboratorio, fuiste capaz de llenar a todos y cada uno de nosotros con tu amor y generosidad. Eres tú quien dio sentido a la palabra familia.

Gracias Irene, por estar pendiente de todos nosotros. Por decir la verdad y no importarte gritar cuando hace falta. Por tu coleta del Tarasca y los cigarros-terapia. Gracias, porque escasea la gente que rellena el frasco lavador cuando le hace falta.

Gracias Elena, por tu ironía que siempre me hace reír. Por no importarte ser directa. Por todas las anécdotas que compartimos. Por venir a visitarnos aunque seamos unos vagos. Por las canciones de iglesia.

Gracias Tamara, por tu dulzura y tus puntos de locura, que siempre me sorprenden favorablemente. Por los videos fluffy. Porque a día de hoy, sigo flipando con tu movimiento de pestañas y tus bailes en el Tarasca.

Gracias a Niu, Lu, Ivana, Nataliya, Surasa por enriquecernos con vuestras culturas y por abrir camino a todos los NanoFar que vendrán. Y para terminar, gracias a los nuevos nanochachos, por renovar la ilusión del laboratorio. Edi, Mireia, Vanesa, Lena, Mati, Cecilia, Catarina, Ricardo, Sergio, Ovidio, Franscesco, Bhanu, Maruthi, Ana Olivera, Sheila, Diego, Paul, Chema, Carmen… En especial, gracias a Andrea, Iago, Germán, Sofía y Carla. Special thanks to Howl, for being hand in hand working next to me in the bench. For your support and smile, even in those days when we both just wanted to scream: Jesúuuuuuusss!!!

Gracias a los juernes de secreto y al Montoto. Viri, Patri, Seo, Colo, Judo, María, Laura(s), Patricia… por las cervezas, la zorcilla y todas las conversaciones con las que intentamos arreglar el mundo. Gracias a Laura también por acompañarme en nuestra aventura americana.

Gracias a mis niñas. Por vuestra amistad durante todos estos años. Por tantas vivencias compartidas. Por las innumerables cañas-terapia en las que todas nos desahogamos, aunque ninguna sepa a ciencia cierta de qué está hablando la otra. Por esa complicidad que hace que nos entendamos aunque hablemos todas a la vez (o eso digan). Por todo vuestro cariño y apoyo. Sois un pilar en mi vida, os quiero.

Gracias a mis niños. Por los Jack Daniels y las rancheras. Por los pacharanes y los bailes forzosos. Por las cenas y las pelis. El reggae y la poesía. Gracias por compartir tantas casas rurales en las que queremos vivir para siempre. Os quiero.

Y por último, gracias a mis padres. Los más importantes. Si he conseguido hacer esto es gracias a vosotros. Gracias por inculcarme la responsabilidad, el compromiso y el pensamiento crítico. Gracias por todas las conversaciones y divagaciones. Por cuidarme y quererme tanto. Por entender mi mal humor. Por todos los viajes. Gracias por apoyarme incondicionalmente y tener el coraje de decirme que me equivoco cuando me hace falta. Sin vosotros, yo no sería nadie. Os quiero con locura.

CONFLICT OF INTEREST

I declare that some of the authors of this work, including myself, have a patent related to the mRNA activated matrices developed in the context of this thesis:

M. García Fuentes, A. Martinez Ledo, A. Vidal Figueroa, Biodegradable scaffold comprising messenger RNA, P201630565; PCT/ES2017/070262, Spain, May 2nd, 2016

Sgd. Adriana Martínez Ledo

USC
UNIVERSIDADE
DE SANTIAGO
DE COMPOSTELA

INDEX

USC
UNIVERSIDADE
DE SANTIAGO
DE COMPOSTELA

Abstract/Resumen

USC
UNIVERSIDADE
DE SANTIAGO
DE COMPOSTELA

ABSTRACT

The main goal of this thesis has been the development of various RNA-based therapies to modulate cell phenotypes in two different disease contexts: cancer and tissue engineering.

In a first step, we developed a nanocarrier aimed to revert the tumor immunosuppression mediated by myeloid derived suppressor cells (MDSCs). To this end, we designed a core-shell nanocapsule with a polyarginine coating capable of adsorbing RNAi sequences targeting the C/EBPβ pathway, and a glycerol-monooleate-based core with an L2 inverse micellar phase that enabled the encapsulation of the CCL2 chemokine. These nanocapsules were able to control the release of the RNA molecules and protect them from RNase degradation when coated with additional polyarginine and hyaluronic acid polymer layers. In vitro, they promoted macrophage chemoattraction and induced a potent MDSC transfection that resulted in the reversion of their immunosuppressive phenotype. In vivo, they reduced C/EBPβ mRNA levels preventing monocyte differentiation into tumor-associated macrophages.

Next, we explored a new concept of gene-activated matrices (GAMs) activated with mRNA-encoded transcription factors (TFs) SOX9 and MYOD, to direct mesenchymal stem cell (MSC) specification to cartilage and muscle tissues, respectively. We nanocomplexed TF mRNAs and loaded them within fibrin matrices. We observed that these mRNA matrices presented a much higher transfection efficiency compared to classical pDNA matrices. In GAMs activated with natural mRNA, gene expression decayed quickly over time, whereas those loaded with chemically-modified mRNAs induced a sustained transgene expression. More importantly, the overexpression of both TFs resulted in an efficient chondrogenic and myogenic differentiation of MSCs, promoting a higher synthesis of tissue specific markers compared to pDNA and control matrices.

Finally, we developed another version of SOX9-GAMs based on collagen-I-alginate interpenetrating polymer networks (IPNs) with the aim to study the role of GAM mechanics in enhancing the differentiation driven by TF overexpression. We first fabricated an IPN set with defined stiffness and adhesion properties. Within this IPN set, we found that the higher transgene expression was achieved for IPNs with the higher adhesion and stiffness. We demonstrated that this positive effect of stiffness was mediated by adhesion and related to an increased cell proliferation and a higher uptake of the condensates. These IPNs promoted the effective chondrogenesis of MSCs with low hypertrophy levels. Even more, IPN-mediated SOX9 transfection resulted in an increased chondrogenic marker expression compared to the encapsulation of 2D SOX9-transfected cells, supporting the value of 3D cell reprogramming strategies.

USC
UNIVERSIDADE
DE SANTIAGO
DE COMPOSTELA

RESUMEN

El principal objetivo de esta tesis ha sido el desarrollo de varias terapias basadas en ARN para modular fenotipos celulares en dos diferentes contextos de enfermedad: el cáncer y la ingeniería de tejidos.

En un primer momento, desarrollamos un nanovehículo enfocado a revertir la inmunosupresión en tumor causada por células supresoras de estirpe mieloide (MDSCs). Para ello, diseñamos una nanocápsula con una cubierta de poliarginina capaz de adsorber secuencias de ARNi dirigidas a la vía C/EBPβ y un núcleo basado en monooleato de glicerol con una fase micelar inversa L2 que permitió encapsular la quimiocina CCL2. Estas nanocápsulas fueron capaces de controlar la liberación de las moléculas de ARN y protegerlas de la degradación por ARNasas cuando fueron recubiertas con poliarginina y ácido hialurónico. In vitro, promovieron la quimioatracción de macrófagos e indujeron una potente transfección de MDSCs que resultó en la reversión de su fenotipo inmunosupresor. In vivo, redujeron los niveles de C/EBPβ previniendo la diferenciación de monocitos en macrófagos asociados a tumor.

A continuación, exploramos un nuevo concepto de matrices activadas genéticamente (GAMs) activadas con los factores de transcripción (TF) SOX9 y MYOD codificados por ARNm, para dirigir la especificación de células madre mesenquimales (MSCs) hacia cartílago y músculo, respectivamente. Nanocomplejamos los ARNm y los cargamos en matrices de fibrina. Observamos que las matrices de ARNm presentaban una eficacia de transfección mucho mayor que las matrices de ADNp clásicas. En GAMs activadas con ARNm natural, la expression génica decayó rápidamente con el tiempo, mientras que aquellas activadas con ARNm modificados químicamente indujeron una expresión sostenida del transgen. Cabe destacar que la sobrexpresión de ambos TF resultó en una eficiente diferenciación condrogénica y miogénica de MSCs, promoviendo una mayor síntesis de marcadores específicos de tejido que las matrices de ADNp y las control.

Finalmente, desarrollamos otra versión de GAMs de SOX9 basadas en entramados poliméricos (IPNs) a base de colágeno I y alginato para estudiar el papel de la mecánica de la GAM en la diferenciación celular promovida por la sobreexpresión de TFs. Primero, fabricamos un set de IPNs con propiedades de adhesión y dureza definidas. Dentro de este set, encontramos que la máxima transfección se daba en IPNs con la mayor adhesión y dureza. Demostramos que este efecto positivo de la dureza está mediado por la adhesión y relacionado con una proliferación celular aumentada y una mayor internalización de los nanocomplejos. Estos IPNs promovieron la condrogénesis efectiva de MSCs con bajos niveles de hipertrofia. Más aún, la transfección mediada por IPN resultó en un aumento de la expresión de marcadores condrogénicos en comparación con la encapsulación de células transfectadas en 2D con SOX9.

USC
UNIVERSIDADE
DE SANTIAGO
DE COMPOSTELA

Resumen *in extenso*

USC
UNIVERSIDADE
DE SANTIAGO
DE COMPOSTELA

RESUMEN *IN EXTENSO*

1. Introducción

La especificación del fenotipo celular es un proceso complejo que implica intricadas redes moleculares. Existen señales tanto químicas como mecánicas que actúan en consonancia para dirigir una serie de cascadas moleculares, de modo que su desregulación da lugar a una alteración en la transcripción y traducción de ciertos genes que conlleva variaciones en la expresión proteica. En último término, la alteración de estas cascadas se traduce en un amplio rango de problemas de desarrollo y enfermedades[1].

Entre los distintos reguladores de la expresión génica, los microARNs (miARNs o miRs) están suscitando una atención creciente. Los miARNs son una clase de ARNs no codificantes que juegan un papel central en la homeostasis celular mediante su unión a ARNs mensajeros (ARNms) complementarios, dando lugar a la inhibición de la traducción de estos ARNms o a su degradación[2]. Aparte de su papel como reguladores del desarrollo, se ha descubierto que numerosas enfermedades están asociadas a procesos de desregulación de miARNs[3]. Por esta razón, los miARNs se presentan como interesantes candidatos para el desarrollo de agentes terapéuticos (conocidos como miARNs miméticos) o para su estudio como dianas terapéuticas (conocidos como antimiARNs).

El ARN mensajero, diana de la acción del miARN, constituye una amplia familia de moléculas de ARN que guardan la información genética almacenada en el ADN actuando como molde para la expresión proteica ribosomal. Los numerosos trabajos publicados desde su descubrimiento en 1961[4], culminaron en la concepción del ARNm como un agente codificador. Esta cualidad fue reconocida hace dos décadas, cuando Wolf et al. demostraron que la inyección directa de ARNm transcrito *in vitro* (IVT) en el músculo esquelético de ratones conducía a la expresión de la proteína codificada[5]. Sin embargo, el análisis del potencial del ARNm fue relegado por el del ADN plasmídico (ADNp) y el AND viral, moléculas más estables, y no fue hasta 1990 cuando se estudió para diversas aplicaciones, incluyendo la sustitución proteica y la vacunación[6]. De hecho, a día de hoy el ARNm ha demostrado ser una herramienta realmente eficiente para conseguir una expresión génica forzada, induciendo tanto una mayor como más rápida síntesis proteica que el ADNp[7–10].

Existen varias diferencias conceptuales entre las terapias basadas en ARN y ADN. El ARN ejerce su actividad en el citoplasma donde el miARN regula la expresión de ARNms nativos y el IVT ARNm es rápidamente traducido. Por el contrario, el ADN necesita entrar en el núcleo para ser transcrito a ARN, y se ha propuesto que el ratio de entrada nuclear,

y la consiguiente funcionalidad del ADN, dependen de la rotura de la membrana nuclear durante la división celular. Además, el ARN no se integra en el genoma, eliminando el riesgo de mutagénesis insercional que el ADN podría presentar. Finalmente, muchas aplicaciones farmacéuticas toman ventaja de la transitoria expresión proteica obtenida mediante ARNm y su degradación metabólica completa[11,12].

La mayor parte de las terapias basadas en miARN y ARNm están orientadas al tratamiento del cáncer. En el caso del miARN, estas terapias están enfocadas a la recuperación de los bajos niveles de miARNs oncosupresores con miARN miméticos o a antagonizar la función de miARNs oncogénicos sobrerregulados con antimiARNs. En estas líneas trabajan compañías como Mirna Therapeutics o miRage Therapeutics, las cuales cuentan con varios candidatos en ensayos clínicos (identificadores de ClinicalTrials.gov NCT01829971, NCT02580552)[13]. En cuanto a las terapias basadas en ARNm, cabe destacar su orientación a la inmunoterapia anti-cáncer, y al desarrollo de vacunas terapéuticas frente al cáncer. Compañías como Curevac o BioNTech han completado varios ensayos clínicos exitosos en este campo.

Una aplicación de las terapias basadas en ARN muy interesante y relativamente menos explorada, es su uso para la modulación del fenotipo de células no tumorales. Tal y como comentamos previamente, el papel de los miARNs en la modulación de la plasticidad celular surge de su preciso control sobre la expresión génica. Dentro de las proteínas que son objeto de modulación del miARN, los factores de transcripción (TFs) son especialmente relevantes ya que regulan naturalmente la diferenciación celular[14]. Los TFs controlan el ratio de transcripción de la información genética del ADN al ARNm mediante su unión a secuencias de ADN específicas. Mientras que los miARNs regulan la expresión génica a un nivel post-transcripcional, los TF operan a nivel transcripcional y se ha demostrado que ambas moléculas cooperan para modular la expresión génica. De hecho, los TFs también regulan la expresión de miARNs y ambos pueden formar circuitos de retroalimentación positiva o negativa que juegan un papel crítico en varios procesos biológicos[15–19]. Un ejemplo de esta regulación cooperativa se observa entre dos moléculas de ARN estudiadas en el contexto de esta tesis: miR-142-3p y TF C/EBPβ, que forman un circuito de retroalimentación activado por la familia de citoquinas IL-6 liberadas por el tumor durante la mioelopoesis inducida por procesos tumorales. Esta mielopoiesis tumoral resulta en la generación de las células supresoras de estirpe mieloide (MDSCs), una población $CD11b^{+}Gr\text{-}1^{+}$ acumulada en el bazo y masa tumoral de pacientes oncológicos que facilita la progresión del tumor. Por esta razón, la modulación de los niveles de C/EBPβ se presenta como una estrategia farmacológica prometedora para controlar el microambiente inmunosupresor y aumentar el efecto de las inmunoterapias frente al cáncer[20,21]. **En consecuencia, en este trabajo hemos estudiado dos estrategias para reducir los niveles de C/EBPβ: el uso de miR 142-3p como un miARN mimético y el uso de shARN contra C/EBPβ. Ambas moléculas han sido**

encapsuladas en nanovehículos junto con otros componentes inmunomoduladores, como se explicará brevemente más adelante y se detallará en el capítulo 1 de la presente memoria.

Junto con el uso de ARN interferente para reducir los niveles de TFs, otra estrategia para modular la diferenciación celular es la expresión forzada de TFs. Así, los TF han sido usados tanto para dirigir la reprogramación celular como para promover su transdiferenciación[22,23]. Distintos TFs o mezclas de TFs han sido identificados con el fin de dirigir la diferenciación celular[24–27]. En 1987, Davis et al. demostraron que fibroblastos murinos podían convertirse en mioblastos mediante el uso de un único ADN copia codificante del TF MyoD[28]. Dos décadas más tarde, Takahashi y Yamanaka descubrieron un conjunto de TFs capaz de reprogramar células somáticas a pluripotencialidad [29]. Sin embargo, aunque la mayor parte de los estudios de regulación transcripcional se han centrado en mecanismos de control de transcripción químicos y genéticos, trabajos recientes sugieren que las fuerzas mecánicas son igualmente importantes reguladores del control transcripcional[1]. De hecho, en los últimos años, la mecanotransducción ha recuperado gran atención como un medio de regular la conversión del fenotipo celular. En este sentido, se ha demostrado que la diferenciación de células madre puede ser modulada mediante la dureza, la elasticidad y las características de estrés-relajación de las matrices en las que estén incorporadas[30–33], así como a través de los contactos célula-célula y célula-matriz[34].

En consonancia con estos estudios, **en este trabajo hemos explorado el uso de los factores de transcripción MyoD, regulador maestro de la miogénesis[28] y SOX9, regulador maestro de la condrogénesis[35,36], en la diferenciación de células madre humanas (hMSCs) para aplicación en ingeniería de tejidos**. Hemos empleado ARNm codificante de TF para evaluar si la cinética de expresión del ARNm podría mimetizar la expresión fisiológica de factores de transcripción, promoviendo así la diferenciación celular. Además, hemos explorado esta estrategia en un contexto tridimensional (3D), desarrollando una matriz activada genéticamente (GAM) en la cual tanto ARNm codificantes de TFs como hMSCs pueden ser incluidos, con el objetivo de crear una plataforma fácilmente inyectable con la capacidad de gelificar *in situ* en el lugar de lesión. Siendo conscientes del impacto del microambiente en el fenotipo celular, nuestro trabajo se ha centrado también en explorar la influencia de las propiedades mecánicas de la GAM en el perfil de diferenciación después de la transfección de los TFs en contextos 3D. Por lo tanto, nuestro objetivo último ha sido el de maximizar los procesos de diferenciación celular mediante la identificación de los microambientes con las propiedades mecánicas óptimas para inducir específicos programas de transcripción mediante expresión forzada de TFs. Además, nuestras matrices 3D constituyen una plataforma adecuada para modelizar los procesos de transferencia génica in vivo que los comúnmente usados modelos 2D. Así, teniendo en cuenta el papel crucial de la

transfección 3D en la actividad de la GAM, en este trabajo también tratamos de investigar la influencia de las propiedades mecánicas de la GAM en la eficacia de transfección de las nanopartículas cargadas con el ARNm. Los capítulos 2 y 3 recogen la información relacionada con esta parte del trabajo experimental.

En conclusión, el objetivo global de esta tesis ha sido el desarrollo de adecuados sistemas de liberación de ARN para modulación del fenotipo celular. Teniendo en cuentala versatilidad de las terapias génicas basadas en ARN, hemos diseñado y estudiado sistemas de liberación de ARN en dos contextos diferentes, la inmunoterapia anti-cáncer y la ingeniería de tejidos. Más concretamente, hemos desarrollado terapias de complejidad creciente abarcando desde sistemas nanoparticulares a hidrogeles en los que nanopartículas y células madre fueron co-encapsuladas construyendo una terapia génica celular 3D. Las propiedades mecánicas de los hidrogeles fueron finalmente exploradas para modular la plasticidad celular y maximizar el potencial de la plataforma tridimensional.

2. Resultados y discusión

2.1 Modulación del fenotipo de células madre supresoras de estirpe mieloide (MDSCs) en inmunoterapia en cáncer

Las MDSCs constituyen un conjunto de células mieloides inmaduras que resultan de procesos de mielopoiesis de emergencia sostenidos ligados a inflamaciones crónicas, enfermedades autoinmunes o cáncer. En base a sus características fenotípicas y bioquímicas, esta categoría de células se dividen en dos suptipos: polimorfonucleares (PMS) y monocíticas (M)-MDSCs, ambos caracterizados por su perfil inmunosupresor y su capacidad de inhibir la función de células T[37].

El origen de las MDSC reside probablemente en la creación de un mecanismo de protección frente a daños tisulares derivados de respuestas inmunes incontroladas. Sin embargo, los tumores pueden utilizar este mecanismo para protegerse de ser eliminados por el sistema inmune, asegurando su propagación[38]. Por esta razón, el desarrollo de terapias que ataquen a las MDSCs constituye un enfoque prometedor para aumentar la eficacia de las inmunoterapias en cáncer, sobre todo en el caso de transferencia adoptiva de células T (ACT)[39].

Las estrategias terapéuticas diseñadas para el tratamiento de MDSCs se basan en diferentes principios: inducir la depleción de MDSCs, afectar su desarrollo, inhibir su actividad supresora del sistema inmune y promover su diferenciación a células mieloides maduras[39]. Como adelantamos previamente, uno de los objetivos de esta tesis ha sido el desarrollo de una nanoterapia de ARNi capaz de promover la diferenciación de MDSCs hacia fenotipos maduros no inmunosupresores. Considerando los efectos tolerogénicos e inmunosupresores derivados de una expresión aberrante de C/EBPβ[20], así como la modulación de C/EBPβ por miR 142-3p[40], hemos investigado dos estrategias de ARNi para modular dicha vía: el uso de miR 142-3p y el uso de un shRNA contra C/EBPβ. Asimismo, aprovechando la versatilidad que ofrecen los nanovehículos diseñados en nuestro laboratorio para la co-administración de varios fármacos con diferentes perfiles farmacológicos, junto a los ARNi hemos encapsulado el antígeno modelo ovalbúmina (OVA), utilizada como modelo, y la proteína quimioatrayente de monocitos 1 (MCP-1 o CCL2).

Dentro del repertorio de quimiocinas, la quimiocina CCL2 es especialmente relevante ya que se encuentra en la mayoría de cánceres sólidos. El eje CCL2-CCR2 está implicado en la migración de células mieloides al tumor, donde MDSCs se acumulan impidiendo la entrada de células T citotóxicas (CTLs), limitando por tanto la eficacia de las inmunoterapias[41–43]. Esta movilización de MDSCs dependiente de CCL2 ejerce una acción predominante en el suptipo monocítico, la población más agresiva, por lo que en este trabajo partimos de la hipótesis de que la incorporación de dicha quimiocina conferiría a nuestro sistema cierto grado de vectorización hacia dicha población[44]. Por

otro lado, CCL2 es nitrada/nitrosilada por especies reactivas de nitrógeno que produce el tumor, impidiendo su habilidad de atraer CTLs pero manteniendo su habilidad para reclutar células mieloides[43,45,46]. Por ello, el objetivo pretendido con nuestra terapia combinada, fue también el de restaurar los niveles nativos de CCL2 dentro del tumor para compensar el ratio incrementado de especies nitradas/nitrosiladas y permitir un reclutamiento adecuado de CTLs. Supusimos además, que el tropismo natural de los nanosistemas hacia el tumor[47] y el bazo[48] nos ayudaría a promover la liberación de CCL2 en los órganos donde se acumulan las MDSCs[49,50].

Para construir esta terapia dual, diseñamos un sistema nanocapsular tipo reservorio con una cubierta polimérica de poliarginina, capaz de adsorber los ARNs mediante fuerzas electrostáticas, y un núcleo a base de monooleato de glicerol (GMO) con una fase micelar inversa L2, adecuada para lograr la encapsulación de péptidos dentro de sus dominios acuosos (**Figura 1**). La poliarginina fue seleccionada como polímero complejante de ARN debido a su mayor biocompatibilidad con respecto a polímeros sintéticos (ej. PEI), y su habilidad de transcitosis, que le confiere propiedades adecuadas para el escape endosomal[51]. Por otro lado, las mesofases basadas en GMO están generando creciente interés como sistemas de liberación de fármacos debido a su nanoestructura interna que permite la incorporación y liberación controlada de fármacos de diversa polaridad y tamaño[52,53]. Teniendo en cuenta que los métodos habitualmente empleados para dispersar estas mesofases implican el uso de altas temperaturas o procesos altamente energéticos que pueden dañar el fármaco encapsulado[54,55], en este trabajo proponemos un método alternativo basado en la auto-emulsificación. En él se utiliza el surfactante no iónico Labrasol® para dispersar espontáneamente un gel cúbico de GMO, previamente cargado con la quimiocina, usando poloxámero 407 como estabilizante.

En un primer paso, evaluamos la capacidad del método de auto-dispersión para dar lugar a emulsiones nanométricas y caracterizamos la eficacia de encapsulación de sus núcleos lipídicos. Las nanoemulsiones (NEs) resultantes presentaron tamaños en torno a 200 nm con bajos índices de polidispersión y cargas superficiales negativas de alrededor de -15 mV. La eficacia de encapsulación del antígeno modelo ovalbúmina fue moderada, cercana a un 30%, mientras que en el caso de la quimiocina CCL2, se consiguió un 50% de eficacia de encapsulación. El recubrimiento de dichas NEs con poliarginina dio lugar a nanocápsulas de tamaño y polidispersión similares pero con una carga superficial invertida (≈40 mV), sugiriendo la adsorción efectiva del polímero catiónico. Considerando que las mesofases basadas en GMO se caracterizan por presentar ordenamientos de tipo cristalino, una vez obtenidas las nanocápsulas procedimos a investigar su cristalinidad. Así, mediante Small Angle X-ray Scattering confirmamos la fase cristalina cúbica del gel de GMO que utilizamos como base de nuestro sistema, y observamos que esta cristalinidad se iba perdiendo a medida que se aumentaba la proporción de Labrasol® en mezclas binarias GMO-Labrasol®. De acuerdo

con esto, las nanocápsulas de poliarginina con una proporción GMO:Labrasol 1:9 p:p presentaron una ordenación de micela inversa L2, dando lugar a núcleos acuosos dentro del núcleo lipídico de la nanoemulsión. Aunque la mesofase de GMO más explorada es la fase cúbica bicontinua reversa (V2), se ha mostrado recientemente que las micelas inversas (L2) pueden ofrecer mejores perfiles de liberación[56], lo que constatan nuestros resultandos, confirmando la utilidad de nuestro método de formulación .

Las nanocápsulas de poliarginina fueron posteriormente usadas para encapsular diferentes secuencias de ARN (miARNs y shARNs control y terapéuticos) demostrando una elevada eficacia de encapsulación (≈70%), una buena estabilidad coloidal y una escasa liberación en medios biológicos relevantes. Cabe destacar que la encapsulación de las secuencias de ARN se mantuvo en las partículas cargadas con la quimiocina CCL2, poniendo de manifiesto la viabilidad del sistema dual. Sin embargo, cuando las partículas cargadas con miARN fueron incubadas en plasma humano, observamos que dichas secuencias podían degradarse aun estando adsorbidas a los sistemas. Para evitar este problema, seguimos dos estrategias: utilizar secuencias de shARN fluoradas resistentes a ARNasas y recubrir nuestras nanocápsulas con unas cubiertas poliméricas a base de poliarginina y ácido hialurónico. Estos sistemas recubiertos mantuvieron un tamaño similar a las partículas cargadas con ARN y una carga superficial que varió dependiendo de la naturaleza del polímero de la cubierta, dando lugar a nanocápsulas con una carga superficial positiva o negativa, dependiendo de que el polímero de recubrimiento fuese simplemente la poliarginina o una combinación de poliarginina-ácido hialurónico, respectivamente. Tanto el uso de dobles recubrimientos como el empleo de las secuencias fluoradas consiguieron evitar el problema de degradación del ARN en plasma, dando lugar a sistemas adecuados para administración intravenosa. Asimismo, los sistemas fueron liofilizados para asegurar la preservación del ARN, consiguiendo mantener su estabilidad coloidal y la integridad de las secuencias tras su almacenamiento durante al menos 1 año.

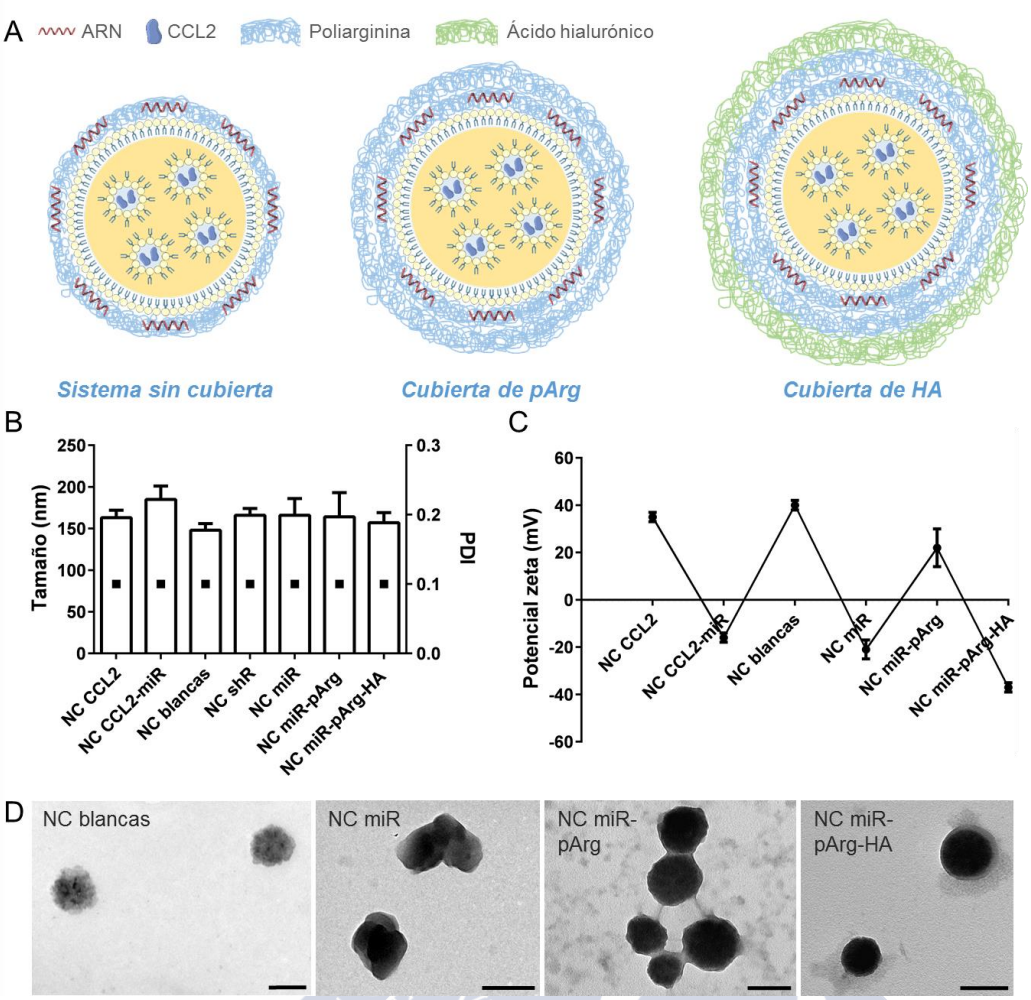

Figura 1. Caracterización de las NCs de poliarginina. A) Esquema de las NCs de poliarginina. B) Tamaños y PDI de las NCs blancas y cargadas según DLS. C) Oscilación de los valores de potencial zeta con la cubierta polimérica. D) Micrografías TEM de las NCs blancas y cargadas con miARN (miR) tras la resuspensión del polvo liofilizado. Escalas = 200 nm.

Finalmente, las nanocápsulas fueron testadas *in vitro*. Una vez descartados fenómenos de toxicidad y efectos inespecíficos sobre el fenotipo de las MDSCs, se llevaron a cabo estudios de transfección de las nanocapsulas cargadas con ARN en los que se evaluó su capacidad para diferenciar las MDSCs a subtipos no inmunosupresores. Dichos ensayos mostraron que las NCs cargadas con shC/EBPβ eran capaces de reducir los niveles de ARNm de C/EBPβ a valores más bajos que el reactivo comercial de referencia. Por su parte, las NCs cargadas con miR 142-3p redujeron la proporción de células $CD11b^{+}$ $Gr\text{-}1^{low\text{-}negative}$, el fenotipo más inmunosupresor, destacando su potencial para reeducar MDSCs (**Figura 2**). A su vez, las nanocapsulas NCs de poliarginina demostraron una elevada actividad quimiotáctica en macrófagos, tanto cargadas con la quimiocina CCL2 como blancas, poniendo de manifiesto la capacidad de vectorización de la terapia. La elevada quimioatracción de las nanocapsulas NCs blancas hacia los macrófagos viene

probablemente derivada al papel de la poliarginina como agonista TLR4[57,58], y resalta el potencial de estos vehículos para la vacunación y la inmunoterapia en cáncer.

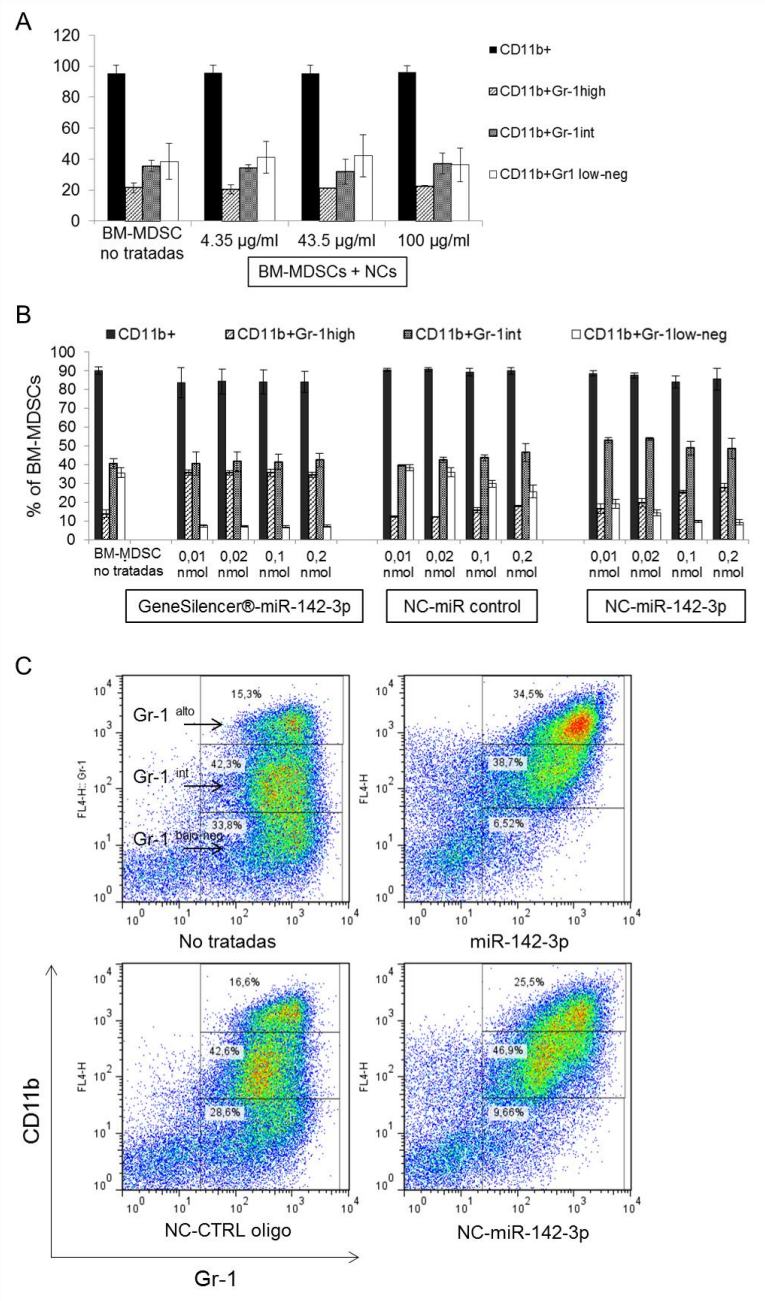

Figura 2. Las nanocápsulas de poliarginina cargadas con miR-142-3p reducen el porcentaje de células Gr-1$^{\text{bajo-negativo}}$ (fracción monocito-macrofágica) en el cultivo de BM-MDSC. A) Las MDSCs fueron tratadas con concentraciones crecientes de NCs blancas para testar su efecto en la distribución de subtipos celulares. Las MDSCs fueron posteriormente transfectadas con 0.01 to 0.1 nmol de miR 142-3p usando un transfectante comercial (GeneSilencer®, Genlantis) o NCs de poliarginina. Se muestran el efecto de direntes dosis de miARN en los subtipos celulares (B) e imágenes representativas de citometría de flujo para la dosis de 0.1 nmol (C). Los valores son la media ± SD de dos experimentos independientes.

Previamente se ha demostrado que el miR 142-3p y el shC/EBPβ son capaces de aumentar la eficacia de la ACT y la vacunación antitumoral *in vivo*, respectivamente, cuando son administrados en dendrímeros 4PD. Nuestras observaciones basadas en datos *in vitro*, sugieren que la combinación de las terapias basadas en ARN y quimiocinas podría ser un enfoque prometedor para aumentar la eficacia de la ACT en inmunoterapia. Además, los resultados relativos a la acumulación de las partículas marcadas en el bazo y el tumor de modelos tumorales murinos, así como el silenciamiento del ARNm de C/ EBPβ en el bazo y tumor después de la administración *in vivo* de las NCs cargadas con shC/EBPβ, evidencian todavía más el potencial de este sistema.

2.2 Modulación del fenotipo de células madre mesenquimales (MSCs) en ingeniería de tejidos

La reparación de tejidos como el cartílago o el músculo esquelético, continúa siendo un objetivo inalcanzado ya que las terapias actuales no consiguen generar tejidos de calidad. En el caso del cartílago, procedimientos quirúrgicos ampliamente usados como la técnica de microfractura, no son capaces de restaurar el cartílago hialino normal. El transplante de tejido osteocondral es la única técnica quirúrgica clásica que regenera el cartílago hialino, pero su uso está limitado debido al riesgo de transmisión de enfermedades y al rechazo inmune derivado de transplantes alogénicos. En línea con esta técnica, existen unos enfoques más avanzados como el implante de condrocitos autólogos (ACI) y el implante de condrocitos autólogos asistido mediante matriz (MACI) pero son muy costosos y precisan protocolos de implantación complejos[59,60]. De la misma manera, las propiedades del músculo esquelético regenerado están todavía lejos de las del músculo nativo. Los tratamientos actuales, incluyendo el transplante autólogo de músculo y la inyección de células de músculo expandidas *ex vivo*, han mostrado un éxito limitado[61–65]. En este sentido, la medicina regenerativa se presenta como una solución para evitar el uso de transplantes y superar el problema de escasez de donantes en el reemplazo de tejidos u órganos dañados. Los avances en biología molecular y ciencia de materiales, han llevado a nuevas estrategias de ingeniería de tejidos que incluyen el desarrollo de matrices 3D que pueden actuar tanto como vehículos de células como de señales para la regeneración tisular[66,67].

Una de las fuentes celulares más ampliamente usadas en ingeniería de tejidos son las células madre mesenquimales (MSCs). Descubiertas por Pittenger et al. en 1999, las MSCs tienen la capacidad de diferenciarse a múltiples linajes mesenquimales y secretar moléculas inmunorreguladoras que ayudan a construir microambientes regeneradores en el lugar de lesión[68]. Además, se pueden extraer de diversas fuentes y pueden ser expandidas *in vitro,* lo que facilita su uso en clínica[69]. Aunque las MSCs muestran un

tropismo natural hacia tejidos dañados incluso tras su inyección intravenosa, se ha demostrado que el uso de sistemas de liberación permite controlar y manipular las células o tejidos implantados con efectos secundarios reducidos[69]. Dentro de estos sistemas de liberación, los hidrogeles, redes poliméricas tridimensionales hidrofílicas, han suscitado gran atención en cuanto a su aplicación en ingeniería de tejidos. Los hidrogeles presentan muchas similitudes con la matriz extracelular y su biocompatibilidad, bioadhesión y biodegradabilidad se pueden modular dependiendo de las necesidades. Además, poseen una estructura altamente porosa que promueve la proliferación celular así como una adecuada cinética de difusión de nutrientes y productos metabólicos. Finalmente, pueden ser formulados en soluciones inyectables que aseguran una administración mínimamente invasiva así como su capacidad de adaptarse a defectos irregulares.

Los hidrogeles se dividen en dos categorías de acuerdo a su origen natural o sintético. Los hidrogeles de polímeros naturales han sido ampliamente usados en ingeniería de tejidos y varios estudios sugieren su superioridad sobre los polímeros sintéticos. Dentro de ellos destacan los hidrogeles de fibrina, alginato y colágeno, polímeros que cuentan ya con varios productos en uso clínico[60,70–72].

La **fibrina** es un producto final de la cascada de coagulación que tiene la capacidad de autoensamblarse formando entramados fibrilares. Puede ser extraída de la sangre del paciente, eliminando, por tanto, cualquier riesgo de respuesta inmune[73]. Ha sido aprobada por la Administración de Alimentos y Medicamentos de EEUU (FDA) como pegamento quirúrgico y se ha usado ampliamente en materiales hemostáticos y apósitos (Tisseel, Artiss, Evicel, Cryoseal etc.). Asimismo, los geles de fibrina presentan una gran bioactividad que ha propiciado su uso en el desarrollo de andamiajes celulares para la liberación de células madre[74].

El **colágeno**, por su parte, es el principal componente de la matriz extracelular de los tejidos mamíferos, y puede formar geles físicos térmicamente reversibles o reticularse químicamente mediante glutaraldehido[75] o difenilfosforilazida[76]. Existen una miríada de productos a base de colágeno aprobados por la FDA, que van desde apósitos (Apligraft, Integra, Gintuit) hasta agentes hemostáticos (Tachosil, Vitagel). Como en el caso de la fibrina, varios dispositivos de colágeno han sido diseñados para su aplicación en ingeniería de tejidos (Chondro-Gide, Infuse, NeuraGen etc) y en diciembre de 2016 la FDA aprobó el primer andamiaje celular para reparar defectos de cartílago de la rodilla (Maci, Vericel Corporation) [77,78].

Finalmente, el **alginato**, también aprobado por la FDA, ha sido empleado para el diseño de productos con aplicaciones diversas, tanto alimentarias como biomédicas, incluyendo sistemas de ingeniería de tejidos y liberación de fármacos. Así, el alginato ha sido usado como excipiente (Tarka, Skelaxin, ROXYBOND, MORPHABOND ER), material

de impresión dental (HygePLUS, Hygedent, Image), apósito (ALGICELL Ag, Suprasorb A + Ag, Phytacare), agente hemostático (Neptune pads) vehículo inyectable de liberación de células (RGD-alginate, ASTM F2315 - 11) y matriz inmobilizadora. Los alginatos son polisacáridos aniónicos e hidrofílicos aislados de algas marrones y bacterias que pueden reticularse con cationes divalentes (p ej. Ca^{2+} o Ba^{2+}) dando lugar a la formación de un entramado de gel.

Estos tres materiales han sido empleados en el contexto de esta tesis para construir **Matrices Activadas Genéticamente (GAMs)** destinadas a la regeneración del cartílago y el músculo esquelético. Como comentamos anteriormente, los hidrogeles se emplean en ingeniería de tejidos como vehículos de células y especialmente, factores de crecimiento que ayuden a guiar el proceso regenerativo. Tradicionalmente, estos factores de crecimiento eran incorporados en forma de proteínas recombinantes como en el caso de OP-1™, una matriz de colágeno cargada con rhBMP-7 o Infuse®, una matriz de colágeno cargada con rhBMP-2, dispositivos ya aprobados por la FDA. Sin embargo, dichos factores normalmente se administran a altas dosis para contrarrestar su corta vida media y los materiales usados actualmente ofrecen un escaso control sobre sus perfiles de liberación. Esto, a su vez, lleva consigo efectos secundarios entre los cuales el riesgo de malignidades es uno de los más graves[79–81].

Intentando superar estas desventajas, se ha empezado a explorar el uso de terapia génica como una alternativa a las proteínas recombinantes, y el concepto de GAM fue descrito[82]. En un primer momento, las GAMs estaban basadas en ADN plasmídico (ADNp), libre o complejado a formulaciones no virales, codificando el factor de crecimiento de interés. Como en el caso de las proteínas recombinantes, este ADNp se cargaba en la matriz polimérica desde la cual sería liberado, produciendo la transfección de las células circundantes y la consiguiente expresión proteica sostenida y localizada. Aunque la mayor parte de estas GAMs estaban basadas en el uso de factores de crecimiento codificados por ADNp, el mismo enfoque se exploró para codificar factores de transcripción esenciales en el desarrollo musculo-esquelético como SOX9, regulador maestro de la condrogénesis, y RUNX2, regulador maestro de la osteogénesis[83,84]. Sin embargo, aunque la liberación de ADNp mediante métodos no virales se prefiere sobre los métodos virales debido a su mayor seguridad, las formulaciones no virales se caracterizan por una baja eficiencia de transferencia génica, lo que en parte condiciona su éxito en clínica. Ello ha llevado al desarrollo de GAMs basadas en ARN, con el objetivo de tomar ventaja de la mayor transferencia génica del ARN[12]. En este sentido, diferentes matrices de ARN han sido exploradas, desde GAMs de siARN a miARN[85], hasta las más recientes GAMs de ARNm, perfiladas por Liu et al. en 2013[86] y descritas por primera vez por Elangovan et al. en 2015 para codificación de proteínas morfogenéticas de hueso (BMPs)[87].

Tomando como base este conocimiento, el segundo objetivo de esta tesis ha sido desarrollar una nueva clase de GAMs de ARNm activadas con factores de transcripción específicos de linaje y cargadas con MSCs, para dirigir la especificación celular en tejidos enfermos o heridos. Para ello, hemos activado hidrogeles con SOX9 (cartílago) [35,36] **y MYOD (músculo)** [28] **para promover la diferenciación condrogénica y miogénica de las MSCs.**

Dado que el requisito fundamental de una GAM es promover la transfección de las células encapsuladas, el primer paso de nuestro trabajo consistió en elaborar unas matrices que consiguieran elevadas eficacias de transfección. Para construir estas GAMs, seleccionamos la fibrina como polímero debido a su amplio uso en clínica, su capacidad para formar sistemas fácilmente inyectables y su historial en dispositivos de transferencia génica[88–94]. Debido a la dificultad de conseguir altas eficacias de transfección en sistemas tridimensionales[95], hemos utilizado el reactivo comercial 3DFectIN, para complejar las secuencias génicas dentro del gel. Salvo en el caso del ARNm de MYOD que fue obtenido comercialmente, estas secuencias génicas han sido sintetizadas mediante transcripción in vitro (IVT) a partir de plásmidos diseñados con el fin de maximizar la síntesis proteica. De esta manera, fue posible comparar las GAMs de ARNm con las correspondientes GAMs de ADNp, previamente estudiadas. Estos ARNm fueron testados primeramente en cultivos en 2D para verificar su actividad, y una vez verificada la funcionalidad de los plásmidos molde, se procedió a optimizar el proceso de transfección en 3D. Los primeros experimentos en 3D fueron realizados con la secuencia reportera de la proteína fluorescente amarilla (YFP), debido a la facilidad para verificar la eficacia de transfección mediante microscopía de fluorescencia. Variables como la concentración del gel, el ratio polinucleótido:transfectante, la densidad celular o el tiempo de ensayo, fueron ajustados en estos experimentos previos. En consecuencia, un rango de concentraciones de fibrina de 2 y 4 mg/ml, un ratio 3DFectIN:polinucleótido 3:1 (µl:µg) y una densidad celular de $1.5x10^6$ células/ml fueron seleccionados para los ensayos de diferenciación.

Paralelamente, los geles elaborados según las condiciones óptimas fueron caracterizados en mayor profundidad. Por un lado, las partículas preparadas en los diferentes ratios fueron caracterizadas en base a su tamaño, polidispersión y distribución dentro del gel. Medidas de espectroscopía de correlación fotónica mostraron diferencias entre las partículas cargadas con ARNm o ADNp. Así, para las partículas de ARNm, un incremento del ratio 3DFectIN:polinucleótido de 2:1 a 3:1 resultó en una disminución del tamaño de partícula hasta alrededor de los 200 nm mientras que el caso del ADNp, el ratio 2:1 resultó insuficiente para complejar el material genético y el tamaño de partícula no consiguió reducirse de ≈1 µm incluso aumentando el ratio a 4:1. En todos los casos, imágenes de microscopia de fluorescencia de las partículas marcadas exhibieron una distribución homogénea dentro del gel,

independientemente del ratio o la concentración de fibrina. Asimismo, ambos tipos de geles mostraron una microarquitectura fibrilar y porosa, observados mediante microcoscopía electrónica de barrido (SEM), adecuada para la proliferación y remodelación celular. La citotoxicidad y los niveles de proliferación celular fueron también testados para el ratio 3:1, mostrando una excelente biocompatibilidad de las GAM.

Una vez realizada esta caracterización inicial, procedimos a caracterizar la cinética de expresión génica de nuestras GAMs de ARNm en comparación con las clásicas GAMs de ADNp. Para ello, utilizamos el ADNp de SOX9 y el ARNm sintetizado *in vitro* a partir de dicho plásmido, y construimos las correspondientes matrices utilizando las dos concentraciones de fibrinógeno (2 y 4 mg/ml) con el fin de comparar también el efecto de la concentración de gel. Los resultados de transfección mostraron expresiones de SOX9 alrededor de tres veces mayores para las matrices activadas con ARNm con respecto a las activadas con ADNp, independientemente de la concentración del gel. Dicha concentración tampoco influyó significativamente en la cinética de expresión, obteniéndose valores de SOX9 que fueron aumentando con el tiempo en el caso de las matrices activadas con ADNp y disminuyendo en las GAMs de ARNm, en consonancia con resultados obtenidos previamente para transfección en 2D[9,96].

A continuación, realizamos los ensayos de diferenciación condrogénica y miogénica con las matrices activadas con SOX9 y MYOD, respectivamente. En el primer caso, comparamos las matrices de ARNm y ADNp además de las dos concentraciones de gel. En el segundo, estudiamos únicamente el efecto de la mecánica del gel. Un primer ensayo de cinética de expresión de marcadores condrogénicos mostró que las GAMs de ARNm promovían una mayor y más rápida expresión génica de agrecano y colágeno con respecto a las matrices de ADNp. Asimismo, la expresión de estos marcadores era mayor en los geles de baja concentración, probablemente debido a una mayor condensación celular derivada de la más rápida degradación de estos geles[97–100], por lo que fueron seleccionados para los experimentos siguientes. Posteriormente, ensayos completos de diferenciación de 21 días mostraron una correlación entre la potente inducción condrogénica de las GAMs de ARNm y la consecución de un tejido cartilaginoso de mejor calidad. Así, la tinción histológica y el análisis inmunohistoquímico de los geles reveló una mayor acumulación de agrecano y colágeno en las matrices activadas con ARNm en comparación con las matrices de ADNp. Esta acumulación fue especialmente mayor en experimentos llevados a cabo con suplementación de TGF-β3, pero la misma tendencia se mostró en ausencia de suplementación, demostrando el potencial de las matrices de ARNm de SOX9. Cabe destacar asimismo, que ambos tipos de matrices consiguieron mejores resultados que el cultivo en pellet estándar, que además de promover una expresión de agrecano y colágeno mucho más baja, dio lugar a una expresión del marcador hipertrófico colágeno X, 600 veces superior (**Figura 3**).

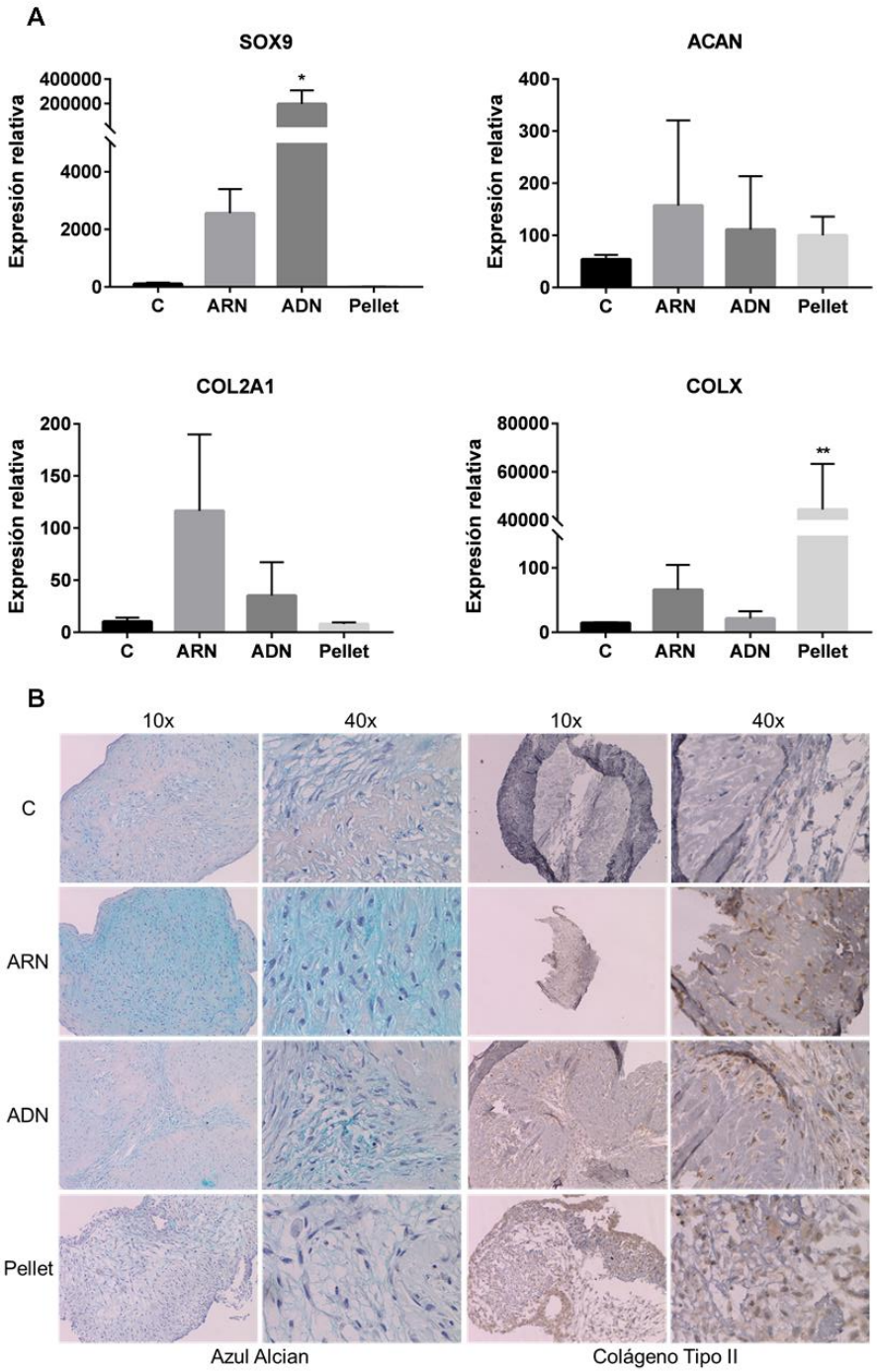

Figura 3. Las hMSCs encapsuladas en matrices de ARNm de SOX9 de 2 mg/ml producen una expresión de marcadores condrogénicos más alta en comparación con sus análogos de ADN en presencia de TGF-β3 soluble. Los hidrogeles fueron cultivados durante 21 días en medio condrogénico completo. A) Niveles de expresión génica de los marcadores condrogénicos SOX9, agrecano (ACAN), colágeno tipo 2 (COL2A1) y colágeno X (COLX). Los valores de expresión génica fueron evaluados mediante qRT-PCR, normalizados frente a la expresión de GAPDH y comparados con los niveles en hMSCs antes de encapsular. Los datos se muestran como la media y desviación estándar de tres replicados en un experimento con el ratio 3DFectIN:polinucleótido 3:1. Se utilizó un análisis two-way ANOVA para comparar los niveles de expresión génica (*P<0.05, **P<0.01). B) Examen inmunohistológico de la deposición de glicosaminoglicanos y colágeno. Los hidrogeles se tiñeron con azul alcian para detectar los glicosaminoglicanos y la expresión de colágeno se detectó mediante inmunohistoquímica. Se muestra un cultivo estándar en pellet a modo de comparación.

Por su parte, las matrices activadas con ARNm de MYOD mostraron una cinética de expresión génica diferente a las matrices de SOX9 previamente estudiadas. En este caso, la expresión de MYOD fue muy potente desde tiempos cortos y no decayó con el tiempo, probablemente debido al hecho de que este ARNm comercial es resistente a ARNasas y por tanto posee una mayor vida media con respecto al ARNm de SOX9. Estas matrices también dieron lugar a una potente inducción miogénica, promoviendo una elevada expresión de los marcadores miogenina y caderina 15 incluso 12h después de la encapsulación de las MSCs. De la misma manera, los ensayos de miogénesis de 15 días demostraron una elevada expresión génica de MYOD, miogenina, y las cadenas pesadas de la miosina 2 y 3, evidenciando un proceso miogénico. Lo que es más importante, el análisis inmunohistoquímico mostró que las matrices de MYOD dieron lugar a la expresión de miosina en las MSCs, proteína crucial en el músculo esquelético. En este caso, los geles de mayor concentración de fibrinógeno (4 mg/ml) son los que consiguieron una mayor expresión de marcadores miogénicos, sobre todo en cuanto a la expresión de miosina a nivel proteico. Esta mayor expresión es probablemente debida a la consecución de un mayor alineamiento celular en los geles de mayor concentración y pone de manifiesto de nuevo la importancia de las propiedades mecánicas de la matriz en la respuesta regenerativa.

En el contexto de la ingeniería de tejidos, varios trabajos han explorado la modulación de las señales mecánicas para dirigir la conversión celular hacia linajes específicos. Para células sembradas sobre sustratos de dos dimensiones (2D), se ha demostrado que la dureza del sustrato y las restricciones geométricas en la adhesión celular pueden afectar la manera en que las células se extienden, su generación de tracción y su destino. Por el contrario, la influencia de las propiedades biofísicas de los ambientes tridimensionales (3D) en el destino celular es más compleja y todavía no se conoce en profundidad. Huebsch et al. demostraron que dentro de hidrogeles de alginato no degradables y reticulados iónicamente, la diferenciación de MSCs era dictada por la dureza de la matriz independientemente de la morfología celular[33]. Tres años después, Khetan et al. identificaron la remodelación celular del gel y la tensión generada por las células como claves en la regulación de su destino[101]. De acuerdo con este trabajo, Chaudhuri et al. establecieron las propiedades de estrés-relajación de los geles como un parámetro crucial para mimetizar la viscoelasticidad de las matrices extracelulares (ECM) naturales y maximizar la remodelación y diferenciación celular[102]. De manera complementaria, otro trabajo reciente desarrollado por Cosgrove et al. ha revelado la importancia de la naturaleza de los ligandos de adhesión celular de los hidrogeles en la interpretación de la dureza de la matriz por parte de las células y los subsiguientes cambios en proliferación y diferenciación celular[103]. Para terminar, se ha demostrado recientemente que una interacción entre los contactos célula-matriz y célula-célula influencia también los estadíos de osteogénesis en hMSCs[34].

A fin de ahondar en la implicación de la mecánica de la matriz en la modulación del fenotipo celular, el último objetivo de esta tesis ha sido el estudio de la influencia de las propiedades de las GAMs en la condrogénesis inducida por SOX9. Sin embargo, los geles de fibrina no permiten un adecuado control sobre las propiedades mecánicas, lo que hace que no sean una plataforma idónea para llevar a cabo este tipo de estudio. Como alternativa, durante la estancia en el grupo del Prof. David Mooney en la Universidad de Harvard, trabajamos con unos IPNs (Interpenetrating Polymer Networks) a base de alginato y colágeno que nos proporcionaron un control preciso sobre la mecánica del gel. Los IPN están constituidos por dos o más polímeros parcialmente entrelazados, formando sistemas híbridos que complementan las propiedades de los polímeros que los forman. Así, los IPNs de colágeno-I-alginato toman ventaja de las propiedades de interacción celular del colágeno para compensar la falta de ligandos de adhesión celular del alginato, a la vez que contrarrestan las pobres propiedades mecánicas de los geles de colágeno con la modulable capacidad de reticulación del alginato[104].

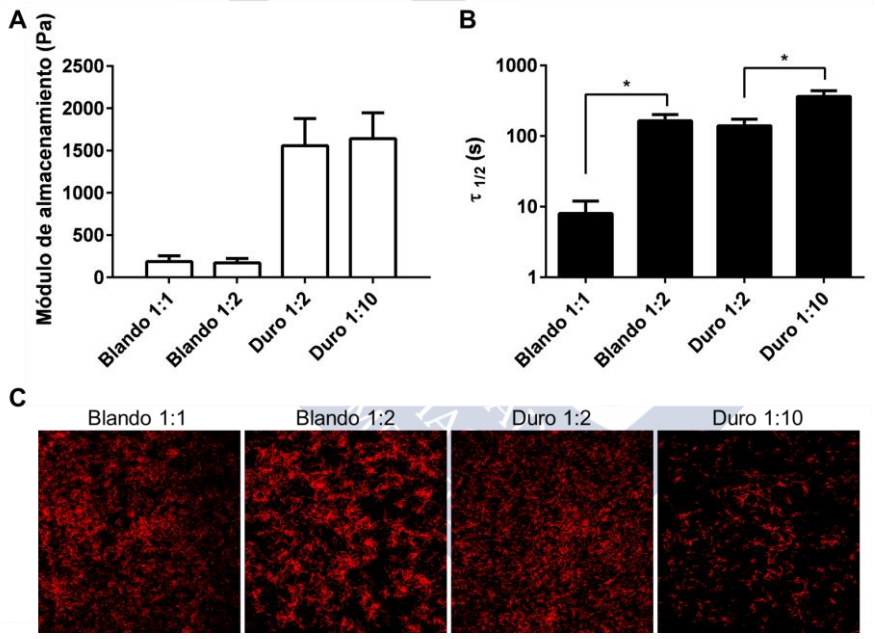

Figura 4. Caracterización reológica y morfológica de los IPNs. A) Módulo de equilibrio de los diferentes IPNs. B) Cuantificación del tiempo en que el estrés se reduce a la mitad de su valor original, $\tau_{1/2}$, en tests de estrés-relajación (One-way ANOVA, n=3, *P<0.05). C) Alineamiento de fibras de colágeno en el conjunto de IPNs. Microscopía confocal de reflectancia de las diferentes composiciones de IPNs.

Con esto en mente, en primer lugar fabricamos un conjunto de IPNs de colágeno-I-alginato de dureza (G' de 150 a 1500 Pa) y adhesión (concentración total de colágeno de 1 y 5 mg/ml) modulables y caracterizamos su reología y fibrilaridad mediante microscopía confocal. Para dar lugar a las diferentes propiedades de adhesión, jugamos con los ratios de los dos polímeros: el alginato, carente de ligandos de adhesión, y el

colágeno, con numerosos dominios de unión a integrinas. La dureza fue modulada mediante la modificación de la concentración del agente reticulante: las micropartículas de carbonato cálcico. La variación de estas variables dio lugar a diferentes composiciones de IPNs que designamos con una notación que describe la dureza del gel en primer lugar, seguida del ratio p:p colágeno:alginato. Consideramos los IPNs Blando 1:1 y Blando 1:2 como los IPNs blandos (G'≈ 150 Pa) y Duro 1:2 y Duro 1:10 como los IPNs duros (G'≈ 1500 Pa). Los experimentos de estrés-relajación mostraron una elevada dependencia del tiempo medio (t ½) de la concentración de alginato. Los IPNs con la concentración más baja exhibieron t ½ de 10 s en comparación con los IPNs de alta concentración de alginato, que presentaron t ½ de 100 s independientemente de la dureza o la concentración de colágeno. Este t ½ concuerda con resultados previos para geles de alginato de bajo peso molecular y baja viscosidad y ha sido identificado como el t ½ óptimo para permitir la remodelación celular de los geles[102], un proceso clave en ingeniería de tejidos (**Figura 4**).

Una vez caracterizados los IPNs, incluimos en ellos las secuencias de SOX9 para elaborar las GAMs de manera análoga a los geles de fibrina y llevar a cabo los experimentos de transfección. Independientemente del tipo de material genético, observamos que la máxima expresión de SOX9 se conseguía en los IPNs Blando 1:1 y Duro 1:2, sugiriendo que ratios colágeno: alginato p:p más bajos ejercen un impacto negativo sobre la transferencia génica (Blando 1:1 > Blando 1:2 IPNs) y que la dureza ejerce un efecto positivo (Duro 1:2 > Blando 1:2), probablemente mediado por ligandos de adhesión celular (Duro 1:2 > Duro 1:10) (**Figura 5A, B**). De hecho, el efecto negativo del alginato en la transfección fue confirmado mediante experimentos en 2D realizados en presencia de concentraciones crecientes de alginato soluble, mientras que su efecto en la agregación de las partículas se mostró mediante análisis de los geles por microscopía de fluorescencia. Por el contrario, el efecto positivo de la adhesión celular en la transfección fue confirmado mediante la reducción de la sobreexpresión de SOX9 después de la adición del inhibidor de ROCK Y-27632. Estudios previos realizados en 2D han ligado el efecto positivo de la dureza en la transfección a unos niveles de proliferación celular incrementados. En este trabajo, no encontramos una diferencia significativa en el crecimiento celular entre los diferentes IPNs, descartando ésta como la causa de la diferente eficacia de transfección. Sin embargo, nuestros estudios muestran un incremento en la internalización celular de las nanopartículas en los geles de mayor dureza, explicando las diferencias en la expresión del transgen entre los diferentes IPNs. Es de destacar que las células transfectadas en 2D con ADNp antes de su encapsulación en los IPNs, exhibieron el mismo patrón de sobreexpresión de SOX9 que tras la transfección en 3D (**Figura 5C, D**). Experimentos complementarios permitieron ligar dicha observación a la encapsulación de partículas de ADNp remanentes (más estables que las partículas de ARNm) junto con las células dentro de los IPNs, confirmando así la importancia de la mecánica de la matriz en la transfección celular.

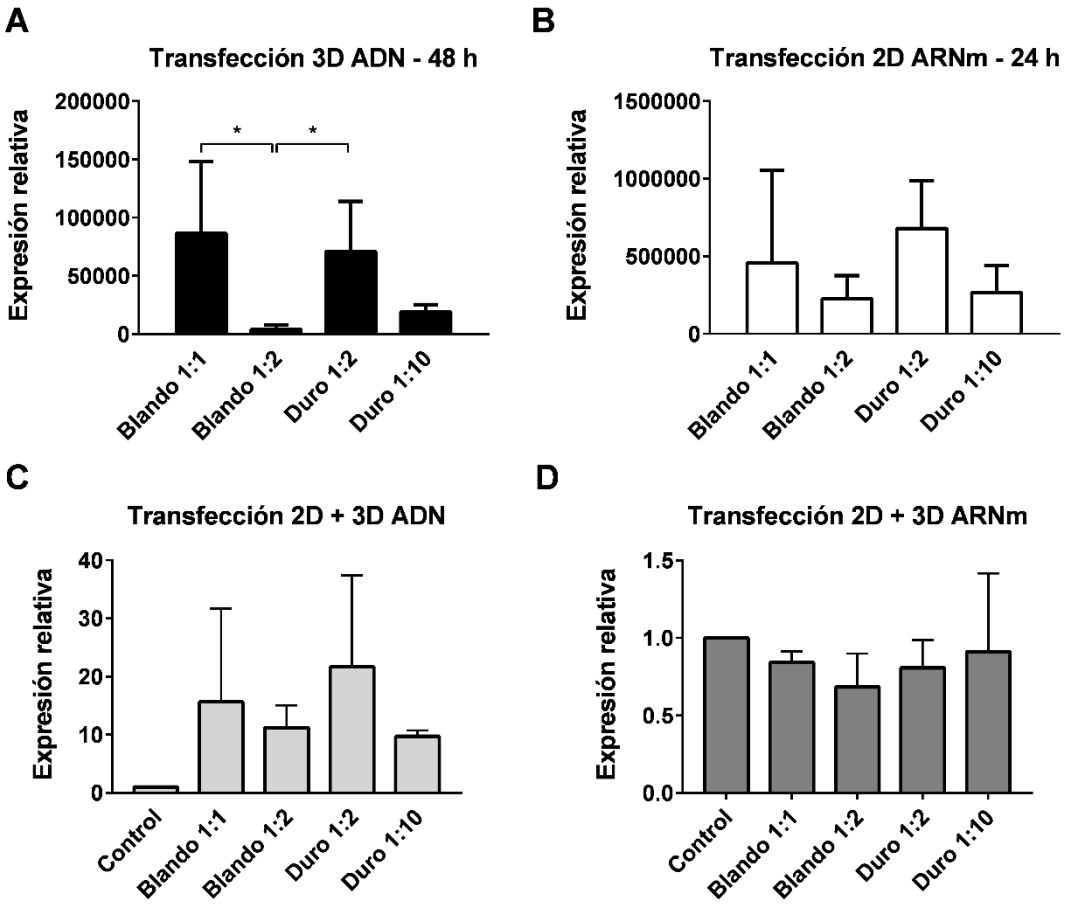

Figura 5. Eficacia de transfección del conjunto de IPNs. A) Sobreexpresión de SOX9 48 h después de la transfección con ADNp. Los niveles de expresión génica fueron comparados mediante un One-way ANOVA (*P<0.05). B) Sobreexpresión de SOX9 24 h después de la transfección con ARNm. C) Sobreexpresión de SOX9 48 h después de la encapsulación de células transfectadas con ADNp (células recuperadas de las placas de cultivo 72 h después de la transfección en 2D). D) Sobreexpresión de SOX9 24 h después de la encapsulación de células transfectadas con ADNp (células recuperadas de las placas de cultivo 24 h después de la transfección en 2D). Los niveles de expression génica fueron normalizados según los niveles de SOX9 a t=0 en células no transfectadas (A-B) y transfectadas en 2D antes de encapsular en los IPNs (C-D).

Posteriormente, procedimos a estudiar el efecto conjunto de la sobrexpresión de SOX9 y la mecánica del IPN. Con el objetivo de evitar las diferencias en la eficacia de transfección entre los distintos IPNs, en un primer momento realizamos la transfección de las MSCs en 2D previamente a su encapsulación en los geles. En comparación con los IPNs de menor dureza, (Blando 1:2), los IPNs más duros (Duro 1:2) mostraron una mayor expresión de marcadores condrogénicos. En base a ello, y dado que los IPNs Duro 1:2 también habían mostrado la mayor eficacia de transfección en los experimentos previos, estos IPNs fueron seleccionados para posteriores experimentos. Al igual que en el caso de la transfección 2D de SOX9, la transfección de SOX9 mediada por los IPNs también indujo una elevada síntesis de marcadores condrogénicos. A diferencia del caso anterior,

la inducción del mRNA de estos marcadores fue mayor para los IPNs-SOX9 que para los IPNs control, especialmente en el caso del colágeno tipo II, cuya expresión no fue sobrerregulada en los IPNs control. Cabe destacar que la expresión forzada de SOX9 dio lugar a la reducción del marcador hipertrófico colágeno X, sugiriendo que los IPNs-SOX9 podrían promover la formación de un tejido cartilaginoso de mejor calidad. Además, el uso del inhibidor BMS-345541 redujo la expresión de COLX en mayor medida, posicionando este inhibidor como un fármaco a considerar en el diseño de biomateriales para la reparación de cartílago.

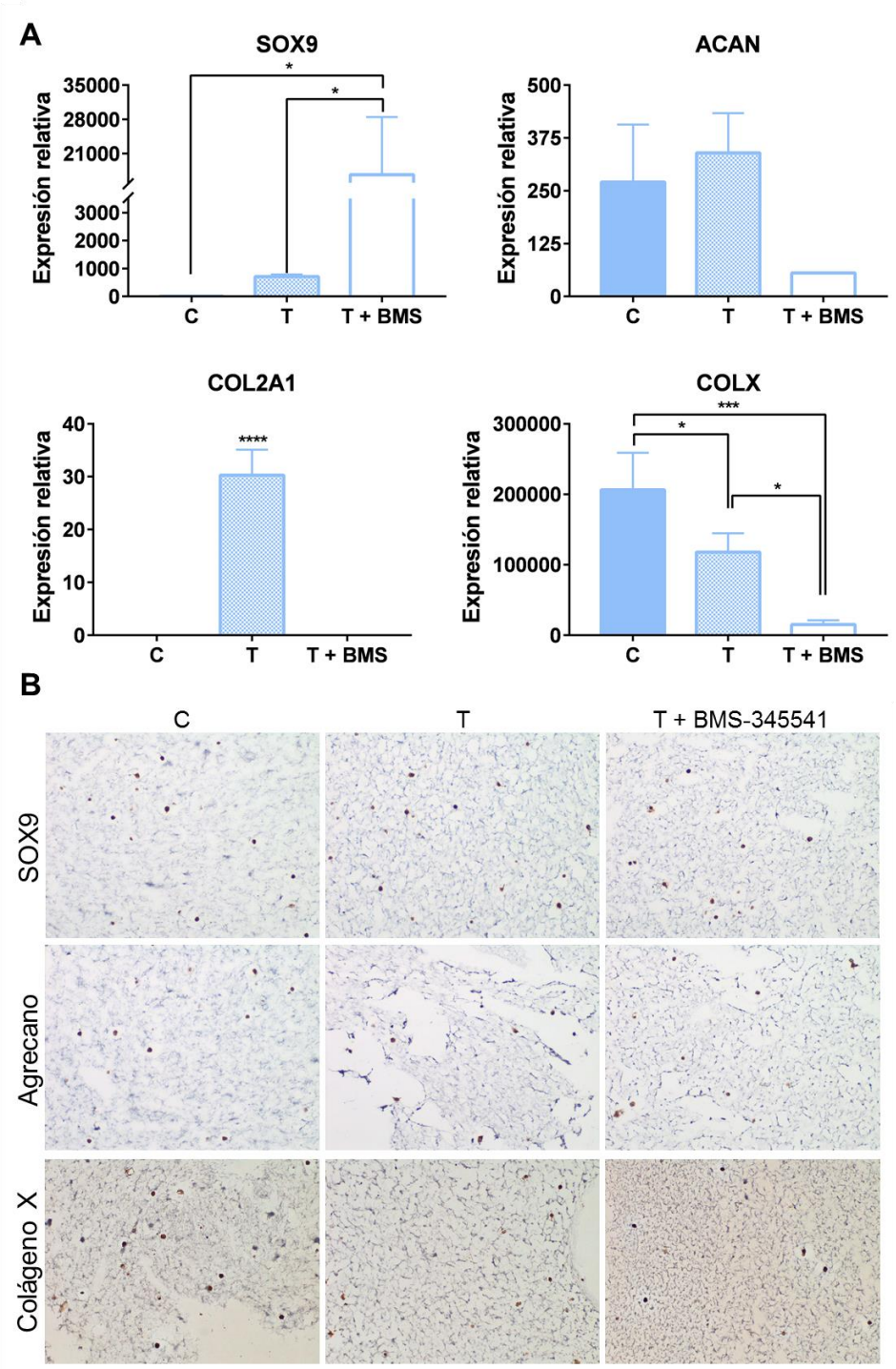

Figura 6. La transfección 3D de SOX9 promueve una mayor expresión de marcadores condrogénicos que la transfección en 2D de MSCs. A) Expresión génica de los marcadores condrogénicos SOX9, agrecano (ACAN), colágeno tipo 2 (COL2A1) y colágeno tipo 10 (COLX). B) Immunohistoquímica de SOX9, agrecano y colágeno tipo 10 en secciones de IPN. Los datos representan la media ±SD. C: células control (no-transfectadas); T: células transfectadas con SOX9; T + BMS: células transfectadas con SOX9 en presencia del inhibidor de NF-κβ inhibitor BMS-345541 (5 μM).

3. Conclusiones

En conjunto, nuestros resultados muestran el potencial de terapias de ARN basadas en biomateriales para desarrollar sistemas de liberación más eficientes, con el objetivo de modular el fenotipo celular en contextos de enfermedad.

Por un lado, hemos diseñado unas nanocápsulas de poliarginina capaces de co-encapsular proteínas y ARNi inmunomoduladores para revertir el fenotipo inmunosupresor de las MDSCs. Estas nanocápsulas han sido elaboradas mediante un nuevo método de auto-emulsificación que resulta en la generación de fases micelares inversas L2 adecuadas para la inclusión de moléculas hidrofílicas. Así, hemos co-asociado en ellas dos secuencias de ARNi, miR 142-3p y shC/EBPβ, adsorbidas a la cubierta catiónica, y dos proteínas inmunomoduladoras, el antígeno modelo ovalbumina y la quimiocina CCL2, encapsuladas en las fases acuosas del núcleo lipídico de GMO. Las nanocápsulas cargadas con el miR 142-3p, mostraron una buena capacidad de transfección de las secuencias de ARN en MDSCs, promoviendo así la reversión del fenotipo inmunosupresor. De manera análoga, cuando el shC/EBPβ fue adsorbido a estos sistemas, se observó una reducción en los niveles de ARNm de C/EBPβ en una línea celular de MDSCs, efecto que también se observó en un modelo murino de fibrosarcoma, dando lugar a la disminución de macrófagos-asociados al tumor. Finalmente, la posibilidad de una terapia dirigida hacia monocitos-macrófagos fue explorada en virtud de la encapsulación de la quimiocina CCL2 en el núcleo lipídico de las nanocápsulas, induciendo una elevada migración de macrófagos hacia las mismas. En general, estas observaciones sugieren que las nanocápsulas de poliarginina constituyen un vehículo prometedor para la co-administración de polinucleótidos y quimiocinas y la consiguiente modulación de la actividad de las MDSCs.

En vista de la capacidad de modulación de las nanocápsulas de poliarginina, decidimos explorar un sistema de liberación más complejo, de tipo andamiaje, con aplicación en ingeniería de tejidos. Así, hemos desarrollado unos geles de fibrina, activados con nanopartículas cargadas con ARNm codificante de los TF maestros SOX9 y MYOD, para dirigir la especificación de células madre hacia cartílago y músculo, respectivamente. Las matrices de ARNm codificantes de TF demostraron una excelente biocompatibilidad y son fácilmente inyectables, constituyendo una adecuada plataforma celular. Cuando comparamos nuestras matrices con matrices cargadas con ADN de TF previamente exploradas, nuestros sistemas fueron capaces de inducir una mayor y más rápida expresión génica de los TF. Esta potente expresión de TF, a su vez, promovió una más rápida iniciación de las cascadas de diferenciación, dando lugar a una síntesis proteica más eficiente de marcadores específicos de tejido. Asimismo, observamos que esta expresión de marcadores de diferenciación dependía de las propiedades mecánicas de la matriz, con matrices menos densas induciendo una mayor expresión de marcadores condrogénicos y matrices más densas promoviendo un mayor grado de miogénesis.

Con el objetivo de profundizar en la influencia de las propiedades mecánicas en la diferenciación celular, a continuación trabajamos con unos IPNs desarrollados en el laboratorio del profesor David Mooney. Estos IPNs, a base de colágeno-I y alginato, nos permitieron controlar la dureza y adhesión de la matriz y estudiar la influencia de estos parámetros en la condrogénesis de MSCs. Desarrollamos un conjunto de cuatro IPNs que caracterizamos en base a su reología y su microarquitectura y determinamos su capacidad de transfección en 3D. Nuestros resultados indicaron un efecto positivo de la dureza y la adhesión del gel en la transfección de MSCs, mediado por una mayor internalización de las nanopartículas portadoras de la terapia génica. Estos IPNs de mayor adhesión y dureza fueron satisfactoriamente empleados para inducir la condrogénesis mediante transfección 3D de SOX9 en MSCs, dando lugar a un tejido cartilaginoso con bajos niveles de hipertrofia. En comparación con los hidrogeles de fibrina previamente estudiados, estos IPNs constituyen un sistema idóneo para la regeneración de cartílago dado que sus propiedades mecánicas se adaptan a las del tejido nativo. Trabajos futuros irán encaminados a potenciar el proceso de diferenciación miogénica mediante matrices optimizadas mecánicamente.

En conclusión, el trabajo desarrollado en esta tesis pone de manifiesto la capacidad de los sistemas de liberación propuestos para la presentación simultánea de diferentes señales implicadas en la modulación celular. Teniendo en cuenta la complejidad de las vías de señalización celular alteradas en contextos de enfermedad, y la importancia de una correcta presentación espacio-temporal de los fármacos, es evidente la necesidad de tecnologías que permitan la generación de este tipo de terapias. Por ello, consideramos que tanto nuestro sistema nanocapsular como los sistemas tipo andamiaje, constituyen herramientas potencialmente útiles para la modulación de fenotipos celulares patológicamente alterados.

Bibliografía

1. Janmey, P. A. *et al.* From tissue mechanics to transcription factors. *Differenciation* **86,** 112–120 (2013).

2. Jonas, S. & Izaurralde, E. Towards a molecular understanding of microRNA-mediated gene silencing. *Nat. Rev. Genet.* **16,** 421–433 (2015).

3. Bracken, C. P., Scott, H. S. & Goodall, G. J. A network-biology perspective of microRNA function and dysfunction in cancer. *Nat. Rev. Genet.* **17,** 719–732 (2016).

4. Brenner, S., Jacob, F. & Meselson, M. An unstable intermediate carrying information from genes to ribosomes for protein synthesis. *Nature* **190,** 576–581 (1961).

5. Wolff, J. A. *et al.* Direct gene transfer into mouse muscle in vivo. *Science* **247,** 1465–1468 (1990).

6. Conry, R. M. *et al.* Characterization of a Messenger RNA Polynucleotide Vaccine Vector. *Cancer Res.* **55,** 1397–1400 (1995).

7. Quabius, E. S. & Krupp, G. Synthetic mRNAs for manipulating cellular phenotypes: An overview. *N. Biotechnol.* **32,** 229–235 (2015).

8. Mandal, P. K. & Rossi, D. J. Reprogramming human fibroblasts to pluripotency using modified mRNA. *Nat. Protoc.* **8,** 568–582 (2013).

9. Andries, O. *et al.* Comparison of the gene transfer efficiency of mRNA/GL67 and pDNA/GL67 complexes in respiratory cells. *Mol. Pharm.* **9,** 2136–2145 (2012).

10. Zou, S., Scarfo, K., Nantz, M. H. & Hecker, J. G. Lipid-mediated delivery of RNA is more efficient than delivery of DNA in non-dividing cells. *Int. J. Pharm.* **389,** 232–243 (2010).

11. Dowdy, S. F. Overcoming cellular barriers for RNA therapeutics. *Nat. Biotechnol.* **35,** 222–229 (2017).

12. Sahin, U., Karikó, K. & Türeci, Ö. mRNA-based therapeutics — developing a new class of drugs. *Nat. Rev. Drug Discov.* **13,** 759–780 (2014).

13. Rupaimoole, R. & Slack, F. J. MicroRNA therapeutics: towards a new era for the management of cancer and other diseases. *Nat. Rev. Drug Discov.* **16,** 203–222 (2017).

14. Vaquerizas, J. M., Kummerfeld, S. K., Teichmann, S. A. & Luscombe, N. M. A census of human transcription factors: function, expression and evolution. *Nat. Rev. Genet.* **10,** 252–263 (2009).

15. Lin, Y. *et al.* Transcription factor and miRNA co-regulatory network reveals shared and specific regulators in the development of B cell and T cell. *Sci. Rep.* **5,** 15215 (2015).

16. Wang, J., Lu, M., Qiu, C. & Cui, Q. TransmiR: A transcription factor microRNA regulation database. *Nucleic Acids Res.* **38,** 119–122 (2009).

17. Lin, Y. *et al.* MiRNA and TF co-regulatory network analysis for the pathology and recurrence of myocardial infarction. *Sci. Rep.* **5,** 9653 (2015).

18. Guo, Z. *et al.* Genome-wide survey of tissue-specific microRNA and transcription factor regulatory networks in 12 tissues. *Sci. Rep.* **4,** 5150 (2015).

19. Le Béchec, A. *et al.* MIR@NT@N: a framework integrating transcription factors, microRNAs and their targets to identify sub-network motifs in a meta-regulation network model. *BMC Bioinformatics* **12,** 67 (2011).

20. Marigo, I. *et al.* Tumor-induced tolerance and immune suppression depend on the C/EBPβ transcription factor. *Immunity* **32,** 790–802 (2010).

21. Sonda, N., Chioda, M., Zilio, S., Simonato, F. & Bronte, V. Transcription factors in myeloid-derived suppressor cell recruitment and function. *Curr. Opin. Immunol.* **23,** 279–285 (2011).

22. Jopling, C., Boue, S. & Belmonte, J. C. I. Dedifferentiation, transdifferentiation and reprogramming: three routes to regeneration. *Nat. Rev. Mol. Cell Biol.* **12,** 79–89 (2011).

23. Merrell, A. J. & Stanger, B. Z. Adult cell plasticity in vivo: de-differentiation and transdifferentiation are back in style. *Nat. Rev. Mol. Cell Biol.* **17,** 413–425 (2016).

24. Rackham, O. J. L. *et al.* A predictive computational framework for direct reprogramming between human cell types. *Nat. Genet.* **48,** 331–335 (2016).

25. Hikichi, T. *et al.* Transcription factors interfering with dedifferentiation induce cell type-specific transcriptional profiles. *Proc. Natl. Acad. Sci.* **110,** 6412–6417 (2013).

26. Almalki, S. G. & Agrawal, D. K. Key transcription factors in the differentiation of mesenchymal stem cells. *Differentiation* **92,** 41–51 (2016).

27. Yamamizu, K. *et al.* Identification of transcription factors for lineage-specific ESC differentiation. *Stem Cell Reports* **1,** 545–559 (2013).

28. Davis, R. L., Weintraub, H. & Lassar, A. B. Expression of a single transfected cDNA converts fibroblasts to myoblasts. *Cell* **51,** 987–1000 (1987).

29. Takahashi, K. & Yamanaka, S. Induction of Pluripotent Stem Cells from Mouse Embryonic and Adult Fibroblast Cultures by Defined Factors. *Cell* **126,** 663–676 (2006).

30. Engler, A. J., Sen, S., Sweeney, H. L. & Discher, D. E. Matrix Elasticity Directs Stem Cell Lineage Specification. *Cell* **126,** 677–689 (2006).

31. Clause, K. C. . L. L. J. . T. K. Directed stem cell differentiation: the role of physical forces. **17,** 48–54 (2012).

32. Guilak, F., Cohen, D. & Estes, B. Control of stem cell fate by physical interactions with the extracellular matrix. *Cell Stem Cell* **5,** 17–26 (2009).

33. Huebsch, N. *et al.* Harnessing traction-mediated manipulation of the cell/matrix interface to control stem-cell fate. *Nat. Mater.* **9,** 518–526 (2010).

34. Mao, A. S., Shin, J. W. & Mooney, D. J. Effects of substrate stiffness and cell-cell contact on mesenchymal stem cell differentiation. *Biomaterials* **98,** 184–191 (2016).

35. Dy, P. *et al.* Sox9 Directs Hypertrophic Maturation and Blocks Osteoblast Differentiation of Growth Plate Chondrocytes. *Dev. Cell* **22,** 597–609 (2012).

36. Bi, W., Deng, J. M., Zhang, Z., Behringer, R. R. & Crombrugghe, B. De. Sox9 is required for cartilage formation. *Nat. Genet.* **22,** 85–89 (1999).

37. Bronte, V. *et al.* Recommendations for myeloid-derived suppressor cell nomenclature and characterization standards. *Nat. Commun.* **7,** 12150 (2016).

38. Ugel, S., De Sanctis, F., Mandruzzato, S. & Bronte, V. Tumor-induced myeloid deviation: When myeloid-derived suppressor cells meet tumor-associated macrophages. *J. Clin. Invest.* **125,** 3365–3376 (2015).

39. De Sanctis, F. *et al.* MDSCs in cancer: Conceiving new prognostic and therapeutic targets. *Biochim. Biophys. Acta - Rev. Cancer* **1865,** 35–48 (2016).

40. Sonda, N. *et al.* miR-142-3p Prevents Macrophage Differentiation during Cancer-Induced Myelopoiesis. *Immunity* **38,** 1236–1249 (2013).

41. Qian, B.-Z. *et al.* CCL2 recruits inflammatory monocytes to facilitate breast-tumour metastasis. *Nature* **475,** 222–225 (2011).

42. Fang, W. Bin *et al.* Targeted gene silencing of CCL2 inhibits triple negative breast cancer progression by blocking cancer stem cell renewal and M2 macrophage recruitment. *Oncotarget* **7,** 49349–49367 (2014).

43. Lesokhin, A. M. *et al.* Monocytic CCR2 + myeloid-derived suppressor cells promote immune escape by limiting activated CD8 T-cell infiltration into the tumor microenvironment. *Cancer Res.* **72,** 876–886 (2012).

44. Sawanobori, Y. & Ueha, S. Chemokine-mediated rapid turnover of myeloid-derived suppressor cells in tumor-bearing mice. *Blood* **111,** 5457–5466 (2008).

45. Molon, B. *et al.* Chemokine nitration prevents intratumoral infiltration of antigen-specific T cells. *J. Exp. Med.* **208,** 1949–1962 (2011).

46. Molon, B., Viola, A. & Bronte, V. Smoothing T cell roads to the tumor: Chemokine post-translational regulation. *Oncoimmunology* **1,** 390–392 (2012).

47. Nakamura, Y., Mochida, A., Choyke, P. L. & Kobayashi, H. Nanodrug Delivery: Is the Enhanced Permeability and Retention Effect Sufficient for Curing Cancer? *Bioconjug. Chem.* **27,** 2225–2238 (2016).

48. Kai, M. P. *et al.* Tumor Presence Induces Global Immune Changes and Enhances Nanoparticle Clearance. *ACS Nano* **10,** 861–870 (2016).

49. Gabrilovich, D. I., Ostrand-Rosenberg, S. & Bronte, V. Coordinated regulation of myeloid cells by tumours. *Nat. Rev. Immunol.* **12,** 253–268 (2012).

50. Bronte, V. & Pittet, M. J. The spleen in local and systemic regulation of immunity. *Immunity* **39,** 806–818 (2013).

51. Szabo, F. K. & Hoffman, G. E. Cell transcytosing poly-arginine coated magnetic nanovector for safe and effective siRNA delivery. *Biomaterials* **32,** 5717–5725 (2011).

52. Drummond, C. J. & Fong, C. Surfactant self-assembly objects as novel drug delivery vehicles. *Curr. Opin. Colloid Interface Sci.* **4,** 449–456 (1999).

53. Clogston, J. & Caffrey, M. Controlling release from the lipidic cubic phase. Amino acids, peptides, proteins and nucleic acids. *J. Control. Release* **107,** 97–111 (2005).

54. Chang, D. P., Jankunec, M., Barauskas, J., Tiberg, F. & Nylander, T. Adsorption of Lipid Liquid Crystalline Nanoparticles: Effects of Particle Composition, Internal Structure, and Phase Behavior. *Langmuir* **28,** 10688–10696 (2012).

55. Barauskas, J., Johnsson, M., Joabsson, F. & Tiberg, F. Cubic Phase Nanoparticles (Cubosome): Principles for Controlling Size, Structure, and Stability. *Langmuir* **21,** 2569–2577 (2005).

56. Phan, S., Fong, W. K., Kirby, N., Hanley, T. & Boyd, B. J. Evaluating the link between self-assembled mesophase structure and drug release. *Int. J. Pharm.* **421,** 176–182 (2011).

57. Yang, Y., Wolfram, J., Fang, X., Shen, H. & Ferrari, M. Polyarginine Induces an Antitumor Immune Response through Binding to Toll-Like Receptor 4. *Small* **10,** 1250–1254 (2014).

58. He, W. *et al.* Re-polarizing Myeloid-derived Suppressor Cells (MDSCs) with Cationic Polymers for Cancer Immunotherapy. *Sci. Rep.* **6,** 24506 (2016).

59. Liu, M. *et al.* Injectable hydrogels for cartilage and bone tissue engineering. *Bone Res.* **5,** 17014 (2017).

60. Vilela, C. A. *et al.* Cartilage Repair Using Hydrogels: A Critical Review of in Vivo Experimental Designs. *ACS Biomater. Sci. Eng.* **1,** 726–739 (2015).

61. Kwee, B. J. & Mooney, D. J. Biomaterials for Skeletal Muscle Tissue Engineering. *Curr. Opin. Biotechnol.* **47,** 16–22 (2017).

62. Ostrovidov, S. *et al.* Skeletal Muscle Tissue Engineering: Methods to Form Skeletal Myotubes and Their Applications. *Tissue Eng. Part B Rev.* **20,** 403–436 (2014).

63. Tedesco, F. S., Dellavalle, A., Diaz-manera, J., Messina, G. & Cossu, G. Repairing skeletal muscle : regenerative potential of skeletal muscle stem cells. *J. Clin.*

Invest. **120,** 11–19 (2010).

64. Wang, Y. X. & Rudnicki, M. A. Satellite cells, the engines of muscle repair. *Nat. Rev. Mol. Cell Biol.* **13,** 127–133 (2011).

65. Almada, A. E. & Wagers, A. J. Molecular circuitry of stem cell fate in skeletal muscle regeneration, ageing and disease. *Nat. Rev. Mol. Cell Biol.* **17,** 267–279 (2016).

66. Hanson, E. T., Lewis, R. L., Auerbach, R., Thomson, J. A. & Applica-, B. Third-Generation Biomedical Materials. *Science* **295,** 1014–1017 (2002).

67. Balakrishnan, B. & Banerjee, R. Biopolymer-based hydrogels for cartilage tissue engineering. *Chem. Rev.* **111,** 4453–4474 (2011).

68. Pittenger, M. F. Multilineage Potential of Adult Human Mesenchymal Stem Cells. *Science* **284,** 143–147 (1999).

69. Wei, X. *et al.* Mesenchymal stem cells: a new trend for cell therapy. *Acta Pharmacol. Sin.* **34,** 747–754 (2013).

70. Jin, R. & Dijkstra, P. J. Hydrogels for Tissue Engineering Applications. *Biomed. Appl. Hydrogels Handb.* **c,** 203–225 (2010).

71. Caliari, S. R. & Burdick, J. A. A practical guide to hydrogels for cell culture. *Nat. Methods* **13,** 405–414 (2016).

72. Li, J. & Mooney, D. J. Designing hydrogels for controlled drug delivery. *Nat. Rev. Mater.* **1,** 16071 (2016).

73. Ye, K. Y. & Black, L. D. Strategies for tissue engineering cardiac constructs to affect functional repair following myocardial infarction. *J. Cardiovasc. Transl. Res.* **4,** 575–591 (2011).

74. Brown, A. C. & Barker, T. H. Fibrin-based biomaterials: Modulation of macroscopic properties through rational design at the molecular level. *Acta Biomater.* **10,** 1502–1514 (2014).

75. Rault, I., Frei, V., Herbage, D., Abdul-Malak, N. & Huc, A. Evaluation of different chemical methods for cross-linking collagen gel, films and sponges. *J. Mater. Sci. Mater. Med.* 215–221 (1996).

76. Chevallay, B., Abdul-Malak, N. & Herbage, D. Mouse fibroblasts in long-term culture within collagen three-dimensional scaffolds: Influence of crosslinking with diphenylphosphorylazide on matrix reorganization, growth, and biosynthetic and proteolytic activities. *J. Biomed. Mater. Res.* **49,** 448–459 (1999).

77. Kon, E., Filardo, G., Roffi, A., Andriolo, L. & Marcacci, M. New trends for knee cartilage regeneration: From cell-free scaffolds to mesenchymal stem cells. *Curr. Rev. Musculoskelet. Med.* **5,** 236–243 (2012).

78. Jaklenec, A., Stamp, A., Deweerd, E., Sherwin, A. & Langer, R. Progress in the

Tissue Engineering and Stem Cell Industry 'Are we there yet?' *Tissue Eng. Part B Rev.* **18,** 155–166 (2012).

79. Kang, D. G., Hsu, W. K. & Lehman, R. A. Complications Associated With Bone Morphogenetic Protein in the Lumbar Spine. *Orthopedics* **40,** e229–e237 (2017).

80. Epstein, N. Complications due to the use of BMP/INFUSE in spine surgery: The evidence continues to mount. *Surg. Neurol. Int.* **4,** 343 (2013).

81. DeVine, J., Dettori, J., France, J., Brodt, E. & McGuire, R. The use of rhBMP in spine surgery: is there a cancer risk? *Evid. Based. Spine. Care. J.* **3,** 35–41 (2012).

82. Bonadio, J., Smiley, E., Patil, P. & Goldstein, S. Localized, direct plasmid gene delivery in vivo: prolonged therapy results in reproducible tissue regeneration. *Nat. Med.* **5,** 753–759 (1999).

83. Im, G. I., Kim, H. J. & Lee, J. H. Chondrogenesis of adipose stem cells in a porous PLGA scaffold impregnated with plasmid DNA containing SOX trio (SOX-5,-6 and -9) genes. *Biomaterials* **32,** 4385–4392 (2011).

84. Umebayashi, M., Sumita, Y., Kawai, Y., Watanabe, S. & Asahina, I. Gene-Activated Matrix Comprised of Atelocollagen and Plasmid DNA Encoding BMP4 or Runx2 Promotes Rat Cranial Bone Augmentation. *Biores. Open Access* **4,** 164–174 (2015).

85. Raisin, S., Belamie, E. & Morille, M. Non-viral gene activated matrices for mesenchymal stem cells based tissue engineering of bone and cartilage. *Biomaterials* **104,** 223–237 (2016).

86. Lui, K. O. *et al.* Driving vascular endothelial cell fate of human multipotent Isl1 + heart progenitors with VEGF modified mRNA. *Cell Res.* **23,** 1172–1186 (2013).

87. Elangovan, S. *et al.* Chemically modified RNA activated matrices enhance bone regeneration. *J. Control. Release* **218,** 22–28 (2015).

88. Spotnitz, W. D. Fibrin sealant: Past, present, and future: A brief review. *World Journal of Surgery* **34,** 632–634 (2010).

89. Spotnitz, W. D. & Burks, S. Hemostats, sealants, and adhesives III: A new update as well as cost and regulatory considerations for components of the surgical toolbox. *Transfusion* **52,** 2243–2255 (2012).

90. Spotnitz, W. D. & Burks, S. State-of-the-art review: Hemostats, sealants, and adhesives II: Update as well as how and when to use the components of the surgical toolbox. *Clin. Appl. Thromb. Hemost.* **16,** 497–514 (2010).

91. Yanke, A. B. & Chubinskaya, S. The state of cartilage regeneration: current and future technologies. *Curr. Rev. Musculoskelet. Med.* **8,** 1–8 (2015).

92. Raut, S. D., Lei, P., Padmashali, R. M. & Andreadis, S. T. Fibrin-mediated lentivirus gene transfer: Implications for lentivirus microarrays. *J. Control. Release* **144,** 213–220 (2010).

93. Padmashali, R. M. & Andreadis, S. T. Engineering fibrinogen-binding VSV-G envelope for spatially- and cell-controlled lentivirus delivery through fibrin hydrogels. *Biomaterials* **32,** 3330–3339 (2011).

94. Lei, P., Padmashali, R. M. & Andreadis, S. T. Cell-controlled and spatially arrayed gene delivery from fibrin hydrogels. *Biomaterials* **30,** 3790–3799 (2009).

95. Zhang, H., Lee, M. Y., Hogg, M. G., Dordick, J. S. & Sharfstein, S. T. High-throughput transfection of interfering RNA into a 3D cell-culture chip. *Small* **8,** 2091–2098 (2012).

96. Warren, L. *et al.* Highly efficient reprogramming to pluripotency and directed differentiation of human cells with synthetic modified mRNA. *Cell Stem Cell* **7,** 618–630 (2010).

97. Almalki, S. G. & Agrawal, D. K. Effects of matrix metalloproteinases on the fate of mesenchymal stem cells. *Stem Cell Res. Ther.* 1–12 (2016).

98. Ahmann, K. A. *et al.* Fibrin Degradation Enhances Vascular Smooth Muscle Cell Proliferation and Matrix Deposition in Fibrin-Based Tissue Constructs Fabricated In Vitro. *Tissue Eng. Part A* **16,** (2010).

99. Page-McCaw, A., Ewald, A. J. & Werb, Z. Matrix metalloproteinases and the regulation of tissue remodelling. *Nat Rev Mol Cell Biol.* **8,** 221–233 (2007).

100. Oh, J. *et al.* Mutations in two matrix metalloproteinase genes , MMP-2 and MT1-MMP , are synthetic lethal in mice. *Oncogene* **23,** 5041–5048 (2004).

101. Khetan, S. *et al.* Degradation-mediated cellular traction directs stem cell fate in covalently crosslinked three-dimensional hydrogels. *Nat. Mater.* **12,** 458–465 (2013).

102. Chaudhuri, O. *et al.* Hydrogels with tunable stress relaxation regulate stem cell fate and activity. *Nat. Mater.* **15,** 326–334 (2015).

103. Cosgrove, B. D. *et al.* N-cadherin adhesive interactions modulate matrix mechanosensing and fate commitment of mesenchymal stem cells. *Nat. Mater.* **15,** 1297–1306 (2016).

104. Branco da Cunha, C. *et al.* Influence of the stiffness of three-dimensional alginate/collagen-I interpenetrating networks on fibroblast biology. *Biomaterials* **35,** 8927–8936 (2014).

Introduction

USC
UNIVERSIDADE
DE SANTIAGO
DE COMPOSTELA

INTRODUCTION

This PhD thesis has been focused on the development of biomaterial-based RNA delivery systems for cell reprogramming. We investigated two main biomaterial-based approaches consisting of 1) a nanocapsular platform with a polyarginine shell and aqueous inner cores for the co-delivery of RNAi and chemokines; and 2) two distinct Gene Activated Matrices (GAMs) based on fibrin hydrogels and collagen-I-alginate interpenetrating polymer networks (IPNs) for the co-delivery of mRNA and Mesenchymal Stem Cells (MSCs). In line with the versatility of RNA-based therapies, we assayed our delivery strategies in two different contexts, namely cancer immunotherapy and tissue engineering. Accordingly, this introduction has been structured in three sections: a first section providing a general overview of cell reprogramming strategies, a second section related to the modulation of Myeloid Derived Suppressor Cells (MDSCs) in cancer immunotherapy, and a last section covering the modulation of MSCs phenotype in tissue regeneration.

With the recent FDA approval of Kymriah® (Novartis) and Yescarta® (Kite Pharma), two CAR T-cell cancer immunotherapies, and the successful engraftment of transgenic stem cells in a patient affected by an incurable genetic skin disease[1], there is no doubt that cell-based gene therapies will be the next revolution in the biomedical field. We are excited to have been able to conduct our research in such a promising topic and hope our work has generated some knowledge that can help the development of better cell-based technologies.

SECTION 1. MODULATION OF TRANSCRIPTION FACTOR EXPRESSION FOR CELL REPROGRAMMING

1.1 RNA-based therapeutics

Cell fate specification is a complex process involving intricate molecular networks. Both mechanical and chemical cues act together in driving these molecular cascades and their dysregulation results in a broad range of developmental problems and diseases[2]. The ultimate effect of these cascades is an alteration of the transcription and translation of certain genes with the consequent change in protein expression. Among the gene expression regulators, microRNAs (miRNAs or miRs) have gained great attention. miRNAs are a class of non-coding RNA molecules that play a central role in cell homeostasis by binding to complementary target mRNAs, a result of which is the mRNA translational inhibition or degradation[3]. Since the discovery of the first miRNA in *Caenorhabditis elegans* in 1993[4], followed by the discovery of the first mammalian

miRNA, let-7, in 2000[5], extensive investigations have revealed the existence of many miRNAs and other non-coding RNAs. Apart from their role as developmental regulators, more and more miRNAs are found to be dysregulated in numerous diseases ranging from cancer to hepatitis, due to genomic events or biogenesis defects[6]. For this reason, miRNAs are interesting candidates as both, therapeutics (known as miRNA mimics) or targets for therapeutics (known as antimiRs).

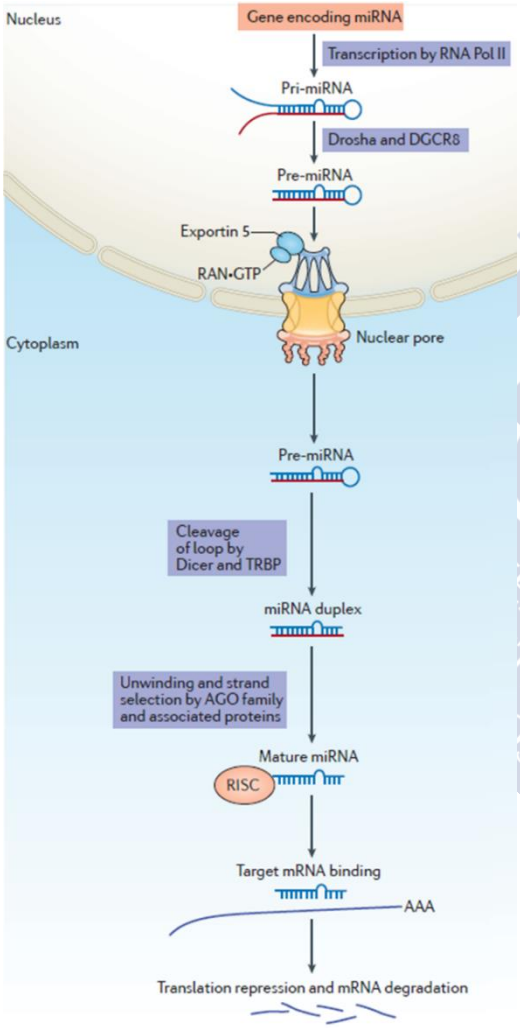

Figure 1. miRNA biogenesis. RNA polymerase II (Pol II) produces the transcription of long primary transcripts that are subsequently cleaved enzymatically to produce mature miRNAs. Drosha, a type III RNase, along with the cofactor protein DGCR8, binds to the primary miRNA (pri-miRNA) transcript and mediate the cleavage of the 3‘ and 5‘ strands of pri-miRNAs to generate pre-miRNA. Next, the exportin 5–RAN•GTP complex mediates the movement of pre-miRNAs from the nucleus into the cytosol. There, the RNase III Dicer and TAR RNA binding protein (TRBP) bind to the pre-miRNAs and cleave the terminal loop, resulting in a miRNA duplex. This miRNA duplex is incorporated into the RNA-induced silencing complex (RISC) where mature miRNA is formed after the unwinding and strand selection mediated by the argonaute (AGO) family of proteins in conjunction with several cofactors such as PACT. Binding of the mature miRNA to RISC leads to the targeting of mRNAs with complementary sites and results in translational repression or mRNA degradation. Adapted from [7] with permission.

Messenger RNA, target of miRNA action, is a large family of RNA molecules that convey the genetic information stored in DNA acting as the template for ribosome protein expression. Since its discovery in 1961[8], a huge body of research has culminated in the conception of mRNA as a drug encoding molecule two decades ago, when Wolff et al. demonstrated that direct injection of in vitro transcribed (IVT) mRNA into the skeletal muscle of mice led to the expression of the encoded protein[9]. However, IVT mRNA was relegated by pDNA and viral DNA, more stable molecules, and it was not until the 1990s

when its preclinical exploration was initiated for diverse applications, including protein substitution and vaccination[10]. Indeed, by now mRNA has proved to be a really efficient tool to boost forced gene expression, inducing both a higher and faster protein synthesis than pDNA[11–14].

There are several conceptual differences between RNA- and DNA-based therapies. RNA exerts its activity in the cytoplasm where miRNA regulates the expression of native mRNAs and IVT mRNA is rapidly translated. By contrast, DNA needs to enter the nucleus to be transcribed into RNA, and it has been proposed that the rate of nuclear entry, and consequently DNA functionality, depends on nuclear envelope breakdown during cell division. In addition, RNA does not integrate into the genome avoiding the risk of insertional mutagenesis that DNA may have. Finally, many pharmaceutical applications take advantage of the transient alteration of protein expression obtained with RNA and its complete metabolic degradation[15,16].

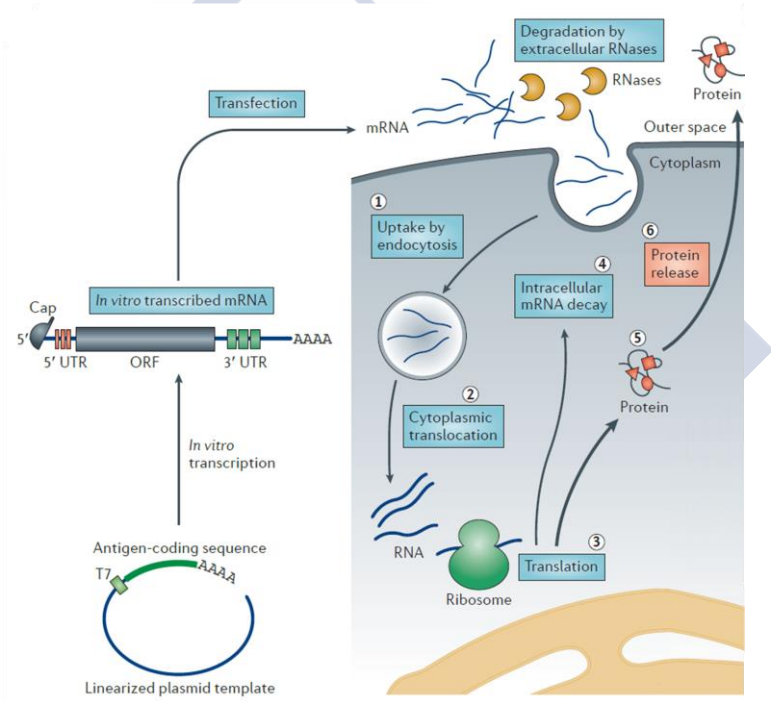

Figure 2. Principles of mRNA-based therapeutics. A linearized DNA plasmid template with the coding sequence is used for *in vitro* transcription. The *in vitro* transcribed mRNA contains the cap, 5'and 3' untranslated regions (UTRs), the open reading frame (ORF) and the poly(A) tail, which determine the translational activity and stability of the mRNA molecule. **Mechanism of protein expression** Step 1: a fraction of exogenous mRNA escapes degradation by ubiquitous RNases and is spontaneously endocytosed by cell-specific mechanisms and enters endosomal pathways. Step 2: release mechanisms of mRNA into the cytoplasm are not fully understood. Step 3: translation of mRNA uses the protein synthesis machinery of host cells. Binding of the mRNA to ribosomes, the eukaryotic initiation factors eIF4E and eIF4G, and poly(A)-binding protein, results in the formation of circular structures and active translation. Step 4: termination of translation by degradation of mRNAs is catalyzed by exonucleases. Step 5: the translated protein product undergoes post-translational modification. Then, the protein can act in the cell in which it has been generated. Step 6: alternatively, the protein product is secreted and may act via autocrine, paracrine or endocrine mechanisms. Adapted from [16] with permission.

In terms of structural features, both miRNA and mRNA are polymeric macromolecules with deoxyribonucleotides as monomer units. miRNA is synthesized as a stem-looped precursor that is enzymatically processed by two ribonucleases-III (RNAses III) yielding single stranded RNA molecules of 21-25 nucleotides (≈0.023 kb)[17,18]. mRNAs are also single stranded molecules but they have an average length of 2.2 kb. Whereas miRNAs are usually obtained by chemical synthesis, mRNAs are commonly synthesized by cell-free In Vitro Transcription (IVT) reactions templated with linearized plasmids or PCR products and performed by T7 or SP6 RNA polymerases in the presence of nucleotides. Contrary to miRNAs, which do not encode specific proteins, mRNAs possess an open reading frame (ORF) encoding the protein of interest, marked by start and stop codons and flanked by untranslated regions (UTRs). Besides, mRNAs contain a 5' cap and a 3' poly(A) tail to maximize their stability. The DNA template can include all the structural elements of the mRNA except for the 5' cap, that is enzymatically synthesized or added as a synthetic cap analogue. Poly(A) tails can either be encoded by the DNA template or enzymatically synthesized after the elongation step[19–25].

1.2 RNAi therapeutics for the modulation of transcription factor expression

The majority of miRNA and mRNA-based therapies are oriented to the treatment of cancer diseases. In the case of miRNA, these therapies are intended to replenish the low levels of oncosuppressor miRNAs with miRNA mimics or to antagonize the function of upregulated oncogenic miRNAs with antimiRs. Among the miRNA mimics, miR-34 is one of the most important families of miRNAs, whereas miR-155 stands out among the most studied anti-miRs. Both types of therapies have candidates undergoing clinical trials. A miR-34 mimics from Mirna Therapeutics has already completed phase I for multiple solid tumors while an anti-miR-155 developed by miRage Therapeutics is in phase I for cutaneous T cell lymphomas and mycosis fungoides (ClinicalTrials.gov identifiers NCT01829971 and NCT02580552, respectively)[7]. Regarding mRNA-based therapies, they have been mostly oriented to cancer immunotherapy and, more specifically, to cancer vaccination. In 1996, it was demonstrated that dendritic cells (DCs) exposed to mRNA encoding tumor antigens or total mRNA extracted from tumor cells, could elicit specific T cell responses and inhibit tumor growth after subcutaneous injection in tumor bearing mice[10]. This success prompted the development and clinical translation of the mRNA-transfected DCs approach and since then the *ex vivo* and *in vivo* transfection of DCs with IVT mRNA has been further optimized. Indeed, several companies such as Curevac or BioNTech have completed successful clinical trials in a broad spectrum of cancers including prostate, non-small-cell lung cancer and melanoma. Currently, more ambitious approaches are being tested for the development of personalized vaccines in patients with melanoma (ClinicalTrials.gov identifier: NCT02035956), where tumor specimens from each patient are subjected to next-generation sequencing to identify individual immunogenic mutations suitable for vaccine design[16].

A very exciting but maybe less explored application of RNA-based therapies is their use for the modulation of non-tumoral cell phenotype. As indicated before, the role of miRNAs in the modulation of cell plasticity comes from their finely tuned control over gene expression. Among all the proteins that are subject of miRNA regulation, transcription factors (TFs) are especially relevant, since they naturally regulate cell differentiation[26]. TFs control the transcription rate of genetic information from DNA to messenger RNA by binding to specific DNA sequences through DNA-binding domains. While miRNA regulates gene expression at a posttranscriptional level, TFs operate at the transcriptional level and it is now clear that both molecules cooperate to tune gene expression. In fact, TFs also regulate miRNA expression and they can form feedback or feed-forward loops, which play critical roles in various biological processes[27–31]. An example of this cooperative regulation is found between two RNA molecules studied in the context of this thesis: miR-142-3p and TF C/EBPβ, which form a feedback loop activated by tumor-released IL-6 family cytokines during tumor-induced myelopoiesis. This tumor-induced myelopoiesis results in the generation of myeloid derived suppressor cells (MDSCs), a $CD11b^{+}Gr\text{-}1^{+}$ population accumulated in the spleen and tumor mass of tumor-bearing hosts that facilitates tumor progression. For this reason, the modulation of C/EBPβ levels appear as a good pharmacological strategy to control the suppressive microenvironment and boost the effect of cancer immunotherapies[32,33].

Indeed, in this work we have studied two strategies to downregulate C/EBPβ levels: the use of miR 142-3p as a miRNA mimics and the use of a shRNA against C/EBPβ. Both molecules have been encapsulated in nanovehicles comprising other immunomodulatory components, as it will be briefly described later on in this introduction and expounded on in Chapter 1.

1.3 mRNA therapeutics for transcription factor enforced expression

Together with RNAi-based approaches to downregulate transcription factor (TF) levels, another strategy to modulate cell differentiation is TF forced expression. Likewise, TFs have been used either to direct cell reprogramming or to promote cell transdifferentiation[34,35]. Cell reprograming consist on the conversion of somatic cells in pluripotent stem cells that can be further differentiated into several cell phenotypes. Cell transdifferentiation is the process of converting from one cell type to another without going through a pluripotent state. Different single TFs or cocktails of TFs have been identified to direct the differentiation towards specific tissue types[36–39]. In 1987, Davis et al. demonstrated that mouse fibroblasts could be converted into myoblasts by the use of a single cDNA encoding the transcription factor MyoD[40]. Nineteen years later, Takahashi and Yamanaka discovered a set of TFs that could reprogram somatic cells to pluripotency[41]. These two breakthroughs flourished in a scientific context fertilized by

the ideas of somatic cell cloning and transdetermination developed over the past five decades, and constructed the dynamic understanding of cell plasticity that we have today[42].

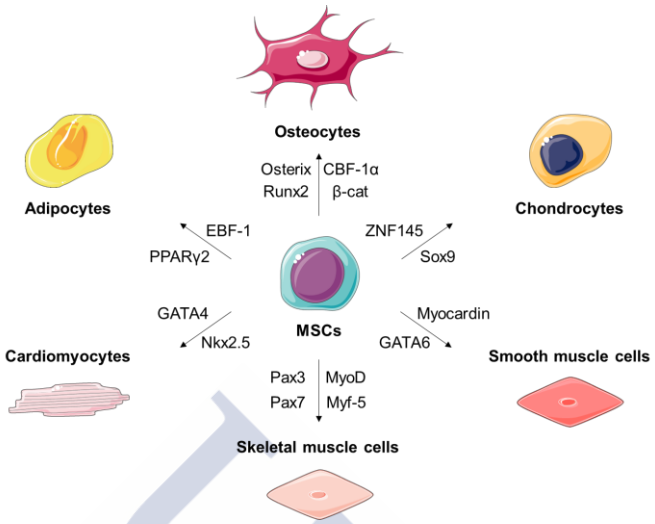

Figure 3. Mesenchymal stem cell (MSC) differentiation through transcription factor (TF) forced expression. Adapted from [38] with permission.

1.4 Mechanical regulation of transcription factor expression

Whereas most studies on transcriptional regulation have focused on genetic or chemical control mechanisms of transcription, recent work suggests that mechanical forces are equally important regulators of transcriptional control[2]. In fact, over the past few years, mechanostransduction has regained great attention as a means to regulate cell fate conversion. Differentiation of mesenchymal stem cells (MSCs) towards specific lineages has proved to be modulated by matrix stiffness and elasticity[43–45]. It is now well stablished that substrates of high stiffness enhance osteogenesis while softer substrates lead to adipogenic and neurogenic marker expression[46]. Besides, for the same optimal stiffness, an increased deposition of osteogenic matrix, was obtained for substrates with higher stress-relaxation[47]. Finally, an interplay between cell-matrix and cell-cell contacts has been recently shown to further impact different stages of osteogenesis in human MSCs (hMSCs)[48].

In line with these studies, in this work we have explored the use of transcription factors MyoD, master regulator of myogenesis[40], and SOX9, master regulator of chondrogenesis[49,50], in the differentiation of hMSCs for tissue engineering applications. We have used mRNA-encoded TFs to test whether mRNA expression kinetics could better mimic the physiological transcription factor expression and maximize the differentiation outcome as compared to DNA-encoded TFs. In addition, we have explored this strategy in a 3D context, developing a Gene Activated Matrix (GAM) in which both mRNA

enconding TFs and hMSCs can be included, aiming to create an easily injectable platform that would gel in situ in the place of injury. Being aware of the impact of the microenvironment on cell phenotype, our research also sought to explore the influence of GAM mechanical properties on the differentiation outcome after TF transfection in 3D contexts. Therefore, we aimed to maximize cell differentiation processes by identifying the right mechanical environments where to induce specific transcriptional programs by forced TF expression. However, owing to the growing interest on studying drug efficacy in 3D culture systems, and given the crucial role of 3D transfection for GAM activity, we further explored the influence of GAM mechanical properties on nanoparticle transfection efficiency. Chapters 2 and 3 will gather the information regarding this part of the experimental work.

SECTION 2. MODULATION OF MYELOID DERIVED SUPPRESSOR CELLS (MDSCS) IN CANCER IMMUNOTHERAPY

Given the increase in allergies and autoimmune diseases, the immune system is now clearly considered to be key in the maintenance of a correct tissue homeostasis. This conception has led to a growing understanding of disease-related inflammation and prompted the development of an exciting new kind of pharmacological approaches aiming to modulate pathological immune responses. One of the diseases with more intensive research in this area is, definitely, cancer, and many immunotherapies have been recently approved for different types of cancer.

Contrary to allergies or autoimmune diseases, where an aberrant exacerbated immune response is the cause of the disease, cancer has the particularity to show both the Yin and Yang of the immune system, with immune cells acting both to kill tumor cells and foster tumor progression. This dual role is even found in the same cell subsets, such as tumor-associated macrophages (TAMs) or tumor-associated neutrophils (TANs), which high plasticity allows them to exert either tumor-promoting or antitumor activities. Conversely, other tumor-associated myeloid cells, called myeloid derived suppressor cells (MDSCs), have been unequivocally linked to a tumor-promoting activity.

2.1 Myeloid derived suppressor cells (MDSCs)

Myelopoiesis is a structured process that takes place in the bone marrow where common precursors acquire specific markers and functions of circulating leucocytes, ensuring the proper turnover of these cells. Several pathological conditions can alter the steady supply of mature leucocytes resulting in emergency myelopoiesis, which provides cells to eliminate potential threats, either abnormal cellular growth, infectious agents or tissue damage. This altered myelopoiesis is normally restored after the trigger is resolved, but in some conditions associated with chronic inflammation, autoimmune diseases and cancer, this aberrant myelopoiesis is sustained resulting in the accumulation of immature myeloid cells. These cells have a pathologic activation program that is different from that of mature myeloid cells: they are poorly phagocytic and produce high levels of anti-inflammatory cytokines as well as reactive oxygen and nitrogen species. As a result, these cells are not able to perform effectively the normal functions of mature leukocytes.

Based on their myeloid origin, their immune-suppressive function and their systemic expansion in cancer-related contexts, these cells have been denominated myeloid derived suppressor cells (MDSCs)[51]. Murine MDSCs constitute a heterogeneous population of cells bearing the markers CD11b and Gr-1 (Ly6C and/or Ly6G). MDSCs include two major subsets based on their phenotypic and morphological features but

also on their unique functional and biochemical characteristics: polymorphonuclear (PMN) and monocytic (M)-MDSCs. In tumor-bearing mice, MO-MDSCs ($Gr1^{lo/int}CD11b^{+}Ly6C^{hi}Ly6G^{-}$) are highly immunosuppressive and exert their effects largely in an antigen-nonspecific manner, whereas PMN-MDSCs ($Gr1^{hi}CD11b^{+}$ $Ly6C^{lo}Ly6G^{+}$) are moderately immunosuppressive and promote T cell tolerance via antigen-specific mechanisms. Although MDSCs are implicated in the suppression of different cells of the immune system, such as NK and B cells, inhibition of T cells is the gold standard for the evaluation of their function.

Attending to their potent immunosuppressive action it is possible that the main role of MDSC is the protection of the host from extensive tissue damage caused by uncontrolled immune responses. Yet, tumors can hijack and amplify this, *a priori* beneficial, activity to protect themselves from elimination by the immune system. One of the mechanisms to exert this immune evasion is through the release of tumor-derived factors (TDFs), which induce tumor-infiltrating MO-MDSC differentiation into immunosuppressive TAMs[52]. However, MDSCs ability to promote tumor growth not only depend on the induction of tumor tolerance but also on their support of angiogenesis, cancer stemness and metastasis dissemination. For this reason, MDSC targeting represents a promising approach to increase the efficacy of cancer immunotherapies, especially in the case of adoptive cell transfer (ACT)[53].

2.2 Therapeutic strategies to modulate MDSCs activity

Several molecular and biochemical hallmarks are associated with MDSCs and could be used as pharmacological targets to modulate their function. Indeed, MDSCs are characterized by the aberrant expression of specific transcription factors and apoptosis regulators, a particular signature of pro- and anti-inflammatory cytokines or chemoattractants affecting MDSCs trafficking and their receptors, as well as enzymes and metabolic by-products contributing to their immune-regulatory behavior. Therapeutic strategies targeting MDSCs include: inducing MDSC depletion, affecting their development, inhibiting their immune suppressive activity and promoting their differentiation into mature myeloid cells[53].

2.2.1 MDSC altered development and depletion

More and more evidence points to the effects of conventional chemotherapy on the host immune system and its influence on tumor eradication by the induction of MDSC depletion. Classical chemotherapeutic agents have shown great cytotoxic action on MDSCs, such as gemcitabine[54,55] or 5-fluorouracil[56], sometimes accompanied by an enforced MDSC differentiation towards non-immune-suppressive cell phenotypes (paclitaxel and docetaxel[57,58]). For this reason, low dose chemotherapy is currently being tested in several clinical trials either alone or in combination with other

immunomodulatory drugs or ACT to increase the efficacy of cancer vaccination (i. e. NCT00801801, NCT00670748, NCT00560963).

Although drugs targeting MDSC development are very diverse in nature, they are all able to reduce MDSC accumulation in tumor microenvironment as well as in blood and secondary lymphoid organs of tumor-bearing mice. Candidates in this category range from amino-bisphosphonates (zoledronic acid[59]), antibodies blocking S100A8/A9 proteins (mAbGB3.1[60]) and CSF1R kinase inhibitors (GW2580, PLX3397, IMC-CS4, RG71555[61–63]) to inhibitors of the H^+/Na^+ and Na^+/Ca^{2+} channels (dimethyl amiloride[64]), histamine receptors antagonists (cimetidine[65]), IL-1 receptor antagonists (anakinra[66]) and antiangiogenic therapies (sunitinib, bevacizumab[67,68]).

2.2.2 Inhibition o MDSCs immune suppressive activity

The reversion of MDSC immune suppression has been addressed with several compounds including selective inhibitors of the JAK2/STAT3 pathway, like cucurbitacin B[69], or phosphodiesterase-5 (PDE-5) inhibitors such as sildenafil and tadalafil[70,71], which have been evaluated in different clinical trials (NCT01374217, NCT008436359, NCT00894413). In addition, given the key role of NO in MDSC-mediated immune suppression, several NOS-inhibiting compounds are under investigation. Nitroaspirin has proved to be effective enhancing the antitumor immunity elicited by cancer vaccination[72] whereas [3-(aminocarbonyl)furoxan-4-yl] methylsalicylate (AT38) is able to decrease MDSC inhibitory activity by reducing CCL2 nitration, as we will explain later. Methyl ester of 2-cyano-3,12-dioxooleana-1,9(11)-dien-28-oic acid (CDDO-Me; bardoxolone methyl) has also been tested to promote the up-regulation of several antioxidant genes reducing intracellular ROS[73] and COX2-inhibitors such as celecoxib have demonstrated activity in reducing prostaglandin E2-mediated ARG1 up-regulation in MDSCs[74].

2.2.3 Reversion of MDSCs phenotype

Finally, drugs promoting MDSC differentiation towards non-suppressive cells have also been investigated. A particular successful example is all-trans retinoic acid (ATRA), which has increased the efficacy of cancer vaccination in conjunction with chemotherapy in a phase II clinical trial in SCLC patients (NCT00618891)[75]. Similar to ATRA, $1,25(OH)_2D_3$ vitamin has also shown benefits in reducing intratumoral $CD34^+$ cells and promoting the maturation of DCs in HNSCC patients[76]. Besides, several RNAi based therapies are currently being explored for MDSC differentiation, especially those targeting the C/EBPβ pathway, as it will be described below. However, as compared to previous compounds, the clinical investigation of these promising drug candidates has been somehow limited by their inherent physicochemical properties that hamper their capability to cross biological barriers and in turn bring the necessity of drug delivery carriers.

2.3 C/EBPβ as a pharmacological target for MDSCs

C/EBP transcription factors are involved in the regulation of granulopoiesis. They share conserved C-terminal regions but they differ in their N-terminal regions that contain transcriptional activation domains. C/EBPα is considered the 'master regulator' of steady-state granulopoiesis where C/EBPε is required for the terminal differentiation and maturation of granulocytes. Whereas C/EBPβ does not seem to be implicated in steady-state granulopoiesis, it controls emergency granulopoiesis induced by cytokines and infections[77]. Given the importance of emergency granulopoiesis in cancer, Marigo et al. generated a hematopoietic lineage-restricted C/EBPβ ablated animal model with the aim to study the role of C/EBPβ in tumor-induced tolerance[32]. They carried out adoptive cell therapy (ACT) experiments in the ablated mice bearing a subcutaneous MCA203 fibrosarcoma by transferring polyclonal cytotoxic T lymphocytes (CTLs) recognizing the mouse telomerase, and demonstrated that absence of C/EBPβ could revert tumor-induced tolerance and provide therapeutic benefit. Indeed, they found that whereas CTLs transfer did not impact tumor progression in partially C/EBPβ ablated (Cebpbflox/+) mice, significant prolongation of survival and complete cure was achieved in more than 60% of C/EBPβ ablated (Cebpbflox/flox) mice in the absence of any prior myeloid and lymphoid ablation by ϒ-irradiation. Overall, their results positioned C/EBPβ as a prominent regulator of the tolerogenic and immunesuppressive environment induced by cancer and set the basis for C/EBPβ targeting in MDSCs.

As we commented before, TFs can cooperate with miRNAs to tune gene expression and both molecules can form feedback or feed-forward loops critical for the regulation of various biological processes. C/EBPβ forms a feedback loop with miR-142-3p activated by tumor-released IL-6 family cytokines during tumor-induced myelopoiesis. There have been described three isoforms of C/EBPβ with different molecular weights: liver-inhibitory protein (LIP), liver-activating protein (LAP), and full-length liver-activating protein (LAP*)[78]. Cytokine binding to IL-6 subunit alters the ratio of these C/EBPβ isoforms, augmenting LAP* and driving macrophage differentiation towards immunosuppressive phenotypes. LAP*, for its part, acts as an inhibitory regulator of miR activity, resulting in IL6 signal transducer (IL6st) upregulation, thus sustaining its downstream pathway. miR-142-3p represses LAP* expression by non-canonical binding to its 5' mRNA coding sequence, so its downregulation increases LAP* expression, closing the loop and further promoting myeloid cell differentiation towards immune-suppressive macrophages[79].

2.4 CCL2 as a targeting molecule for the MDSC monocytic-macrophagic subset

Innate and adaptive immune responses can affect tumor progression with a favorable or detrimental effect depending on the nature of the immune infiltrate. Chemokines,

chemotactic cytokines, can alter the composition and activation state of this immune infiltrate as well as modify the stroma composition. For this reason, an increasing body of research is focusing on the use of these molecules to modulate the tumor microenvironment and enhance the immune rejection of cancer[80]. However, chemokine actions in the tumor microenvironment are very complex as they can either recruit immune cells able to orchestrate the antitumor immune response or sustain tumor survival, progression and metastasis. This contradictory effect among the different chemokines is further complicated by tumor-induced post-translational modifications, which can turn an immune-stimulant chemokine into an immune-suppressive one, adding another layer of regulation[81].

Within the chemokine repertoire, chemokine CCL2 is especially relevant since it is found in the majority of solid cancers. CCL2 tailors macrophage differentiation towards the protumorigenic M2-phenotype and CCL2-CCR2 axis is also implicated in the migration of myeloid cells to the tumor[82,83]. This CCL2-driven MDSCs mobilization depends on MDSCs subsets, as CCR2 deficiency causes a significant loss of monocytic $CD11b^{+}Gr\text{-}1^{int}Ly\text{-}6C^{hi}$ MDSCs, resulting in a predominant $CD11b^{+}Gr\text{-}1^{hi}Ly\text{-}6C^{int}$ granulocytic MDSCs accumulation[84]. In melanoma tumors, CCL2-driven mobilization resulted in the accumulation of CCR2-expressing MDSCs within the tumor site, where they hampered CD8+ T cell entry, thus limiting the efficacy of cancer immunotherapy[85]. Due to this impaired T cell tumor homing, half of the patients failed to respond to ACT for melanoma even though the majority of the transferred circulating CD8+ T cells showed specific antitumor activity[86]. Indeed, the infiltration of primary tumors by memory T cells correlates with a high prognostic value for disease-free and overall survival, further highlighting the importance of developing strategies aimed at boosting proper T cell homing[87,88]. In this sense, a CCL2-related mechanism of tumor escape is being explored to create a new class of adjuvants for cancer immunotherapy. CCL2 is nitrated/nitrosylated by reactive nitrogen species (RNS) produced by the tumor, impeding its ability to attract tumor-specific CTLs but maintaining its capability to recruit myeloid cells[85,89,90]. One of the candidates among these new adjuvants is AT38 [3-(aminocarbonyl)furoxan-4-yl] methylsalicylate, a NO-donating compound that can decrease MDSC inhibitory activity by reducing CCL2 nitration.

2. 5 Nanomedicines for the targeting of MDSCs

In terms of drug delivery, nanotechnology has made great contributions to the field of oncology. For the first nano-oncologicals, based on classical chemotherapeutic agents, the nanoencapsulation of these compounds allowed the improvement of their therapeutic index due a passive tumor targeting effect. Marketed nanomedicines such as Abraxane® or Doxil®, represent, among others, specific milestones in this therapeutic approach. Currently, efforts are oriented to exploit the capability of nanotechnology to enhance the pharmaceutical properties of biomacromolecules,

specially gene therapies and mAbs with intracellular targets. In addition, the versatility of nanocarriers for the co-delivery of various drugs with different actions and physicochemical profiles, is also being widely explored with a special emphasis in cancer immunotherapy. To this end, researches usually take advantage of the inherent immunogenic properties of some nanomaterials looking for synergistic effects. Lastly, but not less important, nanotechnology is making possible the development of more sensitive methods for cancer imaging and diagnosis[91].

The field of nanotechnologies targeting MDSCs is still in its infancy. Several nanoparticles encapsulating some of the previous mentioned compounds have been developed (i.e. PLGA nanoparticles encapsulating bevacizumab[92], heparin and hyaluronic acid nanoparticles encapsulating paclitaxel and all-trans retinoic acid[93,94], galactosylated solid lipid nanoparticles loaded with cucurbitacin B[95]) but their effect on MDSCs has not been assessed.
However, although scarce, a number of drug delivery systems have been specifically designed to target this cell compartment. For example, Albeituni et al. showed how yeast-derived particulate β-glucan (WGP) oral treatment decreased tumor weight in tumor-bearing mice due to a reduced accumulation of PMN-MDSCs. In addition, WGP-treated M-MDSC differentiated into $CD11c^+$ cells with high MHC class II expression *in vivo* and induced decreased tumor burden when inoculated subcutaneously with LCC cells. More importantly, patients with non-small cell lung cancer (NSCLC) that had received WGP prior to other treatment, had a decreased frequency of $CD14^-HLA\text{-}DR^-$ $CD11b^+CD33^+$ MDSCs in the peripheral blood[96]. Another study by Tian et al., linked the effect of WGP on MDSCs to the inhibition of nuclear factor I-A (NFIA) expression, an integral component of myeloid differentiation and lineage commitment[97]. For their part, Lebel et al. demonstrated that intra-tumor administration of papaya mosaic virus nanoparticles (PapMW) significantly slowed down melanoma progression and prolonged survival in tumor-bearing mice, and that this effect was in part mediated by a reduction of MDSCs[98].

Other studies were based in semi-synthetic approaches consisting in modifying naturally occurring nanometric systems or slightly manipulating bacterial products. As an example, Fernández et al. developed very small size proteoliposomes (VSSP) by hydrophobic conjugation of the GM3 ganglioside with the outer membrane protein complex from *Neisseria meningitides* strain 385. When they administered this adjuvant to mice, they observed an increased accumulation of $Cd11b^+$ $Gr\text{-}1^+$ cells in their spleens, which were less immune-suppressive as compared to tumor-induced MDSCs. Indeed, they found that the inoculation of the VSSP adjuvant in EG.7-OVA bearing-mice was sufficient to avoid tumor-induced tolerance and stimulate an immune response against ovalbumin (OVA)[99]. Finally, Sun et al. were the first exploring the use of exosomes as drug carriers. They applied exosomes secreted from the EL-4 mouse lymphoma cell line

to load curcumin and showed a reduction in $Cd11b^{+}Gr^{+}$ cells in the lungs of mice treated with curcumin-loaded exosomes after an LPS induced-sepsis shock[100].

The effect of nanoencapsulated classical chemotherapeutic agents was also studied on the MDSC subset. Yong et al. designed a myeloperoxidase (MPO)-triggered release system in which gold nanoparticles (GNPs) loaded with paclitaxel were used to cork nitrogen-doped carbon nanotube cups (NCNCs) and subsequently promote the opening of the corked NCNCs and paclitaxel release in the presence of neutrophil-secreted MPO. They showed that NCNCs loaded with paclitaxel blocked the ability of tumor-associated MDSCs to suppress proliferation of pre-activated T cells *in vitro*[101]. In addition, Jeanbart et al. studied the effect of ultra-small polymer micelles loaded with 6-thioguanine (MC-TG) in tumor bearing mice and found a dose-dependent depletion on MO-MDSCs in the spleen, G-MDSCs in the draining lymph nodes and Gr^{1int} MO-MDSCs in the tumor. More importantly, MC-TG significantly improved the efficacy of adoptively transferred, OVA-specific $CD8^{+}$ T cells in melanoma cells expressing OVA[102]. Finally, the impact of nanoencapsulated low dose chemotherapy was evaluated by Sasso et al., who showed a reduction of MO-MDSCs in lymphoma and melanoma bearing mice treated with subcutaneous Gemcitabin-loaded lipid nanocapsules (LNCs) and an increased efficacy of adoptive T cell therapy in both animal models[103].

In relation to combinatory drug delivery systems, Kong et al. developed a lipid-coated hollow mesoporous silica nanoparticle for the co-encapsulation of ATRA, doxorubicin and interleukin-2 and observed a modulation of the tumor microenvironment with a down-regulation of immunosuppressive MDSCs in B16F10 tumor-bearing mice[104].

Finally, to our knowledge, there is just one work describing RNAi nanotherapies targeting MDSCs. In this work, Zilio et al. developed G5 PAMAM dendrimers conjugated with a CD124/IL-4Rα-targeting peptide, which has previously proved to be a successful strategy to target MDSCs[105]. They loaded these dendrimers with shRNAs targeting the STAT3 and C/EBPβ transcription factors as well as with miR 142-3p, also implicated in the modulation of the C/EBPβ pathway. They found that, compared with either gene therapies or vaccination alone, the co-administration of dendrimers loaded with shRNA against STAT3 and C/EBPβ enhanced the efficacy of vaccination against AH1, a tumor-specific gp-70-derived antigen. Besides, only the co-administration of dendrimers loaded with miR 142-3p in conjunction with adoptive cell therapy of CTLs against the tumor-associated antigen mTERT, was able to significantly delayed tumor progression if MCA203 fibrosarcoma-bearing mice[106].

2.6 Polyarginine nanocapsules as drug delivery vehicles

Nanocapsules, reservoir type delivery systems, consist of an oily core and a polymeric shell, capable both of entrapping drugs of different charges and polarities. They represent very versatile systems for the co-delivery of various active compounds, a strategy of increasing interest in drug delivery. Among others, our lab has extensively explored the use of nanocapsules for the delivery of cytotoxic drugs[107–110], antigens[111–115] or peptides[116,117]. Several polymers have been investigated to tailor the interaction of the drug delivery vehicles with the cell milieu. In particular, polyarginine has been previously investigated as a polymeric shell in order to associate polynucleotides to the nanocapsule's surface[118] and to boost the immune response towards multi-enveloped vaccines[119].

Although the oily core of nanocapsules is usually employed to entrap hydrophobic drugs, there are also formulation procedures to generate aqueous inner phases capable of entrapping hydrophilic compounds. In this regard, the use of mesophases based on glyceryl monooleate is generating increasing interest due to their suitable properties for the encapsulation and slow release of drugs of various polarities.

2.6.1 Immunomodulatory and cell-penetrating properties of polyarginine

Arginine rich polymers have been widely explored in the drug delivery field due to their properties of cell-penetrating peptides (CPPs)[120,121]. They contain positively charged moieties which aid the interaction with the negatively charged cell membranes thus helping transport molecular cargos across them. However, not only charge is promoting this transport as several studies have demonstrated that polymers of L- or D-arginine entered cells far more efficiently than polymers of equal length composed of lysine, ornithine and histidine[122,123]. Indeed, polyarginine guanidinium groups have been shown to be responsible for this enhanced cellular uptake, and their rigidity has proved to be crucial for their non-endocytic transduction[124]. In addition, various structural investigations have shown the positive role of arginine residues in cell transfection efficiency[118,125–127]. Lastly, a recent study has suggested that these guanidinium groups are not only implicated in the improved ability to cross cell membranes but are also the cause of polyarginine-mediated TLR4 activation, suggesting its potential for immunotherapy[128].

2.6.2 Glyceryl monooleate-based mesophases for peptide encapsulation

Peptide encapsulation within lipid-based carriers has proved to be challenging due to the hydrophilic character of most part of these macromolecules. However, the functionality provided by lipid materials in terms of structural and pharmacological properties, as well as their low toxicity profiles, have led to an intense investigation on their use for peptide encapsulation[115,116,129]. Moreover, many lipid materials hold a

GRAS designation together with a long history as additives for both medical enteral/parenteral nutrition and the food industry, which confers them an adequate regulatory status. Finally, there is already a vast knowledge about lipid carriers for the encapsulation of hydrophobic low molecular weight molecules that can be adapted to the increasing amount of protein/peptide therapeutics.

Solid lipid nanoparticles, microemulsions, nanoemulsions, self-emulsifying systems, liposomes and nanocapsules have been widely explored for peptide encapsulation purposes. Although the study of lipid based liquid crystalline phases has been mainly focus on their structural and thermodynamic understanding, these mesophases are raising increasing interest as drug delivery devices. This is due to their highly ordered, thermodynamically stable internal nanostructure that offers potential as a slow release matrix.

They are spontaneously assembled by adding amphiphilic lipids to water, such as glycerol monooleate (GMO) or phytantriol, which have been specially explored due to their commercial availability and their ability to form liquid crystal phases at physiological temperature. The phase structure formed depends on the type of packing derived from the molecular geometry of the main lipid component[130] but is also affected by other factors such as pH, ionic strength, temperature, pressure and the presence of additives [131–133]. Following the well established phase diagram for the GMO-water binary system, a specific phase assembly can be easily achieved by selecting the adequate lipid proportion at a certain temperature [134]. In ternary and more complex systems, different additives can be incorporated to alter the self-assembly of the lipid packing and consequently control the phase structure to create systems with the desired release profiles[135].

The most explored mesophases used as drug delivery systems are the viscous reversed bicontinuous cubic (V2) and inverse hexagonal phases (H2). However, it has been recently shown that the less studied inverse micellar cubic phase with Fd3m space group (I2) and inverse micelles (L2) could provide better release kinetics than traditional bicontinuous cubic phases[136]. Cubic phases (Q), as well as micellar (L) and hexagonal phases (H) constitute complex three-dimensional architectures in comparison with the simpler monolayer and bilayer (lamellar phase) amphipathic arrangements that surfactants can acquire in aqueous solutions[137]. Whereas lamellar and hexagonal phases are optically birefringent, cubic phases are optically isotropic, what makes cubic phase gels appear as a clear, viscous and jelly material. Surfactant molecules are organized in bilayers forming a bicontinuous water-lipid structure in which these lipid layers separate two non-intersecting water channels. In contrast to the bicontinuous cubic phase, the inverse hexagonal phase forms a hexagonal pattern composed of rod-shaped inverse micelles with closed water channels [138]. The inverse micellar cubic phase also exhibits a

closed structure consisting of tightly packed inverse micelles arranged in a double diamond network[139].

The ordered structure of these complex liquid crystal matrices minimizes the stress and free energy of the system and allows them to have a high inner surface, a property that can be exploited to solubilize and load big quantities of compounds[140]. In addition, due to the presence of both lipidic and aqueous domains, these matrices can incorporate molecules of varying size and polarity. For hydrophilic drugs, release from the matrix is controlled by diffusion through the tortuous aqueous channels, which is affected by temperature changes and lipid identity, whereas release of lipophilic drugs depends also on their partition coefficient[141].

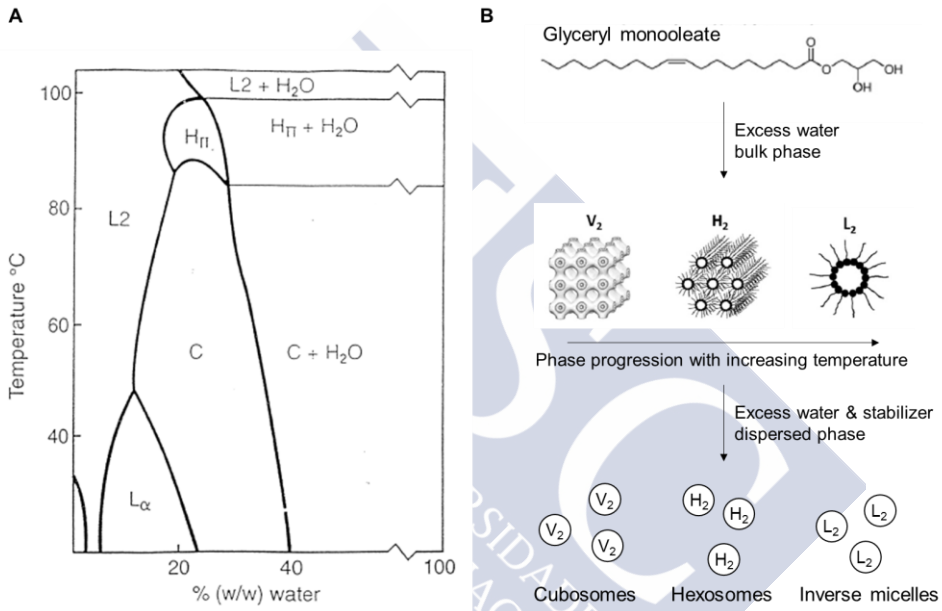

Figure 4. Composition/temperature phase diagram for the monoolein-water system and schematic view of the formulation process. (A) Phase diagram of the glyceryl monooleate–water system depicting the reversed micellar phase (L_2), lamellar phase (L_α), cubic phase (C) and reversed hexagonal phase (H_{II}). (B) Chemical structure of glycerol monooleate and the dispersed bulk phases. Adapted from [136,142,143] with permission.

Commonly employed methods for dispersing bulk crystalline phases yielding cubosomes, hexosomes or sponges usually imply the use of highly energetic procedures such as sonication or homogenization, which represent a risk for the integrity of the drug payload. Another kind of more recent methods incorporate a variety of cosolvents in the formulation process but they generally have a heating step which is also undesirable for labile molecules[144]. However, new easier and less energetic methods for cubic phase dispersion, which do not mean an aggression for mesophase structure or the encapsulated molecule, are desirable from an industrial point of view. In this thesis, we explored a new self-emulsification method that avoids these two damaging processes in which Labrasol® is applied to spontaneously disperse a bulk GMO cubic gel using

poloxamer 407 as stabilizer. CCL2, our chemoattractant peptide, is preloaded in the aqueous phase of the bulk GMO gel before the self-dispersion with Labrasol to yield submicrometric particles. Considering that cargo molecules and excipients can alter the inner structure of the native gel and even disrupt it[145], we determined the crystallinity of our nanoparticles compared to the bulk GMO gel. To our knowledge, there is no previous work studying the role of Labrasol® in redispersing GMO bulk crystalline phases and its implication in crystalline phase behavior[146], which makes the study especially appealing due to the mildness and suitability of this methodology.

In light of these observations, one of the objectives of this thesis was to develop a nanotherapy to promote the differentiation of MDSCs to less immune-suppressive phenotypes. Specifically, like Zilio et al., we aimed to modulate MDSCs phenotype by the use of two RNA sequences oriented to promote the downregulation of transcription factor C/EBPβ: a miR 142-3p mimics and a RNA interference consisting on a shRNA against C/EBPβ. However, together with this RNAi therapy, our nanovehicles were designed to co-encapsulate the chemokine CCL2 for monocyte and T cell chemoattraction, to both direct the RNA to the most immune-suppressive MDSC subset and to restore native CCL2 levels within the tumor site to balance the increased ratio of nitrated/nitrosylated species and enable the adequate CTL recruitment. To this end, we have designed a core-shell nanocapsule with a polyarginine coating intended to adsorb the RNA by electrostatic forces, and a glycerol-monooleate(GMO)-based core with an L2 inverse micellar phase capable of entraping the chemokine within its aqueous domains. Given that TLR4 activation usually results in CCL2 production [147], we speculate that the incorporation of polyarginine in our nanovehicles may increase monocyte/macrophage chemoattraction and activation, further supporting the targeting of the RNA gene therapy. These nanocapsules were additionally coated with polyarginine and hyaluronic acid yielding multi-layered nanocapsules in order to protect the RNA cargo and facilitate targeting purposes.

SECTION 3. MODULATION OF HUMAN MESENCHYMAL STEM CELLS (HMSCS) IN TISSUE REGENERATION

Regenerative medicine appears as a solution to avoid transplantation and overcome donor shortage in the replacement of damaged and diseased organs or tissues. Advances in molecular biology, materials science and specially material-cell interfaces have led to new tissue engineering strategies including the development of 3D matrices that can act both as cell carriers and signal providers for regeneration and healing[148,149]. Among the targets for tissue engineering, cartilage regeneration remains one of the unmet medical goals since current therapies fail to restore a normal hyaline cartilage. Cartilage damage can be caused by a variety of conditions, such as trauma, arthritis, and sports-related injuries. In particular, the high incidence of arthritic diseases due to aging and obesity has a major impact on the quality of life. It is expected that 10-15% of adults over 60 years old show symptoms of arthritic disease whereas osteoarthritis (OA) is estimated to affect 130 million people by 2050 worldwide. Besides, the clinical and economic impact of OA is very high, with an estimated annual cost of $65 billion.

The self-healing of damaged cartilage is limited, due to the lack of progenitor cells as well as vascular, neural and lymphatic networks. Surgical approaches to treat cartilage lesions, such as microfracture and resurfacing techniques, are widely adopted because they are easy to perform, cost competitive and they achieve patient relief. However, their benefits are short-term due to the poor quality of the regenerated tissue, mostly composed by fibrocartilage. Osteochondral grafting is the only classical surgery technique that restores hyaline cartilage, but its use is limited due to the risk of disease transmission and graft-versus-host immune response when allografts are transplanted. In line with this technique, autologous chondrocyte implantation (ACI) and matrix assisted autologous chondrocyte implantation (MACI) constitute more advanced approaches in development but they are expensive and demand complex implantation protocols[150,151].

Another tissue that can benefit from tissue engineering applications is skeletal muscle. As in the case of cartilage, the properties of regenerated skeletal muscles are still far from their natural counterparts. Current treatments including autologous muscle transplantation and injection of muscle cells expanded *ex vivo*, have shown limited success. Autologous transplants lead to donor site morbidity and inadequate innervation and perfusion of the transferred muscle due to the difficulty of removing and re-connecting muscle arties, veins and nerves. Intramuscular injections of cells have shown little benefit in early clinical trials due to poor cell survival, migration and immune rejection. Although skeletal muscle has an inherent ability to regenerate in response to minor injuries, there is a need for engineered muscles as clinical substitutes for reconstructive surgery in several medical conditions including myopathy, traumatic

injury, aggressive tumor ablation and muscle denervation. For this reason, the development of engineered muscles capable of repairing or replacing the normal function of defective native tissues remains a challenge[152–156].

3.1 Regenerative potential of human Mesenchymal Stem Cells (hMSCs)

Mesenchymal Stem Cells were first described by Pittenger et al. in 1999, who characterized them in terms of their ability to proliferate in tissue culture plates showing a fibroblastic morphology, their expression of specific surface proteins (SH2, SH3, CD29, CD44, CD71, CD90, CD106, CD120a and CD14, among others) and their capability to differentiate to multiple mesenchymal lineages[157]. Although first isolated from the bone marrow, MSC can be easily isolated from other sources such as adipose tissue, umbilical cord, fetal liver, muscle, and lung and, more importantly, can be successfully expanded *in vitro*[158]. In addition, MSCs secrete various bioactive macromolecules that are immunoregulatory and help build regenerative microenvironments in the place of injury. For these reasons, MSCs appear as a valuable cell source to regenerate damaged mesenchymal tissues like bone, cartilage, muscle, dermis and other connective tissues[159].

The use of MSC in regenerative medicine has been largely addressed, either alone or in combination with biomaterials that serve as scaffolds to direct their function and facilitate their inclusion. Although MSC show a natural tropism to damaged tissue sites even after intravenous injection, the advantage of MSC delivery systems lies in the ease of controlling and manipulating the implanted cells and tissues with reduced side effects[158]. A number of clinical trials are investigating the potential of autologous and especially allogeneic MSCs for various applications. In particular, MSC therapies oriented to bone/cartilage regeneration are the most studied, due to the lack of current therapeutic interventions that successfully repair the osteochondral tissue. In second place, MSCs are being explored for their role of suppressing T cell proliferation and cytokine production, which makes them an attractive tool to contain the immune rejection in allogeneic grafting. Lastly, the third biggest area of research is the use of MSCs for cardiovascular repair, mainly in patients with severe myocardial infarct[160]. As a result, many companies are taking part in the development of this technology, such as Baxter, Mesoblast, Teva, Aastrom Biosciences, and specially Osiris Therapeutics, which therapy based on allogeneic bone-marrow derived MSCs has been approved in Canada and New Zealand for the treatment of graft-versus-host disease[161].

3.2 Hydrogels for tissue engineering

Hydrogels, crosslinked 3D networks of hydrophilic polymer chains, have attracted great attention for tissue engineering applications. They are similar to the natural extracellular matrix, have a high water content and swelling ability and their biocompatibility,

bioadhesiveness and biodegradability can be tuned depending on the necessities. Besides, they possess a highly porous frame that supports cell transplantation and proliferation as well as an adequate diffusion kinetics of nutrients and metabolic products. Finally, they can undergo volume phase or sol-gel phase transitions in response to physical and/or chemical stimuli, which allows for the formulation of injectable platforms that have the ability to match irregular defects while ensuring minimal invasiveness and target delivery at the preferred site.

Hydrogels are usually divided into two categories according to their natural or synthetic origin. Hydrogels from natural polymers have been widely used for tissue engineering approaches and several reports suggest the beneficial cellular responses of biopolymers and their performance over synthetic polymers. Among the different biopolymer-based hydrogels, those made of fibrin, alginate and collagen are widely explored as injectable systems[151,162–164].

3.2.1 Fibrin hydrogels

Fibrin polymer is an end product of the enzymatic cascade of blood clotting. Its easy assembly into fibrillary networks makes fibrin an attractive biopolymer. Besides, it has the potential to be extracted from patient's blood, constituting an autologous scaffold and thus alleviating any risk of immune reaction[165]. In addition, fibrin has been FDA approved as a surgical sealant and has been used extensively in hemostatic materials, such as fibrin glues, and wound dressings. Currently approved fibrin sealants include Tisseel and Artiss (Baxter), Evicel (Johnson & Johnson) and Cryoseal (Thermogenesis). Some of these sealants are also being used for tissue engineering applications in combination with other polymers or native tissue components, as clot stabilizers in microfracture procedures. Examples of these are Vitagel (Orthovita), BioCartilage (Arthrex), DeNovo NT (Zimmer) or Cartilage Autograft Implantation Systems (CAIS, DePuy Mitek and DePuy Biologics)[166–169].

Apart from their important role in hemostasis, fibrin gels are very bioactive, promoting cell attachment and stimulating hydrogel remodelling, serving as a scaffold for tissue repair following injury. The fibrin network provides a physical support for neutrophil, macrophage, and fibroblast infiltration, which will ultimately lay down fibronectin, collagen and other extracellular matrix (ECM) components to rebuild the damaged tissue. Furthermore, fibrinopeptides, which are released during polymerization of fibrin, and fibrin degradation peptides, are bioactive themselves and contribute to tissue repair due to their mitogenic, chemotactic and proangiogenic activities. Finally, fibrin provides a variety of signals and cues to direct cell behaviors through its numerous binding sites for growth factors, integrins and additional ECM components. For this reason, fibrin has

also been used in the development of cell instructive scaffolds for stem cell differentiation and delivery as well as for the induction of angiogenesis[170].

Fibrin is formed through the polymerization of the soluble precursor molecule fibrinogen, a process that is initiated by the serine protease thrombin, which is activated in response to injury. Fibrinogen is a 45 nm-long peptide made up of 6 paired polypeptide chains $(A\alpha\ B\beta\ \Upsilon)_2$ that are held together by 29 disulfide bonds. Fibrin polymerization is initiated by the thrombin cleavage of fibrinopeptides A (FpA) and B (FpB) from the N-termini of the Aα and Bβ -chains of fibrinogen to produce fibrin monomer $(\alpha\ \beta\ \Upsilon)_2$. The release of FpAs exposes an N-terminal α-chain motif Gly-Pro-Arg (GPR), called knob 'A,' which is complementary to pockets or holes 'a' located in the ϒ-nodules of another fibrin molecule, yielding A:a interactions. Cleavage of FpA and exposure of knobs 'A' are necessary and sufficient to form fibrin clots since A:a interactions are the driving force of fibrin polymerization. These A:a interactions are produced in a half-staggered manner, with 2 A:a knob-hole interactions holding the 2 monomers together. The addition of a third molecule to a half-staggered dimer produces an end-to-end junction where the ends of 2 molecules connect each other, leading to a regular 22.5-nm repeat. The release of FpBs exposes the N-terminal β-chain motif Gly-His-Arg-Pro (GHRP), called knob 'B,' which is complementary to hole 'b' located in the globular β-nodule. However, the affinity of the knob 'B'-mimetic GHRP peptide for fibrinogen (K_d = 140 mM) is relatively low compared with the knob 'A'-mimetic GPRP (K_d = 25mM) and despite evidence for the physical existence of B:b interactions, their physiological role remains unclear.

In addition to the established A:a and B:b knob-hole complexes, there is some evidence for the physical existence of A:b interactions. Moreover, the ϒ275-300 residues form a D-D interface similar to the one located at the end-to-end junction between fibrin monomers. Although D-D interactions are weak and yield first upon forced stretching of fibrin oligomers, studies revealed that they are essential for the elongation of fibrin strands.

The dimers and trimers formed by knob-hole and D-D interactions can lengthen longitudinally to form protofibrils, which aggregate laterally leading to the formation of fibers. The elongation and the thickening of fibrin fibers are accompanied by branching, which is necessary to produce the 3D network that constitutes the fibrin clot or gel. Most branch points consist of the junction of 3 fibers of about the same diameters, and, in general, as the number of branch points increase, the fiber diameters decrease. In addition, during and after polymerization in blood, fibrin is covalently cross-linked by factor XIIIa, activated by thrombin. The C-terminal portion of each of fibrin(ogen)'s ϒ-chain contains 1 cross-linking site at which 2 adjacent molecules form an intermolecular ϒ-glutamyl-e-lysyl covalent bond. The same intermolecular ϒ-glutamyl-e-lysyl bonds

form more slowly between C-terminal portions of fibrin α-chains (αC regions), thereby creating αC polymers. In addition, cross-linking also occurs between α- and ϒ-chains. This dense covalent cross-linking within and between protofibrils makes the polymerization process irreversible and stabilizes fibrin polymers[171,172].

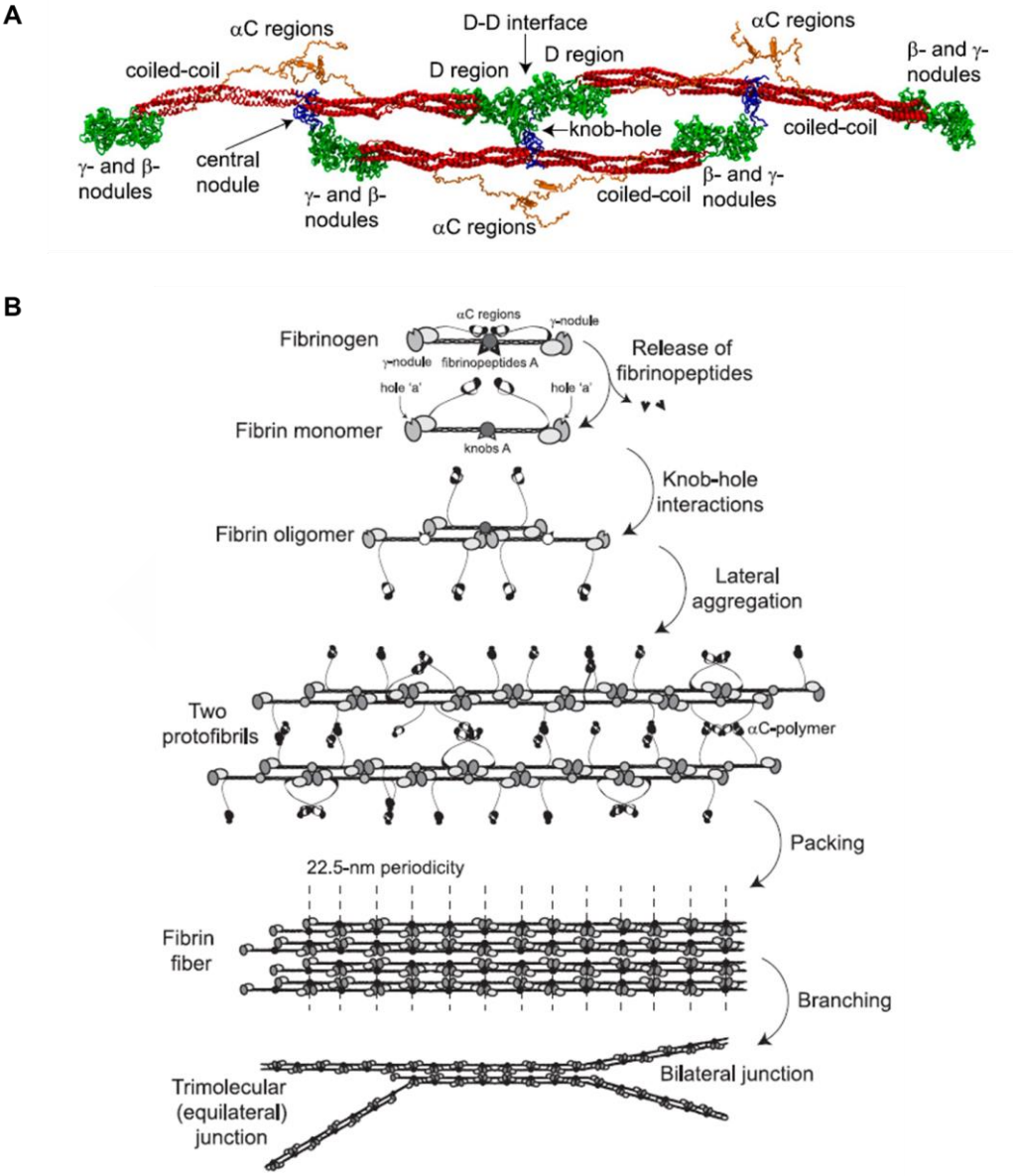

Figure 5. Schematic representation of fibrin oligomer and polimerization. (A) Short oligomer formed by 3 fibrin monomers based on the x-ray crystallographic structure of fibrinogen (Protein Data Bank entry: 3GHG). A:a knob-hole bonds that are the major basis of fibrin polymerization maintain the third (lower) monomer in a half-staggered arrangement. The intermolecular noncovalent coupling and the covalent cross-linking at the D-D interface hold the two (upper) monomers in a linear arrangement. (B) Fibrin polymerization steps: (1) enzymatic release of fibrinopeptides from fibrinogen, the formation of monomeric fibrin-containing exposed knobs, and the partial dissociation of the αC regions; (2) self-assembly of monomeric fibrin via knob-hole interactions and the formation of half-staggered 2-stranded fibrin oligomers; (3) lateral aggregation of protofibrils by αC-αC-interactions; (4) packing of protofibrils into a fiber with a 22.5-nm periodic crossstriation; and (5) fibrin network formation due to the branching of fibers by bilateral or trimolecular junction. Adapted from [171] with permission.

3.2.2 Collagen-I-alginate Interpenetrating Polymer Networks (IPNs)

Despite their good biocompatibility and bioactivity, natural hydrogels usually lack good mechanical properties and pose difficulties to control their degradation rates, which have motivated approaches to modify these polymers as well as to formulate hybrid hydrogels. Bioactive polymers such as fibrin, collagen, gelatin and hyaluronic acid all have good biocompatibility and promote cell adhesion and biological responses but they typically possess low mechanical properties. Alginate and agarose, on the contrary, are easily gelated polymers with highly tunable mechanical properties, but they are limited by their lack of cellular interaction. Strategies to improve the performance of these polymers include the physical mixture of two or more polymers with complementary properties to yield interpenetrating polymer networks (IPNs). The polymers in an IPN are not covalently bonded but at least partially interlaced and their network cannot be pulled apart unless chemical bonds are broken. One good example would be the collagen-I-alginate IPNs, which take advantage of the cell-interactive features of collagen to overcome alginate's lack of adhesion ligands, while surpassing the low mechanical properties of collagen hydrogels with the easily tunable crosslinking capacity of alginate[173].

Collagen is a main component of the extracellular matrix of mammalian tissues and, together with fibrinogen, one of the most widely used natural polymers. It can form thermally reversible physical gels or be chemically crosslinked using glutaraldehyde[174] or diphenylphosphoryl azide[175]. Collagen is composed of different polypeptides that can be recognized by cells and degraded by enzymes. Each collagen molecule consist of three polypeptide chains that contain one or more regions characterized by the repeating amino acid motif (Gly-X-Y). X and Y positions can be constituted by any amino acid but they are often (2S)-proline (Pro, 28%) and (2S,4R)-4-hydroxyproline (Hyp, 38%), respectively, with ProHypGly being the most common triplet (10.5%) in collagen[176]. This motif allows the chains to form a right-handed triple helical structure with the X and Y residues exposed to the surface and all glycine residues towards the core. Depending on the type of collagen, the triple-helical motif can be a major or minor part of the molecule, which also contains other regions comprising different non-collagenous domains.

In humans, there are 28 different proteins known as collagens, as well as about the same number of other members of the collagen superfamily. They can be grouped in subfamilies, with the fibrillary collagens being the ones with most interest from the biochemical point of view. There are 5 fibril-forming collagens (types I, II, III, V and XI) whereas other collagens form networks (types IV, VIII and X) or 11-nm periodic beaded filaments (type VI), associate with fibril surfaces (types IX, XII and XIV) or occur as transmembrane proteins (types XIII and XVII) [177]. Collagen I is the most widely occurring

collagen and can be found in skin, tendon, bone, cornea, lung and vasculature. Type II has a very specific tissue distribution and is essentially limited to cartilage. Type III is found in relatively elastic tissues such as embryonic skin, lung and blood vessels. Finally, types V and XI are less abundant collagens found in association with collagen I in the cornea and collagen II in cartilage, respectively.

Collagen fibrils are characterized by a repeating banding pattern with a D-periodicity of 64-67 nm, depending on the tissue. The three polypetide chains forming the fibrillary collagen molecules are called α chains. These chains can be identical, forming homotrimeric molecules as in collagens II and III, or distinct, yielding heterotypic molecules as in collagen I. All fibrillary collagens possess a long central triple-helical region in each α chain, consisting of a continuous (Gly-X-Y)n repeat, where n is 337-343. In the case of collagens I, II and III, this region is flanked by short non-helical regions called telopeptides at both C- and N- termini. They are synthesized in the ribosome in the form of soluble precursor molecules, called procollagens, with large N- and C-terminal propeptide domains. Procollagens then enter the rough endoplasmic reticulum, where they undergo post-translational modifications resulting in the assembly of procollagen molecules. These molecules transit the Golgi network and they are exported to the extracellular matrix. Procollagen processing occurs during or shortly after secretion followed by assembly of fibrils. C-propeptides are removed by specific metalloproteinases (ADAMTS and BMP1/Tolloid-like families, furin-like proprotein convertases) leaving the short C-telopeptides, while the extent of N-terminal processing depends on collagen type. Finally, fibrils are stabilized by the formation of covalent cross-links initiated by members of the lysyl oxidase family of copper-dependent amine oxidases.

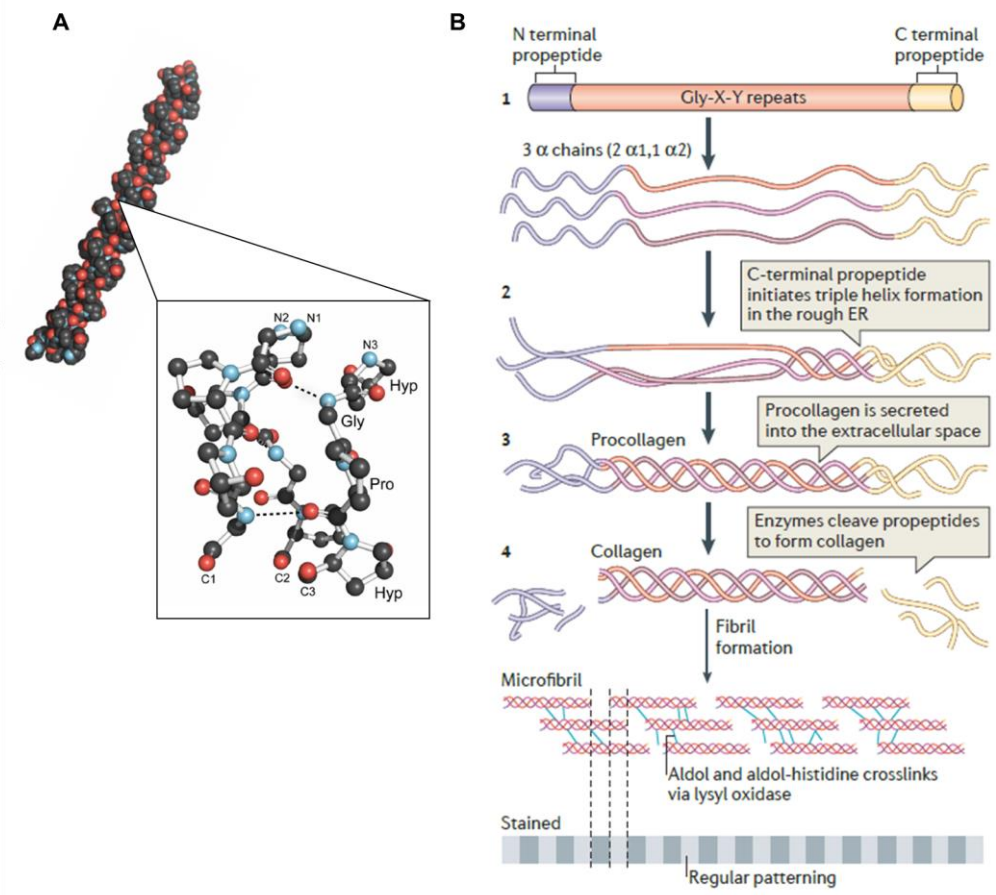

Figure 6. Collagen structure and assembly. (A) Crystal structure of a collagen triple helix formed from $(ProHypGly)_4$–(ProHypAla)–$(ProHypGly)_5$ and ball-and-stick image of one of its segments [Protein Data Bank (PDB) entry 1cag] (19). (B) Process of collagen formation showing the three α-chains of type I collagen (step 1) which are intracellularly assembled into the triple helix following initiation of this process by the C-terminal domain (step 2). Procollagen is secreted by cells into the extracellular space (step 3) and converted into collagen by the removal of the N- and C-propeptides via metalloproteinase enzymes (step 4). After procollagen is secreted into the extracellular space, collagen type-specific metalloproteinase enzymes remove the amino- and carboxy-propeptides. Collagen is assembled into cross-striated microfibrils that occur in the extracellular matrix of connective tissues. Short microfibrils merge into mature fibrils through longitudinal and axial growth. To form mature fibres, lysyl oxidase catalyses the formation of intramolecular and intermolecular covalent crosslinks between collagen molecules. Adapted from [176,178] with permission.

Collagen hydrogels are usually formed by the reconstitution of commercially available acid soluble fibrillary collagens, commonly collagen type I, although there are also pepsin soluble fibrillary collagens. These acid solutions are kept cold and when the pH is adjusted to around neutral and the temperature raised to around physiological, fibril formation occurs spontaneously. Fibril formation is an entropy-driven process, in which self-assembly results in burying surface-exposed hydrophobic residues within the fibril, and proceeds by a nucleation and growth mechanism. The structure of the resulting fibrils is influenced by several parameters including buffer compositions, the presence of other type of macromolecules and the order of the initiating procedure[179].

There are a myriad of FDA approved collagen-based products ranging from wound dressings (Apligraft, Integra, Gintuit) to hemostatic agents (Tachosil, Vitagel). Several devices have been intended for tissue engineering applications, such as Chondro-Gide (Geistlich Pharma), a bilayer collagen matrix for cartilage repair, Infuse (Medtronic), a rBMP-2 loaded collagen sponge for bone regeneration or NeuraGen (Integra LifeSciences), a semi-permeable, Type I collagen tube for peripheral nerve repair. On December 2016, the FDA approved the first, collagen-based, cellularized scaffold for the repair of symptomatic, full-thickness cartilage defects of the knee. Maci, manufactured by Vericel Corporation, consist of a bio-resorbable porcine-derived collagen membrane that is seeded with expanded patient's autologous cells and implanted in the damaged area[180,181].

Together with collagen, as an FDA approved polymer, **alginate** has become one of the most important biomaterials for diverse applications. Ammonium, calcium, potassium, propylene glycol and sodium alginate are GRAS materials with a long trajectory in the food industry were alginate has been widely used as emulsifier, binder and gelling agent. In addition, its biocompatibility and lack of immunogenicity, as well as its gentle gelling behavior, has enabled the use of alginate in a variety of biomedical applications including tissue engineering and drug delivery. It has been used as drug excipient (Tarka, Skelaxin, ROXYBOND, MORPHABOND ER), dental impression material (HygePLUS, Hygedent, Image), wound dressing (ALGICELL Ag, Suprasorb A + Ag, Phytacare), hemostatic (Neptune pads) injectable cell delivery vehicle (RGD-alginate, ASTM F2315 - 11) and immobilization matrix.

Alginates are anionic and hydrophilic polysaccharides isolated from brown algae and bacteria. They are linear unbranched block copolymers composed of (1-4)-linked β-D-mannuronic acid (M units) and its C-5 epimer α-L-guluronic acid (G units) monomers, which are covalently linked together in different sequences or blocks. M and G blocks can be either similar (MMMM, GGGG) or strictly alternating (GMGMGMGM) depending on the alginate source, which also determines their relative amount.
G blocks are stiffer and less soluble at low pH than alternating blocks because of the $^{1}C4$ diaxial links of L-guluronic acid compared to the $^{4}C1$ diequatorial links of D-Mannuronic acid. Two G blocks of adjacent polymer chains can be cross-linked with divalent cations (e.g. Ca^{2+} or Ba^{2+}) through interactions with the carboxylic groups in the sugars, creating ionic interchain bridges which lead to the formation of a gel network.

Alginate solutions have non-Newtonian characteristics (shear thinning) and their viscosity depends on the concentration of the polymer and its MW distribution. The MW distribution, as well as the polymer composition (M/G ratio) also regulates the overall gel stiffness in conjunction with the stoichiometry of the alginate with the chelating cation. Similarly, manipulating polymer MW and composition allows one to tune the

polymer degradation rate, which is especially interesting since alginate is not naturally broken down enzymatically but it degrades via an uncontrollable and unpredictable process involving loss of divalent ions.

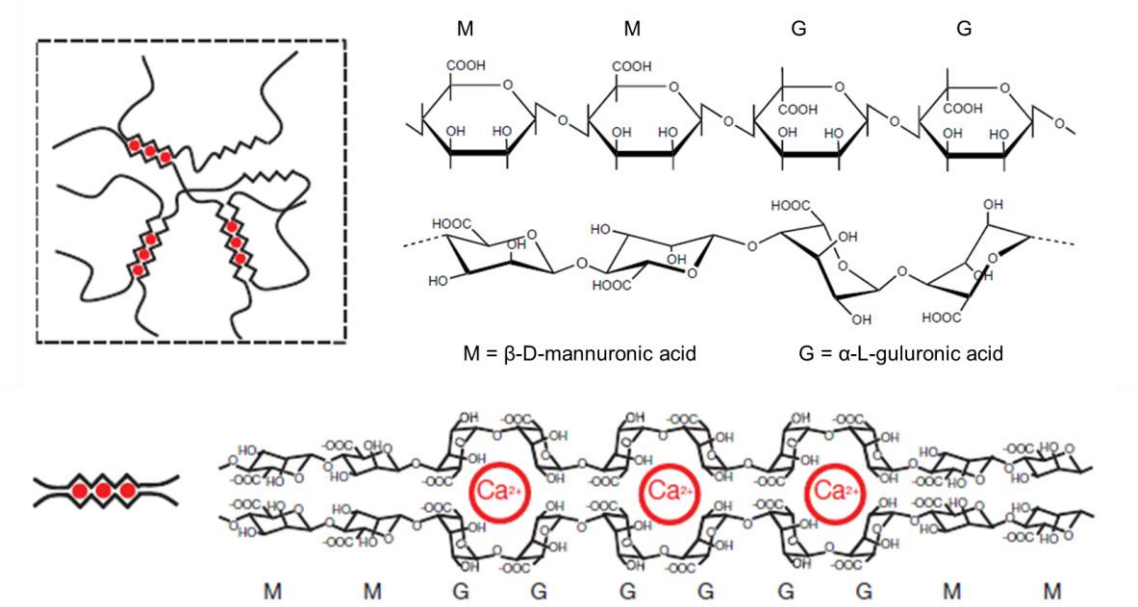

Figure 7. Schematic of an alginate gel. In an alginate gel, the G blocks on different polymer chains form ionic crosslinks through Ca^{2+} (red circles). Adapted from [182,183] with permission.

As a result, alginate mechanical properties and degradation rate can be highly controlled by modulating polymer MW and composition as well as the nature and stoichiometry of the cross-linking agent. In addition, the properties of alginate polymers can be further modulated by the introduction of chemical modifications. Since cells do not naturally adhere to alginate, the most widespread example of these chemical modifications is the use of the fibronectin-derived adhesion peptide arginine glycine aspartic acid (RGD) and its subtypes, to yield cell-interactive alginates. This RGD coupling can be done using carbodiimide chemistry, which is also applied to covalently cross-link alginates, providing an alternative cross-linking method[183–186].

3.3 Gene Activated Matrices (GAMs) for tissue engineering

In tissue engineering approaches, hydrogels are usually employed as vehicles for cells and also growth factors that help directing the regenerative process. Traditionally, these growth factors were included in the form of recombinant proteins which were released in a controlled manner from the polymer matrices. Specific collagen-based devices have reached the clinical setting for the delivery of rhBMP-7 (OP-1™), and rhBMP-2 (Infuse®)[187]. However, these devices have a limited capacity to control the release, so that to extend the effect of the associated growth factors it is necessary to administer

them at high doses. This, in turn, leads to side effects among which the risk of malignancies is one of the biggest concerns[188–190].

Trying to overcome these drawbacks, researchers have started to explore the use of gene therapy as an alternative to recombinant proteins, and this has led to the concept of Gene Activated Matrix (GAM). At the very beginning, GAMs were based on plasmid DNA (pDNA), free or complexed to non-viral formulations, encoding the growth factor of interest. As for recombinant proteins, this complexed pDNA was loaded within a polymer matrix from which it could be slowly released, producing the transfection of surrounding cells and the consequent sustained protein expression. These GAMs were mostly comprised of FDA approved polymers, either natural (alginate, collagen and fibrin) or synthetic (polyethylene glycol (PEG), poly-lactic-co-glycolic acid (PLGA)) and were generally oriented to MSC-based bone and cartilage repair[191]. Although the majority of these GAMs were based on the use of growth factors BMP-2 and TGF-β1 to repair bone and cartilage defects, respectively, this approach was also explored to encode pivotal transcription factors (TF) in musculoskeletal development. As previously described, TFs are DNA binding proteins that regulate gene transcription and several TFs have been identified to direct cell differentiation towards specific tissue types[36–39]. Among them, the SOX trio (SOX9, SOX6 and SOX5) or SOX9 alone, master regulator of chondrogenesis, as well as RUNX2, main regulator of osteogenesis, have been widely assayed[192,193].

Nevertheless, while non-viral delivery of pDNA is preferred over viral vectors due to safety concerns, non-viral formulations are characterized by a low gene transfer efficiency, which in part hampers their clinical success. This prompted the use of RNA-based GAMs, with the aim to take advantage of the superior gene transfer capacity of RNA. In this regard, different RNA GAMs were explored, ranging from siRNA and miRNA GAMs[191], to the more recent mRNA GAMs. Although more and more iRNA mechanisms are being discovered to control crucial developmental processes, and hence iRNA GAMs hold great promise, in the context of this thesis we will focus on the exploration of mRNA GAMs. As we commented before, since their first preclinical exploration in the 1990s, mRNA-based therapies have gained great attention and proved to surpass pDNA in boosting forced protein expression[11–14]. However, mRNA therapies were mostly oriented to cancer vaccination, and it was not until 2013 when Lui et al. first envisioned the concept of mRNA-GAM[194] that would be described by Elangovan et al. two years later. In their work, Elangovan and co-workers used chemically modified mRNA encoding BMP-2, complexed to branched polyethylenimine (PEI) and embedded in a collagen matrix, to study the bone regeneration of rat calvarial defects, and demonstrated its superior biocompatibility and regenerative capacity as compared to a traditional pDNA GAM[195]. One year later, Balmayor et al. compared the use of BMP-2 mRNA within two different biomaterials: fibrin gels and micro-macro biphasic calcium phosphate (MBCP)

granules, both seeded with rat derived BMSCs *in vitro*. They observed a high osteoinductive behavior of what they called transcrip-activated matrices (TAMs) and found that MBCP synergistically enhances the hBMP-2 cmRNA-induced osteogenic pathway, highlighting the role of TAMs mechanical properties in their cell differentiation potential[196]. Finally, in 2017, Khorsand and Elangovan compared the osteoinductive potential of BMP-2 and BMP-9 mRNA with the same settings as in their previous study, observing an increased bone formation of the calvarial defects treated with BMP-9 GAMs[197].

Building on this knowledge, in the context of this thesis we aimed to further explore the concept of mRNA GAMs, developing a new kind of mRNA GAMs activated with lineage-specific TFs. To this end, fibrin hydrogels were activated with SOX9 (cartilage)[49,50] and MYOD (muscle)[40] TFs and hMSCs where encapsulated therein to promote their transfection and investigate their chondrogenic and myogenic differentiation. As mentioned before, TF-activated GAMs have been previously developed for pDNA, however, since mRNA expression kinetics may mimic better the physiological changes in TF expression, we hypothesized that our novel mRNA GAMs could provide a therapeutic benefit compared with these classical pDNA GAMs.

Together with chemical signals, recent work suggests that mechanical forces are equally important regulators of lineage specification. In fact, over the past few years, mechanostransduction has regained great attention as a means to regulate cell fate conversion. For this reason, we next sought to explore the influence of hydrogel mechanical properties on the net differentiation outcome. However, fibrin hydrogels, with poor mechanical properties, are not suitable systems to study the mechanical modulation of cell phenotype. Thereby, collagen-I-alginate IPNs developed at the laboratory of Prof. Mooney, that allow to tune gel stiffness independently of gel architecture, polymer concentration or adhesion ligand density [173], were used to evaluate the influence of hydrogel mechanics on the chondrogenic differentiation driven by SOX9 forced expression.

3.4 Mechanotransduction

The necessity to integrate the effect of mechanical forces in the global understanding of tissue homeostasis and development is becoming crucial to generate new types of therapeutic interventions and improved strategies for tissue engineering and regenerative medicine. For this reason, an increasing body of research is now focusing on the modulation of cell phenotype by tuning the mechanical properties of their substrates either in two-dimensional (2D) or three-dimensional (3D) cell culture systems[43,45,198–203]. In addition, these 3D systems are also being used to get more realistic knowledge about cytotoxicity and drug efficacy, especially in the context of cancer,

where tissue stiffening has been extensively linked to drug resistance and cell malignancy. Indeed, more and more results support the value of 3D cultures as means to overcome the lack of predictability of current 2D *in vitro* models prior to *in vivo* experimentation. Specifically, they are proving to be especially relevant to test new nanoparticulate delivery systems, where diffusion through the extracellular matrix and other complex biological barriers represents a key issue for drug efficacy[204,205].

Mechanical control of gene transcription contributes to the maintenance of pluripotency, determination of cell fate as well as pattern formation and organogenesis thus controlling cell and tissue function throughout embryogenesis and adult life. The mechanisms by which these mechanical forces are translated into transcriptional alterations are varied and complex. This is because cells are not alone, but they are surrounded by neighboring cells and a extracellular matrix (ECM) that generate contractile forces that balance their cytoskeletal actomyosin filaments maintaining them in a tensionally prestressed state. Cells sense this environment by transmembrane surface adhesion receptors, such as integrins and cadherins, which convert the mechanical signals into cytoplasmic biochemical signals within cell surface focal adhesions and cell-cell adhesion complexes. These downstream intracellular signaling cascades, in turn, promote changes in the concentration of second messengers (such as Ca^{2+} flux, inositol triphosphate…) or activate protein signaling molecules (such as MAPKs and Rho-family small GTPases) thus triggering transcriptional changes in the nucleus. Thereby, focal adhesion proteins that physically couple actin filaments to integrins, act as mechanotransducers in part by regulating cytoskeletal tension.

Since cytoskeleton filaments are also coupled to the nuclear membrane, intranuclear scaffolds and chromatin, cytoskeletal tension further results in a dynamic state of the nuclei size and shape. This promotes a prestressed state of the nucleus that balance contractile forces with condensation forces of the chromatin. For this reason, the nucleus itself can act as a mechanosensor and mechanical forces can regulate gene expression directly by altering the transport of transcription factors into the nucleus[206].

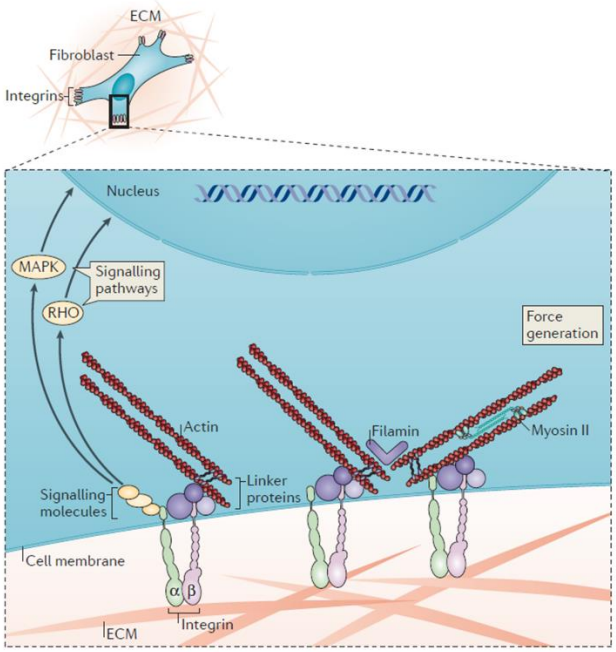

Figure 8. Key components of mechanotransduction pathways. Schematic depicting a fibroblast embedded in the extracellular matrix (ECM), with an expanded view showing cell–ECM interactions. Cells interact mechanically with the ECM via transmembrane receptors called integrins, which in turn interact with intracellular signalling molecules (including focal adhesion kinase (FAK) and SRC) and physically connect to cytoskeletal actin via linker proteins (including talin, vinculin, filamin, α-actinin and the complex involving integrin-linked protein kinase (ILK), PINCH and parvin). Key signalling pathways associated with integrin activation include the RHO–RHO-associated protein kinase (ROCK) and mitogen-activated protein kinase (MAPK) pathways. Reproduced from [207] with permission.

In the context of tissue engineering, several works have explored the modulation of mechanical cues to selectively tune cell phenotype towards specific lineages. For cells seeded atop hydrogels, the modulus of the substrate or geometry constrains on its cell adhesion properties have been shown to affect cell spreading, traction generation and fate. Conversely, the influence of biophysical properties on cell fate within 3D environments is more complicated and not fully understood yet. Huebsch et al. showed that within non-degradable, ionically crosslinked alginate hydrogels, the differentiation of encapsulated MSC is dictated by matrix stiffness irrespective of cell morphology. Despite the lack of hydrogel degradation, the physically crosslinked alginate employed in this system, was adequately mobile to enable cellular reorganization of bound adhesive ligands, traction generation and differentiation[46]. Three years later, Khetan et al. identified these cell-mediated remodeling and cell-generated tension as key for fate regulation. In their model, covalently crosslinked hyaluronic acid hydrogels, cell differentiation is mediated by the generation of degradation-mediated cellular traction, independently of cell morphology or matrix mechanics[208]. In agreement with this work, Chaudhuri et al. established hydrogel stress-relaxation as a key parameter to mimic the viscolasticity of natural ECMs and maximize cell remodeling and differentiation[47]. Further improving this knowledge, another recent work developed by Cosgrove et al. revealed the importance on the nature of hydrogel cell adhesion ligands in cell interpretation of ECM stiffness and subsequent changes in downstream cell proliferation and differentiation[209]. Finally, an interplay between cell-matrix and cell-cell contacts has been recently shown to further impact different stages of osteogenesis in hMSCs[48].

Within this frame, in the context of this thesis we sought to explore the influence of the mechanical properties of SOX9 mRNA GAMs on the chondrogenic differentiation of hMSCs. As mentioned previously, fibrin hydrogels are characterized by their poor mechanical properties precluding them of being a suitable platform to study the interplay between mechanics and SOX9 forced expression. Hence, collagen-I-alginate IPNs developed by the Mooney Lab were selected for these experiments, allowing a precise control over gel mechanical properties. Indeed, these highly tunable systems allowed us to test the effect of adhesion and stiffness to both understand the process of gene transfer in 3D environments and to identify the optimal conditions for cartilage repair. Taking everything together, our goal was, on the one hand, to prove the feasibility and superior profile of TF-activated mRNA GAMs over their pDNA counterparts, and, on the other hand, to further enhance the differentiation behaviour of these mRNA GAMs by optimizing their mechanical properties. Overall, the work summarized in Chapters 2 and 3 of this manuscript was intended to contribute to the increasing knowledge and understanding of cell responses to drugs and substrates in 3D environments, with the aim to exploit cell-material interactions to create better cell therapies and medical devices.

References

1. Aragona, M. & Blanpain, C. Transgenic stem cells replace skin. *Nat. News Views* (2017).
2. Janmey, P. A. *et al.* From tissue mechanics to transcription factors. *Differenciation* **86,** 112–120 (2013).
3. Jonas, S. & Izaurralde, E. Towards a molecular understanding of microRNA-mediated gene silencing. *Nat. Rev. Genet.* **16,** 421–433 (2015).
4. Lee, R. C. The C . elegans Heterochronic Gene lin-4 Encodes Small RNAs with Antisense Complementarity to lin-14. *Cell* **75,** 843–854 (1993).
5. Reinhart, B. J. *et al.* The 21-nucleotide let-7 RNA regulates developmental timing in Caenorhabditis elegans. *Nature* **403,** 901–906 (2000).
6. Bracken, C. P., Scott, H. S. & Goodall, G. J. A network-biology perspective of microRNA function and dysfunction in cancer. *Nat. Rev. Genet.* **17,** 719–732 (2016).
7. Rupaimoole, R. & Slack, F. J. MicroRNA therapeutics: towards a new era for the management of cancer and other diseases. *Nat. Rev. Drug Discov.* **16,** 203–222 (2017).
8. Brenner, S., Jacob, F. & Meselson, M. An unstable intermediate carrying information from genes to ribosomes for protein synthesis. *Nature* **190,** 576–581 (1961).
9. Wolff, J. A. *et al.* Direct gene transfer into mouse muscle in vivo. *Science* **247,** 1465–1468 (1990).
10. Conry, R. M. *et al.* Characterization of a Messenger RNA Polynucleotide Vaccine Vector. *Cancer Res.* **55,** 1397–1400 (1995).
11. Quabius, E. S. & Krupp, G. Synthetic mRNAs for manipulating cellular phenotypes: An overview. *N. Biotechnol.* **32,** 229–235 (2015).
12. Mandal, P. K. & Rossi, D. J. Reprogramming human fibroblasts to pluripotency using modified mRNA. *Nat. Protoc.* **8,** 568–582 (2013).
13. Andries, O. *et al.* Comparison of the gene transfer efficiency of mRNA/GL67 and pDNA/GL67 complexes in respiratory cells. *Mol. Pharm.* **9,** 2136–2145 (2012).
14. Zou, S., Scarfo, K., Nantz, M. H. & Hecker, J. G. Lipid-mediated delivery of RNA is more efficient than delivery of DNA in non-dividing cells. *Int. J. Pharm.* **389,** 232–243 (2010).
15. Dowdy, S. F. Overcoming cellular barriers for RNA therapeutics. *Nat. Biotechnol.* **35,** 222–229 (2017).
16. Sahin, U., Karikó, K. & Türeci, Ö. mRNA-based therapeutics — developing a new class of drugs. *Nat. Rev. Drug Discov.* **13,** 759–780 (2014).
17. He, L. & Hannon, G. J. MicroRNAs: small RNAs with a big role in gene regulation. *Nat. Rev. Genet.* **5,** 631–631 (2004).
18. Ha, M. & Kim, V. N. Regulation of microRNA biogenesis. *Nat. Rev. Mol. Cell Biol.* **15,** 509–24 (2014).
19. Warren, L. *et al.* Highly efficient reprogramming to pluripotency and directed differentiation of human cells with synthetic modified mRNA. *Cell Stem Cell* **7,** 618–630 (2010).
20. Dvir, S. *et al.* Deciphering the rules by which 5 ’-UTR sequences affect protein expression in yeast. *Proc. Natl. Acad. Sci. U. S. A.* **110,** E2792–E2801 (2013).

21. Holcik, M. & Liebhaber, S. a. Four highly stable eukaryotic mRNAs assemble 3' untranslated region RNA-protein complexes sharing cis and trans components. *Proc. Natl. Acad. Sci. U. S. A.* **94,** 2410–2414 (1997).
22. Annweiler, A., Hipskind, R. A. & Wirth, T. A strategy for efficient in vitro translation of cDNAs using the rabbit β-globin leader sequence. *Nucleic Acids Res.* **19,** 3750 (1991).
23. Kozak, M. An analysis of 5'-noncoding sequences from 699 vertebrate messenger rNAS. *Nucleic Acids Res.* **15,** 8125–8148 (1987).
24. Proudfoot, N. J. Ending the message: Poly(A) signals then and now. *Genes Dev.* **25,** 1770–1782 (2011).
25. Kuhn, A. N. *et al.* mRNA as a versatile tool for exogenous protein expression. *Curr. Gene Ther.* **12,** 347–61 (2012).
26. Vaquerizas, J. M., Kummerfeld, S. K., Teichmann, S. A. & Luscombe, N. M. A census of human transcription factors: function, expression and evolution. *Nat. Rev. Genet.* **10,** 252–263 (2009).
27. Lin, Y. *et al.* Transcription factor and miRNA co-regulatory network reveals shared and specific regulators in the development of B cell and T cell. *Sci. Rep.* **5,** 15215 (2015).
28. Wang, J., Lu, M., Qiu, C. & Cui, Q. TransmiR: A transcription factor microRNA regulation database. *Nucleic Acids Res.* **38,** 119–122 (2009).
29. Lin, Y. *et al.* MiRNA and TF co-regulatory network analysis for the pathology and recurrence of myocardial infarction. *Sci. Rep.* **5,** 9653 (2015).
30. Guo, Z. *et al.* Genome-wide survey of tissue-specific microRNA and transcription factor regulatory networks in 12 tissues. *Sci. Rep.* **4,** 5150 (2015).
31. Le Béchec, A. *et al.* MIR@NT@N: a framework integrating transcription factors, microRNAs and their targets to identify sub-network motifs in a meta-regulation network model. *BMC Bioinformatics* **12,** 67 (2011).
32. Marigo, I. *et al.* Tumor-induced tolerance and immune suppression depend on the C/EBPβ transcription factor. *Immunity* **32,** 790–802 (2010).
33. Sonda, N., Chioda, M., Zilio, S., Simonato, F. & Bronte, V. Transcription factors in myeloid-derived suppressor cell recruitment and function. *Curr. Opin. Immunol.* **23,** 279–285 (2011).
34. Jopling, C., Boue, S. & Belmonte, J. C. I. Dedifferentiation, transdifferentiation and reprogramming: three routes to regeneration. *Nat. Rev. Mol. Cell Biol.* **12,** 79–89 (2011).
35. Merrell, A. J. & Stanger, B. Z. Adult cell plasticity in vivo: de-differentiation and transdifferentiation are back in style. *Nat. Rev. Mol. Cell Biol.* **17,** 413–425 (2016).
36. Rackham, O. J. L. *et al.* A predictive computational framework for direct reprogramming between human cell types. *Nat. Genet.* **48,** 331–335 (2016).
37. Hikichi, T. *et al.* Transcription factors interfering with dedifferentiation induce cell type-specific transcriptional profiles. *Proc. Natl. Acad. Sci.* **110,** 6412–6417 (2013).
38. Almalki, S. G. & Agrawal, D. K. Key transcription factors in the differentiation of mesenchymal stem cells. *Differentiation* **92,** 41–51 (2016).
39. Yamamizu, K. *et al.* Identification of transcription factors for lineage-specific ESC differentiation. *Stem Cell Reports* **1,** 545–559 (2013).
40. Davis, R. L., Weintraub, H. & Lassar, A. B. Expression of a single transfected cDNA converts fibroblasts to myoblasts. *Cell* **51,** 987–1000 (1987).

41. Takahashi, K. & Yamanaka, S. Induction of Pluripotent Stem Cells from Mouse Embryonic and Adult Fibroblast Cultures by Defined Factors. *Cell* **126,** 663–676 (2006).
42. Graf, T. Historical origins of transdifferentiation and reprogramming. *Cell Stem Cell* **9,** 504–516 (2011).
43. Engler, A. J., Sen, S., Sweeney, H. L. & Discher, D. E. Matrix Elasticity Directs Stem Cell Lineage Specification. *Cell* **126,** 677–689 (2006).
44. Clause, K. C. . L. L. J. . T. K. Directed stem cell differentiation: the role of physical forces. **17,** 48–54 (2012).
45. Guilak, F., Cohen, D. & Estes, B. Control of stem cell fate by physical interactions with the extracellular matrix. *Cell Stem Cell* **5,** 17–26 (2009).
46. Huebsch, N. *et al.* Harnessing traction-mediated manipulation of the cell/matrix interface to control stem-cell fate. *Nat. Mater.* **9,** 518–526 (2010).
47. Chaudhuri, O. *et al.* Hydrogels with tunable stress relaxation regulate stem cell fate and activity. *Nat. Mater.* **15,** 326–334 (2015).
48. Mao, A. S., Shin, J. W. & Mooney, D. J. Effects of substrate stiffness and cell-cell contact on mesenchymal stem cell differentiation. *Biomaterials* **98,** 184–191 (2016).
49. Dy, P. *et al.* Sox9 Directs Hypertrophic Maturation and Blocks Osteoblast Differentiation of Growth Plate Chondrocytes. *Dev. Cell* **22,** 597–609 (2012).
50. Bi, W., Deng, J. M., Zhang, Z., Behringer, R. R. & Crombrugghe, B. De. Sox9 is required for cartilage formation. *Nat. Genet.* **22,** 85–89 (1999).
51. Bronte, V. *et al.* Recommendations for myeloid-derived suppressor cell nomenclature and characterization standards. *Nat. Commun.* **7,** 12150 (2016).
52. Ugel, S., De Sanctis, F., Mandruzzato, S. & Bronte, V. Tumor-induced myeloid deviation: When myeloid-derived suppressor cells meet tumor-Associated macrophages. *J. Clin. Invest.* **125,** 3365–3376 (2015).
53. De Sanctis, F. *et al.* MDSCs in cancer: Conceiving new prognostic and therapeutic targets. *Biochim. Biophys. Acta - Rev. Cancer* **1865,** 35–48 (2016).
54. Tomihara, K. *et al.* Gemcitabine chemotherapy induces phenotypic alterations of tumor cells that facilitate antitumor T cell responses in a mouse model of oral cancer. *Oral Oncol.* **50,** 457–467 (2014).
55. Suzuki, E., Kapoor, V., Jassar, A. S., Kaiser, L. R. & Albelda, S. M. Gemcitabine selectively eliminates splenic Gr-1+/CD11b + myeloid suppressor cells in tumor-bearing animals and enhances antitumor immune activity. *Clin. Cancer Res.* **11,** 6713–6721 (2005).
56. Vincent, J. *et al.* 5-Fluorouracil selectively kills tumor-associated myeloid-derived suppressor cells resulting in enhanced T cell-dependent antitumor immunity. *Cancer Res.* **70,** 3052–3061 (2010).
57. Naiditch, H., Shurin, M. R. & Shurin, G. V. Targeting myeloid regulatory cells in cancer by chemotherapeutic agents. *Immunol. Res.* **50,** 276–285 (2011).
58. Kodumudi, K. N. *et al.* A novel chemoimmunomodulating property of docetaxel: Suppression of myeloid-derived suppressor cells in tumor bearers. *Clin. Cancer Res.* **16,** 4583–4594 (2010).
59. Sanford, D. E. *et al.* A Study of Zoledronic Acid as Neo-Adjuvant, Perioperative Therapy in Patients with Resectable Pancreatic Ductal Adenocarcinoma. *J. Cancer Ther.* **4,** 797–803 (2013).

60. Sinha, P. *et al.* Proinflammatory S100 Proteins Regulate the Accumulation of Myeloid-Derived Suppressor Cells. *J. Immunol.* **181,** 4666–4675 (2008).
61. Xu, J. *et al.* CSF1R signaling blockade stanches tumor-infiltrating myeloid cells and improves the efficacy of radiotherapy in prostate cancer. *Cancer Res.* **73,** 2782–2794 (2013).
62. Ries, C. H. *et al.* Targeting tumor-associated macrophages with anti-CSF-1R antibody reveals a strategy for cancer therapy. *Cancer Cell* **25,** 846–859 (2014).
63. Priceman, S. J. *et al.* Targeting distinct tumor-infiltrating myeloid cells by inhibiting CSF-1 receptor: Combating tumor evasion of antiangiogenic therapy. *Blood* **115,** 1461–1471 (2010).
64. Chalmin, F. *et al.* Membrane associated Hsp72 from tumor derived exosomes mediates STAT3 depedent immunosuppressive function of mouse and human myeloid derived suppressor cells. *J. Clin. Invest.* **120,** 467–471 (2010).
65. Zheng, Y. *et al.* Cimetidine suppresses lung tumor growth in mice through proapoptosis of myeloid-derived suppressor cells. *Mol. Immunol.* **54,** 74–83 (2013).
66. Bruchard, M. *et al.* Chemotherapy-triggered cathepsin B release in myeloid-derived suppressor cells activates the Nlrp3 inflammasome and promotes tumor growth. *Nat. Med.* **19,** 57–64 (2012).
67. Ko, J. S. *et al.* Sunitinib mediates reversal of myeloid-derived suppressor cell accumulation in renal cell carcinoma patients. *Clin. Cancer Res.* **15,** 2148–2157 (2009).
68. Osada, T. *et al.* The effect of anti-VEGF therapy on immature myeloid cell and dendritic cells in cancer patients. *Cancer Immunol. Immunother.* **57,** 1115–1124 (2008).
69. Lu, P., Yu, B. & Xu, J. Cucurbitacin B Regulates Immature Myeloid Cell Differentiation and Enhances Antitumor Immunity in Patients with Lung Cancer. *Cancer Biother. Radiopharm.* **27,** 495–503 (2012).
70. Serafini, P. *et al.* Phosphodiesterase-5 inhibition augments endogenous antitumor immunity by reducing myeloid-derived suppressor cell function. *J. Exp. Med.* **203,** 2691–2702 (2006).
71. Weed, D. T. *et al.* Tadalafil Reduces Myeloid-Derived Suppressor Cells and Regulatory T Cells and Promotes Tumor Immunity in Patients with Head and Neck Squamous Cell Carcinoma. *Clin. Cancer Res.* **21,** 39–48 (2015).
72. De Santo, C. *et al.* Nitroaspirin corrects immune dysfunction in tumor-bearing hosts and promotes tumor eradication by cancer vaccination. *Proc. Natl. Acad. Sci. U. S. A.* **102,** 4185–4190 (2005).
73. Nagaraj, S. *et al.* Anti-inflammatory triterpenoid blocks immune suppressive function of MDSCs and improves immune response in cancer. *Clin. Cancer Res.* **16,** 1812–1823 (2010).
74. Veltman, J. D. *et al.* COX-2 inhibition improves immunotherapy and is associated with decreased numbers of myeloid-derived suppressor cells in mesothelioma. Celecoxib influences MDSC function. *BMC Cancer* **10,** 464 (2010).
75. Kusmartsev, S. *et al.* All- trans -Retinoic Acid Eliminates Immature Myeloid Cells from Tumor-bearing Mice and Improves the Effect of Vaccination All- trans-Retinoic Acid Eliminates Immature Myeloid Cells from Tumor-bearing Mice and Improves the Effect of Vaccination. *Cancer Res.* **63,** 4441–4449 (2003).

76. Kulbersh, J. S., Day, T. A., Gillespie, M. B. & Young, M. R. I. 1α,25-Dihydroxyvitamin D3 to skew intratumoral levels of immune inhibitory CD34+ progenitor cells into dendritic cells. *Otolaryngol. - Head Neck Surg.* **140,** 235–240 (2009).
77. Hirai, H. *et al.* C/EBPβ is required for 'emergency' granulopoiesis. *Nat. Immunol.* **7,** 732–739 (2006).
78. Qiu, X., Aiken, K. J., Chokas, A. L., Beachy, D. E. & Nick, H. S. Distinct functions of CCAAT enhancer-binding protein isoforms in the regulation of manganese superoxide dismutase during interleukin-1β stimulation. *J. Biol. Chem.* **283,** 25774–25785 (2008).
79. Sonda, N. *et al.* miR-142-3p Prevents Macrophage Differentiation during Cancer-Induced Myelopoiesis. *Immunity* **38,** 1236–1249 (2013).
80. Viola, A., Sarukhan, A., Bronte, V. & Molon, B. The pros and cons of chemokines in tumor immunology. *Trends Immunol.* **33,** 496–504 (2012).
81. De Sanctis, F. *et al.* The emerging immunological role of post-translational modifications by reactive nitrogen species in cancer microenvironment. *Front. Immunol.* **5,** 1–16 (2014).
82. Qian, B.-Z. *et al.* CCL2 recruits inflammatory monocytes to facilitate breast-tumour metastasis. *Nature* **475,** 222–225 (2011).
83. Fang, W. Bin *et al.* Targeted gene silencing of CCL2 inhibits triple negative breast cancer progression by blocking cancer stem cell renewal and M2 macrophage recruitment. *Oncotarget* **7,** 49349–49367 (2014).
84. Sawanobori, Y. & Ueha, S. Chemokine-mediated rapid turnover of myeloid-derived suppressor cells in tumor-bearing mice. *Blood* **111,** 5457–5466 (2008).
85. Lesokhin, A. M. *et al.* Monocytic CCR2 + myeloid-derived suppressor cells promote immune escape by limiting activated CD8 T-cell infiltration into the tumor microenvironment. *Cancer Res.* **72,** 876–886 (2012).
86. Rosenberg, S. A. & Dudley, M. E. Cancer regression in patients with metastatic melanoma after the transfer of autologous antitumor lymphocytes. *Proc. Natl. Acad. Sci. U. S. A.* **101 Suppl,** 14639–45 (2004).
87. Galon, J. Type, Density, and Location of Immune Cells Within Human Colorectal Tumors Predict Clinical Outcome. *Science* **313,** 1960–1964 (2006).
88. Ugel, S. *et al.* Immune Tolerance to Tumor Antigens Occurs in a Specialized Environment of the Spleen. *Cell Rep.* **2,** 628–639 (2012).
89. Molon, B. *et al.* Chemokine nitration prevents intratumoral infiltration of antigen-specific T cells. *J. Exp. Med.* **208,** 1949–1962 (2011).
90. Molon, B., Viola, A. & Bronte, V. Smoothing T cell roads to the tumor: Chemokine post-translational regulation. *Oncoimmunology* **1,** 390–392 (2012).
91. Shi, J., Kantoff, P. W., Wooster, R. & Farokhzad, O. C. Cancer nanomedicine: progress, challenges and opportunities. *Nat. Rev. Cancer* **17,** 20–37 (2016).
92. Sousa, F. *et al.* A new paradigm for antiangiogenic therapy through controlled release of bevacizumab from PLGA nanoparticles. *Sci. Rep.* **7,** 3736 (2017).
93. Hou, L., Yao, J., Zhou, J. & Zhang, Q. Pharmacokinetics of a paclitaxel-loaded low molecular weight heparin-all-trans-retinoid acid conjugate ternary nanoparticulate drug delivery system. *Biomaterials* **33,** 5431–5440 (2012).
94. Yao, J., Zhang, L., Zhou, J., Liu, H. & Zhang, Q. Efficient simultaneous tumor targeting delivery of all-trans retinoid acid and paclitaxel based on hyaluronic acid-based multifunctional nanocarrier. *Mol. Pharm.* **10,** 1080–1091 (2013).

95. Wang, W. *et al.* Galactosylated solid lipid nanoparticles with cucurbitacin B improves the liver targetability. *Drug Deliv.* **17,** 114–122 (2010).
96. Sondike, S. B., Pisetsky, E. M. & Luzier, J. L. Yeast-derived Particulate β-Glucan Treatment Subverts the Suppression of Myeloid-derived Suppressor Cells by Inducing PMN-MDSC Apoptosis and M-MDSC Differentiation to APC in Cancer. *J. Immunol.* **196,** 2167–2180 (2016).
97. Tian, X. *et al.* Particulate β-glucan regulates the immunosuppression of granulocytic myeloid-derived suppressor cells by inhibiting NFIA expression. *Oncoimmunology* **4,** 1–10 (2015).
98. Lebel, M. È. *et al.* Potentiating Cancer Immunotherapy Using Papaya Mosaic Virus-Derived Nanoparticles. *Nano Lett.* **16,** 1826–1832 (2016).
99. Fernandez, A. *et al.* Inhibition of Tumor-Induced Myeloid-Derived Suppressor Cell Function by a Nanoparticulated Adjuvant. *J. Immunol.* **186,** 264–274 (2011).
100. Sun, D. *et al.* A Novel Nanoparticle Drug Delivery System: The Anti-inflammatory Activity of Curcumin Is Enhanced When Encapsulated in Exosomes. *Mol. Ther.* **18,** 1606–1614 (2010).
101. Zhao, Y. *et al.* Nano-gold corking and enzymatic uncorking of carbon nanotube cups. *J. Am. Chem. Soc.* **137,** 675–684 (2015).
102. Jeanbart, L., Kourtis, I. C., van der Vlies, A. J., Swartz, M. A. & Hubbell, J. A. 6-Thioguanine-loaded polymeric micelles deplete myeloid-derived suppressor cells and enhance the efficacy of T cell immunotherapy in tumor-bearing mice. *Cancer Immunol. Immunother.* **64,** 1033–1046 (2015).
103. Sasso, M. S. *et al.* Low dose gemcitabine-loaded lipid nanocapsules target monocytic myeloid-derived suppressor cells and potentiate cancer immunotherapy. *Biomaterials* **96,** 47–62 (2016).
104. Kong, M. *et al.* Biodegradable hollow mesoporous silica nanoparticles for regulating tumor microenvironment and enhancing antitumor efficiency. *Theranostics* **7,** 3276–3292 (2017).
105. Roth, F. *et al.* Aptamer-mediated blockade of IL4Rα triggers apoptosis of MDSCs and limits tumor progression. *Cancer Res.* **72,** 1373–1383 (2012).
106. Zilio, S. *et al.* 4PD Functionalized Dendrimers: A Flexible Tool for In Vivo Gene Silencing of Tumor-Educated Myeloid Cells. *J. Immunol.* **198,** 4166–4177 (2017).
107. Gonzalo, T. *et al.* A new potential nano-oncological therapy based on polyamino acid nanocapsules. *J. Control. Release* **169,** 10–16 (2013).
108. Lollo, G. *et al.* Polyglutamic acid-PEG nanocapsules as long circulating carriers for the delivery of docetaxel. *Eur. J. Pharm. Biopharm.* **87,** 47–54 (2014).
109. Abellan-Pose, R. *et al.* Polyaminoacid nanocapsules for drug delivery to the lymphatic system: Effect of the particle size. *Int. J. Pharm.* **509,** 107–117 (2016).
110. Borrajo, E. *et al.* Docetaxel-loaded polyglutamic acid-PEG nanocapsules for the treatment of metastatic cancer. *J. Control. Release* **238,** 263–271 (2016).
111. Vicente, S. *et al.* A Polymer/Oil Based Nanovaccine as a Single-Dose Immunization Approach. *PLoS One* **8,** 2–9 (2013).
112. Vicente, S., Goins, B. A., Sanchez, A., Alonso, M. J. & Phillips, W. T. Biodistribution and lymph node retention of polysaccharide-based immunostimulating nanocapsules. *Vaccine* **32,** 1685–1692 (2014).
113. Vicente, S. *et al.* Co-delivery of viral proteins and a TLR7 agonist from polysaccharide nanocapsules: A needle-free vaccination strategy. *J. Control.*

Release **172,** 773–781 (2013).
114. Vicente, S. *et al.* Highly versatile immunostimulating nanocapsules for specific immune potentiation. *Nanomedicine* **9,** 2273–2289 (2014).
115. Gonzalez-Aramundiz, J. V. *et al.* Rational design of protamine nanocapsules as antigen delivery carriers. *J. Control. Release* **245,** 62–69 (2017).
116. Niu, Z. *et al.* Rational design of polyarginine nanocapsules intended to help peptides overcoming intestinal barriers. *J. Control. Release* (2017).
117. Thwala, L. N. *et al.* The interaction of protamine nanocapsules with the intestinal epithelium: A mechanistic approach. *J. Control. Release* **243,** 109–120 (2016).
118. Lozano, M. V. *et al.* Polyarginine nanocapsules: A new platform for intracellular drug delivery. *J. Nanoparticle Res.* **15,** (2013).
119. Correia-Pinto, J. F., Peleteiro, M., Csaba, N., González-Fernández, Á. & Alonso, M. J. Multi-enveloping of particulated antigens with biopolymers and immunostimulant polynucleotides. *J. Drug Deliv. Sci. Technol.* **30,** 424–434 (2015).
120. Guo, Z., Peng, H., Kang, J. & Sun, D. Cell-penetrating peptides: Possible transduction mechanisms and therapeutic applications. *Biomed. Reports* 528–534 (2016).
121. Matsumoto, R. *et al.* Effects of the properties of short peptides conjugated with cell-penetrating peptides on their internalization into cells. *Sci. Rep.* **5,** 12884 (2015).
122. Mitchell, D. J., Steinman, L., Kim, D. T., Fathman, C. G. & Rothbard, J. B. Polyarginine enters cells more efficiently than other polycationic homopolymers. *J. Pept. Res.* **56,** 318–325 (2000).
123. Robison, A. D. *et al.* Polyarginine Interacts More Strongly and Cooperatively than Polylysine with Phospholipid Bilayers. *J. Phys. Chem. B* **120,** 9287–9296 (2016).
124. Lättig-Tünnemann, G. *et al.* Backbone rigidity and static presentation of guanidinium groups increases cellular uptake of arginine-rich cell-penetrating peptides. *Nat. Commun.* **2,** 453 (2011).
125. Alhakamy, N. A. & Berkland, C. J. Polyarginine Molecular Weight Determines Transfection Efficiency of Calcium Condensed Complexes. *Mol. Pharm.* **10,** 1940–1948 (2013).
126. Alhakamy, N. A., Dhar, P. & Berkland, C. J. Charge Type, Charge Spacing, and Hydrophobicity of Arginine-Rich Cell-Penetrating Peptides Dictate Gene Transfection. *Mol. Pharm.* **13,** 1047–1057 (2016).
127. Huang, Y. *et al.* Systemic Administration of siRNA via cRGD-containing Peptide. *Sci. Rep.* **5,** 1–5 (2015).
128. Yang, Y., Wolfram, J., Fang, X., Shen, H. & Ferrari, M. Polyarginine Induces an Antitumor Immune Response through Binding to Toll-Like Receptor 4. *Small* **10,** 1250–1254 (2014).
129. Niu, Z., Conejos-Sánchez, I., Griffin, B. T., O'Driscoll, C. M. & Alonso, M. J. Lipid-based nanocarriers for oral peptide delivery. *Adv. Drug Deliv. Rev.* **106,** 337–354 (2016).
130. Schwarz, U. S. & Gompper, G. Bending frustration of lipid-water mesophases based on cubic minimal surfaces. *Langmuir* **17,** 2084–2096 (2001).
131. Fong, W. K., Hanley, T. & Boyd, B. J. Stimuli responsive liquid crystals provide 'on-demand' drug delivery in vitro and in vivo. *J. Control. Release* **135,** 218–226 (2009).

132. Shearman, G. C., Ces, O., Templer, R. H. & Seddon, J. M. Inverse lyotropic phases of lipids and membrane curvature. *J. Phys. Condens. Matter* **18,** S1105–S1124 (2006).
133. Yaghmur, A. *et al.* Effects of pressure and temperature on the self-assembled fully hydrated nanostructures of monoolein-oil systems. *Langmuir* **26,** 1177–1185 (2010).
134. Qiu, H. & Ca, M. The phase diagram of the monoolein / water system : metastability and equilibrium aspects. *Biomaterials* **21,** 223–234 (2000).
135. Lee, K. W. Y., Nguyen, T. H., Hanley, T. & Boyd, B. J. Nanostructure of liquid crystalline matrix determines in vitro sustained release and in vivo oral absorption kinetics for hydrophilic model drugs. *Int. J. Pharm.* **365,** 190–199 (2009).
136. Phan, S., Fong, W. K., Kirby, N., Hanley, T. & Boyd, B. J. Evaluating the link between self-assembled mesophase structure and drug release. *Int. J. Pharm.* **421,** 176–182 (2011).
137. Fraser, S., Separovic, F. & Polyzos, A. Cubic phases of ternary amphiphile-water systems. *Eur. Biophys. J.* **39,** 83–90 (2009).
138. Kaasgaard, T. *et al.* Ordered 2-D and 3-D nanostructured amphiphile self-assembly materials stable in excess solvent. *Phys. Chem. Chem. Phys.* **8,** 4957 (2006).
139. Pouzot, M., Mezzenga, R., Guillot, S. & Glatter, O. Structural and Rheological Investigation of Fd3 mInverse Micellar Cubic Phases. *Langmuir* **23,** 9618–9628 (2007).
140. Drummond, C. J. & Fong, C. Surfactant self-assembly objects as novel drug delivery vehicles. *Curr. Opin. Colloid Interface Sci.* **4,** 449–456 (1999).
141. Clogston, J. & Caffrey, M. Controlling release from the lipidic cubic phase. Amino acids, peptides, proteins and nucleic acids. *J. Control. Release* **107,** 97–111 (2005).
142. Shah, J. C., Sadhale, Y. & Chilukuri, D. M. Cubic phase gels as drug delivery systems. *Adv. Drug Deliv. Rev.* **47,** 229–250 (2001).
143. Zhai, J., Waddington, L., Wooster, T. J., Aguilar, M. I. & Boyd, B. J. Revisiting β-casein as a stabilizer for lipid liquid crystalline nanostructured particles. *Langmuir* **27,** 14757–14766 (2011).
144. Chang, D. P., Jankunec, M., Barauskas, J., Tiberg, F. & Nylander, T. Adsorption of Lipid Liquid Crystalline Nanoparticles: Effects of Particle Composition, Internal Structure, and Phase Behavior. *Langmuir* **28,** 10688–10696 (2012).
145. Tilley, A., Dong, Y.-D., Amenitsch, H., Rappolt, M. & Boyd, B. J. Transfer of lipid and phase reorganisation in self-assembled liquid crystal nanostructured particles based on phytantriol. *Phys. Chem. Chem. Phys.* **13,** 3026–3032 (2011).
146. Libster, D., Aserin, A., Wachtel, E., Shoham, G. & Garti, N. An HII liquid crystal-based delivery system for cyclosporin A: Physical characterization. *J. Colloid Interface Sci.* **308,** 514–524 (2007).
147. Shi, C. & Pamer, E. G. Monocyte Recruitment During Infection and Inflammation. *Nat Rev Immunol* **11,** 762–774 (2014).
148. Hanson, E. T., Lewis, R. L., Auerbach, R., Thomson, J. A. & Applica-, B. Third-Generation Biomedical Materials. *Science* **295,** 1014–1017 (2002).
149. Balakrishnan, B. & Banerjee, R. Biopolymer-based hydrogels for cartilage tissue engineering. *Chem. Rev.* **111,** 4453–4474 (2011).
150. Liu, M. *et al.* Injectable hydrogels for cartilage and bone tissue engineering. *Bone*

Res. **5,** 17014 (2017).
151. Vilela, C. A. *et al.* Cartilage Repair Using Hydrogels: A Critical Review of in Vivo Experimental Designs. *ACS Biomater. Sci. Eng.* **1,** 726–739 (2015).
152. Kwee, B. J. & Mooney, D. J. Biomaterials for Skeletal Muscle Tissue Engineering. *Curr. Opin. Biotechnol.* **47,** 16–22 (2017).
153. Ostrovidov, S. *et al.* Skeletal Muscle Tissue Engineering: Methods to Form Skeletal Myotubes and Their Applications. *Tissue Eng. Part B Rev.* **20,** 403–436 (2014).
154. Tedesco, F. S., Dellavalle, A., Diaz-manera, J., Messina, G. & Cossu, G. Repairing skeletal muscle : regenerative potential of skeletal muscle stem cells. *J. Clin. Invest.* **120,** 11–19 (2010).
155. Wang, Y. X. & Rudnicki, M. A. Satellite cells, the engines of muscle repair. *Nat. Rev. Mol. Cell Biol.* **13,** 127–133 (2011).
156. Almada, A. E. & Wagers, A. J. Molecular circuitry of stem cell fate in skeletal muscle regeneration, ageing and disease. *Nat. Rev. Mol. Cell Biol.* **17,** 267–279 (2016).
157. Pittenger, M. F. Multilineage Potential of Adult Human Mesenchymal Stem Cells. *Science (80-.).* **284,** 143–147 (1999).
158. Wei, X. *et al.* Mesenchymal stem cells: a new trend for cell therapy. *Acta Pharmacol. Sin.* **34,** 747–754 (2013).
159. Caplan, A. I. Adult mesenchymal stem cells for tissue engineering versus regenerative medicine. *J. Cell. Physiol.* **213,** 341–347 (2007).
160. Trounson, A. & McDonald, C. Stem Cell Therapies in Clinical Trials: Progress and Challenges. *Cell Stem Cell* **17,** 11–22 (2015).
161. Sheridan, C. Cardiac stem cell therapies inch toward clinical litmus test. *Nat. Biotechnol.* **31,** 5–6 (2013).
162. Jin, R. & Dijkstra, P. J. Hydrogels for Tissue Engineering Applications. *Biomed. Appl. Hydrogels Handb.* **c,** 203–225 (2010).
163. Caliari, S. R. & Burdick, J. A. A practical guide to hydrogels for cell culture. *Nat. Methods* **13,** 405–414 (2016).
164. Li, J. & Mooney, D. J. Designing hydrogels for controlled drug delivery. *Nat. Rev. Mater.* **1,** 16071 (2016).
165. Ye, K. Y. & Black, L. D. Strategies for tissue engineering cardiac constructs to affect functional repair following myocardial infarction. *J. Cardiovasc. Transl. Res.* **4,** 575–591 (2011).
166. Spotnitz, W. D. Fibrin sealant: Past, present, and future: A brief review. *World Journal of Surgery* **34,** 632–634 (2010).
167. Spotnitz, W. D. & Burks, S. Hemostats, sealants, and adhesives III: A new update as well as cost and regulatory considerations for components of the surgical toolbox. *Transfusion* **52,** 2243–2255 (2012).
168. Spotnitz, W. D. & Burks, S. State-of-the-art review: Hemostats, sealants, and adhesives II: Update as well as how and when to use the components of the surgical toolbox. *Clin. Appl. Thromb. Hemost.* **16,** 497–514 (2010).
169. Yanke, A. B. & Chubinskaya, S. The state of cartilage regeneration: current and future technologies. *Curr. Rev. Musculoskelet. Med.* **8,** 1–8 (2015).
170. Brown, A. C. & Barker, T. H. Fibrin-based biomaterials: Modulation of macroscopic properties through rational design at the molecular level. *Acta Biomater.* **10,** 1502–1514 (2014).

171. Weisel, J. W. & Litvinov, R. I. Mechanisms of fibrin polymerization and clinical implications. *Blood* **121,** 1712–1719 (2013).
172. Li, Y., Meng, H., Liu, Y. & Lee, B. P. Fibrin gel as an injectable biodegradable scaffold and cell carrier for tissue engineering. *Sci. World J.* **2015,** (2015).
173. Branco da Cunha, C. *et al.* Influence of the stiffness of three-dimensional alginate/collagen-I interpenetrating networks on fibroblast biology. *Biomaterials* **35,** 8927–8936 (2014).
174. Rault, I., Frei, V., Herbage, D., Abdul-Malak, N. & Huc, A. Evaluation of different chemical methods for cross-linking collagen gel, films and sponges. *J. Mater. Sci. Mater. Med.* 215–221 (1996).
175. Chevallay, B., Abdul-Malak, N. & Herbage, D. Mouse fibroblasts in long-term culture within collagen three-dimensional scaffolds: Influence of crosslinking with diphenylphosphorylazide on matrix reorganization, growth, and biosynthetic and proteolytic activities. *J. Biomed. Mater. Res.* **49,** 448–459 (1999).
176. McCance, K. L. *et al.* Collagen Structure and Stability. *Annu Rev Biochem* **78,** 929–958 (2009).
177. Hulmes, D. J. S. Building Collagen Molecules, Fibrils, and Suprafibrillar Structures. *J. Struct. Biol.* **137,** 2–10 (2002).
178. Mouw, J. K., Ou, G. & Weaver, V. M. Extracellular matrix assembly: a multiscale deconstruction. *Nat. Rev. Mol. Cell Biol.* **15,** 771–785 (2014).
179. Hulmes, D. J. S. Collagen Diversity, Synthesis and Assembly. *Collagen Struct Mech (ed. Frazt) Springer* 15–47 (2008).
180. Kon, E., Filardo, G., Roffi, A., Andriolo, L. & Marcacci, M. New trends for knee cartilage regeneration: From cell-free scaffolds to mesenchymal stem cells. *Curr. Rev. Musculoskelet. Med.* **5,** 236–243 (2012).
181. Jaklenec, A., Stamp, A., Deweerd, E., Sherwin, A. & Langer, R. Progress in the Tissue Engineering and Stem Cell Industry 'Are we there yet?' *Tissue Eng. Part B Rev.* **18,** 155–166 (2012).
182. Sun, J.-Y. *et al.* Highly stretchable and tough hydrogels. *Nature* **489,** 133–136 (2012).
183. Andersen, T., Auk-Emblem, P. & Dornish, M. 3D Cell Culture in Alginate Hydrogels. *Microarrays* **4,** 133–161 (2015).
184. Augst, A. D., Kong, H. J. & Mooney, D. J. Alginate hydrogels as biomaterials. *Macromol. Biosci.* **6,** 623–633 (2006).
185. Rowley, J. A., Madlambayan, G. & Mooney, D. J. Alginate hydrogels as synthetic extracellular matrix materials. *Biomaterials* **20,** 45–53 (1999).
186. Sun, J. & Tan, H. Alginate-based biomaterials for regenerative medicine applications. *Materials (Basel).* **6,** 1285–1309 (2013).
187. Lo, K. W.-H., Ulery, B. D., Ashe, K. M. & Laurencin, C. T. Studies of bone morphogenetic protein-based surgical repair. *Adv. Drug Deliv. Rev.* **64,** 1277–91 (2012).
188. Kang, D. G., Hsu, W. K. & Lehman, R. A. Complications Associated With Bone Morphogenetic Protein in the Lumbar Spine. *Orthopedics* **40,** e229–e237 (2017).
189. Epstein, N. Complications due to the use of BMP/INFUSE in spine surgery: The evidence continues to mount. *Surg. Neurol. Int.* **4,** 343 (2013).
190. DeVine, J., Dettori, J., France, J., Brodt, E. & McGuire, R. The use of rhBMP in spine surgery: is there a cancer risk? *Evid. Based. Spine. Care. J.* **3,** 35–41 (2012).

191. Raisin, S., Belamie, E. & Morille, M. Non-viral gene activated matrices for mesenchymal stem cells based tissue engineering of bone and cartilage. *Biomaterials* **104,** 223–237 (2016).
192. Im, G. I., Kim, H. J. & Lee, J. H. Chondrogenesis of adipose stem cells in a porous PLGA scaffold impregnated with plasmid DNA containing SOX trio (SOX-5,-6 and -9) genes. *Biomaterials* **32,** 4385–4392 (2011).
193. Umebayashi, M., Sumita, Y., Kawai, Y., Watanabe, S. & Asahina, I. Gene-Activated Matrix Comprised of Atelocollagen and Plasmid DNA Encoding BMP4 or Runx2 Promotes Rat Cranial Bone Augmentation. *Biores. Open Access* **4,** 164–174 (2015).
194. Lui, K. O. *et al.* Driving vascular endothelial cell fate of human multipotent Isl1 + heart progenitors with VEGF modified mRNA. *Cell Res.* **23,** 1172–1186 (2013).
195. Elangovan, S. *et al.* Chemically modified RNA activated matrices enhance bone regeneration. *J. Control. Release* **218,** 22–28 (2015).
196. Balmayor, E. R. *et al.* Modified mRNA for BMP-2 in Combination with Biomaterials Serves as a Transcript-Activated Matrix for Effectively Inducing Osteogenic Pathways in Stem Cells. *Stem Cells Dev.* **26,** 25–34 (2016).
197. Khorsand, B. *et al.* A Comparative Study of the Bone Regenerative Effect of Chemically Modified RNA Encoding BMP-2 or BMP-9. *AAPS J.* **19,** 438–446 (2017).
198. DuFort, C. C., Paszek, M. J. & Weaver, V. M. Balancing forces: architectural control of mechanotransduction. *Nat. Rev. Mol. Cell Biol.* **12,** 308–319 (2011).
199. Yang, C., Tibbitt, M. W., Basta, L. & Anseth, K. S. Mechanical memory and dosing influence stem cell fate. *Nat. Mater.* **13,** 645–652 (2014).
200. Ross, T. D. *et al.* Integrins in mechanotransduction. *Curr. Opin. Cell Biol.* **25,** 613–618 (2013).
201. Cukierman, E. Taking Cell-Matrix Adhesions to the Third Dimension. *Science (80-.).* **294,** 1708–1712 (2001).
202. Das, R. K., Gocheva, V., Hammink, R., Zouani, O. F. & Rowan, A. E. Stress-stiffening-mediated stem-cell commitment switch in soft responsive hydrogels. *Nat. Mater.* **15,** 318–325 (2015).
203. Dupont, S. *et al.* Role of YAP/TAZ in mechanotransduction. *Nature* **474,** 179–183 (2011).
204. Griffith, L. G. & Swartz, M. A. Capturing complex 3D tissue physiology in vitro. *Nat. Rev. Mol. Cell Biol.* **7,** 211–224 (2006).
205. Alonso-Nocelo, M. *et al.* Selective interaction of PEGylated polyglutamic acid nanocapsules with cancer cells in a 3D model of a metastatic lymph node. *J. Nanobiotechnology* **14,** 51 (2016).
206. Mammoto, A., Mammoto, T. & Ingber, D. E. Mechanosensitive mechanisms in transcriptional regulation. *J. Cell Sci.* **125,** 3061–3073 (2012).
207. Humphrey, J. D., Dufresne, E. R. & Schwartz, M. A. Mechanotransduction and extracellular matrix homeostasis. *Nat. Rev. Mol. Cell Biol.* **15,** 802–812 (2014).
208. Khetan, S. *et al.* Degradation-mediated cellular traction directs stem cell fate in covalently crosslinked three-dimensional hydrogels. *Nat. Mater.* **12,** 458–465 (2013).
209. Cosgrove, B. D. *et al.* N-cadherin adhesive interactions modulate matrix mechanosensing and fate commitment of mesenchymal stem cells. *Nat. Mater.* **15,** 1297–1306 (2016).

Background, hypothesis, and objectives

USC
UNIVERSIDADE
DE SANTIAGO
DE COMPOSTELA

BACKGROUND

CHAPTER 1: Co-delivery of RNAi and Chemokine from Polyarginine Nanocapsules enables the modulation of Myeloid Derived Suppressor Cells

This specific activity has been based on the following background:

With regard to the pharmacological approach to achieve MDSCs targeting:

Myeloid Derived Suppressor Cells (MDSCs) constitute an immature myeloid cell population that originates from aberrant myelopoiesis in cancer-related contexts. MDSCs are highly immunosuppressive and promote T cell tolerance, angiogenesis, cancer stemness and metastasis dissemination, thereby supporting tumor growth[1]. Consequently, MDSC targeting represents a promising approach to increase the efficacy of cancer immunotherapies, especially in the case of adoptive cell transfer (ACT)[2].

One of the strategies of MDSC targeting consist on inducing their differentiation into mature myeloid cells. To this end, the modulation of the C/EBPβ pathway has proved beneficial and both shC/EBPβ and miR 142-3p have been shown to enhance the efficacy of cancer vaccination and ACT[3–5]. Given the key role of nitric oxide (NO) in MDSC-mediated immune suppression, several NOS-inhibiting compounds are under investigation to reduce MDSC immune suppressive activity. One of these compounds is AT38, which is able to decrease MDSC inhibitory activity by reducing CCL2 nitration. Nitrosylated CCL2 secreted by the tumor is unable to recruit tumor-specific cytotoxic T cells and, thus, restoring original CCL2 levels appears as another strategy to improve the efficacy of ACT[6–8].

With regard to the contribution of nanotechnology:

Among others, our lab has made significant efforts on the formulation of biomacromolecules, such as proteins and polynucleotides, with the final goal to protect them from degradation and facilitate their transport across biological barriers[9–18]. Among the different delivery carriers, our lab has pioneered the development of nanocapsules with an oily core and a polymer shell[19–23]. Nanocapsules offer a high versatility for the co-delivery of various drugs with different actions and physicochemical profiles, a strategy that is being widely explored in the field of cancer immunotherapy[24]. In general, these NCs have been used for the encapsulation of hydrophobic drugs into the hydrophobic core[25–30] or the adsorption of proteins onto the polymer shell[20,31–34]. However, there are also ways to promote the entrapment of hydrosoluble molecules within oily phases. In this sense, GMO-based mesophases are raising increasing interest due to the presence of aqueous domains within their internal nanostructure, which offers potential for slow drug delivery[35,36]. Commonly employed methods for dispersing

bulk crystalline phases yielding nanometric particles usually imply the use of formulation procedures which may represent a risk for the integrity of the drug payload[37]. Our lab has also contributed to the development of nanocapsules through mild self-emulsification methods[38], a valuable background that could be exploited for mesophase dispersion.

On the other hand, with regard to the nature of the polymer shell, polyarginine-based nanocapsules were developed in our lab in 2013[22] and since then, a number of applications including protein and vaccine delivery have been explored[21,30,39]. The selection of polyarginine as a polymeric coating has been based on its known cell penetration capacity [40,41]. Moreover, various structural investigations have shown the positive role of arginine residues in cell transfection efficiency[22,42–44]. In addition, a recent study has suggested that polyarginine guanidinium groups might also be the cause of polyarginine-mediated TLR4 activation, a fact that would support its use in cancer immunotherapy[45].

CHAPTER 2: mRNA-Activated Matrices Encoding Transcription Factors as Primers of Cell Differentiation in Tissue Engineering

With regard to the selection of hMSCs as a target:

Human Mesenchymal Stem Cells (hMSCs) are known to differentiate to multiple mesenchymal lineages[46]. They can be isolated from the bone marrow, adipose tissue, umbilical cord and other sources and successfully expanded *in vitro*[47]. For these reasons, MSCs are a valuable cell source to regenerate damaged mesenchymal tissues[48] and their use in regenerative medicine has been largely explored, either alone or in combination with biomaterials that serve as scaffolds to direct their function and facilitate their inclusion.

With regard to the use of GAMs as a material systems approach to influence hMSCs activity:

Transcription Factors (TFs) have been identified to direct cell differentiation towards specific tissue types[49–52]. In 1987, Davis et al. demonstrated that mouse fibroblasts could be converted into myoblasts by the use of a single cDNA encoding the transcription factor MyoD[53]. Likewise, TF SOX9 has been identified as the master regulator of chondrogenesis[54,55]. Given the potential of TF-mediated cell specification for tissue engineering applications, pDNA Gene Activated Matrices (GAMs) encoding pivotal TFs have been explored for musculoskeletal regeneration[56,57]. However, pDNA induces a limited forced protein expression compared to mRNA[58–61], which prompted the

development of mRNA GAMs[62–64]. Indeed, these recently explored mRNA GAMs have proved to surpass the bone regeneration capacity of their pDNA counterparts. Nonetheless, to our knowledge, these mRNA GAMs have only been explored for Growth Factors (GFs) and the potential of mRNA-based GAMs encoding TFs has not been investigated yet.

With regard to the design of fibrin-based scaffolds:

Fibrin's easy assembly into fibrillary networks makes it an attractive biopolymer for tissue engineering. It has the potential to be extracted from patient's blood, constituting an autologous scaffold and thus alleviating any risk of immune reaction[65]. In addition, fibrin has been FDA approved as a surgical sealant and has been used extensively in hemostatic materials. More importantly, some of these sealants are also being used in regenerative medicine as clot stabilizers in microfracture procedures[66–69]. Fibrin gels are very bioactive, promoting cell attachment and stimulating hydrogel remodelling, which support its use in the development of cell instructive scaffolds for stem cell differentiation and delivery[70].

CHAPTER 3: Modulation of Gene Activated Matrix mechanics enhances the 3D transfection and SOX9-directed differentiation of Mesenchymal Stem Cells

With regard to the potential of interpenetrating polymer networks (IPNs) in tissue engineering:

The physical mixture of two or more polymers with complementary properties has led to the formation of interpenetrating polymer networks (IPNs) with attractive properties for the purpose of tissue engineering. A good example is represented by the collagen-I-alginate IPNs, which take advantage of the cell-interactive features of collagen to overcome alginate's lack of adhesion ligands, while surpassing the low mechanical properties of collagen hydrogels with the easily tunable crosslinking capacity of alginate. As demonstrated at the laboratory of Prof. Mooney, collagen-I-alginate IPNs allow one to tune gel stiffness independently of gel architecture, polymer concentration or adhesion ligand density[71]. This, in turn, makes them an ideal platform to study the effect of hydrogel mechanics on cell biology.

With regard to the modulation of Gene Activated Matrices (GAMs) mechanics to boost their transfection efficiency and regenerative capacity:

Three-dimension (3D) transfection refers to cell transfection events occurring within 3D matrices where cells are embedded[72–74]. These matrices, termed Gene Activated Matrices (GAMs), consist on polymer matrices loaded with free or complexed nonviral

formulations. When considering 3D transfection efficiency, attention should be paid not only to the physicochemical characteristics of the genetic material formulations, but also to the polymer matrix itself. Matrix properties such as surface charge[75], cell adhesion, stiffness or biodegradability[76–78] are key parameters to ensure a high degree of gene transfer and hence should be carefully considered in GAM design. Consequently, understanding the process involving 3D gene transfer can help guide the development of improved GAMs as well as more efficient nonviral formulations.

On the other hand, over the past few years, mechanostransduction has regained great attention as a means to regulate cell fate conversion[79]. Differentiation of mesenchymal stem cells (MSCs) towards specific lineages has proved to be modulated by matrix stiffness and elasticity[80–82], as well as stress-relaxation[83]. In addition, an interplay between cell-matrix and cell-cell contacts has been recently shown to further impact hMSC differentiation[84]. Considering this, there is no doubt now that mechanostransduction has broad implications in the biomedical field, allowing for the generation of improved biomaterials capable to modulate diseased cells. However, given the high exploration of MSC-biomaterial interactions, tissue engineering represents the most straightforward application. In this regard, the modulation of GAM mechanics appears as a good strategy to synergistically modulate cell phenotype.

References

1. Bronte, V. *et al.* Recommendations for myeloid-derived suppressor cell nomenclature and characterization standards. *Nat. Commun.* **7,** 12150 (2016).

2. De Sanctis, F. *et al.* MDSCs in cancer: Conceiving new prognostic and therapeutic targets. *Biochim. Biophys. Acta - Rev. Cancer* **1865,** 35–48 (2016).

3. Marigo, I. *et al.* Tumor-induced tolerance and immune suppression depend on the C/EBPβ transcription factor. *Immunity* **32,** 790–802 (2010).

4. Sonda, N. *et al.* miR-142-3p Prevents Macrophage Differentiation during Cancer-Induced Myelopoiesis. *Immunity* **38,** 1236–1249 (2013).

5. Zilio, S. *et al.* 4PD Functionalized Dendrimers: A Flexible Tool for In Vivo Gene Silencing of Tumor-Educated Myeloid Cells. *J. Immunol.* **198,** 4166–4177 (2017).

6. Molon, B. *et al.* Chemokine nitration prevents intratumoral infiltration of antigen-specific T cells. *J. Exp. Med.* **208,** 1949–1962 (2011).

7. Lesokhin, A. M. *et al.* Monocytic CCR2 + myeloid-derived suppressor cells promote immune escape by limiting activated CD8 T-cell infiltration into the tumor microenvironment. *Cancer Res.* **72,** 876–886 (2012).

8. Molon, B., Viola, A. & Bronte, V. Smoothing T cell roads to the tumor: Chemokine post-translational regulation. *Oncoimmunology* **1,** 390–392 (2012).

9. Blanco, M. D. & Alonso, M. J. Development and characterization of protein-loaded poly(lactide-co-glycolide) nanospheres. *European Journal of Pharmaceutics and Biopharmaceutics* **43,** 287–294 (1997).

10. Calvo, P., Remuñán-López, C., Vila-Jato, J. L. & Alonso, M. J. Novel hydrophilic chitosan-polyethylene oxide nanoparticles as protein carriers. *J. Appl. Polym. Sci.* **63,** 125–132 (1997).

11. Quellec, P. Protein encapsulation within polyethylene glycol-coated nanospheres. I. Physicochemical characterization. *J. Biomed. Mater. Res.* **15,** 274–54 (1998).

12. Fernánzed-Urrusuno, R., Calvo, P., Remuñán-López, C., Vila-Jato, J. L. & Alonso, M. J. Enhancement of nasal absorption of insulin using chitosan nanoparticles. *Pharm. Res.* **16,** 1576–81 (1999).

13. Sánchez, A., Tobío, M., González, L., Fabra, A. & Alonso, M. J. Biodegradable micro- and nanoparticles as long-term delivery vehicles for interferon-alpha. *Eur. J. Pharm. Sci.* **18,** 221–229 (2003).

14. García-Fuentes, M., Torres, D. & Alonso, M. J. Design of lipid nanoparticles for the oral delivery of hydrophilic macromolecules. *Colloids Surfaces B Biointerfaces* **27,** 159–168 (2003).

15. Garcia-Fuentes, M., Torres, D. & Alonso, M. J. New surface-modified lipid nanoparticles as delivery vehicles for salmon calcitonin. *Int. J. Pharm.* **296,** 122–

132 (2005).

16. Vila, A. *et al.* PLA-PEG particles as nasal protein carriers: The influence of the particle size. *Int. J. Pharm.* **292,** 43–52 (2005).

17. Teijeiro-osorio, D., Remun, C. & Alonso, M. J. New Generation of Hybrid Poly/Oligosaccharide Nanoparticles as Carriers for the Nasal Delivery of Macromolecules New Generation of Hybrid Poly / Oligosaccharide Nanoparticles as Carriers for the Nasal Delivery of Macromolecules. *Biomacromolecules* **10,** 243–249 (2009).

18. Csaba, N., Köping-Höggård, M. & Alonso, M. J. Ionically crosslinked chitosan/tripolyphosphate nanoparticles for oligonucleotide and plasmid DNA delivery. *Int. J. Pharm.* **382,** 205–214 (2009).

19. Thwala, L. N. *et al.* The interaction of protamine nanocapsules with the intestinal epithelium: A mechanistic approach. *J. Control. Release* **243,** 109–120 (2016).

20. Gonzalez-Aramundiz, J. V. *et al.* Rational design of protamine nanocapsules as antigen delivery carriers. *J. Control. Release* **245,** 62–69 (2017).

21. Niu, Z. *et al.* Rational design of polyarginine nanocapsules intended to help peptides overcoming intestinal barriers. *J. Control. Release* (2017). doi:10.1016/j.jconrel.2017.02.024

22. Lozano, M. V. *et al.* Polyarginine nanocapsules: A new platform for intracellular drug delivery. *J. Nanoparticle Res.* **15,** (2013).

23. Prego, C., Torres, D. & Alonso, M. J. Chitosan nanocapsules: A new carrier for nasal peptide delivery. *J. Drug Deliv. Sci. Technol.* **16,** 331–337 (2006).

24. Shi, J., Kantoff, P. W., Wooster, R. & Farokhzad, O. C. Cancer nanomedicine: progress, challenges and opportunities. *Nat. Rev. Cancer* **17,** 20–37 (2016).

25. Abellan-Pose, R. *et al.* Polyaminoacid nanocapsules for drug delivery to the lymphatic system: Effect of the particle size. *Int. J. Pharm.* **509,** 107–117 (2016).

26. Borrajo, E. *et al.* Docetaxel-loaded polyglutamic acid-PEG nanocapsules for the treatment of metastatic cancer. *J. Control. Release* **238,** 263–271 (2016).

27. Alonso-Nocelo, M. *et al.* Selective interaction of PEGylated polyglutamic acid nanocapsules with cancer cells in a 3D model of a metastatic lymph node. *J. Nanobiotechnology* **14,** 51 (2016).

28. Lollo, G. *et al.* Polyglutamic acid-PEG nanocapsules as long circulating carriers for the delivery of docetaxel. *Eur. J. Pharm. Biopharm.* **87,** 47–54 (2014).

29. Gonzalo, T. *et al.* A new potential nano-oncological therapy based on polyamino acid nanocapsules. *J. Control. Release* **169,** 10–16 (2013).

30. Reimondez-Troitiño, S. *et al.* Polymeric nanocapsules: a potential new therapy for corneal wound healing. *Drug Deliv. Transl. Res.* **6,** 708–721 (2016).

31. Vicente, S. *et al.* A Polymer/Oil Based Nanovaccine as a Single-Dose Immunization Approach. *PLoS One* **8,** 2–9 (2013).

32. Vicente, S., Goins, B. A., Sanchez, A., Alonso, M. J. & Phillips, W. T. Biodistribution and lymph node retention of polysaccharide-based immunostimulating nanocapsules. *Vaccine* **32,** 1685–1692 (2014).

33. Vicente, S. *et al.* Co-delivery of viral proteins and a TLR7 agonist from polysaccharide nanocapsules: A needle-free vaccination strategy. *J. Control. Release* **172,** 773–781 (2013).

34. Vicente, S. *et al.* Highly versatile immunostimulating nanocapsules for specific immune potentiation. *Nanomedicine* **9,** 2273–2289 (2014).

35. Drummond, C. J. & Fong, C. Surfactant self-assembly objects as novel drug delivery vehicles. *Curr. Opin. Colloid Interface Sci.* **4,** 449–456 (1999).

36. Clogston, J. & Caffrey, M. Controlling release from the lipidic cubic phase. Amino acids, peptides, proteins and nucleic acids. *J. Control. Release* **107,** 97–111 (2005).

37. Chang, D. P., Jankunec, M., Barauskas, J., Tiberg, F. & Nylander, T. Adsorption of Lipid Liquid Crystalline Nanoparticles: Effects of Particle Composition, Internal Structure, and Phase Behavior. *Langmuir* **28,** 10688–10696 (2012).

38. Jakubiak, P. *et al.* Solvent-free protamine nanocapsules as carriers for mucosal delivery of therapeutics. *Eur. Polym. J.* **93,** 695–705 (2017).

39. Lollo, G. *et al.* Polyarginine Nanocapsules as a Potential Oral Peptide Delivery Carrier. *J. Pharm. Sci.* **106,** 611–618 (2017).

40. Guo, Z., Peng, H., Kang, J. & Sun, D. Cell-penetrating peptides: Possible transduction mechanisms and therapeutic applications. *Biomed. Reports* 528–534 (2016).

41. Matsumoto, R. *et al.* Effects of the properties of short peptides conjugated with cell-penetrating peptides on their internalization into cells. *Sci. Rep.* **5,** 12884 (2015).

42. Alhakamy, N. A. & Berkland, C. J. Polyarginine Molecular Weight Determines Transfection Efficiency of Calcium Condensed Complexes. *Mol. Pharm.* **10,** 1940–1948 (2013).

43. Alhakamy, N. A., Dhar, P. & Berkland, C. J. Charge Type, Charge Spacing, and Hydrophobicity of Arginine-Rich Cell-Penetrating Peptides Dictate Gene Transfection. *Mol. Pharm.* **13,** 1047–1057 (2016).

44. Huang, Y. *et al.* Systemic Administration of siRNA via cRGD-containing Peptide. *Sci. Rep.* **5,** 1–5 (2015).

45. Yang, Y., Wolfram, J., Fang, X., Shen, H. & Ferrari, M. Polyarginine Induces an Antitumor Immune Response through Binding to Toll-Like Receptor 4. *Small* **10,** 1250–1254 (2014).

46. Pittenger, M. F. Multilineage Potential of Adult Human Mesenchymal Stem Cells. *Science* **284,** 143–147 (1999).

47. Wei, X. *et al.* Mesenchymal stem cells: a new trend for cell therapy. *Acta Pharmacol. Sin.* **34,** 747–754 (2013).

48. Caplan, A. I. Adult mesenchymal stem cells for tissue engineering versus regenerative medicine. *J. Cell. Physiol.* **213,** 341–347 (2007).

49. Rackham, O. J. L. *et al.* A predictive computational framework for direct reprogramming between human cell types. *Nat. Genet.* **48,** 331–335 (2016).

50. Hikichi, T. *et al.* Transcription factors interfering with dedifferentiation induce cell type-specific transcriptional profiles. *Proc. Natl. Acad. Sci.* **110,** 6412–6417 (2013).

51. Almalki, S. G. & Agrawal, D. K. Key transcription factors in the differentiation of mesenchymal stem cells. *Differentiation* **92,** 41–51 (2016).

52. Yamamizu, K. *et al.* Identification of transcription factors for lineage-specific ESC differentiation. *Stem Cell Reports* **1,** 545–559 (2013).

53. Davis, R. L., Weintraub, H. & Lassar, A. B. Expression of a single transfected cDNA converts fibroblasts to myoblasts. *Cell* **51,** 987–1000 (1987).

54. Dy, P. *et al.* Sox9 Directs Hypertrophic Maturation and Blocks Osteoblast Differentiation of Growth Plate Chondrocytes. *Dev. Cell* **22,** 597–609 (2012).

55. Bi, W., Deng, J. M., Zhang, Z., Behringer, R. R. & Crombrugghe, B. De. Sox9 is required for cartilage formation. *Nat. Genet.* **22,** 85–89 (1999).

56. Im, G. I., Kim, H. J. & Lee, J. H. Chondrogenesis of adipose stem cells in a porous PLGA scaffold impregnated with plasmid DNA containing SOX trio (SOX-5,-6 and -9) genes. *Biomaterials* **32,** 4385–4392 (2011).

57. Umebayashi, M., Sumita, Y., Kawai, Y., Watanabe, S. & Asahina, I. Gene-Activated Matrix Comprised of Atelocollagen and Plasmid DNA Encoding BMP4 or Runx2 Promotes Rat Cranial Bone Augmentation. *Biores. Open Access* **4,** 164–174 (2015).

58. Quabius, E. S. & Krupp, G. Synthetic mRNAs for manipulating cellular phenotypes: An overview. *N. Biotechnol.* **32,** 229–235 (2015).

59. Mandal, P. K. & Rossi, D. J. Reprogramming human fibroblasts to pluripotency using modified mRNA. *Nat. Protoc.* **8,** 568–582 (2013).

60. Andries, O. *et al.* Comparison of the gene transfer efficiency of mRNA/GL67 and pDNA/GL67 complexes in respiratory cells. *Mol. Pharm.* **9,** 2136–2145 (2012).

61. Zou, S., Scarfo, K., Nantz, M. H. & Hecker, J. G. Lipid-mediated delivery of RNA is more efficient than delivery of DNA in non-dividing cells. *Int. J. Pharm.* **389,** 232–243 (2010).

62. Elangovan, S. *et al.* Chemically modified RNA activated matrices enhance bone

regeneration. *J. Control. Release* **218,** 22–28 (2015).

63. Balmayor, E. R. *et al.* Modified mRNA for BMP-2 in Combination with Biomaterials Serves as a Transcript-Activated Matrix for Effectively Inducing Osteogenic Pathways in Stem Cells. *Stem Cells Dev.* **26,** 25–34 (2016).

64. Khorsand, B. *et al.* A Comparative Study of the Bone Regenerative Effect of Chemically Modified RNA Encoding BMP-2 or BMP-9. *AAPS J.* **19,** 438–446 (2017).

65. Ye, K. Y. & Black, L. D. Strategies for tissue engineering cardiac constructs to affect functional repair following myocardial infarction. *J. Cardiovasc. Transl. Res.* **4,** 575–591 (2011).

66. Spotnitz, W. D. Fibrin sealant: Past, present, and future: A brief review. *World Journal of Surgery* **34,** 632–634 (2010).

67. Spotnitz, W. D. & Burks, S. Hemostats, sealants, and adhesives III: A new update as well as cost and regulatory considerations for components of the surgical toolbox. *Transfusion* **52,** 2243–2255 (2012).

68. Spotnitz, W. D. & Burks, S. State-of-the-art review: Hemostats, sealants, and adhesives II: Update as well as how and when to use the components of the surgical toolbox. *Clin. Appl. Thromb. Hemost.* **16,** 497–514 (2010).

69. Yanke, A. B. & Chubinskaya, S. The state of cartilage regeneration: current and future technologies. *Curr. Rev. Musculoskelet. Med.* **8,** 1–8 (2015).

70. Brown, A. C. & Barker, T. H. Fibrin-based biomaterials: Modulation of macroscopic properties through rational design at the molecular level. *Acta Biomater.* **10,** 1502–1514 (2014).

71. Branco da Cunha, C. *et al.* Influence of the stiffness of three-dimensional alginate/collagen-I interpenetrating networks on fibroblast biology. *Biomaterials* **35,** 8927–8936 (2014).

72. Padmashali, R. M. & Andreadis, S. T. Engineering fibrinogen-binding VSV-G envelope for spatially- and cell-controlled lentivirus delivery through fibrin hydrogels. *Biomaterials* **32,** 3330–3339 (2011).

73. Raut, S. D., Lei, P., Padmashali, R. M. & Andreadis, S. T. Fibrin-mediated lentivirus gene transfer: Implications for lentivirus microarrays. *J. Control. Release* **144,** 213–220 (2010).

74. Lei, P., Padmashali, R. M. & Andreadis, S. T. Cell-controlled and spatially arrayed gene delivery from fibrin hydrogels. *Biomaterials* **30,** 3790–3799 (2009).

75. Zhang, H., Lee, M. Y., Hogg, M. G., Dordick, J. S. & Sharfstein, S. T. High-throughput transfection of interfering RNA into a 3D cell-culture chip. *Small* **8,** 2091–2098 (2012).

76. Dhaliwal, A., Oshita, V. & Segura, T. Transfection in the third dimension. *Integr Biol* **5,** 1206–1216 (2013).

77. Shepard, J. A., Huang, A., Shikanov, A. & Shea, L. D. Balancing cell migration with matrix degradation enhances gene delivery to cells cultured three-dimensionally within hydrogels. *Journal of Controlled Release* **146,** 128–135 (2010).

78. Shiva, G., Talar, T. & Segura, T. Utilizing Cell-matrix Interactions to Modulate Gene Transfer to Stem Cells Inside Hyaluronic Acid Hydrogels. *Mol. Pharm.* **8,** 1582–1591 (2011).

79. Janmey, P. A. *et al.* From tissue mechanics to transcription factors. *Differenciation* **86,** 112–120 (2013).

80. Engler, A. J., Sen, S., Sweeney, H. L. & Discher, D. E. Matrix Elasticity Directs Stem Cell Lineage Specification. *Cell* **126,** 677–689 (2006).

81. Clause, K. C. . L. L. J. . T. K. Directed stem cell differentiation: the role of physical forces. **17,** 48–54 (2012).

82. Guilak, F., Cohen, D. & Estes, B. Control of stem cell fate by physical interactions with the extracellular matrix. *Cell Stem Cell* **5,** 17–26 (2009).

83. Chaudhuri, O. *et al.* Hydrogels with tunable stress relaxation regulate stem cell fate and activity. *Nat. Mater.* **15,** 326–334 (2015).

84. Mao, A. S., Shin, J. W. & Mooney, D. J. Effects of substrate stiffness and cell-cell contact on mesenchymal stem cell differentiation. *Biomaterials* **98,** 184–191 (2016).

HYPOTHESIS

CHAPTER 1: Co-delivery of RNAi and Chemokine from Polyarginine Nanocapsules enables the modulation of Myeloid Derived Suppressor Cells

H1. Nanoemulsions (NE) based on glycerol monooleate (GMO) mesophases can be prepared by a mild self-emulsifying method and be used to encapsulate protein and peptide drugs.

H2. GMO NEs can be coated with the cationic polymer polyarginine, thereby forming nanocapsules (NCs) onto which RNA molecules can be associated and further protected by the addition of extra polymeric coating layers (polyarginine, sodium hyaluronate).

H3. The nanocomplexation of RNA sequences (miR 142-3p and shCEBP/β) in polyarginine nanocapsules can promote their cell penetration and induce the differentiation of Myeloid Derived Suppressor Cells (MDSCs) towards a non-immunosuppressive phenotype.

H4. The natural tropism of the nanosystems represents a way of passive targeting to tumor and spleen, where MDSCs accumulate. This passive targeting can be improved by promoting the recruitment of the monocyte-macrophagic MDSC fraction through the inclusion of the chemokine CCL2 in the NCs.

CHAPTER 2: mRNA-Activated Matrices Encoding Transcription Factors as Primers of Cell Differentiation in Tissue Engineering

H1. Polymer matrices loaded with nanocomplexed mRNA induce an efficient forced protein expression in encapsulated Human Mesenchymal Stem Cells (hMSCs).

H2. mRNA matrices encoding pivotal transcription factors (TF) can be used to direct hMSC specification more efficiently than previously explored pDNA matrices.

H3. This mRNA-induced hMSC specification can be further modulated through mRNA dose, matrix composition and mechanical properties.

CHAPTER 3: Modulation of Gene Activated Matrix mechanics enhances the 3D transfection and SOX9-directed differentiation of Mesenchymal Stem Cells

H1. IPN composition and mechanical properties can affect the transfection efficiency of mRNA- and pDNA- activated matrices.

H2. IPN mechanical properties can be tuned to enhance SOX9 mRNA-driven hMSC specification towards chondroblasts.

OBJECTIVES

CHAPTER 1: Co-delivery of RNAi and Chemokine from Polyarginine Nanocapsules enables the modulation of Myeloid Derived Suppressor Cells

The main goal of this work was to develop a multifunctional nanocapsular system capable of co-encapsulating immunomodulatory peptide and RNA drugs intended to revert the immunosuppressive activity of Myeloid Derived Suppressor Cells (MDSCs) in the context of cancer immunotherapy. This goal has been associated to the following practical specific objectives:

O1. To design and develop a Glycerol Monooleate-based nanoemulsion (GMO NE) by a mild self-emulsifying method, capable of encapsulating the chemoattractant peptide CCL2.

O2. To design and develop polyarginine nanocapsules (NCs) based on the use of the optimized GMO NE, and to associate RNA molecules to the NCs shell.

O3. To design and develop multilayer NCs having a polyarginine/RNA/sodium hyaluronate sandwich-like structure that protects RNA from enzymatic degradation.

O4. To evaluate the cytotoxicity, cell uptake and transfection efficiency of RNA-loaded systems and the chemoattracting capacity of CCL2-loaded NCs.

CHAPTER 2: mRNA-Activated Matrices Encoding Transcription Factors as Primers of Cell Differentiation in Tissue Engineering

The principal aim of this research was to develop a new kind of mRNA Gene Activated Matrices (GAMs) encoding pivotal Transcription Factors (TFs) and to explore their potential for tissue engineering applications compared to traditional TF pDNA GAMs.

O1. To design, synthesize and test In vitro Transcribed (IVT) mRNAs encoding reporter sequences (Yellow Fluorescence Protein, YFP) and pivotal Transcription Factors (SOX9) for MSC specification.

O2. To develop biocompatible Gene Activated Matrices (GAMs) loaded with nanocomplexed mRNA encoding YFP and SOX9, and characterize their transfection efficiency and gene expression kinetics in human Mesenchymal Stem Cells (hMSCs) compared to traditional pDNA-activated GAMs.

O3. To evaluate the cytotoxicity, cell proliferation and bioactivity of the GAMs and to carry out chondrogenesis (SOX9 GAMs) and myogenesis (MYOD GAMs) differentiation assays by determining the expression of tissue specific markers by qRT-PCR, histology and immunohistochemistry.

CHAPTER 3: Modulation of Gene Activated Matrix mechanics enhances the 3D transfection and SOX9-directed differentiation of Mesenchymal Stem Cells

The main goal of this work was to elaborate a set of collagen-I-alginate IPNs with different stiffness and cell adhesion properties to check the effect of these two parameters on the 3D transfection and chondrogenesis of human Mesenchymal Stem Cells (hMSCs).

O1. To develop a set of collagen-I-alginate IPNs with different stiffness and cell adhesion properties.

O2. To activate these IPNs with nanocomplexed SOX9 mRNA and pDNA and study the influence of IPN mechanics and composition and the type of genetic material on the transfection efficiency of encapsulated hMSCs.

O3. To carry out chondrogenesis differentiation assays in SOX9 mRNA IPNs by determining the expression of tissue specific markers by qRT-PCR and immunohistochemistry and to relate the chondrogenesis capacity of SOX9 mRNA IPNs to SOX9 overexpression and IPN mechanical properties.

Chapter 1

USC
UNIVERSIDADE
DE SANTIAGO
DE COMPOSTELA

CHAPTER 1

RNAi and Chemokine-loaded Polyarginine Nanocapsules Enable the Modulation of Myeloid Derived Suppressor Cells

This work has been done in collaboration with the University of Padova (Italy), the University of Verona (Italy) and with Monash University (Australia)

ABSTRACT

Myeloid Derived Suppressor Cells (MDSCs), immunosuppressive cells that promote tumor growth, represent an attractive target in cancer immunotherapy. However, the clinical success of this strategy is limited by the lack of efficient drug delivery vehicles targeting this cell compartment. The objective of this work was to develop a delivery carrier named as polyarginine nanocapsules, with the capacity to co-encapsulate two types of immunomodulatory drugs aimed to revert MDSC-mediated immunosuppression. The chemokine CCL2, intended to attract monocytic-macrophagic MDSCs, was encapsulated within the L2 inverse micellar aqueous domains of the lipid core of these nanocapsules. Two different RNAi sequences that modulate the C/EBPβ pathway, shC/EBPβ and miR 142-3p, were successfully associated to their cationic surface. These RNAi sequences were subsequently layered with polyarginine and hyaluronic acid, thereby creating multi-layered assemblies that protected them and facilitated their targeted delivery. shC/EBPβ-loaded nanocapsules led to the downregulation of C/ EBPβ levels in tumor and spleen, preventing monocyte differentiation into tumor-associated macrophages. Additionally, the encapsulation of CCL2 within the nanocapsules was found to induce a potent macrophage chemoattraction that could be used to direct the therapy to the most suppressive cell subsets. In conclusion, the polyarginine nanocapsules described here are efficient vehicles for the co-delivery of proteins and RNA and are potential candidates for the modulation of MDSCs.

Key words: Nanocapsules, RNAi, C/EBPβ, CCL2, MDSCs

USC
UNIVERSIDADE
DE SANTIAGO
DE COMPOSTELA

1. Introduction

Emergency myelopoiesis is a defense mechanism that helps eliminate infectious agents and other potential threats, however, sustained aberrant myelopoiesis in cancer-related contexts results in the accumulation of myeloid derived suppressor cells (MDSCs), immature myeloid cells that impair T cell activity.[1] MDSCs include two major subsets: polymorphonuclear (PMN) and monocytic (M)-MDSCs, both supporting tumor growth by inducing tumor tolerance and boosting angiogenesis, cancer stemness and metastasis dissemination.[2] For this reason, MDSC targeting represents a promising approach to increase the efficacy of cancer immunotherapies, especially in the case of adoptive T cell transfer (ACT).[3–5]

Several molecular and biochemical hallmarks are associated with MDSCs and could be used as pharmacological targets to modulate their function. Among the different targets, C/EBPβ transcription factor (TF) holds a special interest since it is a prominent regulator of the tolerogenic and immunesuppressive environment induced by cancer.[6] During tumor-induced myelopoiesis, C/EBPβ forms a feedback loop with miR-142-3p promoting myeloid cell differentiation towards immunosuppressive macrophages.[7] Bearing this in mind, some authors have explored the use of RNAi-linked poly(amidoamine) (PAMAM) dendrimers and proved that both, absence of C/EBPβ and miR-142-3p overexpression are able to revert tumor-induced tolerance and provide therapeutic benefit in tumor-bearing mice.[8] However, despite these promising results, to our knowledge, this is the only work exploring RNAi-based therapies to target the C/EBPβ pathway in MDSCs.

On the other hand, chemokine targeting is another valuable therapeutic strategy to modulate the tumor immune infiltrate and enhance the immune-mediated rejection of cancer.[9] In particular, the targeting of chemokine CCL2, secreted by the majority of solid cancers, has been extensively investigated.[10–14] The CCL2-CCR2 axis is implicated in the migration of MDSCs to the tumor,[15] with a preferential effect on the monocytic subset,[10,16,17] and this MDSCs accumulation has been shown to hamper CD8+ T cell recruitment, thus limiting the efficacy of cancer immunotherapy.[18,19] Moreover, CCL2 is nitrated/nitrosylated by reactive nitrogen species produced by the tumor, impeding its ability to attract tumor-specific cytotoxic T cells (CTLs) but maintaining its capability to recruit myeloid cells, further promoting the mechanism of tumor escape.[18,20,21] From a pharmaceutical perspective, chemotactic signals have been successfully employed in various cancer vaccination strategies to attract host immune cells to drug delivery devices and help direct adaptive immune responses.[22–24]

The information available regarding the use of cationic polymers for RNA condensation and delivery highlights the value of polyarginine based on its good biocompatibility and its transcytotic and endosomal scape abilities.[25] In addition, recent works have

underlined the capacity of polyarginine and other cationic polymers to induce antitumor responses mediated by MDSCs modulation, thereby acting as TLR4 agonists.[26–29] These attractive properties of polyarginine should be linked to the previous experience of our research group on its use to construct multi-enveloped vaccines[30] and to facilitate intracellular drug delivery.[31–33]

Based on this background information, the goal of this work was to develop polyarginine nanocapsules particularly adapted for the co-delivery of two immunomodulatory drugs: RNAi polynucleotides with the capacity to modulate the C/EBPβ pathway, and the chemokine CCL2 intended to attract monocytes and T cells. More specifically, we have investigated two RNAi strategies involving the use of either miR 142-3p or a C/EBPβ-targeting shRNA. On the other hand, given that the monocytic-macrophagic subset is the most aggressive MDSCs population, we hypothesized that including CCL2 in our RNA-loaded nanocapsules, we could preferentially direct this therapy to the most immunosuppressive MDSCs. With this combined therapy, we also aimed to restore native CCL2 levels within the tumor in order to balance the increased ratio of nitrated/nitrosylated species and enable the adequate CTL recruitment. We further relied on the natural tropism of the nanosystems to the tumor[34] and spleen[35] of tumor-bearing mice, to promote a CCL2 release in the organs where MDSCs accumulate.[36,37]

In order to achieve the association of both, RNA and protein molecules to the nanocapsules, we took advantage of the RNA condensing capacity of the polyarginine shell and we created a glycerol-monooleate (GMO)-based core with an L2 inverse micellar phase capable of entrapping the chemokine within its aqueous domains. GMO was selected as an inner core for the formation of nanocapsules based on its capacity to form mesophases that are highly ordered, thermodynamically stable and adequate for the incorporation of hydrosoluble drugs.[38,39] These nanocapsules were additionally coated with polyarginine and hyaluronic acid to protect the RNA cargo and facilitate targeting purposes. The nanocapsules were extensively characterized in terms of their physicochemical properties and structural organization as well as with regard to their macrophages chemoattractant capacity and ability to downregulate C/EBPβ splenic and tumor levels in a mouse model of fibrosarcoma. Overall, this work describes the development and assessment of a new immunomodulatory nanovehicle capable of both, attracting myeloid cells and promoting the reversion of their immunosuppressive phenotype by modulating the C/EBPβ pathway.

2. Materials and Methods

2.1 Preparation of ovalbumin and CCL2-loaded nanocapsules

Preparation of GMO NEs through the "gel method" consisted on the preformation of a GMO cubic phase gel loaded with OVA, which was subsequently mixed with Labrasol® and dispersed in the Pluronic F127® aqueous solution. To prepare the GMO cubic gel, 5 mg of GMO (Danisco) were melted at 37-40°C and mixed with 1.67 µL of warm water (blank NEs) or the same volume of a warm solution containing 125 µg OVA (InvivoGen) (OVA-loaded NEs). The mixture was vortexed (30 s, 2000 rpm) and equilibrated for 2 days at room temperature to yield 6.7 mg of the cubic phase gel. After the equilibration process, 45 µl of Labrasol® (Gatte-fossé) (1:9 GMO:Labrasol w:w ratio) were mixed with the gel by vortexing (30 s, 2000 rpm) and the aqueous solution containing 5.75 mg Pluronic F127® (Sigma) was subsequently added. NEs were magnetically stirred for 30 min at 300 rpm and stored at 4°C until further use.

Polyarginine nanocapsules (NCs) were elaborated by the adsorption of polyarginine onto pre-formed GMO NEs. Concretely, 2.2 mL (5.75 mg) of the Pluronic F127® solution were poured over the lipid phase under magnetic stirring (5 min, 300 rpm) before adding 250 µL of poly-L-argininine hydrochloride (MW 5-15 KDa, Sigma) solution (5 mg/mL) to reach the final volume of NCs (2.5 mL). For the preparation of CCL2-loaded NCs, the GMO cubic phase gel was formed as previously described containing 0.625, 1.25 or 2.5 µg of CCL2 (Peprotech) to yield 0.25, 0.5 and 1 µg/mL CCL2-loaded NCs. Both the NEs and NCs were isolated by ultracentrifugation (1 h, 25000 rpm and 15°C) in an Ultracentrifuge Beckman Coulter ProteomeLab™ XL-A/XL-I to determine the encapsulation efficiency of the peptide payloads. All NCs were prepared in ultrapurified water (Milli-Q Plus water purification system, Millipore).

2.2 Preparation of RNA-loaded polyarginine nanocapsules

RNA-loaded NCs were prepared by incubating purified polyarginine NCs with a RNA solution (2 µg/µL) (IDT) at a theoretical polyarginine:RNA ratio of 1:1 or 2:1 (w/w), i.e. 24.7 mg/mL of NCs were loaded with 0.4 or 0.2 mg/mL of RNA. After the association, the formulation was immediately vortexed for 30 seconds and left 20 min for stabilization. RNA-loaded NCs at ratio 1:1 (w/w) were then incubated with another layer of polyarginine or with a double layer of polyarginine and hyaluronic acid to formulate: coated 1:1:1 pArg:RNA:pArg NCs or double-coated 1:1:1:6 pArg:RNA:pArg:HA NCs. NCs were lyophilized before storage. For the preparation of the polyarginine-coated system, 0.2 volumes of a polyarginine solution (2 µg/µL) were added over 1 volume of RNA-loaded polyarginine NCs, immediately mixed by vortex (30 sec, 2000 rpm), and incubated 20 min at room temperature. An extra layer of sodium hyaluronate (MW 40 KDa, Lifecore) could be added by mixing polyarginine-coated NCs with a hyaluronic acid solution (10 µg/µL) following the same protocol. Particles incorporating both active

components, chemokine and RNA, were prepared by incubating CCL2-loaded NCs with the RNA solution. All RNA-loaded NCs were prepared in RNAse free water (Life Technologies).

2.3 Physicochemical and morphological characterization of the nanocapsules

Particle mean size and polidispersity index (PDI) were determined by dynamic light scattering (DLS) and zeta potential was calculated from the eletrophoretic mobility values obtained by laser Doppler anemometry in a Nanosizer ZS® (Malvern Instruments) equipped with a red laser light beam (λ= 632.8 nm). Measurements were made at 25°C with a 1/100 (v/v) sample dilution in ultrapure water. The results shown are the mean of three successive measurements of at least three independent samples. For the evaluation of the colloidal stability of the NCs in different relevant media, NCs were diluted 1/10 (v/v) in media, incubated for the desired timeframe and further diluted 1/10 (v/v) in ultrapure water before DLS measurements. Sample morphology was assessed by transmission electron microscopy (JEOL JEM-1011). NCs were stained with osmium tetroxide, vacuum dried, and placed on cupper grids before observation.

2.4 Determination of OVA encapsulation efficiency

The encapsulation efficiency of ovalbumin in the NEs was analyzed by UPLC. UPLC analysis was conducted on an Acquity H-class system equipped with an Acquity UPLC Peptide BEH300 C18 1.7 micron, 2.1x50 mm column. Samples were analyzed using 0.1% trifluoroacetic acid (TFA) in water (Mobile Phase A) and 0.08% TFA in acetonitrile (Mobile Phase B) with the following gradient: 0 min-2%B, 1 min-70%B, 2 min-73.2%B, 4 min-73.2%B, 6 min-80%B, 7 min-2%B, 8 min-2%B. The flow rate was 0.2 mL/min and the column temperature was 60°C. Injection volume was 5 µL and detection was conducted at 214 nm. Nanoemulsions with a theoretical amount of 50 µg/mL were prepared and isolated by ultracentrifugation as previously described. Resultant supernatants and isolated fractions were diluted with 0.08% TFA acetonitrile before injection. OVA concentration was calculated based on calibration curves made in diluted supernatans and isolated fractions of blank particles. The encapsulation efficiency percentage (EE%) was referred as a mass ratio of the amount of OVA in the isolated fractions to the total amount of OVA in the complete sample.

2.5 Determination of CCL2 encapsulation efficiency

The encapsulation of CCL2 within the lipidic core of the particles was determined by a sandwich ELISA. Encapsulation efficiency was investigated in the nanoemulsions due to a high interference of polyarginine in epitope recognition when nanocapsules were assayed. Nanoemulsions with a theoretical amount of 0.25 µg/mL CCL2 were prepared and isolated by ultracentrifugation. Supernatants were diluted with PBS and CCL2 concentration was calculated from a calibration curve made in diluent (0.05% (w/v) Tween 20, 0.1% (w/v) BSA in PBS). The total amount of CCL2 was calculated by extracting

CCL2 from samples of nanocapsules with Triton X-100 before isolation. In this case, CCL2 concentration was calculated from a calibration curve made in diluent supplemented with 0.08% (w/v) Triton X-100, the final amount of Triton X-100 in extracted samples. CCL2 was detected with a secondary antibody conjugated with horseradish peroxidase (HRP) and quantification was made spectrophotometrically, after the incubation (10 min, 37°C) with HRP substrate 2,2'-azino-di-(3-ethylbenzthiazoline sulfonic acid) (ABTS). Absorbance readings were performed at 405 nm, with wavelenght correction at 650 nm, in a Multiskan FC microplate photometer (Thermo Fisher Scientific). Supernatants and total samples of blank nanoemulsions were used as blanks to subtract non -specific background signals. Percentage encapsulation efficiency was calculated as previously described.

The loading of CCL2 was calculated by dividing the total amount of encapsulated CCL2 by the total weight of nanocapsules. The total weight of nanocapsules was obtained by calculating the weight of nanocapsules after their isolation, which represents the yield of NC formation. For this, 2 mL of nanocapsules were isolated by ultracentrifugation and 500 µL of reconstituted isolated nanocapsules and 250 µL of non-isolated nanocapsules were lyophilized in previously weighted 1.5 mL tubes. Tubes were weighted after lyophilization and the yield of NC formation was obtained by dividing the mass of isolated by the mass of non-isolated nanocapsules.

2.6 Evaluation of RNA association and integrity

For the qualitative determination of the association efficiency of RNA onto the surface of the nanocapsules, samples were loaded in agarose (2% w/v in Tris Acetate-EDTA buffer) or polyacrylamide gels (15% w/v in Tris Borate-EDTA buffer) before and after the incubation with an excess of heparin for RNA displacement. Each gel lane was loaded with the same amount of RNA (from 0.4 to 1 µg), either adsorbed to the nanocapsules or displaced from their surface with heparin to check both the adsorption efficiency and integrity of the RNA. For heparin displacement, heparin was added (25:1 w:w heparin:RNA) and samples were incubated for 30 min at 37°C and 300 rpm (Incubator 1000, Heidolph). Control lanes (RNA only) were included to check for smeared bands. Gels were run for 1 h at 90 and 120 V, in a Sub -Cell GT cell 96/192 (Bio-Rad, Hercules, CA, USA) for agarose and polyacrylamide gels, respectively. Loading buffer contained 0.1% w/v glycerol, and 1x SYBR®Gold nucleic acid stain (Life Technologies, Carlsbad, CA, USA) for sample visualization. Gels were imaged with a Molecular Imager® Gel DocTM XR System (Bio-Rad). A quantification of RNA association efficiency was performed by determining the concentration of RNA in the supernatant of nanocapsules after centrifugation (20817 RCF, 1h, Centrifuge 5430R, Eppendorf). Supernatants were measured in a Nanodrop® 2000 UV-Vis Spectrophotometer (Thermo Fisher Scientific) using the supernatant of blank nanocapsules as blank. Adsorption efficiency (AE%) was then calculated based on the theoretical loading of miRNA.

2.7 *In vitro* release of OVA and RNA

OVA release was determined upon the incubation of the NEs in PBS at 1/10 dilution under horizontal shaking (Incubator 1000, Heidolph). NEs were isolated by ultracentrifugation and the concentrated isolated fraction was diluted in PBS pH 7.4 and incubated for 0, 4 and 6 h at 37°C and 300 rpm. Samples were then ultracentrifuged and supernatants were collected for UPLC analysis. RNA release assays after incubation of NCs in full human plasma, PBS or complete culture medium (DMEM 10% FBS, 100 U/mL penicillin and 100 µg/mL streptomycin) were performed with displacement assays using polyacrylamide gels. Nanocapsules were incubated with the media at various dilutions (1/10, 1/50, 1/100) for 4, 8 and 12 h at 37°C and 300 rpm under horizontal shaking. At the desired time points, samples were retrieved and a volume of diluted NCs and diluted NCs incubated with heparin corresponding to a total amount of 400-800 ng RNA were loaded in 15% polyacrylamide gels. Gel displacement assays were performed as described in section 2.6 with the exception of samples incubated in plasma. In this case, heparin incubation was performed during 30 min on ice, giving a 30 s vortex each 5 min, to avoid RNA degradation. For the same reason, electrophoresis was also performed on ice. In addition, samples were diluted at least 1/2.5 for gel loading to avoid plasma autofluorescence.

2.8 SAXS sample preparation and analysis

Bulk GMO phases were prepared with increasing GMO content. GMO was weighed into glass HPLC vials and heated at 40°C until it melted, when the appropriate amount of water was added. Mixtures were immediately vortexed and allowed to equilibrate for ≥48 h. GMO-Labrasol mixtures with increasing Labrasol content were also prepared. GMO gel was weighed into glass vials and mixed with Labrasol by vortex. Finally, nanocapsules and nanoemulsions were elaborated as previously described (Section 2.2). Bulk samples were transferred to a stainless steel paste cell (approx 2 mm diameter, 1 mm sample thickness) and sealed with Kapton tape on both sides, while dispersed nanocapsule systems were transferred to quartz capillaries (1.5 mm diameter, Charles Supper). Capillaries were then inserted into a thermostatted metal heating block controlled by a waterbath to 37±0.1 ◦C. Sample temperature was established by a thermocouple inserted into a spare sample position in the holder. Measurements were performed on the SAXS/WAXS beamLine at the Australian Synchrotron[40]. An X-ray beam with a wavelength of 0.83 Å (11 keV) was selected. The 2D SAXS patterns were collected using a Pilatus 1 M detector (170 mm ×170 mm) that was located 900 mm from the sample position. The total q range for the instrument configuration outlined above was $0.02 < q < 1.06$ $^{\circ}A^{-1}$. 2D SAXS patterns were collected for 1 s and the computer software Scatterbrain used to acquire and reduce the 2D patterns to 1D intensity vs. q profiles. Phase structures were identified by indexing Bragg peaks to known relative spacing ratios and lattice dimensions, a, were calculated using known relationships described by Hyde[41]. Calibration was done against silver behenate.

2.9 Migration assay in RAW 264.7 macrophages

Macrophage migration in response to encapsulated CCL2 was analyzed by a transwell assay using 24 well inserts (6.5 mm) with 8 µm pore size polycarbonate membranes (Corning). RAW264.7 cells were grown in DMEM high glucose with L-glutamine supplemented with 10% v/v fetal bovine serum (FBS), 100 U/mL penicillin and 100 µg/mL streptomycin (Life Technologies). Cells were maintained at 37 °C in a humidified incubator supplied with 5% CO_2, and split by scrapping at 80% confluency. Macrophages were starved for 12 h by culturing them in migration buffer (DMEM supplemented with 1% FBS, 100 U/mL penicillin and 100 µg/mL streptomycin). Then, $0.5x10^6$ cells in 100 µL of migration buffer were added to the upper chamber of the insert. The lower chamber contained 600 µL with either blank or CCL2-loaded NCs. NCs were prepared as previously described, concentrated 2 times after ultracentrifugation and mixed with 3X migration buffer and PBS to reach a dose of 100 ng CCL2 in the basal compartment. Blank NCs were mixed in the same proportions and used as controls. After 12 h of migration at 37 °C in a 5% CO_2 atmosphere, cells in the upper chamber that had not migrated were carefully removed with cotton swabs. Migrated cells were then fixed in paraformaldehyde and stained with DAPI. RAW264.7 cells found on the membrane facing the lower chamber were counted as cells having performed chemotaxis and mean fluorescence intensity (MFI) was quantified with ImageJ software [42]. Ten random fields at 10x magnification were used for cell counting and fluorescence quantification. Mean values and standard deviation were calculated for each independent experiment.

2.10 Transfection and differentiation assays in MDSCs

MDSCs were generated *in vitro* as previously described [6] and incubated for 4 days at 37°C with 5% CO_2. MSC1 cells, an immortalized MDSC cell line, were grown in RPMI 1640 supplemented with L-Glutamine, Na-Pyruvate and 10% FBS (Life Technologies). For transfection experiments, MDSCs and MSC1 cells were plated in 24 well-plates (50000 cells/well) 24 h before transfection with 0.1 nmol of miRNA and 15 pmol of shRNA per well. Naked sequences were complexed with Gene Silencer® (Genlantis) or Lipofectamine® RNAiMAX (Invitrogen) following manufacturer's instructions, as positive controls. The day of transfection, medium was replaced to RPMI without antibiotics (Lipofectamine® RNAimax, NCs) or without antibiotics and serum (GeneSilencer®) and complexes were mixed with RPMI and added over the cells. Lyophilized NCs were reconstituted in a small amount of RNAse free water (3-4 µL), mixed with RPMI and added over the cells. Cells were analyzed 24 h later. MDSCs from the non-adherent and adherent fraction were collected by rinsing the plates with PBS 2 mM EDTA and phenotypic markers were evaluated by flow cytometry. Silencing of C/EBPβ in MSC1 was quantified by qRT-PCR.

2.11 Cytofluorimetric analysis

MDSCs were washed with cold PBS and incubated 10 min at 4°C with purified anti-FcγR antibody (clone 2.4G2) to minimize non-specific antibody binding. Antibodies of interest were added to cell suspensions following FcγR blocking and incubated 20 min at 4°C in the dark. Employed antibodies were: anti-CD11b PE-Cy7 (clone M1/70), anti-CD11b PerCP-Cy5.5 (clone M1/70), anti-LY6G APC-Cy7 (clone 1A8) and anti-LY6C eFluor 450 (clone HK1.4) (all from eBioscience). Aqua LIVE/DEAD®dye (Invitrogen) was used to analyze cell viability. Flow data were acquired with a BD LSRII or BD FACS Calibur instrument and analyzed with FlowJo (Tree Star, Inc.) software.

2.12 RNA extraction and qRT-PCR

TRIzol® reagent (Invitrogen) was added directly to the culture plate after medium removal, and total RNA was extracted according to the TRIzol® extraction protocol. Following TRIzol® extraction, genomic DNA contaminants were removed using the TURBO DNA-free™ Kit (Ambion). cDNA was generated using the reverse transcriptase SuperScript II and polydT12-18 primers (Invitrogen). PCR and fluorescence detection were performed using the ABI 7900HT fast real-time PCR Systems in a reaction volume of 20 µl containing 1× TaqMan Universal PCR Master Mix (Applied Biosystems) and 50 ng cDNA. For quantification of mouse Cebpb and Rn18s the 1× TaqMan Gene Expression Assays Mm00843434_s1 and Mm03928990_g1 (Applied Biosystems) were used. All measurements were performed in duplicates and data were analyzed by the ΔΔCt relative quantification method. Gene expression levels were normalized to the respective endogenous control (Rn18s), and compared with the reference samples.

2.13 Mice

C57BL/6 (WT), congenic CD45.1 (Ly5+) mice and OT-I transgenic mice (C57BL/6-Tg (TcraTcrb)1100Mjb/Crl) were purchsed from Charles River Laboratories (Italy) and maintained under specific pathogen-free conditions in the animal facilities of the Istituto Oncologico Veneto (Padova, Italy). OT-I/CD45.1 F1 mice were obtained by crossbreeding OT-I and CD45.1 mice. Female C57BL/6 (WT) and female/male CD45.1 OT-I transgenic mice 8-12 weeks old were chosen for these experiments. Experiments involving animals were performed according to the national guidelines and approved by the local ethics committee.

2.14 *In vivo* treatments on tumor bearing mice

MCA-203 (aplotype H-2b) fibrosarcoma cells were obtained from the American Type Culture Collection and cultured in DMEM 10% FBS (Gibco) supplemented with 2 mM L-glutammine, 10 mM HEPES, 20 µM 2β-Mercaptoethanol, 150 U/ml streptomycin, 200 U/ml penicillin. To establish tumors, MCA203 cells ($1x10^6$ cells/mouse) were injected subcutaneously on the left flank of C57BL/6 mice, and tumor growth was monitored every 2 days by digital calipers. Intravenous injections of shRNA-loaded polyarginine

nanocapsules (PolyArg NCs), were started at day 11 from MCA203 tumor cell injection, when tumor surfaces were approximately 35 mm^2, and repeated 3 times with 48 hours intervals (RNA dose= 20 μg/mouse/treatment).

2.15 Statistical Analysis

The statistical analysis was performed using GraphPad Prism. Where applicable, data are reported as the mean ±SD. Data were compared using the unpaired two-tailed Student's t-test and p-values less than 0.05 were considered to be statistically significant.

3. Results

3.1 Development of GMO-Polyarginine nanocapsules for the co-association of proteins and polynucleotides

3.1.1. Development of the core nanoemulsion that enables the encapsulation of proteins

A critical goal of this work was to design a nanocarrier that could co-allocate two different molecules, a protein (CCL2) and a polynucleotide (shRNA C/EBPβ and miR 142-3p). To this end, we conceived the idea of producing nano-oily cores specially adapted to encapsulate proteins, and to cover them with a polymer shell with the capacity to associate polynucleotides. Hence, the first step was the definition of an oily core that would enable the entrapment of protein molecules. Considering the literature of protein encapsulation, we identified glyceryl monooleate-based mesophases as promising structures to conform the core of our carriers[38,39]. Glyceryl monooleate (GMO) is an amphiphilic lipid capable of forming various crystalline phases upon dilution with water[43]. These phases are usually dispersed by highly energetic procedures to yield nanoparticles, subsequently stabilized by the surfactant Pluronic F127®[44,45]. Given that these procedures may represent a risk for the encapsulated payload[46], in this work we decided to study the use of the self-emulsifying compound Labrasol® as a co-surfactant to promote a mild mesophase dispersion.

Based on the GMO-water phase diagram, a cubic phase gel suitable for protein encapsulation is obtained at physiological temperature and pressure[47]. Accordingly, this cubic gel was selected as a bulk material for the core composition (75% GMO + 25% water) and its liquid crystalline structure was confirmed by small angle X-ray scattering (SAXS). In agreement with previous literature,[43] the GMO gel showed a cubic structure with a lattice parameter that changed from an "Ia3d" to a "Pn3m" phase upon hydration (**Figure S1A, Supporting information**). However, the addition of Labrasol® to promote the nanodispersion of the GMO gel could alter its cubic phase, therefore the phase distribution of the GMO-Labrasol-water ternary system at 37°C was investigated. The

results in **Figure 1A** indicate that the cubic phase was maintained when the amount of Labrasol® incorporated to the GMO gel was below 10% (90% GMO in excess water). At 20% Labrasol®/80% GMO, the crystalline structure changed from an inverse bicontinuous cubic phase of the double diamond (Pn3m) space group, to an inverse hexagonal phase coexisting with an L2 inverse micellar phase, and above that quantity it shifted entirely to an L2 inverse micellar phase. These L2 inverse micellar phases, together with bicontinuous hexagonal phases, are particularly adequate for achieving controlled peptide release profiles[45]. Hence, the co-surfactant Labrasol® was selected to investigate its capability to disperse the bulk GMO gel, yielding GMO-based nanocarriers suitable for protein encapsulation.

The formulation method, which we termed the "gel method", consisted of the preformation of a GMO cubic phase gel loaded with the model protein ovalbumin (OVA),[47] which was subsequently mixed with Labrasol® and dispersed in the Pluronic F127® aqueous solution (**Figure 1B, Figure S2**, **Supporting Information**). In a first step, different GMO:Labrasol® w:w ratios (i.e. 1:0.5, 1:2, 1:4, 1:9) at a fixed GMO:Pluronic F127® w:w ratio (1:1.15) were evaluated in terms of particle size and polydispersity index to generate GMO-based nanoemulsions. Based on this initial screening, a GMO:Labrasol® ratio of 1:9 was selected to constitute the nanoemulsion core, yielding monodisperse nanoemulsions with a size and zeta potential of about 200 nm and -20 mV, respectively (**Figure 1C**; **Table S1**, **Supporting Information**). These nanoemulsions were further coated with polyarginine to elaborate the final nanocapsular system and both, nanoemulsions (NEs) and nanocapsules (NCs) were analyzed by SAXS. The presence of the characteristic wave of the L2 phase at ≈ 0.15 A^{-1} was observed in both systems, and especially appreciated when the particles were concentrated by centrifugation (**Figure 1D**), thus confirming the suitability of the formulation method to obtain L2 phases for peptide encapsulation. Indeed, GMO-based NEs showed encapsulation efficiencies of OVA of 35% as assessed by UPLC and these NEs were able to retain most part of the protein (60%) upon high dilution in phosphate buffer saline (**Figure 1E**). SAXS analysis of the raw materials confirmed that the L2 phase arrangement corresponds to the NE/NC structure and not to an inherent property of the materials used (**Figure S1B, Supporting Information**).

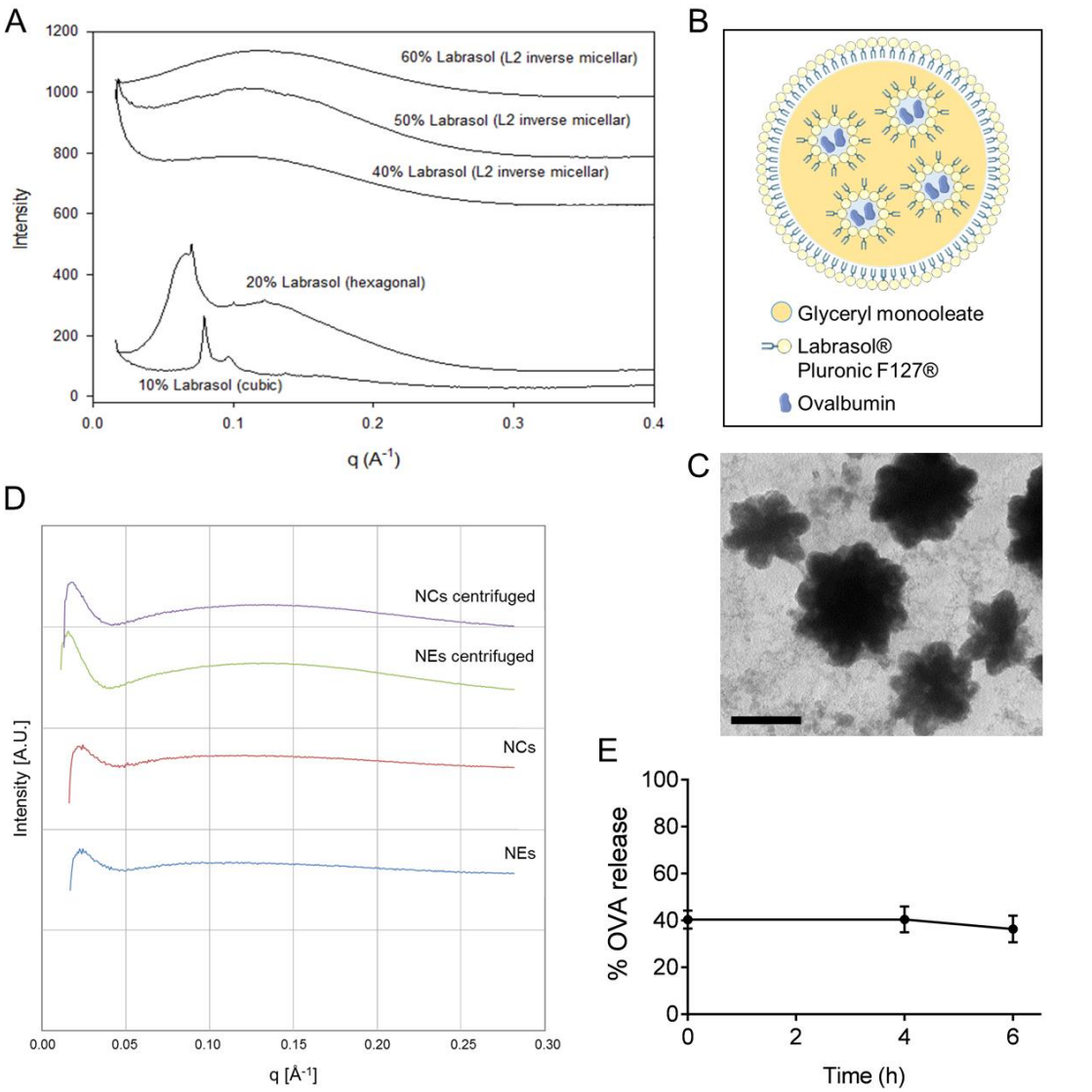

Figure 1. Physicochemical characterization of NEs as the NCs core compositions. A) SAXS profiles showing crystalline phase changes in the GMO precursor gel in excess water with increasing Labrasol® content. B) Schematic showing the structure of the GMO-based NEs. C) TEM image of OVA-loaded NEs. Scale bar = 200 nm. D) SAXS of polyarginine NCs and the corresponding NEs before (bottom) and after concentration by centrifugation (top). E) Release of OVA upon dilution of the NEs in PBS pH 7.4. Values represent the mean ± SD (n=9).

3.1.2 Design and development of RNAi and CCL2-loaded nanocapsules

Once we defined the composition of the NE to be used as a template for the formation of the polymer shell (**Figure 2A**), we analyzed the assembly of one or multiple polymer layers and the co-encapsulation of the chemokine CCL2 and two different types of RNA interference (RNAi) sequences: miRNA (miR) and shRNA (shR). In a first step, CCL2 was encapsulated within the GMO-water gel and the NCs were produced following the experimental conditions defined for the formation of the NEs (**Materials and Methods**), by adding polyarginine into the external aqueous phase. Three nominal CCL2

concentrations, 0.25, 0.5 and 1 µg/mL were tested, resulting in sizes and surface charges of 150 nm and +40 mV, respectively, similar to those of blank (non-loaded) NCs (**Figure 2B, C**). CCL2 encapsulation within the nanoemulsions was also adequate, showing a 50% efficiency as assessed by ELISA (**Figure 3B**).

Next, NCs were loaded with increasing RNA amounts and characterized according to their physicochemical properties. Two RNA:polyarginine w:w ratios, 2:1 and 1:1, were tested during this initial screening, resulting in NCs with adequate physicochemical properties (**Figure 2B, C, D**) and RNA association efficiencies. The association of RNA to the nanocapsules was firstly assessed qualitatively by gel retardation assays. NCs with miRNA and shRNA payloads were loaded in electrophoresis gels before and after the incubation with and excess of heparin. This highly negatively charged polymer is added to the particles to compete with RNA for its adsorption to their cationic surface and to promote its displacement. As observed in **Figure 3A**, RNA bands are only visible after the addition of heparin, suggesting an effective association of the RNA molecules to the NCs surface. Importantly, CCL2-loaded NCs were able to efficiently adsorb the RNAi sequences, demonstrating the potential of polyarginine NCs for the co-allocation of peptides and polynucleotides. In the case of miRNA-loaded systems, encapsulation efficiency was confirmed by a Nanodrop® spectrophotometer after centrifuging the nanoparticles and measuring the resultant supernatant to detect the unbound RNA. The results in **Figure 3B** indicate that the association efficiency obtained by this method was 70%, further supporting the results obtained by gel retardation assays.

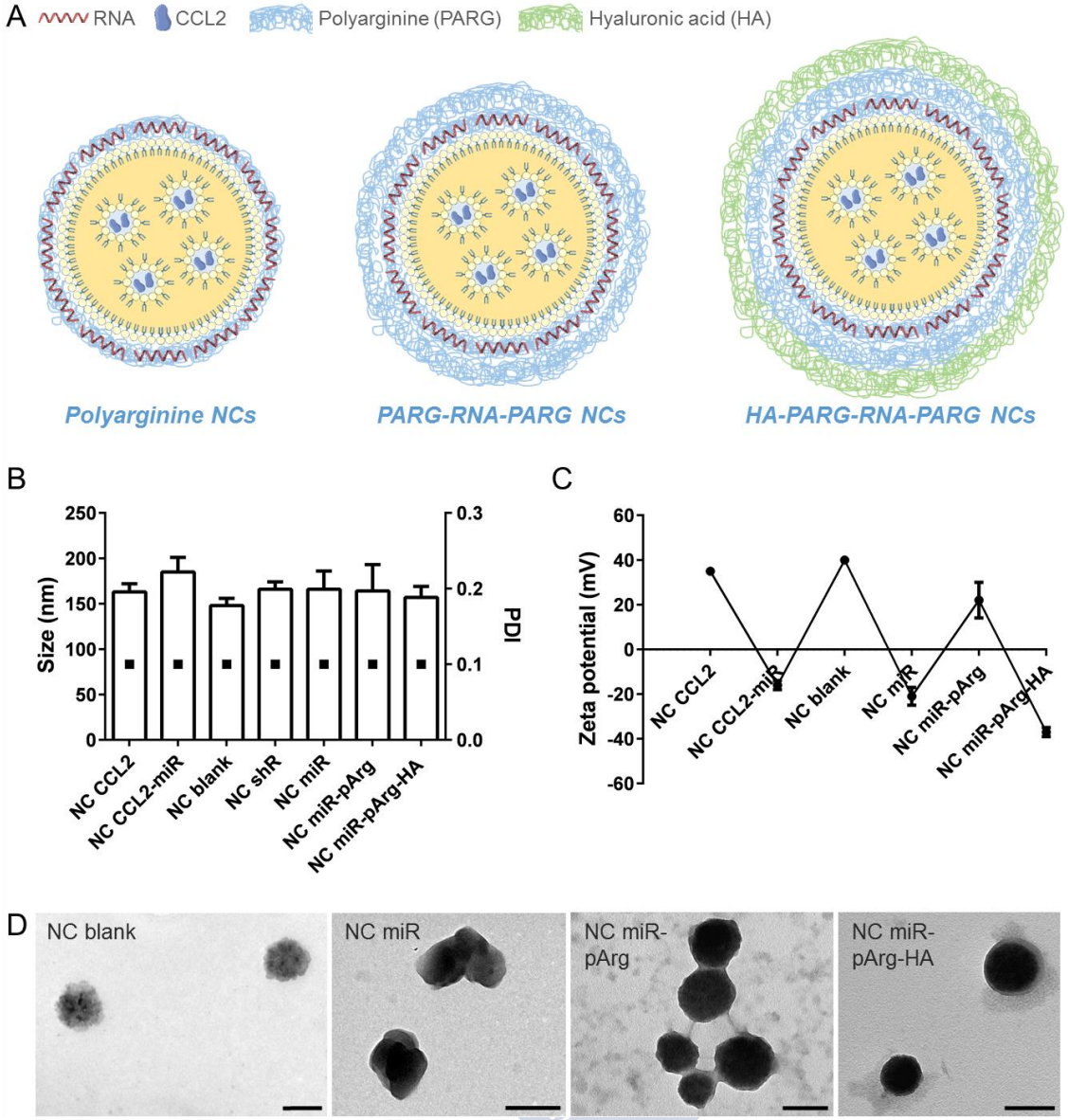

Figure 2. Characterization of polyarginine NCs. A) Schematic representation of single and multiple layer polyarginine NCs. B) Size and PDI of blank and loaded polyarginine NCs as measured by DLS. C) Zeta potential values of blank and loaded polyarginine NCs. D) TEM micrographs of blank and miRNA-loaded NCs after resuspension from a freeze-dried powder. All scale bars = 200 nm.

3.1.3 Assembly of single and multiple-layer RNAi-loaded nanocapsules

Based on their RNA encapsulation efficiency and colloidal properties, NCs with the highest RNA loading (1:1 ratio) were selected for in vitro experiments and to generate single and multiple-layer NCs for improved RNA protection (**Figure 2A**). To this end, RNA-loaded NCs were coated with a single layer of polyarginine or a double layer of polyarginine-hyaluronic acid. Several polymer weight ratios were explored to construct these multi-enveloped nanocapsules, with 1:1:1 and 1:1:1:6 pArg:RNA:pArg and pArg:RNA:pArg:HA w:w ratios resulting in the best colloidal properties (**Figure 2B, C**).

Size, polydispersity index (PDI) and surface charge were evaluated by dynamic light scattering (DLS) and laser doppler electrophoretic mobility, respectively. DLS measurements indicated that both, blank and RNA loaded particles had an average hydrodynamic diameter between 150 nm - 200 nm and a PDI close to 0.1. Zeta potential oscillated from positive to negative values depending on the charge of the polymeric coating (**Figure 2B, 2C**, **table S1**). Examination of the nanocapsules using transmission electron microscopy (TEM) revealed particles within the range predicted by DLS measurements. As observed in **Figure 2D**, blank NCs exhibited a size of around 200 nm and a spherical shape while miRNA-loaded NCs presented a bigger and sharper shape. The larger size of the loaded particles, as well as their more electron dense surface, provide an indication of the effective adsorption of the RNA. The morphology of miRNA-loaded NCs was slightly altered in the presence of the polymeric coatings, yielding electron dense particles with more spherical shapes.

3.2 Stability and release profile of CCL2 and RNAi-loaded nanocapsules upon storage and incubation in bio-relevant media

3.2.1 Stability of CCL2 and RNAi-loaded nanocapsules upon freeze-drying

Stability of nanoparticles in the form of a dried powder is a basic prerequisite from a pharmaceutical development standpoint. Consequently, RNA-loaded nanocapsules were freeze-dried and their behavior after resuspension was analyzed in terms of particle size and RNA association and integrity. Powder nanocapsules were stored for different periods of time at -20°C and then resuspended and loaded in electrophoresis gels before and after incubation with heparin. RNA bands were only observed after the incubation with heparin, indicating that storage time did not induce payload release (**Figure 3D**). Moreover, displaced RNA bands exhibited the same appearance as the control bands, demonstrating the integrity of the cargo even after 1 year storage (**Figure 3D**). Finally, the results obtained by DLS after powder resuspension revealed the same size and polydispersity index as freshly prepared nanocapsules, thus confirming the colloidal stability of the systems (**Figure 3C**).

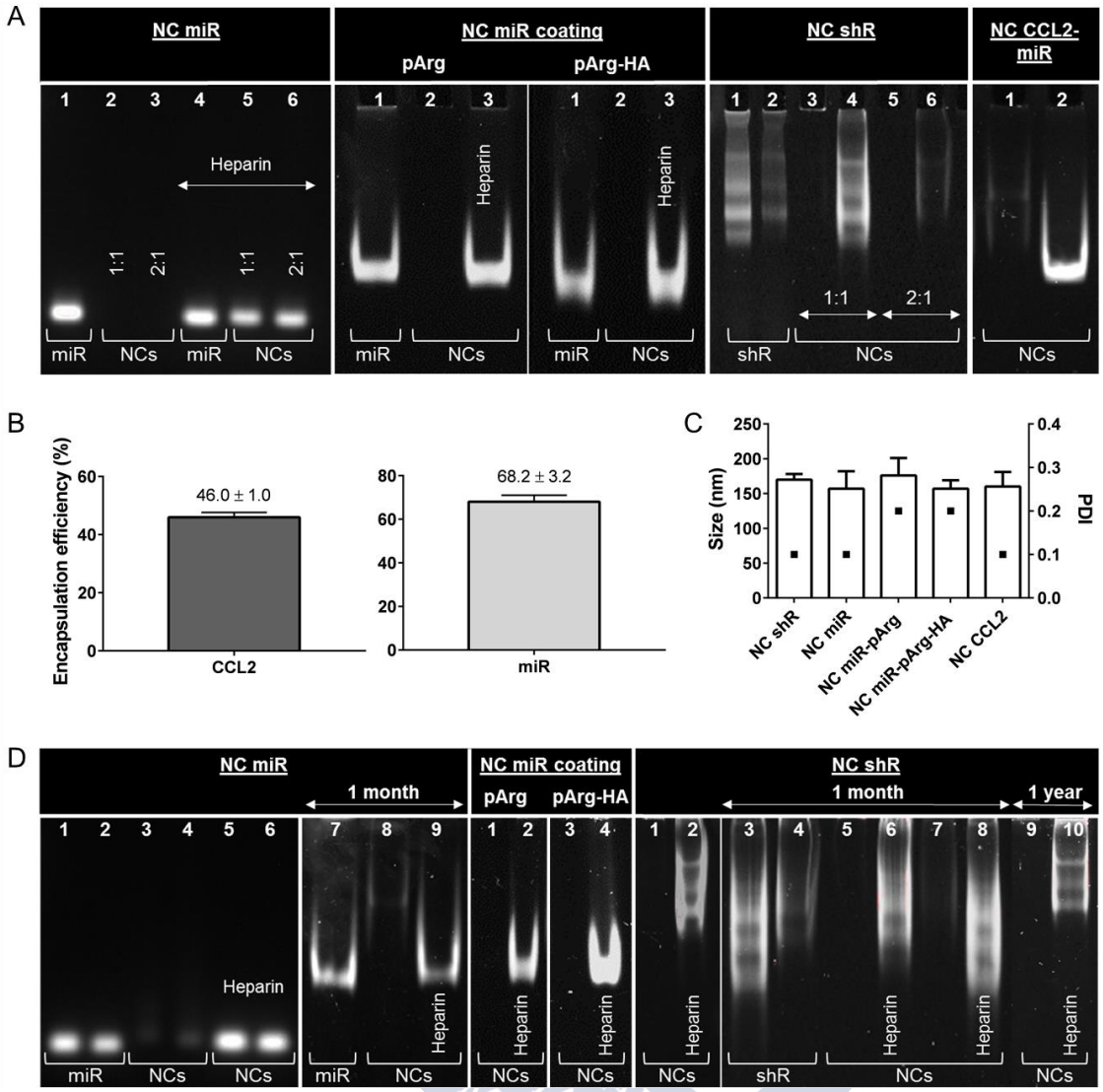

Figure 3. Physicochemical properties and encapsulation efficiency of fresh and freeze-dried RNA and CCL2-loaded NCs. A) RNA association assay by gel electrophoresis. NC miR lanes: (1) miR control sequence in solution, (2) and (3) NCs with 1:1 and 2:1 polyarginine:miR w:w ratios, (4) miR control incubated with heparin, (5) and (6) NCs 1:1 and 2:1 incubated with heparin. NC miR coating lanes: (1) miR control sequence in solution, (2) Coated NCs, (3) Coated NCs incubated with heparin. NC shR lanes: (1) and (2) 800 and 400 ng shR in solution, (3) and (5) NCs 1:1 and 2:1 polyarginine:shR (800 and 400 ng shR), (4) and (6) NCs 1:1 and 2:1 incubated with heparin. NC CCL2-miR lanes: (1) NCs CCL2-miR, (2) NC CCL2-miR incubated with heparin. B) Encapsulation and association efficiency of CCL2 and miR in NCs as assessed by UPLC and spectrophotometry, respectively. Values represent the mean ± SD (n=3). C) Particle size and PDI of freeze-dried NCs after resuspension. Values represent the mean ± SD (n=3). D) RNA stability after reconstitution of fresh, 1 month- and 1 year-stored freeze-dried NCs. NC miR lanes: (1) and (2) miR control and miR 142-3p in solution, (3) and (4) NCs miR control and NCs miR 142-3p, (5) and (6) NCs miR control and NC miR 142-3p incubated with heparin (7) miR control, (8) NCs miR control, (9) NCs miR control incubated with heparin. NC miR coating lanes: (1) and (3) pArg coated NCs and pArg- HA coated NCs, (2) and (4) pArg coated NCs and pArg- HA coated NCs incubated with heparin. NC shR lanes: (1) NCs shR control, (2) NCs shR control incubated with heparin, (3) and (4) shR control and shCEBP/β in solution, (5) and (7) NCs shR control and NCs shCEBP/β, (6) and (8) NCs shR control and NCs shCEBP/β incubated with heparin, (9) NCs shR control, (10) NCs shR control incubated with heparin.

3.2.2 Study of the stability of RNAi associated to the nanocapsules and assessment of their release s in plasma

The release and stability of RNA upon incubation of RNAi-loaded NCs in plasma were investigated by gel retardation assays. miRNA-loaded NCs were incubated in human plasma for 4 hours with a 1/10 dilution (theoretical concentration of NCs and RNAi, 2 mg/ml and 40 µg/ml, respectively). After 4h, aliquots of the release media were loaded in 15% polyacrylamide gels before and after the incubation with heparin. As observed in **Figure 4**, RNA bands were only detected after incubation with heparin, suggesting that there was no release during the assay. However, the fact that the bands were faint indicated that miRNA molecules were partially degraded even though they remained associated to the NCs (**Figure 4A**, **Figure S3**). Two alternative approaches were tested to circumvent this problem: the use of RNase resistant shRNA sequences and the coating of the NCs with single and multiple polymer layers (**Figure 2**). The use of RNase resistant sequences confirmed the absence of release from polyarginine NCs (**Figure 4B**) whilst polyarginine and polyarginine-hyaluronic acid coated systems, were able to protect the labile miRNA sequence from its degradation while preventing its release (**Figure 4C, D**). Further release studies performed in different biorelevant media also showed the absence of free miRNA (**Figure S4** and **Figure S5, Supporting Information**), highlighting the adequate release profile of these NCs. Colloidal stability in these media was confirmed by DLS measurements (**Figure S6, Supporting Information**).

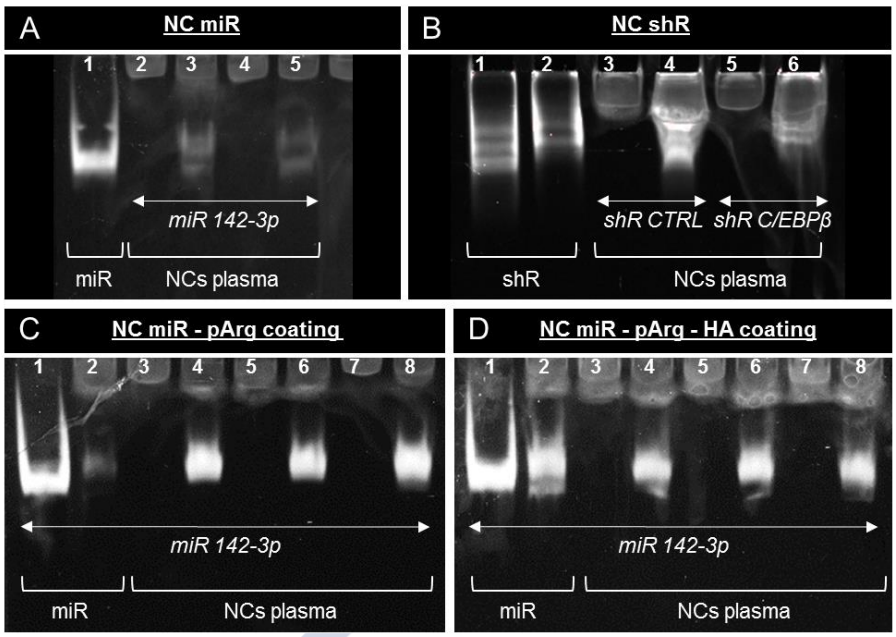

Figure 4. Release and degradation of RNAi-loaded NCs after 4 h of incubation in human plasma is controlled by NC engineering with single and multiple polymeric layers and the use of RNAse resistant sequences. Non-coated nanocapsules (A, B), polyarginine coated nanocapsules (C) and hyaluronic acid-polyarginine coated nanocapsules (D) were diluted 1/10 in human plasma. After 4 h incubation, samples were loaded in 15% polyacrylamide gels with a theoretical RNA amount of 800 ng per well. NC miR lanes: (1) miR- 142-3p sequence in solution; (2) and (4) miR 142-3p loaded NCs incubated in plasma; (3) and (5) miR 142-3p loaded NCs incubated with heparin (30 min on ice). NC shR lanes: (1) and (2) shCTRL and shC/EBPβ in solution, (3) and (5) shCTRL and shC/EBPβ loaded NCs incubated in plasma, (4) and (6) shCTRL and shC/EBPβ loaded NCs incubated with heparin. NC miR-pArg coating lanes: (1) miR 142-3p sequence in solution; (2) miR 142-3p incubated 30 minutes with heparin and plasma on ice; (3), (5) and (7) miR 142-3p loaded NCs incubated in plasma; (4), (6) and (8) miR 142-3p loaded NCs incubated with heparin. NC miR-pArg-HA coating lanes: (1) miR 142-3p sequence in solution; (2) miR 142-3p incubated 30 minutes with heparin and plasma on ice; (3), (5) and (7) miR 142-3p loaded NCs incubated in plasma; (4), (6) and (8) miR 142-3p loaded NCs incubated with heparin.

3.3 In vitro an in vivo evaluation of behavior and perfomance

3.3.1 CCL2 migration assay

Transwell migration assays with RAW264.7 macrophages were performed to test the bioactivity of the encapsulated CCL2. RAW264.7 macrophages were seeded on top of the transwell membranes and treatments were added in the wells underneath. Cell migration towards CCL2 was evaluated based on the amount of cells that crossed the membrane. Given that polyarginine is a known TLR4 activator, blank NCs were first tested to evaluate basal macrophage migration. Indeed, treatment with increasing concentrations of blank particles was found to induce macrophage migration in a dose-dependent manner (**Figure 5A**). Based on these results, polyarginine NCs with a CCL2 loading of 1 µg/mL were selected to perform the migration assays. Considering both,

CCL2 encapsulation efficiency and the yield of NCs production, a dose of 100 ng CCL2 corresponded to a dose of 3 mg NCs (60 µg polyarginine) that presented the minimum basal migration in the previous assays (**Figure 5B**). In these conditions, CCL2-loaded NCs induced significantly higher cell migration compared to blank NCs, suggesting the potential of CCL2-loaded NCs for monocyte-macrophage targeting (**Figure 5C**).

In addition, a T cell invasion assay towards CCL2 was performed to mimic the process of cytotoxic T cell (CTL) recruitment to the tumor. To this end, Matrigels® of 10 mg/ml were loaded with soluble CCL2 (60 ng per 100 µl gel), or maintained as such (blank gels) and allowed to gel at 37°C in a cell incubator. T cells were then added on top of the gels and incubated for 48 h, after which gels were washed and the cells that remained associated to the gels were stained and imaged. As observed in **Figure S7**, CCL2-matrigels promoted a higher T cell invasion, suggesting that the accumulation of CCL2-loaded NCs within the tumor site might represent a valuable strategy to restore the impaired balance of native vs. nitrated/nitrosylated CCL2, in order to rescue CTL recruitment.

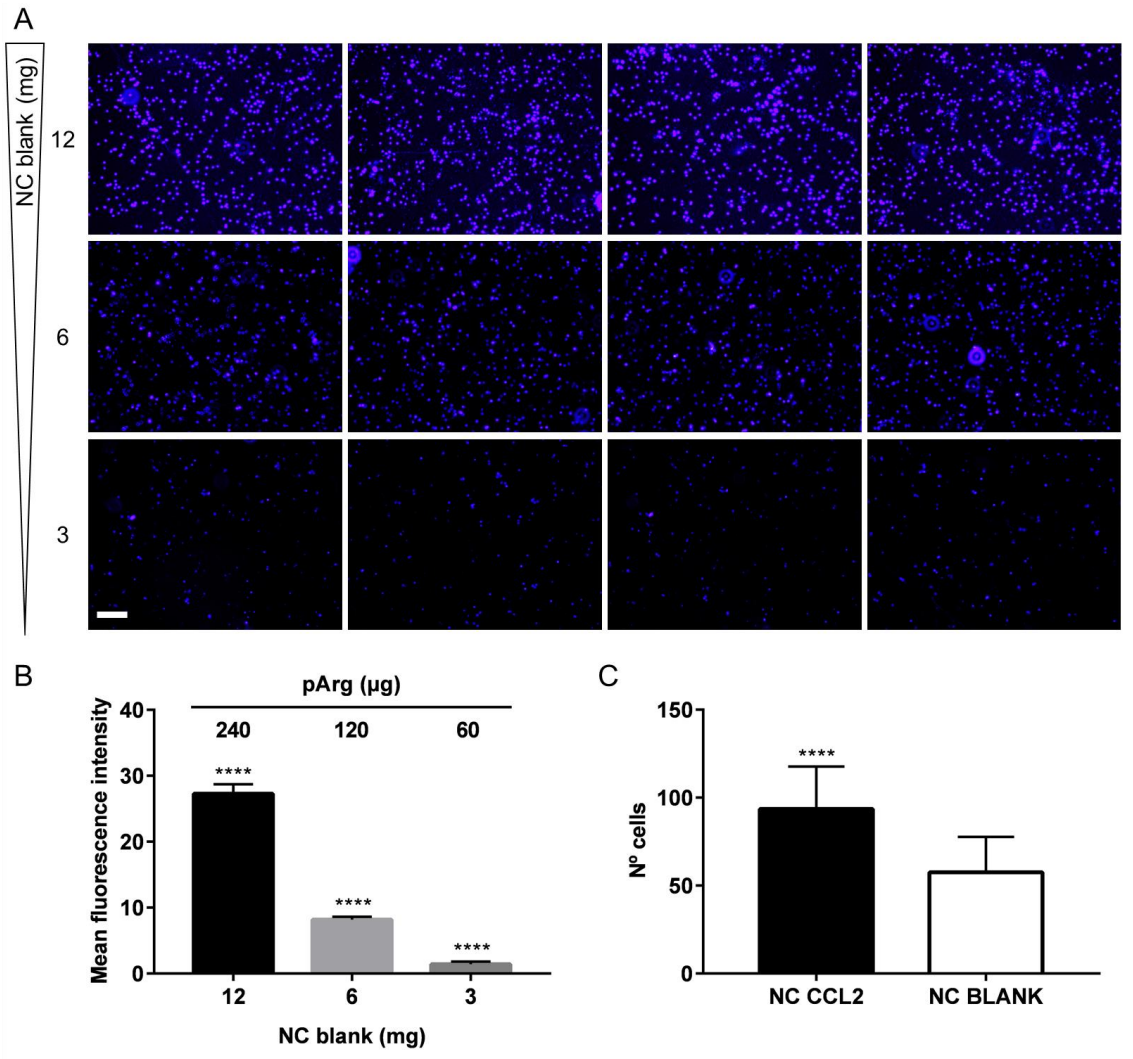

Figure 5. RAW264.7 macrophages migrate towards pArg NC in a dose dependent manner and this migration is increased by encapsulated CCL2. Transwell assays were performed with blank and CCL2-loaded NCs and cells migrated to the basal side of the membrane were DAPI-stained and counted. A) Migration of RAW264.7 macrophages towards decreasing concentrations of blank NCs. Scale bar = 100 µm for all the images. B) Mean fluorescence intensity quantification of (A). C) Macrophage migration to CCL2-loaded NCs as compared to blank NCs. Values represent the mean ± SD of three independent experiments. Data was analyzed using a two-tailed t-Student test (**** P<0.0001).

3.3.2 Effect of miR 142-3p-loaded nanocapsules on BM-MDSC phenotype

Both human and murine MDSCs express the markers CD11b and Gr-1. Granulocytic MDSCs present a high Gr-1 expression and are less immunosuppressive than monocytic- and macrophagic-like MDSCs that possess and intermediate and low-negative expression, respectively.[48] It has been shown that in BM-MDSC cultures, miR-142-3p overexpression prevents the formation of the macrophagic fraction ($CD11b^{+}Gr\text{-}1^{low\text{-}neg}$), which is endowed with the strongest immunosuppressive activity.[7] Consequently, one of the objectives of this study was to investigate the capacity of polyarginine NCs to deliver miR 142-3p and modulate BM-MDSCs. In a first step, the ability of NCs to

facilitate the uptake of RNAi by macrophages was first evaluated using a fluorescent RNAi and the RAW264.7 macrophage cell line. A 5'-fluorescein-conjugated miR 142-3p was associated to polyarginine NCs and incubated with the macrophages for 2 h. Free RNAi was also incubated with the macrophages as control. According to the confocal images shown in **Figure S8**, non-coated polyarginine NCs were able to promote RNAi internalization, whereas no detectable signal was observed for free RNAi. Subsequently, the effect of blank polyarginine NCs on MDSC viability and subset cell distribution was studied. The results showed that polyarginine NCs were highly biocompatible, preserving an adequate cell viability even at a concentration of 100 µg/mL (**Figure S7, Supporting Information**). Although this concentration slightly reduced the Gr-1 low-negative fraction (**Figure 6A**), only concentrations lower than 50 µg/mL were necessary for the differentiation experiments, neglecting the contribution of blank NCs on the modulation of MDSCs phenotype.

In a second step, the immunomodulatory activity of miR 142-3p-loaded NCs was evaluated. MDSCs were transfected with 0.01 to 0.2 nmol of miR 142-3p using a commercial transfection reagent (GeneSilencer®, Genlantis) or polyarginine nanocapsules, and percentages of the differentent cell subsets were quantified by flow cytometry. An scramble miRNA sequence was also loaded in the NCs as control. As depicted in **Figure 6B**, miR 142-3p complexed to GeneSilencer® promoted a dramatic reduction of the Gr-1 low negative fraction at the lowest dose of 0.01 nmol. In the case of miR 142-3p-loaded NCs, a dose of around 0.02 nmol was required to exert the same response. For NCs loaded with miR control, the highest dose of 0.2 nmol produced a high reduction on the Gr-1 low negative subset and, consequently, a dose of 0.1 nmol of encapsulated miR 142-3p was selected for further experiments. Representative flow cytometry plots corresponding to transfections performed with the 0.1 nmol dose are depicted in **Figure 6C**, visually reflecting the switch towards the Gr-1 high phenotype after miR 142-3p treatment. Overall, these results demonstrate the activity of miR 142-3p after NC freeze-drying as well as their transfection efficiency and capacity to modulate MDSCs.

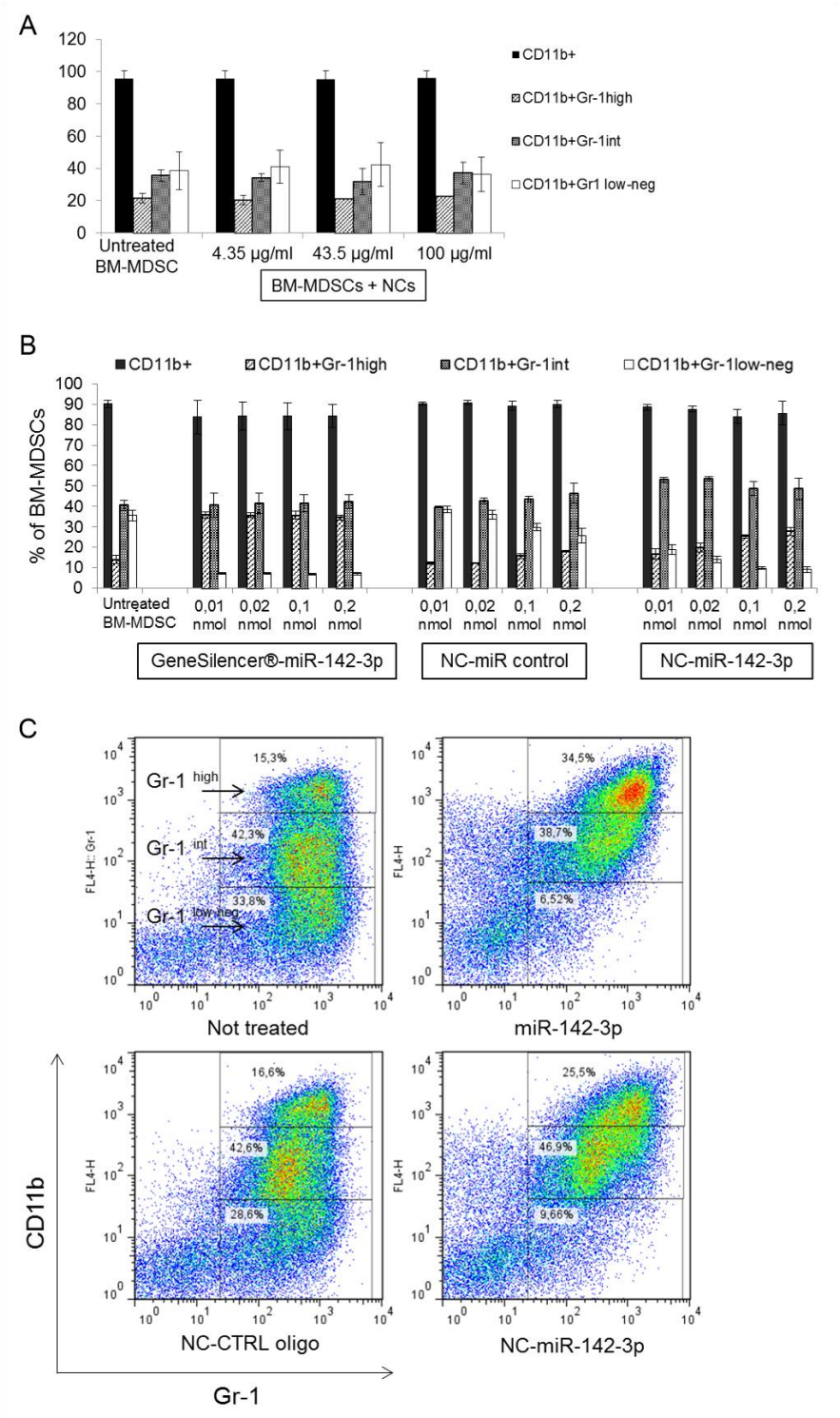

Figure 6. Polyarginine nanocapsules loaded with miR-142-3p reduce the percentage of Gr-1 $^{low\text{-}negative}$ cells (monocyto-macrophagic fraction) in a BM-MDSC culture. A) MDSCs were treated with increasing concentrations of blank polyarginine NCs to check their effect on subset cell distribution. MDSCs were then transfected with 0.01 to 0.1 nmol of miR 142-3p using a commercial transfection reagent (GeneSilencer®, Genlantis) or polyarginine nanocapsules. The effect of the different doses of miR on bone marrow subsets (B) and representative flow cytometry images for the 0.1 nmol dose (C) are shown. The effects were compared to cells treated with nanocapsules and a scrambled miR sequence. Values are means ±SD of two independent experiments.

3.3.3 In vitro transfection efficiency and in vivo efficacy of C/EBPβ-loaded nanocapsules

As described in the Introduction, C/EBPβ creates a feedback loop with miR-142-3p promoting myeloid cell differentiation towards immunosuppressive macrophages during tumor-induced myelopoiesis.[7] Consequently, C/EBPβ downregulation represents a promising approach to control the immunosuppressive environment and revert tumor-induced tolerance. Here, a strategy was explored consisting on the use of shRNA-loaded polyarginine nanocapsules to silence C/EBPβ in MDSCs. To this end, the transfection efficiency of shC/EBPβ-loaded NCs was first evaluated in MSC1 cells, an immortalized cell line derived from primary MDSCs, using Lipofectamine RNAiMAX® as positive control. The amount of shC/EBPβ was titrated from 5 to 25 pmol/well to find the optimal dose (maximum silencing with minimum non-specific silencing by control sequences) and a concentration of 15 pmol/well was fixed for the comparative experiments. The shC/EBPβ-loaded NCs produced a significant down-regulation of C/EBPβ mRNA as compared to non-treated cells or cells treated with nanocapsules and a scrambled sequence. This effect was comparable to the one achieved with the positive control Lipofectamine RNAiMax**,** highlighting the potential of polyarginine nanocapsules for gene delivery and MDSC modulation (**Figure 7A**).

Next, the in vivo efficacy of shC/EBPβ NCs was assessed in a mouse tumor model. The MCA203 sarcoma was selected because of the relevant C/EBPβ expression in both tumor infiltrating and splenic myeloid cells, as previously reported[6]. Mice bearing established MCA203 tumors were intravenously injected with NC-shC/EBPβ or non-loaded NCs. Treatments were started at day 11 from tumor injection when tumor surfaces were approximately 35 mm^2, and repeated 3 times with 48 hours intervals (RNA dose= 20 µg/mouse/treatment, **Figure 7B**). Animals were sacrificed 48 hours after the last treatment and $CD11b^+$ myeloid cells were isolated from spleens and tumors by immunomagnetic sorting. C/EBPβ mRNA levels were significantly reduced in both splenic and tumor-infiltrating $CD11b^+$ cells in mice treated with NC-shC/EBPβ as compared to controls (**Figure 7C**). C/EBPβ downregulation was around 50% in splenic myeloid cells and 30% in tumor-infiltrating myeloid cells. No evident signs of toxicity were observed during the treatment period.

To investigate the impact of C/EBPβ downregulation on tumor-associated myelopoiesis, we performed a phenotypic analysis of myeloid cell subsets in lymphoid organs (spleen and bone marrow) and at the tumor site. While our analysis revealed no differences in bone marrow and splenic myeloid populations (data not shown), a significant decrease in the frequency of tumor-associated macrophages was observed in the NC-shC/EBPβ group compared to controls (**Figure 7D**). Such macrophage reduction correlated with a significant increase in monocytic cells (phenotypically definable as M-MDSCs), thus

suggesting that C/EBPβ downregulation by RNAi might result in a partial impairment of monocyte differentiation into tumor-associated macrophages.

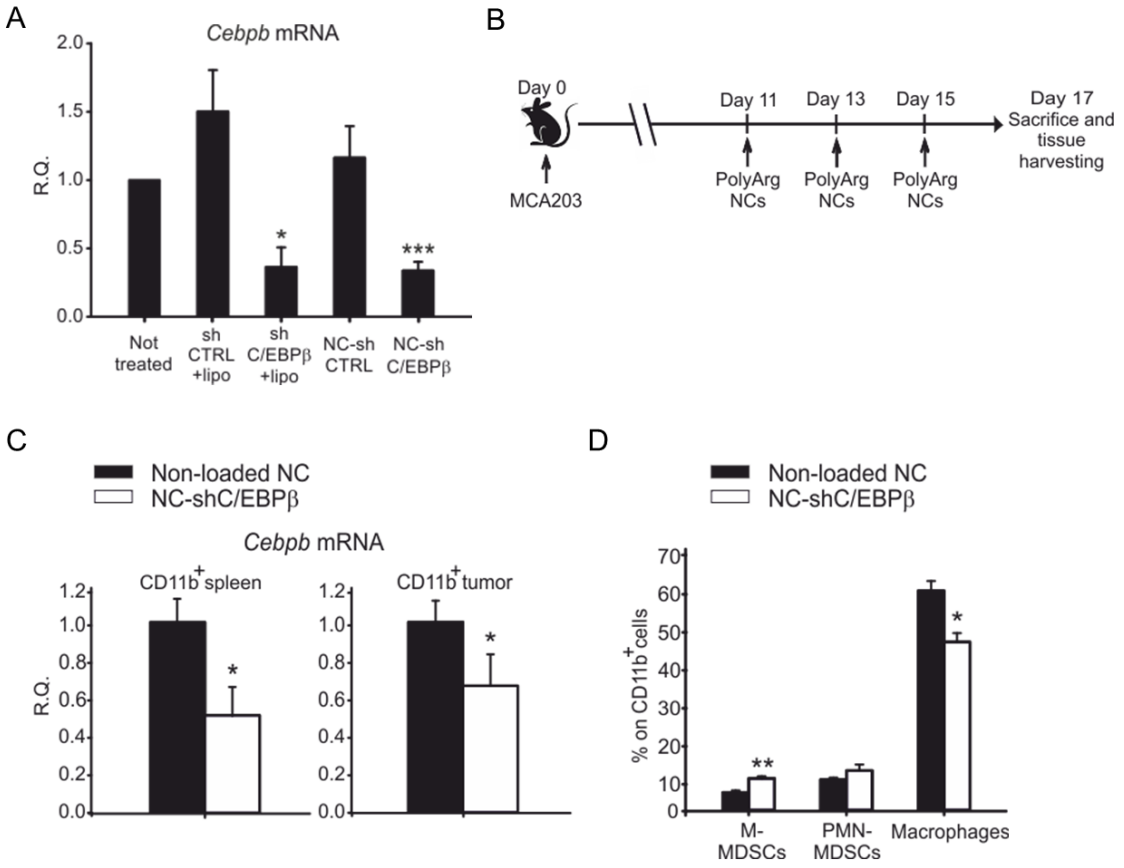

Figure 7. Polyarginine NCs loaded with C/EBPβ-targeting shRNA downregulate C/EBPβ expression in vitro and in vivo. A) Transfection assay in MSC1 cells with the modified shRNA. MSC1 cells were transfected with the C/EBPβ-targeting shRNA (shC/EBPβ) or a scrambled shRNA (shCTRL) either loaded on PolyArg NCs (NC-shC/EBPβ) or complexed with Lipofectamine RNAi Max® reagent (Invitrogen), and harvested 24 hours later. C/EBPβ mRNA levels were quantified by RT-qPCR and normalized with respect to an endogenous control (Rn18S). Data are expressed as relative quantification (R.Q.), normalized to non-transfected (not treated) cells. Means ± SD (n=3). Statistical comparison between each group and the untreated control, *p<0.05, ***p<0.001, Student's *t*-test. B) Schematic representation of the treatment schedule for the in vivo efficacy assay. C57BL/6 mice bearing MCA203 subcutaneous tumors received three intravenous injections of PolyArg NCs, either unloaded or loaded with C/EBPβ-targeting shRNA (20 µg RNA/mouse/treatment). Mice were sacrificed 48 hours after the last treatment. C) C/EBPβ mRNA levels within $CD11b^+$ cells isolated from spleens and tumors of mice treated with either unloaded NCs or NCs loaded with the C/EBPβ-targeting shRNA (NC-shC/EBPβ). C/EBPβ mRNA levels were quantified by RT-qPCR and normalized to an endogenous control (Rn18S). Data (means ± SE) are expressed as relative quantification (R.Q.) normalized to the average cycle threshold value for the control group receiving unloaded NCs. D) Percentage of M-MDSCs, PMN-MDSC and macrophages on total CD11b± cells within the tumor (means ± SD). Cell populations were defined according to the gating strategy reported in figure S10. n=4 mice (unloaded NC) and n=3 mice (NC-shC/EBPβ). *p<0.05 **p<0.01 ***p<0.001, Student's *t*-test.

4. Discussion

The success of adoptive T cell therapy (ACT) for cancer treatment has been evidenced by the recent approval of two Chimeric Antigen Receptor (CAR) T-cell therapies by the Food and Drug Administration (FDA) in 2017. However, this success is somehow shadowed by the fact that these treatments need to be preceded by immune-depleting preparative treatments, which are associated with severe toxicities[49,50] and, hence, less aggressive alternatives are needed. In this regard, researchers have identified MDSCs as a key immune cell population promoting T cell immunosuppression, and MDSCs depletion and RNAi-based re-education have recently proved to be good strategies to improve ACT efficacy.[8,51]

In this work, we hypothesized that the therapeutic efficacy of RNAi-based therapies in vivo will be compromised if they are not integrated in a suitable carrier capable of enhancing their biological half-life and deliver them to their target cell subset. This hypothesis is supported by the fact that the majority of the RNAi therapies under clinical trials have in common the use of a delivery platform[52]. Our therapeutic proposal is that we can re-educate MDSCs through the use of a RNAi-loaded nanocarrier delivered to the most immunosuppressive monocytic-macrophagic MDSCs[7] by the co-encapsulation of the chemoattractant CCL2[10,16,17]. To this end, we have developed a nanocapsular system in which a GMO lipid core is used to promote CCL2 encapsulation while RNAi sequences targeting the C/EBPβ pathway are adsorbed onto a cationic polyarginine coating. By providing CCL2 release within the tumor site, we also aim to restore native CCL2 levels over tumor-nitrated/nitrosylated species to enable the adequate T cell recruitment.[18,20,21]

We selected a GMO lipid core for CCL2 encapsulation due to the favorable structure of GMO-based mesophases for the incorporation and slow release of peptide drugs.[38,39] Although GMO-based mesophases have been widely used for peptide encapsulation, commonly employed methods for mesophase dispersion imply the use of formulation procedures that may damage the drug payload.[46,53] In this work, we explored a new mild self-emulsification method, based on the use of the non-ionic surfactant Labrasol® to disperse a GMO cubic gel loaded with the peptide, yielding polyarginine nanocapsules. Based on the phase diagram of GMO-water binary system, we selected a proportion of 25:75 water:GMO w:w to generate a cubic gel with known properties for protein encapsulation[43]. To be able to select the adequate amount of Labrasol® to disperse this cubic gel, we constructed the phase diagram of the GMO-Labrasol®-water ternary system and evaluated the impact of GMO:Labrasol® w:w ratios on the physicochemical properties of the nanocarriers. As expected, the use of increasing amounts of Labrasol® to disperse the cubic gel led to a change from cubic (10% Labrasol®/90% GMO in excess water) to inverse micellar (>20% Labrasol®/80% GMO) phase arrangements. In addition, Labrasol® amounts higher than 20% were also needed to obtain monodisperse

nanometric particles with adequate colloidal stability over time. Consequently, a GMO:Labrasol® w:w ratio of 1:9 was selected to prepare CCL2-loaded nanocapsules, achieving adequate peptide encapsulation efficiencies of 50%. L2 inverse micellar phases, together with hexagonal phases, have been recently identified to provide improved protein release profiles compared to traditionally explored cubic phases.[45] Therefore, the fact that one can promote the nanodispersion of bulk GMO cubic phases by means of mild formulation procedures, leading to the formation of L2 micellar phases suitable for peptide encapsulation, constitute a relevant result from the pharmaceutical development standpoint.

Polyarginine nanocapsules were successfully loaded with RNAi sequences showing a high encapsulation efficiency of 70%, and adequate physicochemical properties (sizes about 200 nm and PDIs close to 0.1). Importantly, the encapsulation of the highest dose of CCL2 (1 µg/mL) did not impede the adsorption of miR 142-3p molecules, confirming the suitability of this nanocapsular system for the co-delivery of diverse payloads. RNA stability during storage was accomplished by the use of powdered formulations, preserving RNA integrity and the colloidal properties of the nanocapsules for at least 1 year. In addition, RNA stability and release in relevant biological media was controlled by the use of fluorinated RNA sequences[54] and the assembly of polymeric coatings following previously explored layer-by-layer approaches[55–57]. Indeed, multiple layer hyaluronic acid-polyarginine-RNA-polyarginine shells created a “sandwich-like” organization with the RNAi molecules that conferred protection to miR 142-3p sequences during at least 4 h of incubation in human plasma.

As expected, it was observed that RNAi was taken up by macrophages more efficiently when loaded in polyarginine nanocapsules than when administered in free form. This enhancement of RNAi uptake resulted in a high transfection efficiency of shC/EBPβ-loaded NCs suggesting an adequate degree of endosomal escape that is consistent with the buffer capacity of polyarginine.[25] When polyarginine NCs were loaded with miR 142-3p, they were able to modulate MDSCs, switching their most aggressive monocytic-macrophagic fraction towards the less immunosuppressive Gr-1^{high} subset, thus confirming the potential of polyarginine nanocapsules as gene therapy immunomodulating nanocarriers. More importantly, shC/EBPβ-loaded NCs promoted a downregulation of C/EBPβ mRNA of 50% and 30% in splenic and tumor-infiltrating myeloid cells, respectively, suggesting the adequate biodistribution of polyarginine NCs to spleen and tumor. Furthermore, this C/EBPβ downregulation translated into a decrease in the frequency of tumor-associated macrophages and a significant increase in monocytic cells. Together, these results suggest that C/EBPβ downregulation by RNAi might result in a partial impairment of monocyte differentiation into tumor-associated macrophages. In addition, polyarginine nanocapsules induced a potent chemotactic activity in RAW264.7 macrophages, either when loaded with the chemokine CCL2 or in their blank form, probing their potential to target the most immunosuppressive

monocytic-macrophagic MDSCs. The increase of macrophage chemoattraction by blank nanocapsules likely stems from the recently discovered role of polyarginine as a TLR4 agonist[26] and highlights the potential of these vehicles for cancer immunotherapy and vaccination. In this context, the versatility of payload loading underlined before, would allow for the encapsulation of antigens, adjuvants and immunomodulatory molecules of different nature allowing the generation of tunable immune responses. More specifically, due to the high transfection efficiency of these systems, we consider they could be also relevant for mRNA-based vaccination approaches. Further studies would be needed to investigate whether CCL2-loaded nanocapsules are able to revert T cell anergy and preferentially target the most immunosuppressive MDSCs subsets as compared to blank nanocapsules. Given the tumor targeting capacity of polyarginine NCs, and the Matrigel®-invasion capacity of Jurkat T cells towards a CCL2 gradient, we anticipate that CCL2-loaded nanocapsules could represent a valuable strategy to restore native CCL2 levels within the tumor site and rescue cytotoxic lymphocyte recruitment, enhancing the efficacy of ACT.

miR 142-3p and shC/EBPβ were previously reported to boost the efficacy of ACT and antitumoral DNA vaccination in vivo, respectively, when administered loaded in 4PD dendrimers.[8] The results presented here show a significant silencing of C/EBPβ mRNA within spleen and tumor after in vivo administration of shC/EBPβ-loaded nanocapsules, and a potent migration of macrophages and T cells towards CCL2 in vitro. Altogether, these observations suggest that the combination of the RNAi and chemokine therapies, could be a promising approach to boost ACT efficacy in cancer immunotherapy.

5. Conclusions

A new mild self-emulsifying method was developed for the generation of polyarginine nanocapsules, which enabled the co-encapsulation of chemokines and polynucleotides. The method was based on the dispersion of a GMO cubic gel, which resulted in the formation of L2 inverse micellar phases adequate for the entrapment of hydrophilic payloads (i.e. CCL2). In addition, the polyarginine polymer layer facilitated the attachment of RNAi molecules, which were then protected with a single polyarginine or a double polyarginine/HA polymer layers. When loaded with miR 142-3p, these nanocapsules enhanced RNAi transfection in MDSCs and promoted the reversion of their highly immunosuppressive phenotype. More importantly, nanocapsules loaded with shC/EBPβ were able to reduce C/EBPβ mRNA levels within the spleen and tumor of a murine fibrosarcoma model, resulting in the impairment of monocyte differentiation into tumor-associated macrophages. Finally, the feasibility of a monocyte-macrophage targeting was explored when the chemokine CCL2 was loaded within the GMO core, promoting a high degree of macrophage migration towards the particles. Overall, the observations presented in this work suggest that polyarginine nanocapsules represent a

promising carrier for the co-delivery of RNAi and chemokines, which may help modulating the activity of MDSCs.

Acknowledgements

This work was supported by LYMPHOTARG (ERA-NET EuroNanoMed ProgramISCIII, ref PS09/02670) and NICHE projects (ERA-NET EuroNanoMed II framework by ISCIII through CIBER-BBN), which received funding from the European Union's Seventh Framework Programme. A. M. L. was supported by a FPU fellowship from the Spanish Ministry of Education. The authors thank Dr. Bruno Dacuña and Dr. Marc Malfois for scientific discussions, and Raquel Antón and Dr. Mercedes Rivas for helping with transmission and confocal microscopy. The authors specially thank Dr. Rubén Varela for providing the RAW264.7 cell line and for scientific discussions.

References

1. Sica, A. & Bronte, V. Altered macrophage differentiation and immune dysfunction in tumor development. *J. Clin. Invest.* **117,** 1155–1166 (2007).
2. Gil-Bernabé, A. M. *et al.* Recruitment of monocytes/macrophages by tissue factor-mediated coagulation is essential for metastatic cell survival and premetastatic niche establishment in mice. *Blood* **119,** 3164–3175 (2012).
3. De Sanctis, F. *et al.* MDSCs in cancer: Conceiving new prognostic and therapeutic targets. *Biochim. Biophys. Acta - Rev. Cancer* **1865,** 35–48 (2016).
4. Arina, A. & Bronte, V. Myeloid-derived suppressor cell impact on endogenous and adoptively transferred T cells. *Curr. Opin. Immunol.* **33,** 120–125 (2015).
5. Torres Andón, F. & Alonso, M. J. Nanomedicine and cancer immunotherapy – targeting immunosuppressive cells. *J. Drug Target.* **23,** 656–671 (2015).
6. Marigo, I. *et al.* Tumor-induced tolerance and immune suppression depend on the C/EBPβ transcription factor. *Immunity* **32,** 790–802 (2010).
7. Sonda, N. *et al.* miR-142-3p Prevents Macrophage Differentiation during Cancer-Induced Myelopoiesis. *Immunity* **38,** 1236–1249 (2013).
8. Zilio, S. *et al.* 4PD Functionalized Dendrimers: A Flexible Tool for In Vivo Gene Silencing of Tumor-Educated Myeloid Cells. *J. Immunol.* **198,** 4166–4177 (2017).
9. Viola, A., Sarukhan, A., Bronte, V. & Molon, B. The pros and cons of chemokines in tumor immunology. *Trends Immunol.* **33,** 496–504 (2012).
10. Qian, B.-Z. *et al.* CCL2 recruits inflammatory monocytes to facilitate breast-tumour metastasis. *Nature* **475,** 222–225 (2011).
11. Loberg, R. D. *et al.* CCL2 as an Important Mediator of Prostate Cancer Growth In Vivo through the Regulation of Macrophage Infiltration. *Neoplasia* **9,** 556–562 (2007).
12. Chang, A. L. *et al.* CCL2 produced by the glioma microenvironment is essential for the recruitment of regulatory T cells and myeloid-derived suppressor cells. *Cancer Res.* **76,** 5671–5682 (2016).
13. Chun, E. *et al.* CCL2 Promotes Colorectal Carcinogenesis by Enhancing Polymorphonuclear Myeloid-Derived Suppressor Cell Population and Function. *Cell Rep.* **12,** 244–257 (2015).
14. Hale, M. *et al.* Obesity triggers enhanced MDSC accumulation in murine renal tumors via elevated local production of CCL2. *PLoS One* **10,** 1–15 (2015).
15. Huang, B. *et al.* CCL2/CCR2 pathway mediates recruitment of myeloid suppressor cells to cancers. *Cancer Lett.* **252,** 86–92 (2007).
16. Fang, W. Bin *et al.* Targeted gene silencing of CCL2 inhibits triple negative breast cancer progression by blocking cancer stem cell renewal and M2 macrophage recruitment. *Oncotarget* **7,** 49349–49367 (2014).
17. Sawanobori, Y. & Ueha, S. Chemokine-mediated rapid turnover of myeloid-derived suppressor cells in tumor-bearing mice. *Blood* **111,** 5457–5466 (2008).
18. Lesokhin, A. M. *et al.* Monocytic CCR2 + myeloid-derived suppressor cells promote immune escape by limiting activated CD8 T-cell infiltration into the tumor microenvironment. *Cancer Res.* **72,** 876–886 (2012).
19. Rosenberg, S. A. & Dudley, M. E. Cancer regression in patients with metastatic melanoma after the transfer of autologous antitumor lymphocytes. *Proc. Natl. Acad. Sci. U. S. A.* **101 Suppl,** 14639–45 (2004).

20. Molon, B. *et al.* Chemokine nitration prevents intratumoral infiltration of antigen-specific T cells. *J. Exp. Med.* **208,** 1949–1962 (2011).
21. Molon, B., Viola, A. & Bronte, V. Smoothing T cell roads to the tumor: Chemokine post-translational regulation. *Oncoimmunology* **1,** 390–392 (2012).
22. Bencherif, S. A. *et al.* Injectable Cryogel-based Whole Cell Cancer Vaccines. *Nat. Commun.* **6,** 7556–7587 (2016).
23. Kim, J. *et al.* Injectable, spontaneously assembling, inorganic scaffolds modulate immune cells in vivo and increase vaccine efficacy. *Nat. Biotechnol.* **33,** 64–72 (2014).
24. Ali, O. A., Tayalia, P., Shvartsman, D., Lewin, S. & Mooney, D. J. Inflammatory cytokines presented from polymer matrices differentially generate and activate DCs in situ. *Adv. Funct. Mater.* **23,** 4621–4628 (2013).
25. Szabo, F. K. & Hoffman, G. E. Cell transcytosing poly-arginine coated magnetic nanovector for safe and effective siRNA delivery. *Biomaterials* **32,** 5717–5725 (2011).
26. Yang, Y., Wolfram, J., Fang, X., Shen, H. & Ferrari, M. Polyarginine Induces an Antitumor Immune Response through Binding to Toll-Like Receptor 4. *Small* **10,** 1250–1254 (2014).
27. He, W. *et al.* Re-polarizing Myeloid-derived Suppressor Cells (MDSCs) with Cationic Polymers for Cancer Immunotherapy. *Sci. Rep.* **6,** 24506 (2016).
28. Huang, Z. *et al.* Anti-tumor immune responses of tumor-associated macrophages via toll-like receptor 4 triggered by cationic polymers. *Biomaterials* **34,** 746–755 (2013).
29. Chen, H. *et al.* The promotion of type 1 T helper cell responses to cationic polymers in vivo via toll-like receptor-4 mediated IL-12 secretion. *Biomaterials* **31,** 8172–8180 (2010).
30. Correia-Pinto, J. F., Peleteiro, M., Csaba, N., González-Fernández, Á. & Alonso, M. J. Multi-enveloping of particulated antigens with biopolymers and immunostimulant polynucleotides. *J. Drug Deliv. Sci. Technol.* **30,** 424–434 (2015).
31. Lozano, M. V. *et al.* Polyarginine nanocapsules: A new platform for intracellular drug delivery. *J. Nanoparticle Res.* **15,** (2013).
32. Lollo, G. *et al.* Polyarginine Nanocapsules as a Potential Oral Peptide Delivery Carrier. *J. Pharm. Sci.* **106,** 611–618 (2017).
33. Niu, Z. *et al.* Rational design of polyarginine nanocapsules intended to help peptides overcoming intestinal barriers. *J. Control. Release* (2017).
34. Nakamura, Y., Mochida, A., Choyke, P. L. & Kobayashi, H. Nanodrug Delivery: Is the Enhanced Permeability and Retention Effect Sufficient for Curing Cancer? *Bioconjug. Chem.* **27,** 2225–2238 (2016).
35. Kai, M. P. *et al.* Tumor Presence Induces Global Immune Changes and Enhances Nanoparticle Clearance. *ACS Nano* **10,** 861–870 (2016).
36. Gabrilovich, D. I., Ostrand-Rosenberg, S. & Bronte, V. Coordinated regulation of myeloid cells by tumours. *Nat. Rev. Immunol.* **12,** 253–268 (2012).
37. Bronte, V. & Pittet, M. J. The spleen in local and systemic regulation of immunity. *Immunity* **39,** 806–818 (2013).
38. Drummond, C. J. & Fong, C. Surfactant self-assembly objects as novel drug delivery vehicles. *Curr. Opin. Colloid Interface Sci.* **4,** 449–456 (1999).
39. Clogston, J. & Caffrey, M. Controlling release from the lipidic cubic phase. Amino

acids, peptides, proteins and nucleic acids. *J. Control. Release* **107,** 97–111 (2005).
40. Kirby, N. M. *et al.* A low-background-intensity focusing small-angle X-ray scattering undulator beamline. *J. Appl. Crystallogr.* **46,** 1670–1680 (2013).
41. Hyde, S. T. Identification of Lyotropic Liquid Crystalline Mesophases. *Handb. Appl. Surf. Colloid Chem.* 299–332 (2001).
42. Schneider, C. A., Rasband, W. S. & Eliceiri, K. W. NIH Image to ImageJ: 25 years of image analysis. *Nat. Methods* **9,** 671–675 (2012).
43. Qiu, H. & Ca, M. The phase diagram of the monoolein / water system : metastability and equilibrium aspects. *Biomaterials* **21,** 223–234 (2000).
44. Zhai, J., Waddington, L., Wooster, T. J., Aguilar, M. I. & Boyd, B. J. Revisiting β-casein as a stabilizer for lipid liquid crystalline nanostructured particles. *Langmuir* **27,** 14757–14766 (2011).
45. Phan, S., Fong, W. K., Kirby, N., Hanley, T. & Boyd, B. J. Evaluating the link between self-assembled mesophase structure and drug release. *Int. J. Pharm.* **421,** 176–182 (2011).
46. Chang, D. P., Jankunec, M., Barauskas, J., Tiberg, F. & Nylander, T. Adsorption of Lipid Liquid Crystalline Nanoparticles: Effects of Particle Composition, Internal Structure, and Phase Behavior. *Langmuir* **28,** 10688–10696 (2012).
47. Rizwan, S., Hanley, T., Boyd, B., Rades, T. & Hook, S. Liquid crystalline systems of phytantriol and glyceryl monooleate containing a hydrophilic protein: characterisation, swelling and release kinetics. *J. Pharm. Sci.* **98,** 4191–4204 (2009).
48. Dolcetti, L. *et al.* Hierarchy of immunosuppressive strength among myeloid-derived suppressor cell subsets is determined by GM-CSF. *Eur. J. Immunol.* **40,** 22–35 (2010).
49. Rosenberg, S. A. *et al.* Durable Complete Responses in Heavily Pretreated Patients with Metastasic Melanoma Using T Cell Transfer Immunotherapy. *Clin. Cancer Res.* **17,** 4550–4557 (2011).
50. Besser, M. J. *et al.* Adoptive transfer of tumor-infiltrating lymphocytes in patients with metastatic melanoma: Intent-to-treat analysis and efficacy after failure to prior immunotherapies. *Clin. Cancer Res.* **19,** 4792–4800 (2013).
51. Sasso, M. S. *et al.* Low dose gemcitabine-loaded lipid nanocapsules target monocytic myeloid-derived suppressor cells and potentiate cancer immunotherapy. *Biomaterials* **96,** 47–62 (2016).
52. Rupaimoole, R. & Slack, F. J. MicroRNA therapeutics: towards a new era for the management of cancer and other diseases. *Nat. Rev. Drug Discov.* **16,** 203–222 (2017).
53. Barauskas, J., Johnsson, M., Joabsson, F. & Tiberg, F. Cubic Phase Nanoparticles (Cubosome): Principles for Controlling Size, Structure, and Stability. *Langmuir* **21,** 2569–2577 (2005).
54. Sahin, U., Karikó, K. & Türeci, Ö. mRNA-based therapeutics — developing a new class of drugs. *Nat. Rev. Drug Discov.* **13,** 759–780 (2014).
55. Tan, Y. F. *et al.* Layer-by-layer nanoparticles as an efficient siRNA delivery vehicle for SPARC silencing. *Small* **10,** 1790–1798 (2014).
56. Elbakry, A. *et al.* Layer-by-layer assembled gold nanoparticles for siRNA delivery. *Nano Lett.* **9,** 2059–64 (2009).
57. Chen, Z., Zhang, L., He, Y., Shen, Y. & Li, Y. Enhanced shRNA delivery and ABCG2

silencing by charge-reversible layered nanocarriers. *Small* **11,** 952–962 (2015).

USC
UNIVERSIDADE
DE SANTIAGO
DE COMPOSTELA

SUPPORTING INFORMATION

Supplementary methods

Synthesis of fluorinated short hairping (sh) RNAs

shRNA C/EBPβ and scramble shRNA (control) were synthetized *in vitro* via PCR and T7 RNA polymerase. PCR was performed in a 50 µl final reaction volume containing 1x PCR buffer, 2.5 mM MgCl2 , 0.2 mM dNTPs, 1 U Taq DNA polymerase (Invitrogen) and the following ssDNA primers (Eurofins MWG Operon) at 20 µM: ScrambleF 5'-TAATACGACTCACTATAAGGGCAGTAGCATGGTCCGTTGAGATTCAAGAGATCT-3'; ScrambleR 5'-AAGGCAGTAGCATGGTCCGTTGAGATCTCTTGAATC-3'; C/EBPβF 5'-TAATACGACTCACTATAGGGCGGCGACTTCCTCTCCGACCTCTTCTTCAAGAGAGAAGAGG-3'; and C/EBPβR 5'-AAAAACGACTTCCTCTCCGACCTCTTCTCTCTTGAAGAAG-3'. A single PCR cycle was run with the following protocol: 95°C 10 min, 60°C 1 min, 72°C 20 min. The resulting dsDNA was purified using the Wizard® SV Gel and PCR Clean-up system (Promega) according to manufacturer's instructions.

One ug of dsDNA was used as template to transcribe shRNA molecules in a single *in vitro* transcription (IVT) reaction, using the DuraScribe® T7 transcription kit (Epicentre). IVT reaction was run overnight at 37°C in a temperature-controlled oven. DNA template was removed by DNase I digestion and shRNAs were purified using the miRNeasy Micro Kit (Qiagen). Purified shRNAs were quantified by spectrophotometer and correct molecule length was checked by denaturing gel electrophoresis (polyacrylamide 15%, urea 7M).

Lyophilization of nanocapsules

Nanocapsules were frozen overnight at -20°C and lyophilized in a VirTis Genesis 25L equipment (SP Industries) for their storage. Initial freezing temperature was set at -30°C and samples were equilibrated at -40°C before a 46 h drying process, divided in two steps. In the first drying step, temperature was slowly increased in 10°C intervals until reaching 20°C, when a 3 h secondary drying started. Samples were then reconstituted to the initial concentration with ultrapure water by vortexing until complete resuspension, when physicochemical properties and morphology were assessed as described in the experimental section. The integrity of RNA after this process was also evaluated by gel retardation assays.

Nanocapsules uptake in RAW 264.7 macrophages

For cell uptake studies, RAW 264.7 macrophages ($0.9x10^5$) were seeded in an 8 Chambered Borosilicate coverglass system (Lab-Tek) and left overnight. A dose of 1.25 µg of both free and encapsulated 5'-FAM labelled miRNA 142-3p was added to the cells diluted in 100 µL supplemented DMEM and incubated for 2 hours at 37°C. Then media was aspirated and cells were washed with PBS. Subsequently, cells were fixed with a 4% paraformaldehyde solution and stained with DAPI and phalloidin tetramethylrhodamine B isothiocyanate (Sigma) before observation by confocal microscopy (Leica TCS SP5).

Matrigel® invasion assay

T cell invasion in response to CCL2 was analyzed by a Matrigel® invasion assay. Jurkat cells were grown in modified RPMI-1640 medium containing 2 mM L-glutamine, 10 mM HEPES, 1 mM sodium pyruvate, 4500 mg/L glucose, and 1500 mg/L sodium bicarbonate and supplemented with 10% v/v fetal bovine serum (FBS), 100 U/mL penicillin and 100 µg/mL streptomycin (Life Technologies). Cells were maintained at 37 °C in a humidified incubator supplied with 5% CO_2, at a density of 0.1-1x10^6 cells/ml. Matrigels (10 mg/ml) were prepared in 8-well chambered coverslips (Ibidi) containing CCL2 (Peprotech) (CCL2 matrigels) or medium alone (Blank matrigels). For this, an ice-cold Matrigel® stock (11.6 mg/ml) was carefully mixed with the CCL2 OptiMEM solution (60 ng) or OptiMEM alone in a final volume of 100 µl. Ice-cold mixtures were pipetted on each well creating a thin layer of material and allowed to gel in a humidified incubator at 37 °C for 30 min. Then, 300 µl of Jurkat cells (0.15x10^6 cells) suspended in migration buffer (DMEM supplemented with 1% FBS, 100 U/mL penicillin and 100 µg/mL streptomycin) were added on top of each gel. After 48 h of incubation at 37 °C in a 5% CO_2 atmosphere, gels were washed carefully with PBS. Invasive cells were then fixed in paraformaldehyde and stained with DAPI before observation by confocal microscopy (Leica TCS SP5).

Supporting figures

Table S1. Physicochemical characterization of loaded nanosystems indicating: mean particle size, polidispersity index and zeta potential. Nanoemulsions were loaded with 50 µg/ml OVA. Nanocapsules (24.7 mg/mL) were loaded with 0.4 mg/mL RNA and 1 µg/ml CCL2. Values are means ± S.D., n=6 (OVA, RNA) and n=3 (CCL2).

Systems	Loading	Size (nm)	Polidispersity Index	Zeta potential (mV)
Nanoemulsions	*OVA*	172 ± 6	0.1	- 13 ± 1
Nanocapsules	*miRNA control*	186 ± 27	0.1	- 25 ± 7
	shRNA control	174 ± 13	0.1	-
	CCL2 freeze-dried	160 ± 21	0.1	26 ± 6

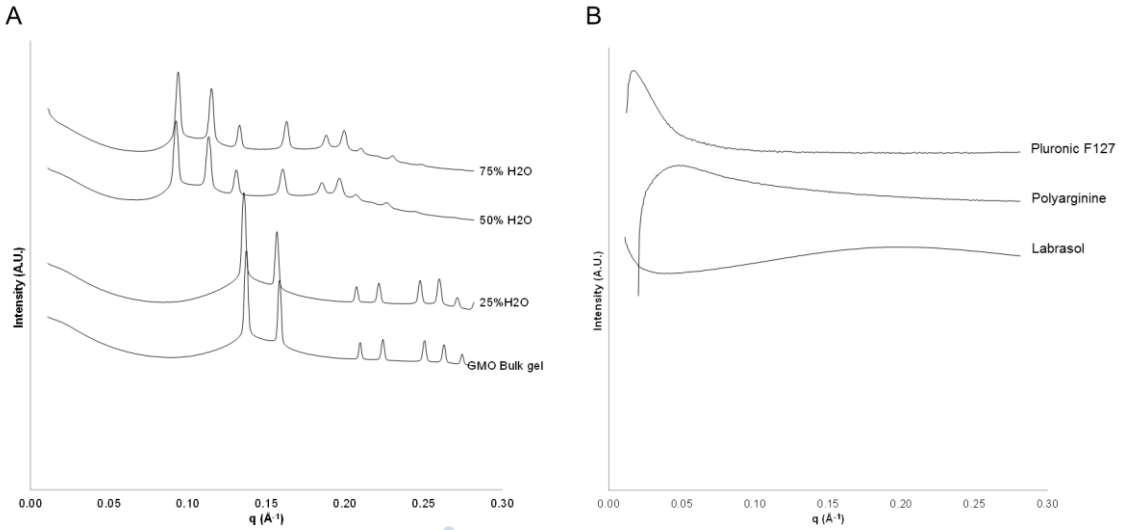

Figure S1. SAXS characterization of the precursor materials. A) SAXS analysis of GMO precursor gel, showing the transition from a Ia3d to a Pn3m phase arrangement upon increasing hydration. B) SAXS profile of raw materials.

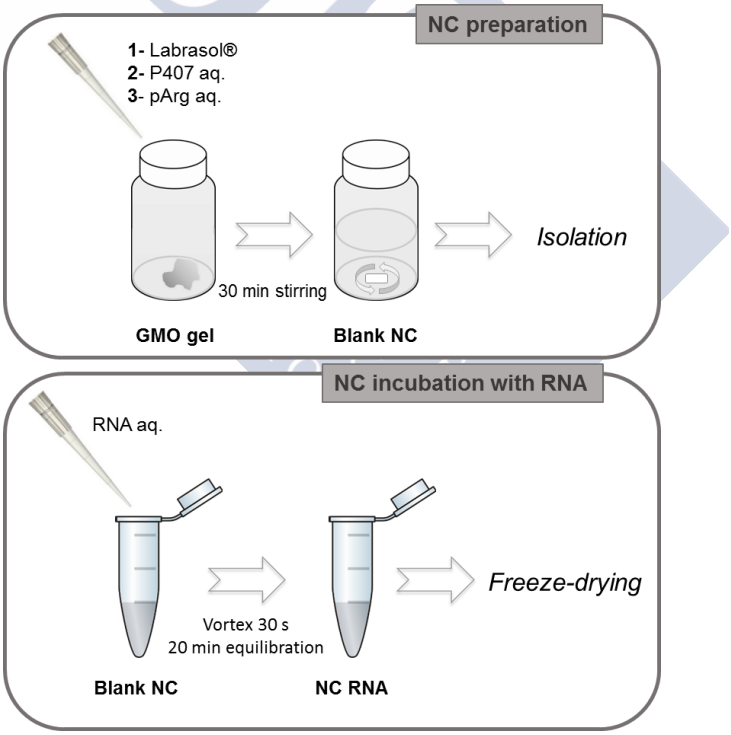

Figure S2. Scheme of the method used for nanocapsules preparation. Objects in figure are not drawn to scale. pArg: polyarginine; P407: Poloxamer 407, aq.: aqueous; GMO: glycerol monooleate; NC: nanocapsules.

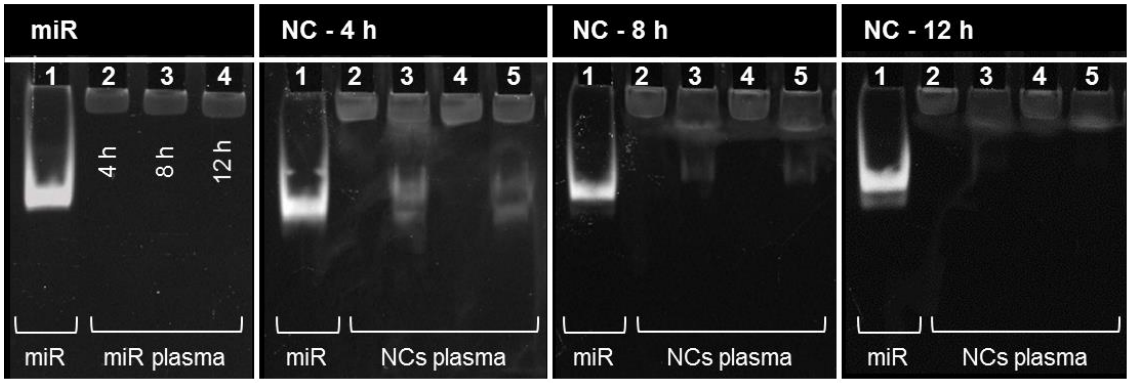

Figure S3. miR 142-3p stability and release from NCs in human plasma after 4, 8 and 12 h incubation. NCs were diluted 1/10 in plasma and at the desired time points samples were loaded in a 15% polyacrylamide gel with a theoretical miR amount of 400 ng per well. Lanes miR sequences: (1) miR 142-3p in solution; (2), (3) and (4) miR 142-3p incubated 4, 8 and 12h in plasma, respectively. Lanes 4 h assay: (1) miR 142-3p in solution; (2) and (4) NCs miR 142-3p incubated 4h in plasma; (3) and (5) NCs miR 142-3p incubated with heparin. Lanes 8 h assay: (1) miR 142-3p in solution; (2) and (4) NCs miR 142-3p incubated 8h in plasma; (3) and (5) NCs miR 142-3p incubated with heparin. Lanes 12h assay: (1) miR 142-3p in solution; (2) and (4) NCs miR 142-3p incubated 12h in plasma; (3) and (5) NCs miR 142-3p incubated with heparin.

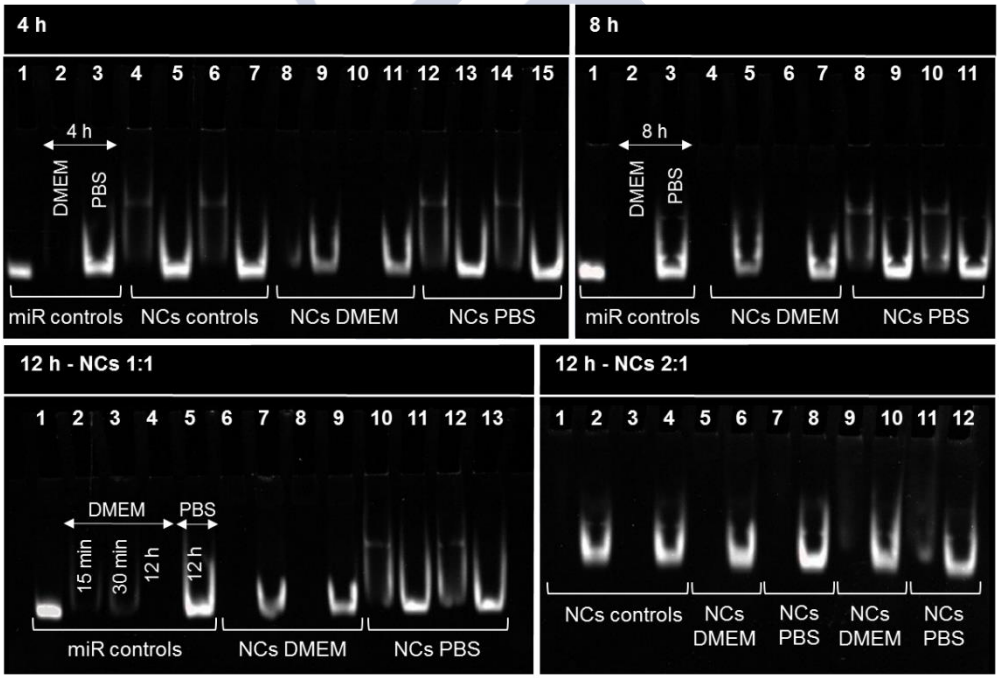

Figure S4. miR release assay in supplemented DMEM (10% FBS + 1% Pen/Strep) and PBS pH 7.2 after 4, 8 and 12 h incubation. NCs were diluted 1/10 in the correspondent media and at the desired timepoints samples were loaded in a 15% polyacrylamide gel with a theoretical miR amount of 800 ng per well. Lanes 4 h assay: (1) miR 142-3p in solution; (2) and (3) miR sequence in DMEM and PBS after 4h incubation, respectively; (4) and (6) fresh NCs; (5) and (7) fresh NCs incubated with heparin; (8) and (10) NCs incubated 4h in DMEM; (9) and (11) NCs DMEM incubated with heparin; (12) and (14) NCs incubated 4h in PBS; (13) and (15) NCs PBS incubated with heparin. Lanes 8 h assay: (1) miR 142-3p in solution; (2) and (3) miR sequence in DMEM and PBS after 8h incubation, respectively; (4) and (6) NCs incubated 8h in DMEM; (5) and (7) NCs DMEM incubated with heparin; (8) and (10) NCs incubated 8h in PBS; (9) and (11) NCs PBS incubated with heparin. Lanes 12h assay polyarginine:miR ratio 1:1: (1) miR 142-3p in solution;

(2) and (3) miR in DMEM after 15 and 30 minutes incubation, respectively; (4) and (5) miR in DMEM and PBS after 12h incubation, respectively; (6) and (8) NCs incubated 12h in DMEM; (7) and (9) NCs DMEM incubated with heparin; (10) and (12) NCs incubated 12h in PBS; (11) and (13) NCs PBS incubated with heparin. Lanes 12h assay ratio 2:1: (1) and (3) NCs miR; (2) and (4) NCs incubated with heparin; (5) and (9) NCs incubated 12h in DMEM; (6) and (10) NCs DMEM incubated with heparin; (7) and (11) NCs incubated 12h in PBS; (8) and (12) NCs PBS incubated with heparin.

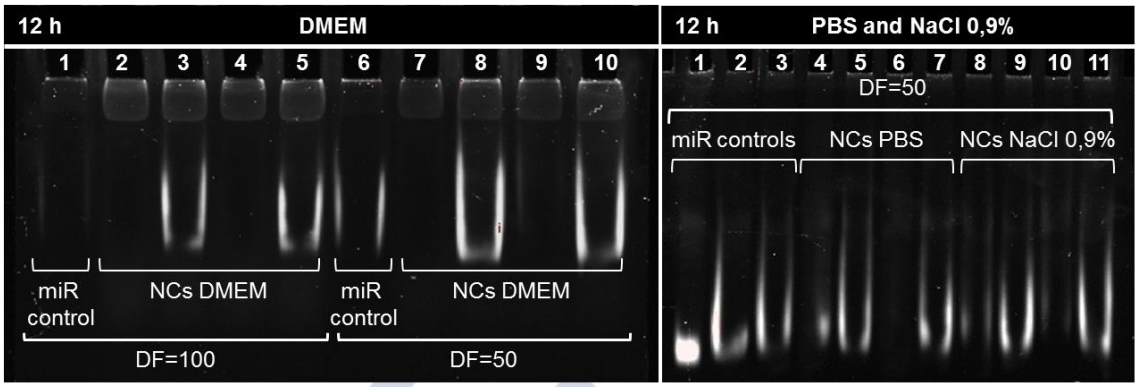

Figure S5. miR release assay in supplemented DMEM (10% FBS + 1% Pen/Strep), PBS pH 7.2 and saline solution after 12 h incubation. NCs (ratio 1:1) were diluted 1/100 and 1/50 in DMEM and 1/50 in PBS and saline solution. After 12 h incubation, samples were loaded in a 15% polyacrylamide gel with a theoretical miR amount of 400 ng per well. Lanes DMEM assay: (1) miR 142-3p sequence incubated 12h in DMEM with a 1/100 dilution; (2) and (4) NCs incubated 12h in DMEM with a 1/100 dilution; (3) and (5) NCs DMEM 1/100 incubated with heparin; (6) miR 142-3p sequence incubated 12h in DMEM with a 1/50 dilution; (7) and (9) NCs incubated 12h in DMEM with a 1/50 dilution; (8) and (10) NCs DMEM 1/50 incubated with heparin. Lanes PBS and saline assay: (1) miR 142-3p sequence in solution; (2) and (3) miR 142-3p sequence incubated 12h in PBS and saline with a 1/50 dilution, respectively; (4) and (6) NCs incubated 12h in PBS with a 1/50 dilution; (5) and (7) NCs PBS 1/50 incubated with heparin; (8) and (10) NCs incubated 12h in saline solution with a 1/50 dilution; (9) and (11) NCs saline 1/50 incubated with heparin.

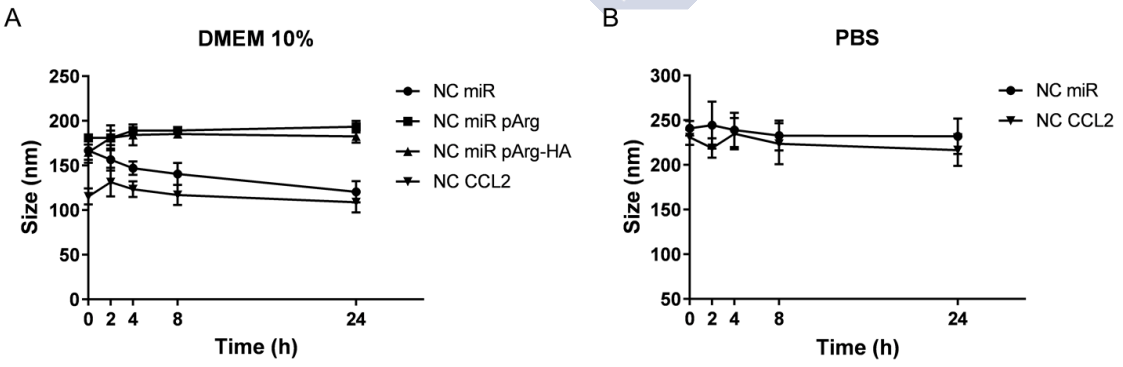

Figure S6. Colloidal stability of polyarginine NCs in supplemented DMEM (10% FBS + 1% Pen/Strep) and PBS pH 7.2.

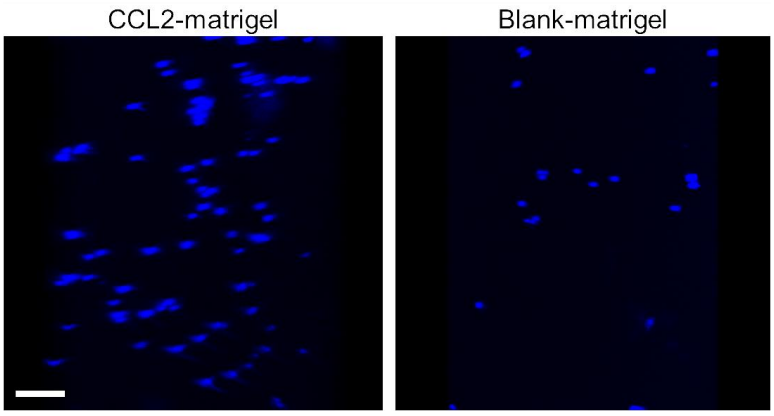

Figure S7. Jurkat cells invade the tumor-mimicking Matrigel® system in response to CCL2. Fluorescence images of DAPI stained-cells associated to the matrigels after a 48 h invasion assay. Representative z-stacks for CCL2 and blank-matrigels. Scale bar = 100 µm for all the images.

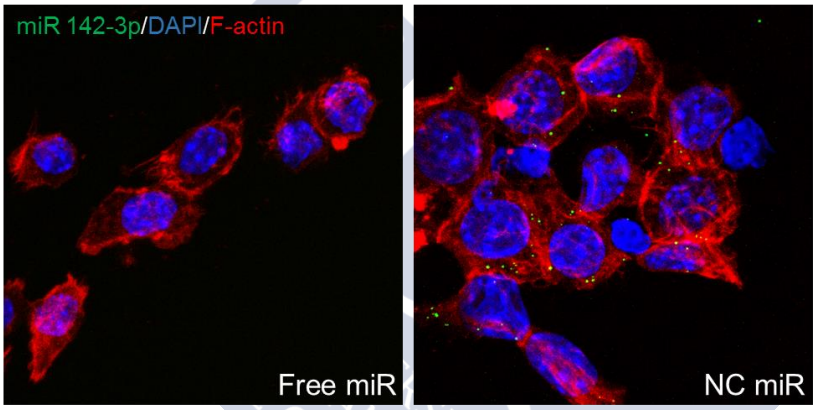

Figure S8. Polyarginine NCs promote RNAi macrophage uptake. Confocal laser microscopy images of RAW264.7 cells incubated with either fluorescently labelled Free RNAi or with the same RNAi loaded in polyarginine NCs.

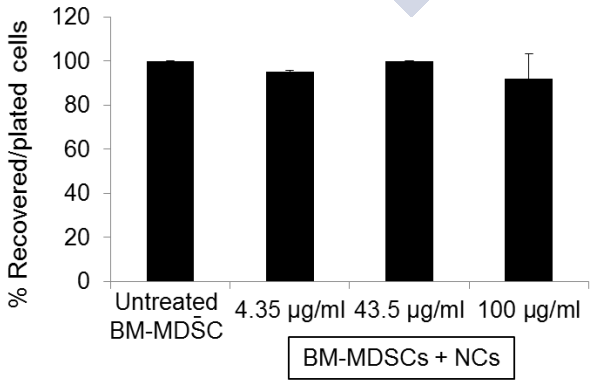

Figure S9. Polyarginine blank NCs do not affect the viability of the BM-MDSCs culture. Cells were treated with different concentrations of blank NCs and cytotoxicity was assessed by calculating the percentage of viable recovered cells on plated cells. Values are means ± SD of two independent experiments.

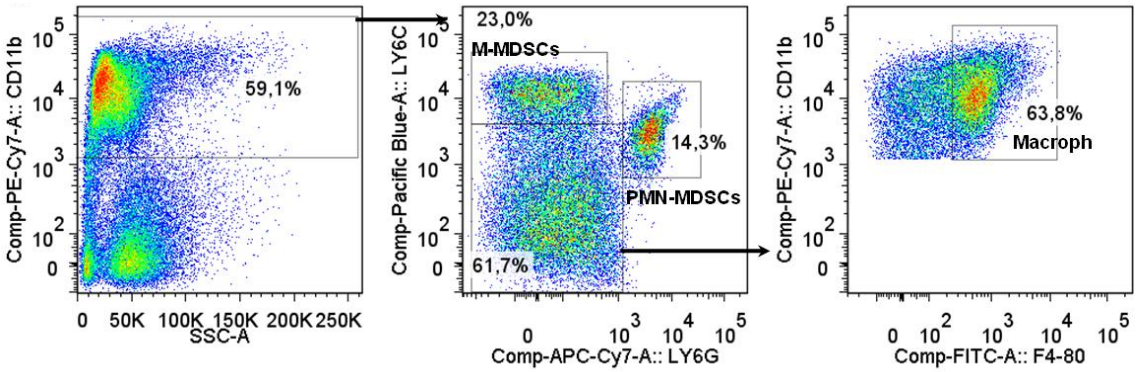

Figure S10. Gating strategy for the identification of PMN-MDSCs (CD11b+Ly6G+Ly6Cint), M-MDSCs (CD11b+Ly6G-Ly6Chigh) and macrophages (CD11b+Ly6G- Ly6Clow/- F4/80+) in the tumor. All analysis were performed after selection of living single cells by morphologic gating, doublets exclusion and dead cell exclusion by LIVE/DEAD® dye staining.

USC
UNIVERSIDADE
DE SANTIAGO
DE COMPOSTELA

Chapter 2

USC
UNIVERSIDADE
DE SANTIAGO
DE COMPOSTELA

CHAPTER 2

mRNA-Activated Matrices Encoding Transcription Factors as Primers of Cell Differentiation in Tissue Engineering

This work has been done in collaboration with the Department of Physiology at the University of Santiago de Compostela

ABSTRACT

Gene-activated matrices (GAMs) encoding pivotal transcription factors (TFs) represent a powerful tool to direct stem cell specification for tissue engineering applications. However, current TF-based GAMs involving the use of pDNA have shown a limited potential and the current expectations rely mainly on the use of mRNA-GAMs. Here, we report a new GAM technology based on mRNA-encoded TFs SOX9 (cartilage) and MYOD (muscle) nanocomplexed to activate *in situ* gelling fibrin hydrogels. We find that mRNA GAMs induce a much higher and faster transgene expression compared to pDNA GAMs, especially in the case of RNase resistant mRNA sequences. This potent TF expression, in turn, induces a higher synthesis of cartilage- and muscle-specific markers at the gene and protein level. Interestingly, we show that the differentiation process is modulated by the mRNA-GAM environment, with low fibrin content matrices inducing better chondrogenesis and high fibrin content matrices promoting improved myogenesis. Taken together, these observations demonstrate the potential of this new kind of gene activated matrices for regenerative medicine.

Key words: GAMs, 3D transfection, mRNA, SOX9, MYOD, tissue engineering

USC
UNIVERSIDADE
DE SANTIAGO
DE COMPOSTELA

1. Introduction

Polymer matrices have been largely explored as tissue engineering devices. Since the FDA approval of the first collagen-based dermal regeneration template Omnigraft®[1] (Integra Life Sciences, Plainsboro NJ), several materials systems have reached the market and paved their way into the clinical setting. Although the first devices largely consisted on biocompatible scaffolds used as fillers or protective patches, polymer matrices soon started to comprise growth factors and other recombinant proteins to help direct the regenerative process. OP-1™ (Stryker Biotech, Hopkinton, MA), a rhBMP-7-loaded collagen carrier, Infuse® (Medtronic, Minneapolis, MN), a rhBMP-2 loaded collagen sponge, or Regranex® (OMJ Pharmaceuticals, Raritan, NJ) a sodium carboxymethylcellulose-based gel loaded with rhPDGF, represent some successful examples[2]. However, these factors are often administered at high doses to overcome their short half-life and currently used materials offer a poor control over their release profiles. This in turn leads to side effects, among which, the risk of malignancies is one of the biggest concerns[3–5].

Trying to overcome these limitations, researchers started to explore the use of gene therapy as an alternative to recombinant proteins, and the concept of Gene Activated Matrix (GAM) was described[6]. Initially, GAMs were based on plasmid DNA (pDNA), free or complexed to non-viral formulations, encoding the growth factor of interest. As for recombinant proteins, this complexed pDNA was loaded within a polymer matrix from which it would be released, producing the transfection of surrounding cells and the consequent sustained and localized transgene expression[7]. Nevertheless, while nonviral delivery of pDNA is preferred over viral vectors due to safety concerns, non-viral formulations are characterized by a low gene transfer efficiency, which in part hampers their clinical success. This scenario has prompted the development of RNA-based GAMs, based on the superior gene transfer capacity of RNA[8]. In this regard, different RNA GAMs were explored, ranging from siRNA and miRNA GAMs[7], to the more recent mRNA GAMs, first described by Elangovan et al. two years ago[9]. In their work, Elangovan and co-workers used chemically modified mRNA encoding the growth factor BMP-2, to study the bone regeneration in rat calvarial defects, and demonstrated its superior biocompatibility and regenerative capacity compared to traditional pDNA-GAMs. Subsequent works explored the use of other GFs and material systems to fabricate mRNA-based GAMs, further highlighting the value of this strategy[10,11].

Compared to growth factors, transcription factors (TFs) have higher potency and specificity to drive cell reprogramming and directed differentiation[12–16]. Realizing their potential for tissue engineering applications, researchers investigated the use of GAMs encoding pivotal TFs in musculoskeletal development, and stablished TF-activated GAMs as promising alternatives to “traditional” growth factor-activated GAMs[17,18].

However, although it has been recently demonstrated that mRNA-encoded TFs can efficiently modulate cell phenotype[16,19–21], to the best of our knowledge, TF-based GAMs have only been explored for pDNA. In this work, we developed a new kind of mRNA GAMs activated with lineage specific TFs and loaded with hMSCs, to direct cell specification in injured or diseased tissues. To this end, fibrin hydrogels were activated with nanocomplexed mRNA encoding SOX9 (cartilage)[22,23] and MYOD (muscle)[24] to promote MSC chondrogenic and myogenic differentiation. Compared to previously explored TF pDNA GAMs, we hypothesized that the rapid gene modulation induced by mRNA could trigger a faster onset of the differentiation cascades, improving the quality of the regenerated tissue. Indeed, we demonstrate that these new GAMs are able to upregulate tissue-specific genes faster than their pDNA counterparts and show how this rapid upregulation results in a higher synthesis of tissue-specific proteins. Overall, this work describes the generation of a novel mRNA GAM concept that could provide therapeutic benefit compared to classical pDNA GAMs.

2. Materials and methods

2.1 Cell culture

Human adipose derived Mesenchymal Stem Cells (hMSCs) were acquired from tebu-bio (Le Perray-en-Yvelines, France) and ATCC (Manassas, VA, USA) and cultured in α-MEM (Gibco, Life Technologies, Carlsbad, CA, USA) supplemented with 10% fetal bovine serum (Gibco), 1% penicillin-streptomycin (Gibco) and 10 ng/ml bFGF (Peprotech, Rocky Hill, NJ, USA). Cells were detached from the plates using TrypLE solution (Gibco) and plated at 5000-7500 cells/cm2. Media was changed every 2-3 days and cells were split at 70-80% confluency.

2.2 Plasmid design and mRNA synthesis

Yellow Fluorescent Protein (YFP) and SOX9 mRNAs were in vitro transcribed (IVT) from plasmid templates (**Fig. S1**). To construct the YFP plasmid, the YFP coding sequence (CDS) and a SV40 polyadenilation signal were sequentially digested from a pIRES YFP vector (Clontech, Mountain View, CA, USA) using the XhoI and SmaI sites, and ligated into a pBluescript KS (+) vector (Stratagene, San Diego, CA, USA). Digestion products were separated in agarose gels and purified with the Wizard SV Gel and PCR Clean-up system kit (Promega, Madison, WI, USA) before overnight ligation at room temperature with T4 DNA ligase (Promega). For SOX9 plasmid, the SOX9 CDS, a Kozak consensus sequence and the 3' UTR of the α globin gene[16,25,26] were synthesized and cloned into a pCMVTnT expression vector (Promega, Madison, WI, USA) by Genewiz (South Plainfield, NJ, USA). Both plasmids were sequence-verified (Stab Vida, Caparica, Portugal) and DH5α *E. Coli* bacteria were transformed for their propagation. Plasmids were extracted from the bacterial cultures and purified with the NucleoSpin Plasmid Kit (Macherey-Nagel, Dueren, Germany) according to manufacturer's instructions. Corresponding

mRNA sequences were synthesized with the Anti-Reverse Cap Analog (ARCA) technology, using the mMESSAGE mMACHINE T7 Ultra kit (Ambion, Foster City, CA, USA) following the manufacturer's protocol. Briefly, plasmids were linearized using XhoI and BamHI restriction enzymes (Promega) and 2-7 enzyme units per µg of pDNA. Endonuclease digestion was confirmed by gel electrophoresis and 1.35 µg of linearized plasmids were used to template each 20 µl reaction. mRNAs were purified via phenol-chloroform extraction using Phase Lock 1.5 ml tubes (5 Prime, Hilden, Germany) followed by ethanol precipitation and quantification by Nanodrop (Thermo Fisher Scientific, Waltham, MA, USA). MYOD mRNA was purchased from Stemgent (Cambridge, MA, USA) and used as supplied.

2.3 Preparation and characterization of 3DFectIN complexes

For 3D transfection experiments, 50 µl of 3DfectIN complexes (OZ Biosciences, Marseille, France), in the specified 3DFectIN:DNA/RNA ratios (µl:µg), were prepared in OptiMEM (Gibco) following manufacturer's instructions. Briefly, a solution containing 1 µg of mRNA/pDNA was added over a solution containing 1, 2, 3 or 4 µl of 3DFectIN reagent in a 1/1 v/v ratio, mixed by pipetting up-down and incubated for 20 min at room temperature. Particle mean size and polydispersity index were analyzed by Dynamic Light Scattering (Nanosizer ZS®, Malvern, Worcestershire, UK) without further dilution. Distribution of the complexes within the hydrogels was assessed after the encapsulation of SYBR®Gold-labeled pDNA complexes and by their visualization under fluorescence microscopy (Olympus IX51 operated with a U-RFL-T lamp). To this end, an aqueous solution of genetic material was labeled by mixing with a 50X DMSO solution of SYBR®Gold Nucleic Acid Gel Stain (Invitrogen) in a ratio 1:1 (µg:µl) and incubated for 5 min at room temperature before complexes were prepared.

2.4 Hydrogel preparation and 3D transfection

Human plasma derived fibrinogen and thrombin were purchased from Sigma-Aldrich (St. Louis, MO, USA). Both materials were reconstituted in Ca^{2+} and Mg^{2+} free phosphate buffered saline (Invitrogen) at 50 mg/ml and 100 U/ml, respectively, and further diluted with the same buffer before hydrogel formation. Fibrin hydrogels of 2 and 4 mg/ml were prepared using 0.625 thrombin units per mg of fibrinogen and casted in tissue culture plates (Thermo Fisher Scientific). Transfection and characterization assays were performed with 100 µl gels casted in 96 well plates. In differentiation assays, 200 µl gels were casted in 48 well plates. For 100 µl gels, 20 µl of the fibrinogen solution (20 or 40 mg/ml) were added to the bottom of the plate. Then, the cell suspension (control gels), the cell suspension mixed with 50 µl 3DFectIN complexes (gene-activated gels), or 60 µl of OptiMEM (blank gels) were thoroughly blended with fibrinogen by pipetting up-down. After this, 20 µL of the thrombin solution (12.5 U/ml) were quickly mixed with the previous hydrogel blend ($1.5x10^6$ cells/ml of gel) avoiding the formation of bubbles. Plates were placed in the cell incubator at 37 °C for 1 h to allow gelation. Finally, 200 µl

of culture medium were added on top of each gel. For 200 µl gels, the same procedure was followed but quantities were doubled.

2.5 Scanning electron microscopy

Blank and cell-seeded fibrin hydrogels were prepared as previously described (**section 2.4**). Blank gels were frozen at -80°C after the gelation process, while hMSCs seeded gels were kept 1 week in culture before freezing. All gels were freeze-dried in a VirTis Genesis 25 ES freeze-drier (SP Industries, Warminster, PA, USA) under the following program: primary drying at -35 °C for 24 h, secondary drying at 0 °C for 24 h and 14 h at room temperature. Freeze-dried samples were carefully removed from the plates and metalized with iridium using a Sputer Coater Quorum Q150T-S (Guelph, Ontario, Canada). Samples were visualized in a Zeiss FESEM Ultra Plus with EDX operated at 5 kV.

2.6 Cell toxicity and proliferation assays

Toxicity derived from the encapsulation of hMSCs in gene-activated gels was evaluated by MTT assays (Sigma-Aldrich). Cell proliferation was investigated by monitoring the DNA content using the Quant-iT PicoGreen dsDNA assay kit (Invitrogen, Life Technologies, Carlsbad, CA, USA). hMSCs were encapsulated in fibrin hydrogels with or without 3DFectIN complexes at a density of $1.5x10^5$ and $1.5x10^6$ cells/ml for MTT and PicoGreen assays, respectively. For MTT assays, gels were cultured during 24 and 48 h and PicoGreen assays were run for 12, 24 and 48 h (short assays) or 3, 7 and 10 days (long assays), preserving some gels for day 0 controls. At the desired time points, gels were digested with 100 µl of a 2.5% trypsin solution (30 min, 37 °C) and transferred to 2 ml tubes. In the case of MTT assays, formazan crystals were solubilized with a 1/1 v/v mix of 20 % SDS in PBS and isopropanol by vortexing for 15 min at 2000 rpm in an Eppendorf MixMate® (Eppendorf, Hamburg, Germany) followed by absorbance reading (570 nm with 690 wavelenght correction) in a Multiskan GO spectrophotometer (Thermo Scientific). The reading values in gene-activated gels were converted to the percentage of the control (non-activated) gels. For proliferation assays, DNA was extracted with a sequential lysis process using an SDS solution (0.1% w/v in PBS) for the first step and a Triton X-100 solution (1% in PBS) for the second step. Samples were vortexed in an Eppendorf MixMate® (15 min at 2000 rpm for each step) to help extraction. Fluorescence readings were performed at 480/520 excitation/emission wavelengths in an EnVision multilabel plate reader (Perkin Elmer, Whaltam, MA, USA). Blank gels were included to subtract the fluorescence background and calibration was performed against a λ DNA standard.

2.7 Hydrogel degradation assay

Cell-mediated degradation of fibrin hydrogels was determined by digesting the gels and measuring the change in protein content over time. Non-activated hydrogels seeded with hMSCs were prepared as previously described (**section 2.4**) and incubated in

culture media at 37 °C and 5% CO_2 for 5 days. At day 1, 2 and 5, the cell media was aspirated and gels were digested with 100 µl of a 2.5% trypsin solution (30 min, 37 °C). After digestion, samples were diluted with water and protein content was quantified as described in Section 2.10. Percentage weight change was normalized to day 0.

2.8 Chondrogenic differentiation

Chondrogenesis assays were performed in hMSCs below passage 10. For experiments evaluating the kinetics of chondrogenic marker expression, 2 and 4 mg/ml hydrogels were casted in 96 well plates and cultured for 7 and 21 days in Complete Chondrogenic Medium (CCM) consisting of DMEM high-glucose 1 mM pyruvate (Gibco), 100 nM dexamethasone (Sigma-Aldrich), 50 µg/ml ascorbic acid 2-phosphate (Sigma-Aldrich), 40 µg/ml L-proline (Sigma-Aldrich), 1% ITS Premix supplement (Becton Dickinson), 1% penicillin/streptomycin (Gibco) and 10 ng/ml transforming growth factor-β3 (Peprotech). Hydrogels (100 µl) were activated with two doses of SOX9 mRNA and pDNA, namely 1 and 0.25 µg per gel, and at desired time points total RNA was extracted to check for the presence of chondrogenic markers SOX9, aggrecan (ACAN) and collagen type II (COL2A1) by qRT-PCR. For experiments evaluating the quality of the cartilage-like tissue, fibrin hydrogels of 2 mg/ml (0.5 µg mRNA per 200 µl gel) were casted in 48 well plates and cultured in CCM and CCM without TGF-β3 (Incomplete Chondrogenic Medium, ICM) for 21 days. At the end of the experiments, SOX9-activated gels were retrieved from the plates and the expression of chondrogenic markers was assessed and compared to non-activated gels cultured in the same conditions. Gene expression of SOX9, ACAN, COL2A1 and collagen type X (COLX) was assessed by qRT-PCR. Alcian blue staining and collagen type II immunohistochemistry (IHC) were used to analyze the deposition of extracellular matrix. Media was changed every 3 days in both experiments.

2.9 Myogenic differentiation

Two protocols were assayed for myogenic differentiation. For both protocols, fibrin hydrogels of 2 and 4 mg/ml were casted in 48 well plates and cultured for 14 days. In the first protocol, hydrogels were activated with 0.5 µg of MYOD mRNA per gel and cultured in complete growth media for the first day changing to DMEM high glucose supplemented with 2% horse serum (Gibco) and 1% penicillin-streptomycin for the rest of the assay. In the second protocol, hydrogels were activated with 0.25 µg of MYOD and cultured in α-MEM supplemented with 5% fetal bovine serum and 1% penicillin-streptomycin for the first 7 days (growth phase) switching to DMEM high glucose supplemented with 2% horse serum, 1% penicillin-streptomycin and 10 ng/ml IGF-I (Peprotech) for the rest of the assay (differentiation phase). At the end of the experiments, hydrogels were retrieved and the expression of myogenic markers was assessed and compared to non-activated gels cultured in the same conditions. Gene expression of myogenic differentiation 1 (MYOD), myogenin (MYOG), cadherin 15 (CDH15), myosin heavy chain 2 (MYH2) and myosin heavy chain 3 (MYH3) was evaluated

by qRT-PCR whereas myosin IHC was used to analyze myotube formation. Media was changed every 2 days in both experiments.

2.10 Total RNA extraction

Two hydrogels (100 µl) or one hydrogel (200 µl) per condition were used for RNA extraction. Hydrogels were removed from the plates with the help of a spatula and placed in 1.5 ml tubes. In transfection experiments, gels were washed with 0.5 ml of PBS and centrifuged in an Eppendorf 5430R centrifuge (4000 rpm, 5 min, 4 °C) to remove any remaining media before the extraction. In the case of chondrogenic differentiation experiments, gels and pellets were washed with PBS, digested with 700 collagenase units (Gibco) for 15 min at 37 °C and washed again before starting the extraction protocol. Centrifugation speed during the washing steps was set at 4000 and 1000 rpm for the gels and pellets, respectively. For each RNA extraction, 350 µl of lysis buffer were used and samples were digested by vortexing 15 min at 2000 rpm in an Eppendorf MixMate® with the help of two 2.8 mm stainless steel grinding balls (Ops Diagnostics, Lebanon, NJ, USA). Cell lysates were extracted with the SPEEDTOOLS total RNA extraction kit (Biotools, Madrid, Spain) following manufacturer's instructions. RNA was quantified by UV absorbance using a Nanodrop 2000 spectrophotometer (Thermo Scientific).

2.11 cDNA synthesis and qRT-PCR

Reverse transcription was carried out using 100-500 ng of total RNA per sample in a 30 µl final reaction volume. First, total RNA was mixed with random primers and dNTPs (Invitrogen) and kept at 65 °C for 5 min. Samples were then incubated with a mix of RNAse OUT, 5x first strand buffer and DTT (Invitrogen) for 2 min at 37 °C and subsequently placed on ice. Finally, reverse transcriptase (M-MLV, Invitrogen) was included and the cycle was continued as follows: 10 min at 25 °C, 50 min at 37 °C and 15 min at 70 °C. The resulting cDNA (5-30 ng) was used to assemble qRT-PCR reactions in a final volume of 20 µl containing Universal PCR Mastermix and TaqMan assays (Applied Biosystems, **Table S1**). The thermal cycling was done in a StepOne Real Time PCR System (Applied Biosystems) performing a 10 min hold at 95 °C followed by 40 cycles of 15 sec at 95 °C and 1 min at 60 °C. No template controls were used in each reaction as negative control. Gene expression values were normalized to internal controls (Actin β and GAPDH) and presented as a fold change relative to cells plated in 2D before the experiments using the comparative $2^{-\Delta\Delta Ct}$ method[27].

2.12 Immunohistochemistry

Hydrogels were retrieved from tissue culture plates, washed with PBS and fixed with 10% buffered formalin at room temperature for less than 24 h. After fixation, samples were maintained in 70% ethanol before dehydration and paraffin sectioning. Sections of 4 µm thickness were cut and allowed to adhere to poly-L-lysine treated glass slides

overnight at 55 °C. Before staining, sections were dewaxed in xylene and hydrated with graded ethanol. Samples from chondrogenic differentiation experiments were stained for deposited sGAG and collagen content with alcian blue (pH 2.5) and Sirius red, respectively. Immunohistochemical staining (IHC) was performed to check for the presence of collagen type II (II-II6B3, DSHB, Iowa City, IA, USA) and myosin heavy chain (clone MY-32 Sigma-Aldrich), after chondrogenic and myogenic differentiation experiments, respectively. Antigen retrieval was performed in Tris-EDTA buffer during 20 min at 95 °C in a PT Link (Agilent, Santa Clara, CA, USA). Samples were pretreated with hydrogen peroxide and blocked with serum free protein block (Dako; Agilent, Santa Clara, CA, USA). Primary antibodies were diluted 1:100 in antibody diluent (Dako) and incubated overnight at 4 °C followed by the incubation with goat secondary antibodies labeled with HRP (Dako) at 1:100 for 1 h and the staining with 3,3'-diaminobenzidine (DAB). Negative controls for histology consisted of hydrogels maintained in regular culture conditions. IHC negative controls were obtained by omitting the primary antibodies (**Fig. S2**). All samples were observed using an Olympus BX43 microscope equipped with an Olympus XC50 camera.

2.13 Statistical Analysis

The statistical analysis was performed using GraphPad Prism. Where applicable, data are reported as the mean ±SD. Data were compared using One- or Two-way ANOVA and p-values less than 0.05 were considered to be statistically significant.

3. Results

3.1 Synthesis and characterization of gene activated matrices (GAMs)

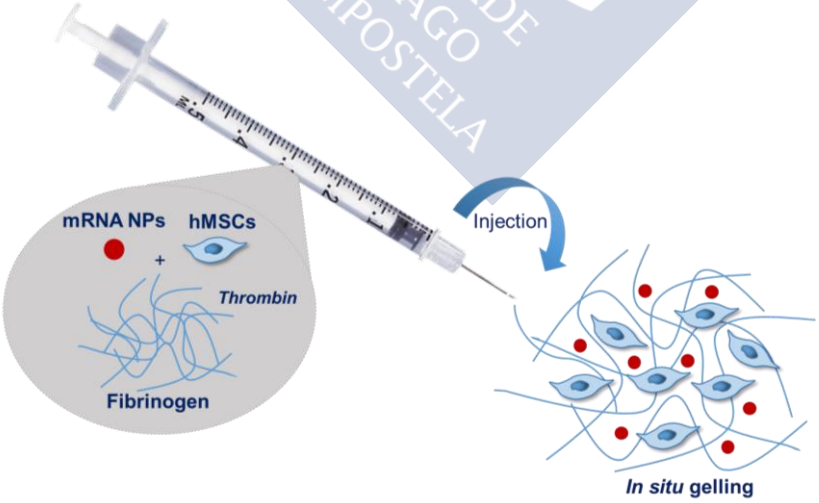

Figure 1. Schematic of human Mesenchymal Stem Cells (hMSCs) encapsulated within mRNA-activated fibrin matrices. mRNA nanocomplexes coding for key transcription factors (TFs) and hMSCs are mixed with fibrinogen and crosslinked with thrombin. Transfection occurs when hMSCs invade the resulting gel leading to forced TF expression and phenotype specification. Objects are not drawn to scale.

Fibrin hydrogels were activated with mRNA and plasmid DNA (pDNA) nanocomplexes coding for transcription factors that are master regulators of cell lineage specification: SOX9 (cartilage) and MYOD (muscle). Both polynucleotides were complexed with 3DfectIN® transfection reagent and mixed with human mesenchymal stem cells (hMSCs) and fibrinogen to yield gene activated matrices (GAMs) upon thrombin crosslinking (**Fig. 1**). In a first step, different 3DfectIN:polynucleotide ratios were evaluated in terms of nanocomplex size, polydispersity index, and payload encapsulation efficiency. All ratios resulted in a homogeneous distribution of 3DfectIN:pDNA complexes within the matrices, that was independent of the fibrinogen concentration (2 or 4 mg/ml) (**Fig. 2A**). Increasing 3DfectIN:polynucleotide ratios from 2:1 to 4:1 (µl:µg) produced smaller and less polydisperse mRNA nanocomplexes, whereas low ratios were needed to obtain small monodisperse pDNA complexes (**Fig. 2B**). Ratio 1:1 exhibited the best compromise for both polynucleotides in terms of particle size and polydispersity index, but this ratio showed an incomplete complexation of the payload (**Fig. S3**). Ratio 2:1 ratio produced polydisperse mRNA complexes with an average size of about 500 nm, while pDNA complexes prepared at the same ratio exhibited a micrometric size. 3:1 and 4:1 ratios resulted in monodisperse mRNA complexes of around 200 nm and micrometric pDNA complexes.

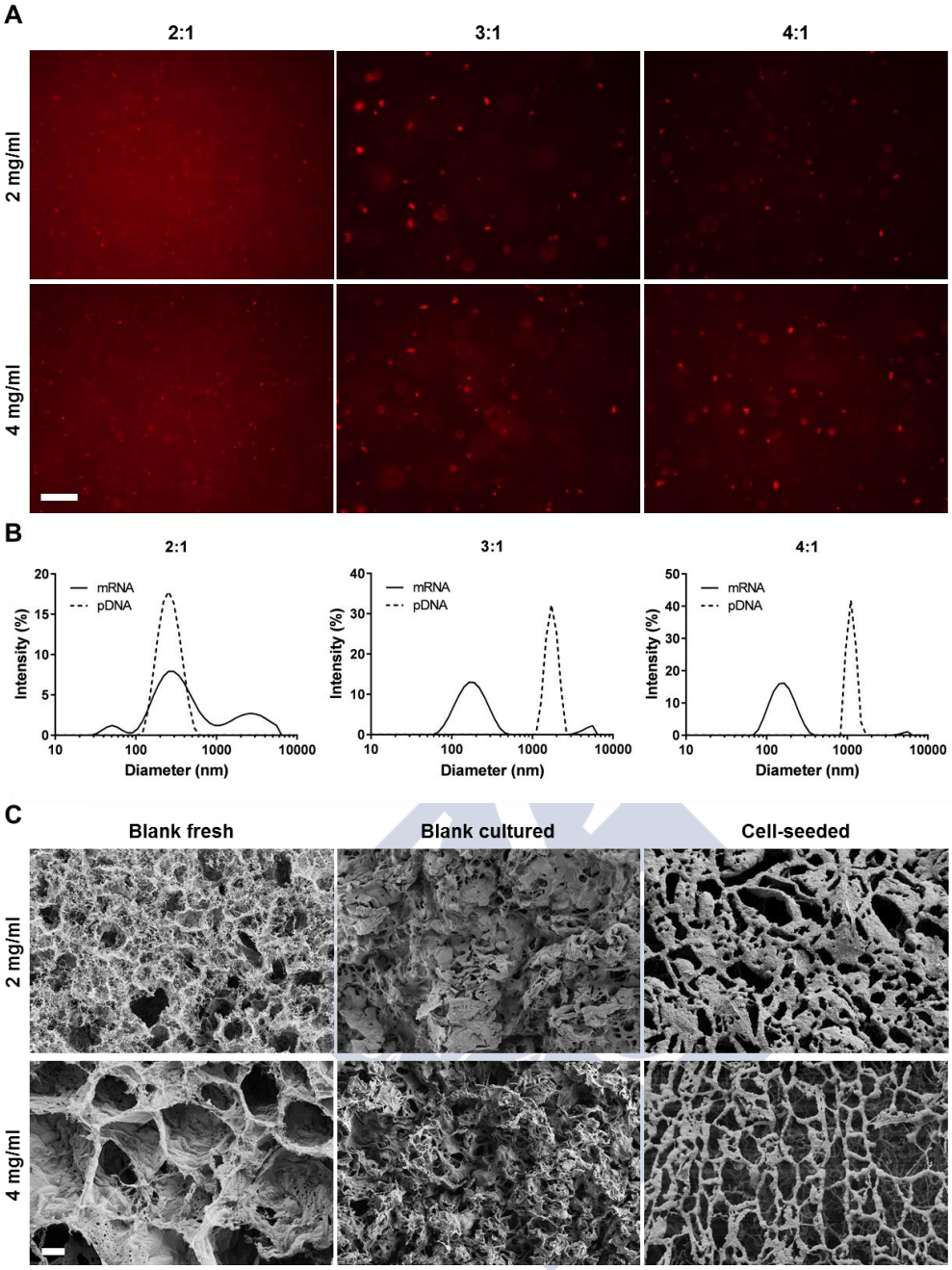

Figure 2. Physicochemical characterization and structural analysis revealed a monodisperse population of 3DFectIN® complexes and highly porous and fibrillar matrices. A) Fluorescence micrographs of SYBR®Gold labelled pDNA complexes (2:1 to 4:1 3DFectIN:pDNA µl:µg ratios) loaded in 2 and 4 mg/ml fibrin hydrogels. Scale bar = 50 µm for all the images. B) Representative size intensity distributions of mRNA and pDNA 3DFectIN complexes as measured by DLS. C) SEM analysis of microarchitecture of fibrin hydrogels. The scale bar corresponds to 20 µm for all the images.

Both concentrations of fibrin hydrogels, 2 and 4 mg/ml, showed a highly porous and fibrillar microarchitecture as observed by SEM (**Fig. 2C**). As expected, the lower fibrinogen concentration of 2 mg/ml gels led to an increased porosity compared to the more concentrated 4 mg/ml gels. Although a few cells can be visualized, there is a notable increase in hydrogel porosity accompanied by a thicker fibrillar network in both seeded gels compared to their blank counterparts. These changes in gel architecture are

likely due to mechanical forces exerted by attached cells and their matrix deposition, that cause hydrogel remodeling.

3.2 Optimization of mRNA 3D transfection

Once the GAMs were characterized in terms of nanocomplexes properties and microarchitecture, a model cell line was encapsulated therein to evaluate their 3D transfection efficiency and cytotoxicity profile. YFP and SOX9 mRNAs were transcribed *in vitro* and transfected in 2D cell cultures to test their functionality by fluorescence microscopy and western blot, respectively (**Fig. S4)**. Functional mRNAs were then used to optimize the 3D transfection process within 4 mg/ml GAMs. In a first step, YFP transfection was performed to quickly screen different 3DFectIN:polynucleotide ratios and doses by fluorescence microscopy. Given that 1:1 ratio had previously shown an incomplete encapsulation of the cargo (**Fig. S3**), this ratio was not included in this initial screening. Thus, nanocomplexes containing 1 or 2 µg mRNA were prepared at three ratios (2:1, 3:1, 4:1 µl:µg), mixed with U87MG cells and encapsulated within the fibrin matrices. Optical and fluorescence micrographs acquired 24 h later suggested that nanocomplexes with 1 µg mRNA at 3:1 ratio provided the best balance between cytotoxicity and transfection efficiency (**Fig. S5, S6**). Next, ratios 2:1 and 3:1 were selected to elaborate SOX9 nanocomplexes and run quantitative transfection and toxicity experiments. Both qRT-PCR and MTT toxicity assays performed in SOX9 GAMs confirmed the qualitative results obtained for YFP GAMs (**Fig. S7**), and consequently a 3:1 3DFectIN:mRNA ratio was selected for hMSCs experiments. Although a 2:1 ratio resulted in pDNA particles below the micrometric size and effectively encapsulated the payload (**Fig. S3**), a 3:1 ratio was also selected for pDNA complexes since it was able to transfect as efficiently (**Fig. S5, S7**) and provided a more consistent benchmark for mRNA-activated matrices prepared at 3:1 ratio.

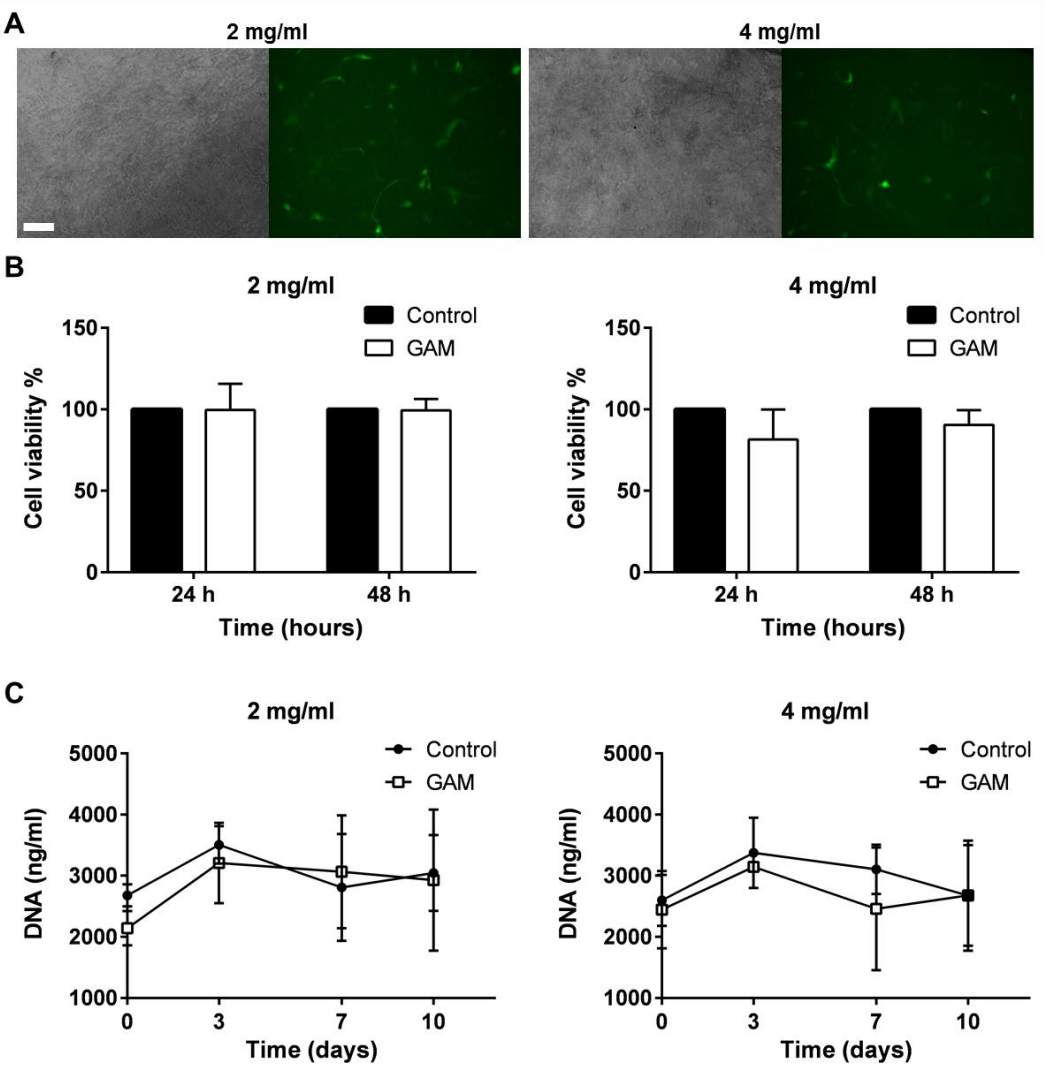

Figure 3. mRNA activated fibrin matrices induce high protein expression levels in encapsulated hMSCs and show very good biocompatibility. A) Representative fluorescence and visible micrographs showing YFP protein expression in hMSCs 24 h after mRNA transfection in 2 and 4 mg/ml fibrin gels. Scale bar = 100 µm for all the images. B) MTT toxicity assay 24 and 48 h after the encapsulation hMSCs and 3DFectIN complexes within 2 and 4 mg/ml gels. C) Ten days proliferation curves for hMSCs in 2 and 4 mg/ml fibrin matrices. Data are shown as mean and standard deviation of three independent experiments at 3:1 3DFectIN:mRNA ratio.

To evaluate the influence of the GAM environment on hMSCs differentiation, we first characterized the transfection efficiency and toxicity profile of YFP mRNA-GAMs. As observed in **figure 3A**, both hydrogel concentrations exhibited a similar level of reporter protein expression 24 h after cell encapsulation. Likewise, MTT toxicity assays carried out at 24 h and 48 h, showed no significant impact on hMSCs viability regardless of the fibrin concentration in the activated gel (**Fig. 3B**). Given the duration of the differentiation experiments, we wanted to check the long-term effect of the RNA complexation reagent on cell proliferation. To this end, we conducted DNA quantitation assays and confirmed that the inclusion of mRNA complexes within fibrin matrices had no significant effect on cell growth as compared to control matrices (**Fig. 3C**). In addition,

the results showed that cell proliferation rates are very similar between both activated and non-activated matrices. Fibrin matrices presented an increase in the cellular DNA content from day 0 to day 3 followed by a slight drop at day 7 that was maintained until day 10.

3.3 Effect of the type of GAM on gene expression kinetics and cell-mediated remodeling

Having characterized 3DfectIN:polynucleotide complexes at different ratios and doses in terms of hMSC toxicity and transfection efficiency, we next studied the influence of matrix remodeling and the type of polynucleotide (mRNA vs. pDNA) on target gene expression during chondrogenic and myogenic differentiation. To this end, we conducted several experiments to compare 2 a 4 mg/ml fibrin matrices in terms of degradation and gene expression kinetics. We first sought to determine whether there was a correlation between YFP and SOX9 transfection, as previously observed in the model cell line (**Fig. S5, S7**). For this, SOX9 expression in hMSCs encapsulated within SOX9-activated matrices was quantified by qRT-PCR. In line with the results for YFP, mRNA-activated matrices induced a higher SOX9 expression compared to their pDNA counterparts, with almost a two fold increase. These SOX9 expression levels were always well over 4 orders of magnitude above those of the control matrices (hMSCs cultured in non-activated matrices), regardless of the type of polynucleotide activating the GAM. Conversely, no differences in transgene expression levels could be observed between matrices with 2 mg/ml and 4 mg/ml of fibrin, independently of whether they were activated with mRNA or pDNA (**Figure 4A**). Likewise, gene expression kinetics was mostly determined by the type of polynucleotide regardless of the matrix concentration, with transgene expression peaking at early and late time points for mRNA and pDNA, respectively (**Figure 4C**). Matrices of 2 mg/ml seemed to induce faster increments and decrements in gene expression, but no statistical differences with 4 mg/ml matrices could be found due to the high standard deviation among the different experiments.

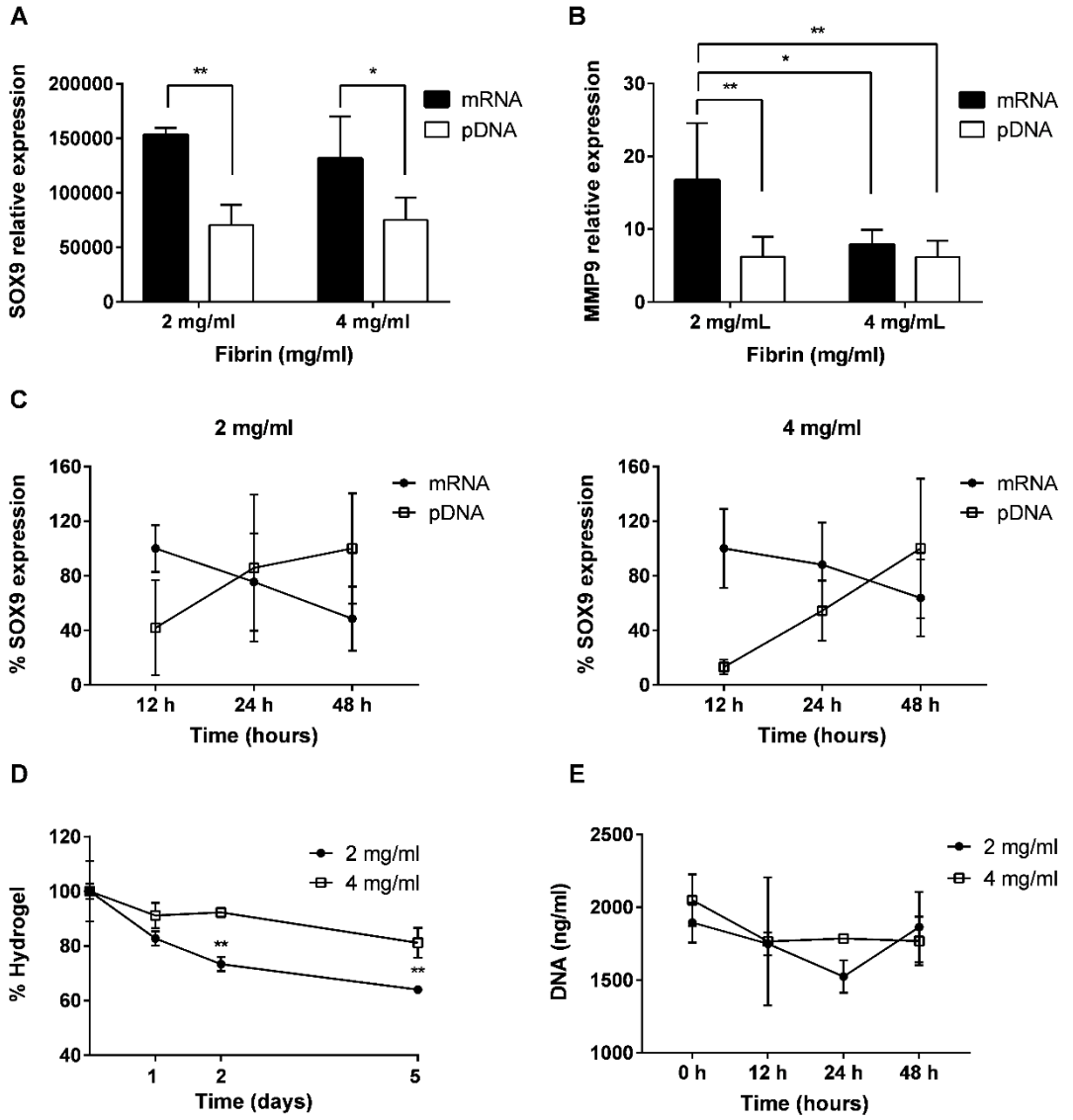

Figure 4. SOX9 3D transfection and gene expression kinetics is determined by the type of polynucleotide used for activation, but not by fibrin matrix concentration. A) SOX9 expression 24 h after hMSCs encapsulation within SOX9 activated 2 and 4 mg/ml fibrin gels (Two-way ANOVA, n =6, *P<0.05, **P<0.01). B) MMP9 expression 24 h after hMSCs encapsulation within SOX9 activated matrices (Two-way ANOVA, n =4, *P<0.05, **P<0.01). C) SOX9 expression kinetics of hMSCs encapsulated in 2 mg/ml and 4 mg/ml fibrin matrices activated with mRNA and pDNA. D) Degradation rates of 2 and 4 mg/ml matrices loaded with hMSCs (Two-way ANOVA, n=3, **P<0.01). E) Short-term proliferation curves (48 h) for hMSCs encapsulated in 2 mg/ml and 4 mg/ml fibrin matrices activated with mRNA and pDNA. Gene expression levels were measured by qRT-PCR and normalized to β-actin expression. Maximum levels of expression were arbitrary set as 100% in graphs shown in C as a way to highlight the tendencies with time. Data are shown as mean and standard deviation of three independent experiments with two replicates per experiment. All experiments were performed at 3:1 3DFectIN:polynucleotide ratio.

Since hydrogel remodeling is linked to cell-mediated degradation, an experiment was performed to monitor the mass loss of cell-seeded hydrogels overtime. Although no significant differences could be observed between both types of matrices at 24 h, the

percentage of mass recovery was lower for 2 mg/ml fibrin matrices at days 2 and 5, indicating their faster degradation (**Fig. 4D**). To test whether this faster degradation was a consequence of a higher cell proliferation rate in the less concentrated gels, we carried out DNA quantitation assays. Our results indicate that cell growth is not significantly different between both matrices, since no differences could be found at any of the time points tested (**Fig. 4E**). Given that Matrix Metalloproteinases (MMPs) have been shown to be involved in the degradation of fibrin hydrogels[28], we next aimed to test if the faster degradation of 2 mg/ml gels was a consequence of an increased MMP secretion. We carried out qRT-PCR analysis to check for the levels of the early marker MMP9 and we found that mRNA-activated matrices induced a slightly higher MMP9 gene expression compared to their pDNA counterparts (**Fig. 4B**). This effect seemed to be more dramatic at lower fibrinogen concentrations since mRNA-activated 2 mg/ml matrices exhibited the highest MMP9 expression, and it partially provides an explanation for the different degradation behavior.

3.4 Chondrogenic differentiation

We next sought to explore whether we could use the differences in transgene expression kinetics and gel remodeling to maximize the expression of tissue differentiation markers. To this end, mRNA- and pDNA-activated matrices codifying for SOX9 were assayed for chondrogenic differentiation. We first conducted a screening experiment to understand the kinetics of chondrogenic marker expression induced by our devices, and to select the best conditions for further analysis. We tested the two concentrations of fibrin hydrogels (2 and 4 mg/ml) with both types of polynucleotides (pDNA and mRNA) at two different polynucleotide doses (1 and 0.25 µg per 100 µl hydrogel). As a reference standard culture for chondrogenic differentiation, we included high-density cell pellet cultures. Gels and pellets were cultured in Complete Chondrogenic Medium (CCM) for 7 and 21 days and the expression of chondrogenic markers SOX9, aggrecan (ACAN) and collagen type-II (COL2A1) was assessed by qRT-PCR (**Fig. 5**). At day 7, gels activated with 1 µg of pDNA produced the highest SOX9 upregulation followed by gels activated with 1 µg mRNA. Gels activated with 0.25 µg of both pDNA and mRNA induced a lower SOX9 expression although their levels were still higher than those of standard cell pellet cultures. The highest ACAN expression at this time point was obtained for both mRNA activated hydrogels, with no statistical differences between them. Conversely, ACAN levels in pDNA-activated hydrogels and cell pellets were much lower than those corresponding to mRNA-activated hydrogels. Regarding COL2A1 expression, mRNA gels achieved the highest gene expression again, followed by pDNA gels and pellet cultures, which showed very low expression compared to both gels. No statistical differences were found between 2 and 4 mg/ml hydrogels at this time point (7 days) (**Fig. 5, left**). At 21 days, SOX9 expression did not change significantly compared to the expression observed at 7 days, except for the hydrogels

activated with 0.25 µg of pDNA, which increased their expression levels more than five times during this time frame. Differences between 2 and 4 mg/ml matrices were observed at this time point. Indeed, 2 mg/ml matrices induced significantly higher ACAN and COL2A1 expression compared to 4 mg/ml matrices for almost all the conditions tested. Further, 4 mg/ml matrices only induced detectable COL2A1 Ct levels when activated with 1 µg of mRNA. The concentration of polynucleotides did not have a significant impact on ACAN induction, with similar ACAN levels achieved for both the high and the low doses. On the contrary, hydrogels activated with 1 µg f mRNA and 0.25 µg of pDNA promoted the highest COL2A1 expression (**Fig. 5, right**). Together, these results show that 2 mg/ml mRNA-activated matrices induce the higher chondrogenic marker expression and that this expression is similar for both mRNA concentrations, namely 0.25 and 1 µg of mRNA per matrix.

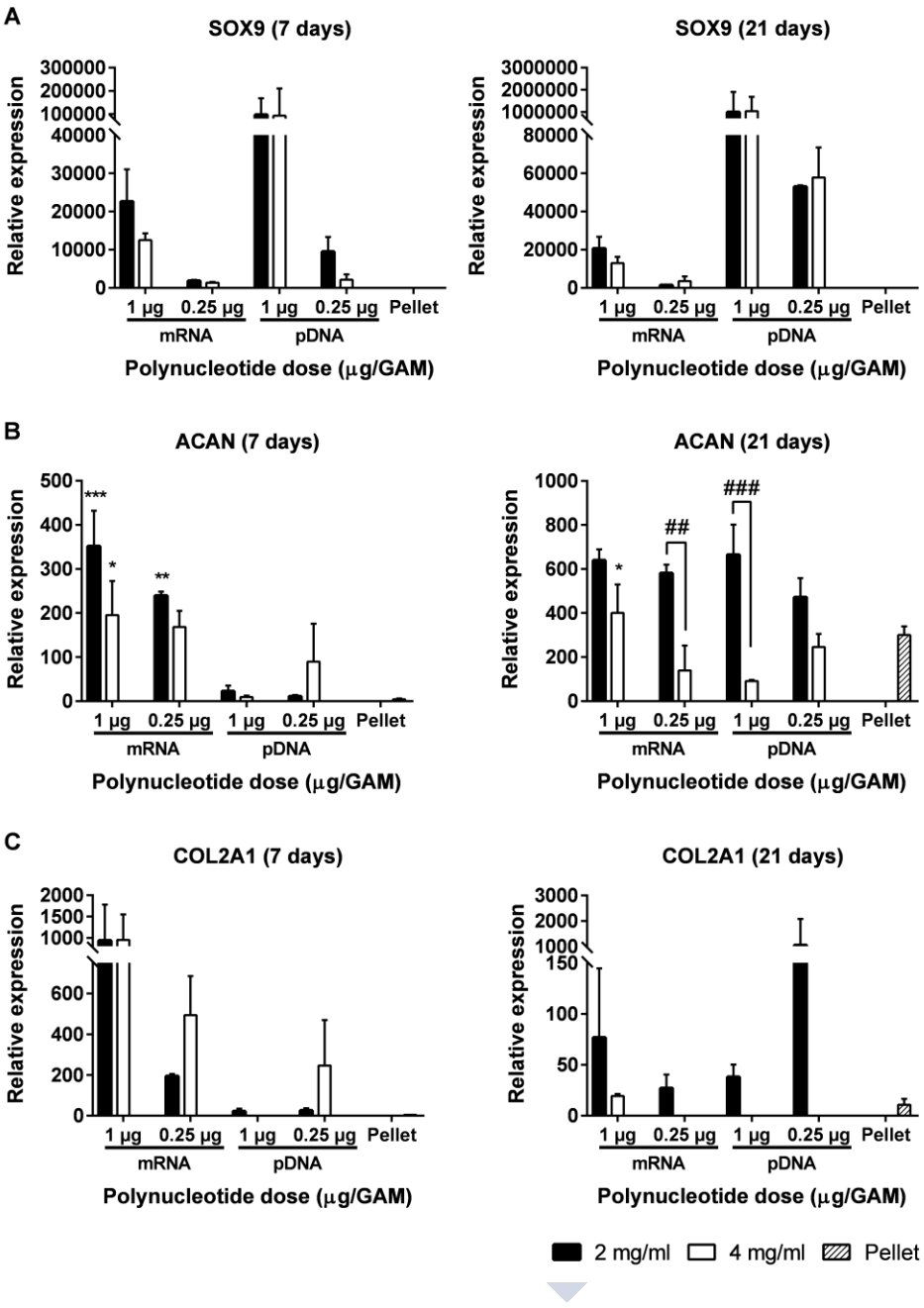

Figure 5. mRNA-activated matrices coding for SOX9 with low fibrin concentration (2 mg/ml) induce the highest gene expression of chondrogenic markers after a 21 days induction assay. Chondrogenic marker expression of hMSCs encapsulated within 2 and 4 mg/ml mRNA and pDNA activated-fibrin hydrogels cultured for 7 days (left) and 21 days (right) in complete chondrogenic media. Two doses of mRNA were tested, namely 1 and 0.25 µg per 100 µl gel. Gene expression levels of SOX9 (A), aggrecan (B) and collagen type-II (C) were measured by qRT-PCR, normalized to GAPDH expression and compared to the levels in hMSCs before encapsulation. Data are shown as mean and standard deviation of two replicates in one experiment performed at 3:1 3DFectIN:polynucleotide ratio. Two-way ANOVA was performed to compare gene expression levels in mRNA and pDNA activated matrices of the same dose and concentration (*P<0.05, **P<0.01, ***P<0.001) and to compare 2 mg/ml and 4 mg/ml matrices with the same dose and genetic material (##P<0.01, ###P<0.001). High-density cell pellet cultures are shown as a benchmark for comparison purposes.

Having observed that 2 mg/ml GAMs exhibited the highest chondrogenic marker expression and that the lowest dose of 0.25 μg of SOX9 effectively induced the upregulation of ECM-related genes, we selected these conditions to compare the differentiation of hMSCs encapsulated in SOX9-activated and non-activated matrices. We conducted these induction assays for 21 days in complete and incomplete chondrogenic media (with and without TGF-β3), in order to explore the influence of growth factor supplementation on the differentiation outcome. Results from both, gene expression analysis and histological evaluation indicated that GAMs cultured in complete chondrogenic media (CCM) exhibited the highest chondrogenic marker expression. Indeed, SOX9, ACAN, COL2A1 and COLX gene expression was around 100 times higher in CCM compared to incomplete chondrogenic media (ICM) (**Fig. 6A, S9A**). Interestingly, ACAN and COLX expression were slightly down-regulated in ICM gels as compared to the levels at day 0. Although no statistical differences could be found among the different hydrogels for most part of the chondrogenic markers, a trend was observed for higher gene expression levels in activated gels compared to non-activated ones. Statistical significance was achieved for SOX9 expression, for which levels in pDNA-activated matrices were 100 and 10 times higher than their mRNA counterparts in CCM and ICM conditions, respectively (**Fig. 6A, S9A**). Gene expression of the hypertrophic marker COLX in reference pellet cultures was also significantly higher compared to all the gel treatments (**Fig. 6A**).

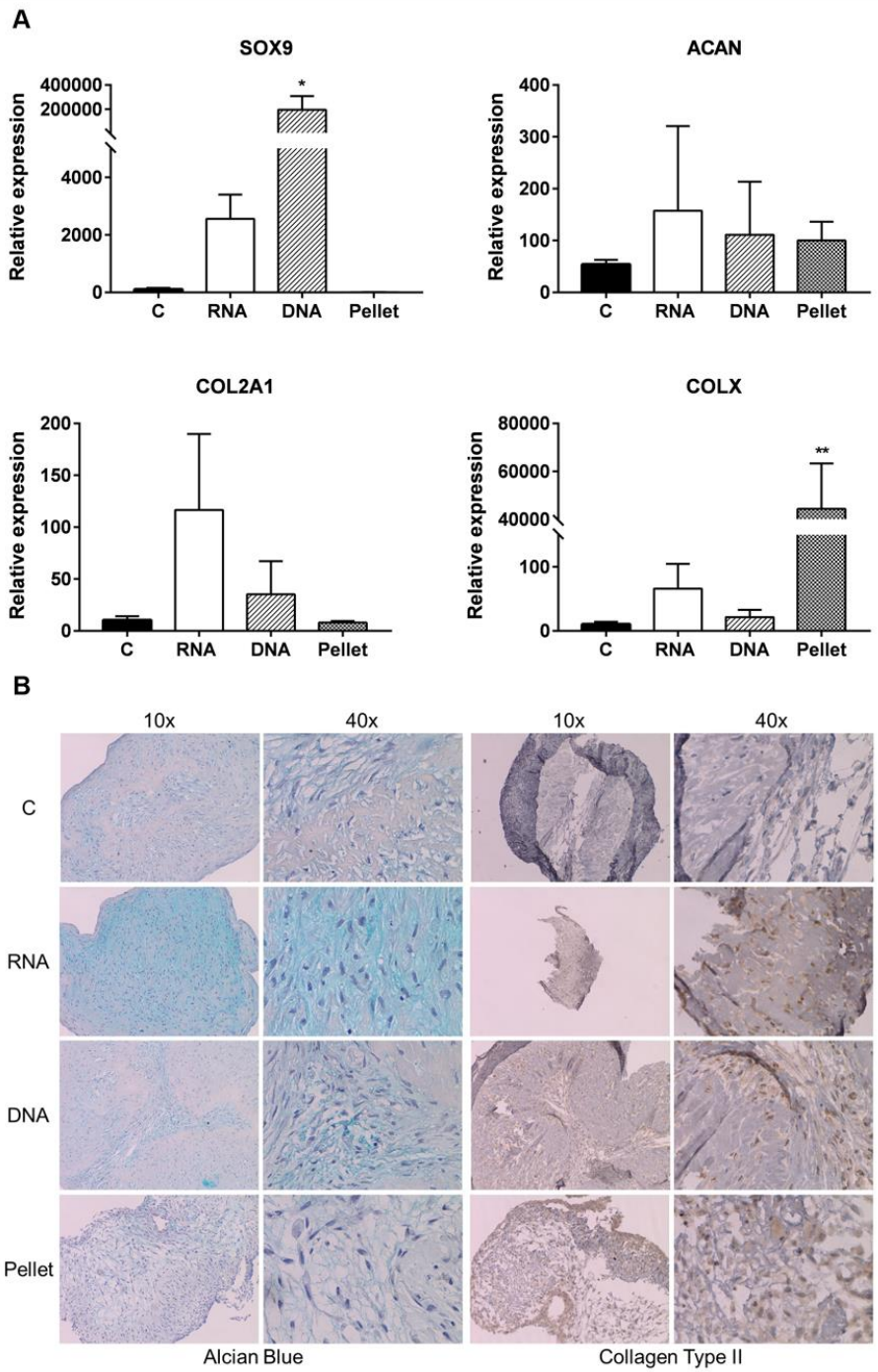

Figure 6. Higher chondrogenic marker expression is observed in hMSCs encapsulated within 2 mg/ml SOX9 mRNA-matrices as compared to their pDNA counterparts in the presence of soluble TGF-β3. Hydrogels were cultured for 21 days in complete chondrogenic media. A) Gene expression levels of chondrogenic markers SOX9, aggrecan (ACAN) and collagen type-II (COL2A1), and the hypertrophy marker collagen type-X (COLX) were measured by qRT-PCR, normalized to GAPDH expression and compared to the levels in hMSCs before encapsulation. Data are shown as mean and standard deviation of three replicates in one representative experiment performed at 3:1 3DFectIN:gene ratio. A one-way ANOVA was performed to compare gene expression levels (*P<0.05, **P<0.01). B) Immunohistological examination of glycosaminoglycan and collagen deposition. Hydrogels were stained with alcian blue for sGAG detection while collagen was detected by immunohistochemistry. Standard cell pellet culture is shown for comparison.

Histological evaluation of SOX9 mRNA-GAMs cultured in CCM showed an extensive glycosaminoglycan (sGAG) accumulation as assessed by Alcian Blue staining. sGAG deposition was much lower in the rest of conditions, especially in the case of the reference cell pellet cultures (**Fig. 6B**). Immunohistochemical analysis of collagen type-II revealed a similar trend, with SOX9 mRNA-GAMs inducing a more homogeneous collagen II expression compared to their pDNA counterparts. Reference cell pellet cultures exhibited a notably high collagen II expression in contrast to their low sGAG secretion. Conversely, control matrices did not show appreciable collagen II protein expression as assessed by immunohistochemistry. For experiments performed without TGF-β3 supplementation, a lower sGAG deposition was observed, suggesting a synergistic effect between SOX9- and TGF-β3-mediated signaling in MSC chondrogenic differentiation. However, in agreement with the experiments performed in CCM, both GAMs exhibited a slightly higher Alcian Blue staining compared to control gels (**Fig. S9B**). This tendency was also observed for collagen stained with Sirius red, with the presence of more dense areas in the case of activated matrices, highlighting the value of SOX9-GAMs for chondrogenic differentiation even in the absence of TGF-β supplementation.

3.5 Myogenic differentiation

Encouraged by the good results obtained for the chondrogenic differentiation experiments, in a last step we assessed the potential of mRNA matrices for myogenic differentiation. To this end, we activated fibrin gels (2 and 4 mg/ml) with MYOD mRNA and evaluated the expression of myogenic markers in hMSCs. First, we evaluated the kinetics of myogenic gene expression after transfection within the matrices. As it was the case for SOX9-mRNA GAMs, the expression of MYOD in hMSCs was highly upregulated at 12 h post transfection (**Fig. 7A**), reaching expression levels which are 8 orders of magnitude as compared to the original ones. Interestingly, contrary to the gradual decay in transcription factor expression observed in SOX9 mRNA matrices over time (12-48 h), this high MYOD expression was maintained over the entire experiment (48 h). This is most probably related to the fact that this mRNA was chemically modified to increase its resistance to RNases, while for SOX9 we used non-modified sequences. MYOD matrices were also able to induce a high upregulation of MYOD direct transcriptional targets implicated in myogenesis; myogenin (MYOG) expression was upregulated by 5 orders of magnitude while the integrin cadherin 15 (CDH15) was upregulated by 3 orders of magnitude. These upregulations occurred as fast as the induction of MYOD expression, suggesting the onset of a myogenic differentiation program coinciding with the encapsulation of hMSCs within the matrices. A similar myogenic marker expression trend was observed for both, 2 and 4 mg/ml MYOD matrices, with no significant differences between them.

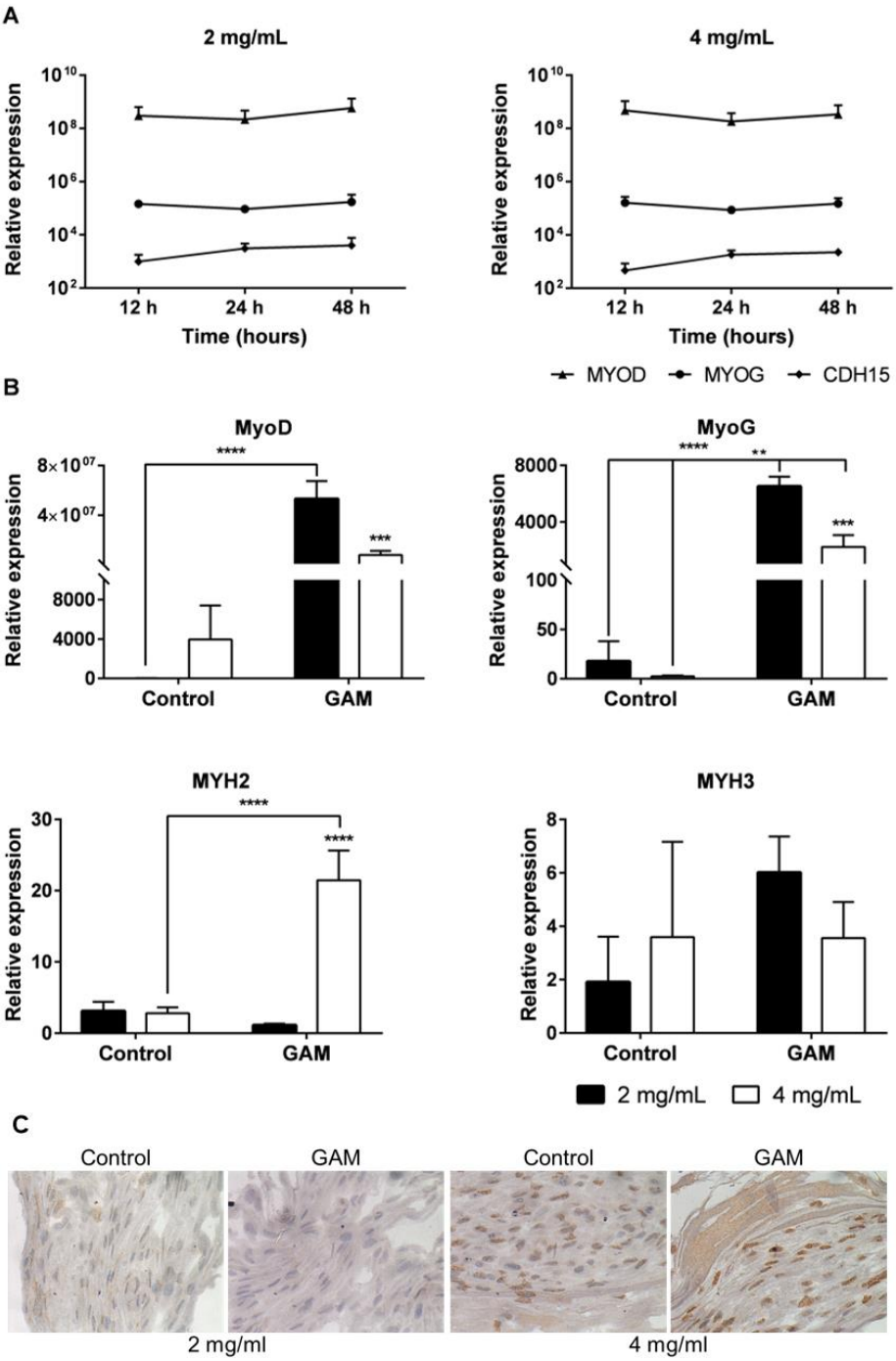

Figure 7. MYOD-activated fibrin hydrogels induce a rapid onset of myogenic differentiation in hMSCs. A) Kinetics of myogenic marker expression in hMSCs cultured in MYOD-matrices for 2 days. Cells were maintained in growth media (α-MEM 10% FBS). Data are shown as mean and standard deviation of two independent experiments. B-C) Myogenic differentiation experiment. Hydrogels were cultured for 7 days in α-MEM (5% FBS) followed by a 7 days culture in DMEM high glucose (2% HS, 10 ng/ml IGF-1). B) Gene expression levels of myogenic markers MYOD, myogenin (MYOG), myosin heavy chain type 2 (MYH2) and myosin heavy chain type 3 (MYH3) were measured by qRT-PCR, normalized to β-actin expression and compared to the levels in hMSCs before encapsulation. Data are shown as mean and standard deviation of three replicates in one experiment at 3:1 3DFectIN:mRNA ratio. Two-way ANOVA was performed to compare gene expression levels (*P<0.05, **P<0.01, ***P<0.001). C) Examination of myosin heavy chain expression by immunohistochemistry.

Next, hMSCs were cultured for 14 days within the matrices to perform myogenic differentiation experiments. Two doses and two differentiation schedules were tested to maximize the differentiation output. In a first set of experiments, fibrin matrices were activated with 0.5 µg mRNA per 100 µL gel and encapsulated hMSCs were cultured in growth medium for one day and DMEM high glucose supplemented with 2% horse serum (HS) during the rest of the experiment. In a second set of experiments, matrices were activated with 0.25 µg mRNA per 100 µL gel and hMSCs were cultured following a two-step schedule consisting of a growth phase and a differentiation phase. During the growth phase, hMSCs were cultured in α-MEM supplemented with 5% fetal bovine serum (FBS) for 7 days. Subsequently, media was changed to DMEM high glucose supplemented with 2% HS and 10 ng/ml insulin growth factor 1 (IGF-1) for the next 7 days (differentiation phase). At the end of the experiments, gels were retrieved and myogenic marker expression was assessed by qRT-PCR and immunohistochemistry (IHC). In agreement with our previous kinetics experiments, MYOD and MYOG mRNA expression was very high regardless of the schedule (**Fig. S10A, Fig. 7B**). Interestingly, whereas mRNA dose directly affected MYOD relative expression in hMSCs, with the lowest dose yielding 1000 times less MYOD expression, MYOG maximum expression was maintained, suggesting that MYOD might be well above its saturation levels for affecting its direct transcriptional targets such as MYOG (**Fig. S10A, Fig. 7B**). In addition, myosin heavy chain 2 and 3 (MYH2 and MYH3) mRNA expression was higher when the low mRNA dose and IGF-1 were used (**Fig. S10A, Fig.7B**), leading to higher myosin heavy chain protein synthesis, which was confirmed by IHC (**Fig. S10B, Fig.7C**). Differences between 2 and 4 mg/ml gels also arose in the IGF-1 set of experiments. Indeed, while MYOD and MYOG levels in 2 mg/ml matrices were similar to the ones observed for the high dose experiments, their values were much lower for the 4 mg/ml fibrin hydrogels (**Fig. S10A**, **Fig. 7B**). Conversely, MYH2 expression was significantly higher in hMSCs encapsulated within 4 mg/ml mRNA GAMs (**Fig. 7B**), a tendency that seems to be also observed for MYH3, although the variations did not reach statistical significance (**Fig. S10A, Fig. 7B**).

4. Discussion

In this work, we show that mRNA-activated matrices encoding pivotal transcription factors (TF) in musculoskeletal development can efficiently direct hMSCs lineage specification for tissue engineering applications. Several recent studies have investigated the use of mRNA-GAMs encoding growth factors (GF) for bone regeneration, and demonstrated their superior performance compared to their pDNA counterparts[10,11,29]. While this approach has been successful for some straightforward cell differentiation processes like in bone engineering, this has not been the case for more complex tissues such as cartilage[30]. As compared to GFs, TFs have been identified as powerful tools to induce cell reprogramming or directed differentiation[12–16], and their

use in pDNA-GAMs has proven successful for cartilage and bone regeneration[17,18]. Based on this knowledge, we hypothesized that the efficacy of mRNA-induced transgene expression could enhance the regenerative potential of TF-based GAMs. To address this possibility, mRNA sequences encoding two TFs, SOX9 and MYOD, were nanocomplexed and homogeneously loaded into fibrin hydrogels together with hMSCs, in order to promote stem cell transfection and directed differentiation in a three-dimensional (3D) context. Fibrin has been FDA approved as a surgical sealant for almost 20 years, is amenable for in situ gel formation and has a positive record on reverse and 3D transfection[31–33], which support its applicability for clinically useful mRNA activated gels. In addition, fibrin can be extracted from the patient's blood, constituting an autologous scaffold and thus alleviating any risk of immune reaction[34].

In agreement with previous literature, our results show that fibrin-based GAMs are very bioactive, promoting cell attachment and stimulating hydrogel remodeling and the deposition of extracellular matrix (ECM)[35]. This is a critical characteristic for 3D transfection, since gene transfer has been described to occur while cells proliferate and colonize the 3D matrices, thus taking up the entrapped nanoparticles[31–33,36–38]. Indeed, our fibrin matrices induced a high transfection efficiency of encapsulated hMSCs, showing at least a 50,000-fold increase in transgene expression levels compared to control cells (Fig. 4). This expression was higher for mRNA-activated gels, and especially potent for RNase resistant mRNA sequences, which is consistent with previous studies performed in 2D (Fig. 7)[16]. Gene expression kinetics also proved to be in agreement with previous 2D experiments, where mRNA transfection induces rapid changes in gene expression while pDNA transfection gradually increases over time[16,39]. Interestingly, whereas transgene expression in non-modified mRNA matrices decreased over time, transgene expression levels in RNase-resistant-mRNA matrices remained constant for at least two days, and probably maintained for at least two weeks (Fig. 7). This different behavior highlights the importance of selecting the appropriate sequences to obtain the best gene expression profile depending on the desired application.

Stem cell directed differentiation experiments confirmed the value of SOX9 and MYOD mRNA GAMs over previously explored pDNA GAMs. Compared to SOX9 pDNA-GAMs, SOX9 mRNA-GAMs induced a much faster mRNA upregulation of chondrogenic markers, an effect that was already evident at day 7 after hMSCs encapsulation. MYOD mRNA GAMs further supported this rapid induction of tissue-specific markers, by promoting the upregulation of myogenic markers as early as 12 h after hMSCs encapsulation, even in the absence of myogenic induction media. Importantly, this potent tissue marker expression in SOX9 and MYOD mRNA GAMs was translated into the generation of cartilage-like and muscle-like tissues of improved quality. Together, these results suggest that the fast TF upregulation induced by mRNA GAMs results in a faster onset of the cell differentiation programs that may be beneficial for tissue regeneration. This

might have implications for the clinical translation of GAM-based technologies, where a rapid tissue formation is especially crucial to avoid material loss and cell clearance at the damaged tissue. Interestingly, our observations also bring insights on the significance of mRNA dose to induce TF-driven differentiation and suggest that, in contrast to the general perception, maintenance of very high TF expression levels as differentiation progresses might be counterproductive. In the case of chondrogenic differentiation, reducing SOX9 mRNA dose four times resulted in a dramatic decrease in SOX9 expression, but produced only a slight effect on aggrecan levels, suggesting that there is a plateau in SOX9-induced aggrecan expression. Similarly, whereas reducing mRNA dose to the half resulted in a 1000-times lower MYOD expression in hMSCs, MYOG maximum expression was maintained. Previous works have shown that high levels of TFs can exert a negative feedback on target gene expression[40–42]. Similarly, Yamanaka et al. have shown that TF induction needs to be stopped during induced pluripotent stem cell reprogramming for the process to be successful[43]. In light of these observations, one could anticipate that TF mRNA dose and pharmacokinetics must be considered as important design parameters for TF mRNA GAMs.

A number of works have unveiled the role of the mechanical properties of materials systems to direct cell specification[44–46]. In agreement with these studies, we found that the GAM environment dramatically influences MSC chondrogenic and myogenic differentiation. Indeed, our results show that 2 mg/ml SOX9-GAMs induce a more potent upregulation of chondrogenic markers compared to 4 mg/ml GAMs. For myogenic differentiation, 2 mg/ml MYOD-GAMs generated again the highest levels of immature markers, but it was the 4 mg/ml MYOD-GAMs that induced a higher expression of the mature markers (i.e. myosin heavy chain) (Fig. 7). Previous studies have highlighted the importance of matrix remodeling through proteolytic degradation as a critical process for tissue formation. Encapsulated cells must proliferate and secrete ECM components that allow them to eventually substitute the scaffold template[47–50]. In this sense, material systems have been engineered to respond to MMP secretion by adapting scaffold architecture to cell-remodeling events[51–53]. This is especially relevant for MSCs chondrogenesis, where hydrogel remodeling may lead to mesenchymal condensation, a process that is critical for the onset of the differentiation program[54–57]. The results from cell-mediated degradation experiments of both fibrin matrices showed that 2 mg/ml matrices were degraded faster. These 2 mg/ml mRNA GAMs also promoted a higher upregulation of MMP9 expression, a result that is consistent with previous literature exploring the role of MMPs on fibrin hydrogel breakdown[28]. These results are consistent with the higher ECM synthesis observed in less concentrated mRNA-GAMs, likely related to their faster degradation that results in hydrogel breakdown and cell condensation. This was especially notorious in the case of the ECM protein collagen type-II, which mRNA failed to be upregulated in the more concentrated GAMs. In the case of muscle regeneration, manipulations on material systems have been mostly oriented to mimic

the elasticity and topography of the native tissues. Indeed, maximum myotube striation has been shown to occur in materials with a Young's modulus of ≈ 12 kPa[58,59], whereas myotube alignment has been augmented through material patterning and mechanical stimulation[60–62]. Although our work has not focused on the engineering of MYOD-mRNA GAM to mimic the properties of the muscular tissue, we suggest that the increased myogenic marker expression observed in 4 mg/ml GAMs could be related to a better cell alignment derived from their more slowly degradation.

Overall, this work provides the first evidence of a mRNA-activated matrix encoding transcription factors as a new tool for controlling cell differentiation. Our results show several strengths for this technology in tissue engineering: (i) potent and fast induction of specific differentiation programs, (ii) controllable transcription factor expression kinetics that allows the process to proceed in self-regulated fashion once triggered, (iii) broad applicability to many different tissue engineering problems, (iv) capacity to upregulate pivotal differentiation markers, reaching levels higher than most data reported in the literature. Already in this first approximation, we were able to apply this technology to successfully generate cartilage- and muscle-like tissues as confirmed by gene expression and histological analysis. In addition, we identified some of the critical parameters affecting the performance of mRNA-GAMs encoding TFs, such as mRNA dose and chemical modification (i.e. its biological stability), and the mechanical properties of the scaffold. Although our results provide some insights on how to modulate these factors in order to improve GAM design, further studies will be required to better elucidate the influence of these variables to be able to better adapt these GAMs to their target application.

5. Conclusions

mRNA-activated fibrin hydrogels encoding pivotal transcription factors (TF) SOX9 and MYOD were developed to direct stem cell specification for tissue engineering applications. When compared to previously explored TF codifying pDNA activated matrices, these systems could effectively induce a higher and faster TF gene expression. This potent TF expression, in turn, promoted a faster onset of the corresponding differentiation cascades, resulting in a more efficient protein synthesis of tissue-specific markers. mRNA-activated matrices are cell compatible and easily injectable, representing a suitable cell-based platform. Modulation of mRNA dose and matrix mechanics could further tune the system performance, allowing for the generation of optimized devices. Based on these attractive properties, we believe that mRNA-activated matrices encoding TFs may become a centerpiece in a new generation of systems intended for tissue engineering and regenerative medicine.

Acknowledgements

This work has been funded by Ministerio de Economía y Competitividad (MINECO-RETOS, Grant MAT2017-84361-R, Feder Funds), Fundación BBVA 2014-PO0110 and Xunta de Galicia (Grupos de Referencia Competitiva, Feder Funds; Convenio para fomentar a actividade investigadora do persoal investigador finalista nas convocatorias de axudas do ERC no marco da H2020). AML was a recipient of a FPU grant from Ministerio de Economía y Competitividad

References

1. Yannas, I. V, Lee, E., Orgill, D. P., Skrabut, E. M. & Murphy, G. F. Synthesis and characterization of a model extracellular matrix that induces partial regeneration of adult mammalian skin. *Proc. Natl. Acad. Sci. U. S. A.* **86,** 933–7 (1989).
2. Lo, K. W.-H., Ulery, B. D., Ashe, K. M. & Laurencin, C. T. Studies of bone morphogenetic protein-based surgical repair. *Adv. Drug Deliv. Rev.* **64,** 1277–91 (2012).
3. Kang, D. G., Hsu, W. K. & Lehman, R. A. Complications Associated With Bone Morphogenetic Protein in the Lumbar Spine. *Orthopedics* **40,** e229–e237 (2017).
4. Epstein, N. Complications due to the use of BMP/INFUSE in spine surgery: The evidence continues to mount. *Surg. Neurol. Int.* **4,** 343 (2013).
5. DeVine, J., Dettori, J., France, J., Brodt, E. & McGuire, R. The use of rhBMP in spine surgery: is there a cancer risk? *Evid. Based. Spine. Care. J.* **3,** 35–41 (2012).
6. Bonadio, J., Smiley, E., Patil, P. & Goldstein, S. Localized, direct plasmid gene delivery in vivo: prolonged therapy results in reproducible tissue regeneration. *Nat. Med.* **5,** 753–759 (1999).
7. Raisin, S., Belamie, E. & Morille, M. Non-viral gene activated matrices for mesenchymal stem cells based tissue engineering of bone and cartilage. *Biomaterials* **104,** 223–237 (2016).
8. Sahin, U., Karikó, K. & Türeci, Ö. mRNA-based therapeutics — developing a new class of drugs. *Nat. Rev. Drug Discov.* **13,** 759–780 (2014).
9. Elangovan, S. *et al.* Chemically modified RNA activated matrices enhance bone regeneration. *J. Control. Release* **218,** 22–28 (2015).
10. Balmayor, E. R. *et al.* Modified mRNA for BMP-2 in Combination with Biomaterials Serves as a Transcript-Activated Matrix for Effectively Inducing Osteogenic Pathways in Stem Cells. *Stem Cells Dev.* **26,** 25–34 (2016).
11. Khorsand, B. *et al.* A Comparative Study of the Bone Regenerative Effect of Chemically Modified RNA Encoding BMP-2 or BMP-9. *AAPS J.* **19,** 438–446 (2017).
12. Makiko Iwafuchi-Doi and Kenneth S. Zaret. Pioneer transcription factors in cell reprogramming. *Genes Dev.* **28,** 2679–2692 (2014).
13. Takahashi, K. & Yamanaka, S. A decade of transcription factor-mediated reprogramming to pluripotency. *Nat. Rev. Mol. Cell Biol.* **17,** 183–193 (2016).
14. Liang, Q. Le *et al.* Transcription factor directed differentiation of human embryonic stem cells into the pancreatic endocrine lineage. *Cell Res.* **18,** S109–S109 (2008).
15. Graf, T. & Enver, T. Forcing cells to change lineages. *Nature* **462,** 587–594 (2009).
16. Warren, L. *et al.* Highly efficient reprogramming to pluripotency and directed differentiation of human cells with synthetic modified mRNA. *Cell Stem Cell* **7,** 618–630 (2010).
17. Im, G. I., Kim, H. J. & Lee, J. H. Chondrogenesis of adipose stem cells in a porous PLGA scaffold impregnated with plasmid DNA containing SOX trio (SOX-5,-6 and -9) genes. *Biomaterials* **32,** 4385–4392 (2011).
18. Umebayashi, M., Sumita, Y., Kawai, Y., Watanabe, S. & Asahina, I. Gene-Activated Matrix Comprised of Atelocollagen and Plasmid DNA Encoding BMP4 or Runx2 Promotes Rat Cranial Bone Augmentation. *Biores. Open Access* **4,** 164–174 (2015).
19. Mandal, P. K. & Rossi, D. J. Reprogramming human fibroblasts to pluripotency

using modified mRNA. *Nat. Protoc.* **8,** 568–582 (2013).
20. Guo, X. R. *et al.* PDX-1 mRNA-induced reprogramming of mouse pancreas-derived mesenchymal stem cells into insulin-producing cells in vitro. *Clin. Exp. Med.* **15,** 501–509 (2014).
21. Aini, H. *et al.* Messenger RNA delivery of a cartilage-anabolic transcription factor as a disease-modifying strategy for osteoarthritis treatment. *Sci. Rep.* **6,** 18743 (2016).
22. Dy, P. *et al.* Sox9 Directs Hypertrophic Maturation and Blocks Osteoblast Differentiation of Growth Plate Chondrocytes. *Dev. Cell* **22,** 597–609 (2012).
23. Bi, W., Deng, J. M., Zhang, Z., Behringer, R. R. & Crombrugghe, B. De. Sox9 is required for cartilage formation. *Nat. Genet.* **22,** 85–89 (1999).
24. Davis, R. L., Weintraub, H. & Lassar, A. B. Expression of a single transfected cDNA converts fibroblasts to myoblasts. *Cell* **51,** 987–1000 (1987).
25. Kozak, M. An analysis of 5'-noncoding sequences from 699 vertebrate messenger rNAS. *Nucleic Acids Res.* **15,** 8125–8148 (1987).
26. Holcik, M. & Liebhaber, S. a. Four highly stable eukaryotic mRNAs assemble 3' untranslated region RNA-protein complexes sharing cis and trans components. *Proc. Natl. Acad. Sci. U. S. A.* **94,** 2410–2414 (1997).
27. Pfaffl, M. W. A new mathematical model for relative quantification in real-time RT-PCR. *Nucleic Acids Res.* **29,** 45e–45 (2001).
28. Tamer, A. A. E., Griffith, M. & Hincke, M. Characterization and Inhibition of Fibrin Hydrogel–Degrading Enzymes During Development of Tissue Engineering Scaffolds. *Tissue Eng.* **13,** (2007).
29. Elangovan, S. *et al.* Chemically modified RNA activated matrices enhance bone regeneration. *J. Control. Release* **218,** 22–28 (2015).
30. Huey, D. J., Hu, J. C. & Athanasiou, K. A. Unlike bone, cartilage regeneration remains elusive. *Science* **338,** 917–921 (2012).
31. Lei, P., Padmashali, R. M. & Andreadis, S. T. Cell-controlled and spatially arrayed gene delivery from fibrin hydrogels. *Biomaterials* **30,** 3790–3799 (2009).
32. Raut, S. D., Lei, P., Padmashali, R. M. & Andreadis, S. T. Fibrin-mediated lentivirus gene transfer: Implications for lentivirus microarrays. *J. Control. Release* **144,** 213–220 (2010).
33. Padmashali, R. M. & Andreadis, S. T. Engineering fibrinogen-binding VSV-G envelope for spatially- and cell-controlled lentivirus delivery through fibrin hydrogels. *Biomaterials* **32,** 3330–3339 (2011).
34. Ye, K. Y. & Black, L. D. Strategies for tissue engineering cardiac constructs to affect functional repair following myocardial infarction. *J. Cardiovasc. Transl. Res.* **4,** 575–591 (2011).
35. Brown, A. C. & Barker, T. H. Fibrin-based biomaterials: Modulation of macroscopic properties through rational design at the molecular level. *Acta Biomater.* **10,** 1502–1514 (2014).
36. Zhang, H., Lee, M. Y., Hogg, M. G., Dordick, J. S. & Sharfstein, S. T. High-throughput transfection of interfering RNA into a 3D cell-culture chip. *Small* **8,** 2091–2098 (2012).
37. Thoma, C. R. *et al.* A High-Throughput–Compatible 3D Microtissue Co-Culture System for Phenotypic RNAi Screening Applications. *J. Biomol. Screen.* **18,** 1330–1337 (2013).

38. Plank, C. *et al.* Gene activated matrices for bone and cartilage regeneration in arthritis. *Eur. J. Nanomedicine* **4,** 17–32 (2012).
39. Andries, O. *et al.* Comparison of the gene transfer efficiency of mRNA/GL67 and pDNA/GL67 complexes in respiratory cells. *Mol. Pharm.* **9,** 2136–2145 (2012).
40. Kypriotou, M. *et al.* SOX9 Exerts a Bifunctional Effect on Type II Collagen Gene (COL2A1) Expression in Chondrocytes Depending on the Differentiation State. *DNA Cell Biol.* **22,** 119–129 (2003).
41. Harada, A. *et al.* Spatial re-organization of myogenic regulatory sequences temporally controls gene expression. *Nucleic Acids Res.* **43,** 2008–2021 (2015).
42. Cho, H. C., Mallappa, C., Hernández-Hernández, J. M., Rivera-Pérez, J. A. & Imbalzano, A. N. Contrasting roles for MyoD in organizing structures during embryonic skeletal muscle development. *Dev. Dyn.* **244,** 43–55 (2015).
43. Takahashi, K. & Yamanaka, S. Induction of Pluripotent Stem Cells from Mouse Embryonic and Adult Fibroblast Cultures by Defined Factors. *Cell* **126,** 663–676 (2006).
44. Huebsch, N. *et al.* Harnessing traction-mediated manipulation of the cell/matrix interface to control stem-cell fate. *Nat. Mater.* **9,** 518–526 (2010).
45. Chaudhuri, O. *et al.* Hydrogels with tunable stress relaxation regulate stem cell fate and activity. *Nat. Mater.* **15,** 326–334 (2015).
46. Mao, A. S., Shin, J. W. & Mooney, D. J. Effects of substrate stiffness and cell-cell contact on mesenchymal stem cell differentiation. *Biomaterials* **98,** 184–191 (2016).
47. Almalki, S. G. & Agrawal, D. K. Effects of matrix metalloproteinases on the fate of mesenchymal stem cells. *Stem Cell Res. Ther.* 1–12 (2016). doi:10.1186/s13287-016-0393-1
48. Ahmann, K. A. *et al.* Fibrin Degradation Enhances Vascular Smooth Muscle Cell Proliferation and Matrix Deposition in Fibrin-Based Tissue Constructs Fabricated In Vitro. *Tissue Eng. Part A* **16,** (2010).
49. Page-McCaw, A., Ewald, A. J. & Werb, Z. Matrix metalloproteinases and the regulation of tissue remodelling. *Nat Rev Mol Cell Biol.* **8,** 221–233 (2007).
50. Oh, J. *et al.* Mutations in two matrix metalloproteinase genes , MMP-2 and MT1-MMP , are synthetic lethal in mice. *Oncogene* **23,** 5041–5048 (2004).
51. Parmar, P. A. *et al.* Collagen-mimetic peptide-modifiable hydrogels for articular cartilage regeneration. *Biomaterials* **54,** 213–225 (2015).
52. Parmar, P. A. *et al.* Temporally degradable collagen e mimetic hydrogels tuned to chondrogenesis of human mesenchymal stem cells. *Biomaterials* **99,** 56–71 (2016).
53. Anderson, S., Lin, C., Kuntzler, D. & Anseth, K. The performance of human mesenchymal stem cells encapsulated in cell-degradable polymer-peptide hydrogels. *Biomaterials* **32,** 3564–3574 (2011).
54. Ghone, N. V. & Grayson, W. L. Recapitulation of mesenchymal condensation enhances in vitro chondrogenesis of human mesenchymal stem cells. *J. Cell. Physiol.* **227,** 3701–3708 (2012).
55. Ray, P. & Chapman, S. C. Cytoskeletal reorganization drives mesenchymal condensation and regulates downstream molecular signaling. *PLoS One* **10,** 1–24 (2015).
56. Bian, L., Guvendiren, M., Mauck, R. L. & Burdick, J. A. Hydrogels that mimic

developmentally relevant matrix and N-cadherin interactions enhance MSC chondrogenesis. *Proc. Natl. Acad. Sci.* **110,** 10117–10122 (2013).

57. Cosgrove, B. D. *et al.* N-cadherin adhesive interactions modulate matrix mechanosensing and fate commitment of mesenchymal stem cells. *Nat. Mater.* **15,** 1297–1306 (2016).
58. Engler, A. J., Sen, S., Sweeney, H. L. & Discher, D. E. Matrix Elasticity Directs Stem Cell Lineage Specification. *Cell* **126,** 677–689 (2006).
59. Engler, A. J. *et al.* Myotubes differentiate optimally on substrates with tissue-like stiffness: Pathological implications for soft or stiff microenvironments. *J. Cell Biol.* **166,** 877–887 (2004).
60. Page, R. L. *et al.* Restoration of Skeletal Muscle Defects with Adult Human Cells Delivered on Fibrin Microthreads. *Tissue Eng. Part A* **17,** 2629–2640 (2011).
61. Heher, P. *et al.* A novel bioreactor for the generation of highly aligned 3D skeletal muscle-like constructs through orientation of fibrin via application of static strain. *Acta Biomater.* **24,** 251–265 (2015).
62. Chen, S., Nakamoto, T., Kawazoe, N. & Chen, G. Engineering multi-layered skeletal muscle tissue by using 3D microgrooved collagen scaffolds. *Biomaterials* **73,** 23–31 (2015).

USC
UNIVERSIDADE
DE SANTIAGO
DE COMPOSTELA

SUPPORTING INFORMATION

Supplementary methods

2D Lipofectamine® 2000 transfection

For 2D transfections, cells were plated in 96 well plates approximately 12 h prior to transfection at a density of 90000 (U87MG) or 75000 (hMSCs) cells/cm^2. Four hours before transfection, media was changed to OptiMEM reduced serum medium (Gibco). Then, 50 µl of Lipofectamine complexes (Gibco), at 0.5:1 Lipofectamine:DNA/RNA ratios (µl:µg), were prepared in OptiMEM following manufacturer's instructions. Briefly, a solution containing 1 µg of mRNA/pDNA was added over a solution containing 0.5 µl of Lipofectamine®2000 reagent in a 1/1 v/v ratio, mixed by pipetting up-down and incubated for 20 min at room temperature. Complexes were added over the cells drop-by-drop and incubated for 6 hours. Subsequently, complexes were aspirated and cells were maintained in regular growing media until analysis. The transfection reaction was escalated for plates of higher surface areas.

Protein extraction from 2D cultures

Cells were retrieved from the plates, pelleted by centrifugation (5 min, 15 °C, 1000 rpm) and washed two times with PBS. RIPA buffer supplemented with protease inhibitor cocktail (Sigma-Aldrich) was added to the clean pellet (0.5 ml per 60 mm dish) followed by a 20 min incubation on ice. Samples were then sonicated in a Branson Digital Sonifier 250 (30% amplitude, 5 pulses of 1 sec), centrifuged (15 min, 16000xg, 4 °C) and supernatants were collected for further analysis. Protein concentration was determined by UV absorbance using a Multiskan GO spectrophotometer (Thermo Scientific) and the Bradford method. A bovine serum albumin (BSA) calibration curve and the 590/450 nm linearization method[1].

Western blot

Protein extracts (25-50 µg) were mixed with 5x Laemmli buffer, denaturated at 95 °C in a Thermoblock for 5 min and separated in 10% PAGE gels. Then, proteins were electroblotted onto a PVDF membrane using a semi-dry blotter (Sigma-Aldrich) operated at 1.2 mA/cm^2 membrane for 1 h. Non-specific binding sites were blocked for 2 hours at room temperature with 5% nonfat milk in 0.05% TNT buffer. The membrane was incubated overnight at 4 °C with SOX9 rabbit primary antibody (Santa Cruz Biotechnologies, Dallas, TX, USA) and Tubulin mouse primary antibody (Sigma-Aldrich) using a 1:500 and 1:3000 dilution in 1% TNT, respectively. The membrane was then washed three times with 1% TNT for 10 min and further incubated for 45 min with HRP-conjugated secondary antibodies (GE Healthcare, Chicago, IL, USA) at room temperature and 1:20000 dilution in 0.5% TNT. After three more washes with 0.5% TNT, the immunoblots were finally visualized following the addition of HRP SuperSignal® West Dura Extended Duration Substrate (Thermo Scientific).

Supporting figures

Table S1. List of Taqman assays employed for qRT-PCR experiments.

TaqMan assays (Applied Biosystems)	
SOX9 (human)	Hs00165814_m1
ACAN (human)	Hs 00153936_m1
COL2A1 (human)	Hs00264051_m1
COL10A1 (human)	Hs00166657_m1
MYOD1 (human)	Hs00159528_m1
MYOG (human)	Hs01072232_m1
CDH15 (human)	Hs00170504_m1
MYH2 (human)	Hs00430042_m1
MYH3 (human)	Hs01074230_m1
ACT B (human)	Hs99999903_m1
GAPDH (human)	Hs99999905_m1

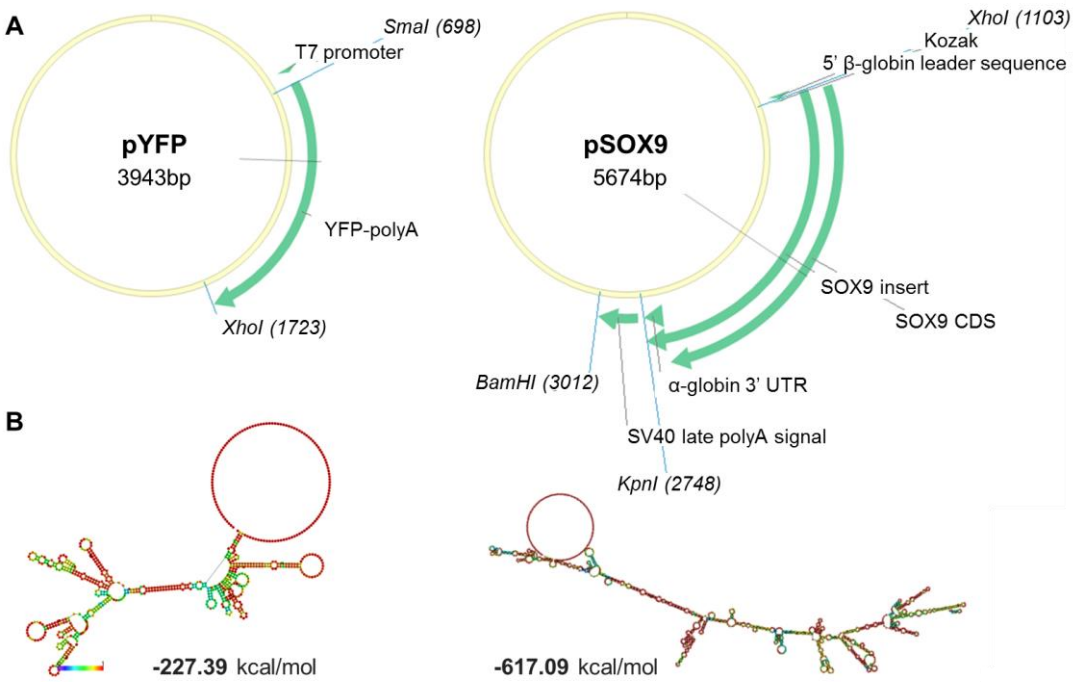

Fig. S1. Scheme of the plasmid templates used for In Vitro Transcription (IVT) reactions and the most probable secondary structrures of the corresponding mRNAs. (A) SOX9 coding sequence (CDS) and the 3' UTR of the α globin gene were cloned into a pCMVTnT expression vector (Promega). YFP coding sequence and the SV40 polyadenilation signal were digested from a pIRES YFP vector (Clontech) and ligated into a pBluescript KS (+) vector. (B) Minimun Free Energy base pair probabilities according to Vienna RNA website (Gruber AR et al, Nucleic Acids Res. 2008) yield a value of -227.39 and -617.09 kcal/mol free energy for the thermodynamic ensemble of YFP and SOX9 RNA molecules, respectively.

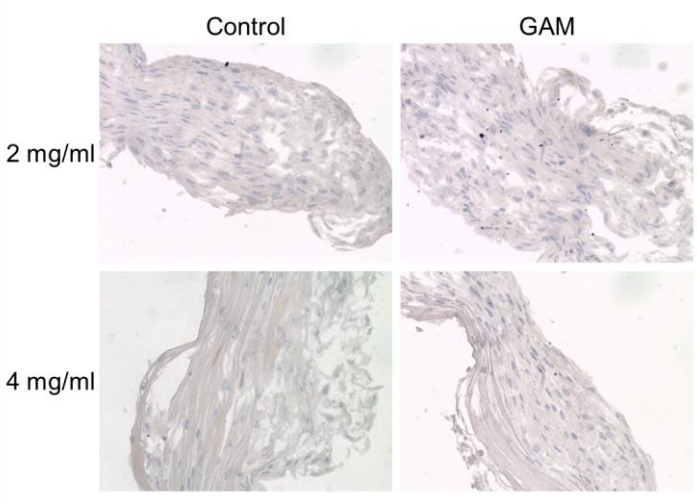

Fig. S2. Negative controls for Myosin Heavy Chain detection by immunohistochemistry. Negative controls were processed in the same way as samples but without the addition of the primary antibody. Controls correspond to the experiment with the two step schedule: 7 days in α-MEM (5% FBS) followed by a 7 days in DMEM high glucose (2% HS, 10 ng/ml IGF-1).

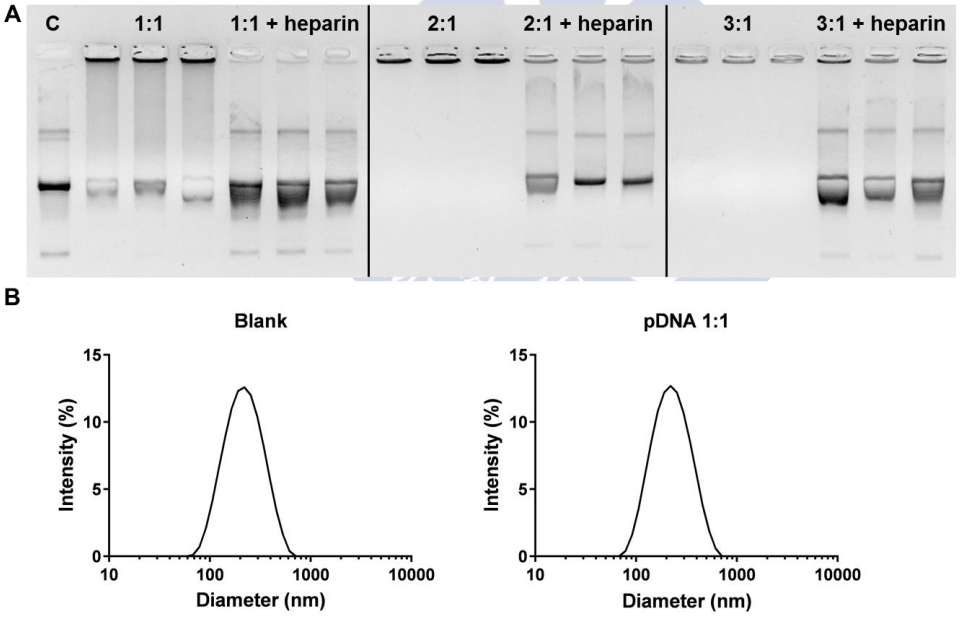

Fig. S3. 3DFectIN:pDNA particles at 1:1 ratio show an incomplete encapsulation of the pDNA cargo. A) Agarose displacement test of 1:1 YFP pDNA loaded 3DFectIN complexes as compared to 2:1 and 3:1 complexes (µL 3DFectIN:µg pDNA). B) Representative size intensity distributions of blank (non-loaded) and pDNA-loaded 3DFectIN complexes prepared at 1:1 ratio as measured by DLS.

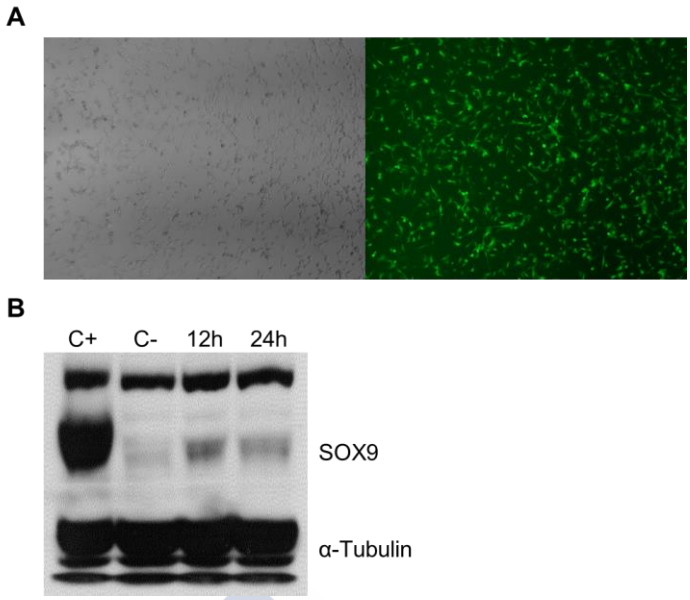

Fig. S4. *In vitro* transcribed mRNAs induce an efficient protein expression after 2D transfection. (A) Fluorescent micrograph (right) and corresponding optical micrograph (left) showing YFP protein expression 12 h after YFP mRNA transfection in U87MG cells. (B) SOX9 protein expression 12 and 24 h after SOX9 mRNA transfection in HEK293 cells. Protein lysates of untreated and pDNA-transfected cells were used as negative (C-) and positive (C+) controls, respectively.

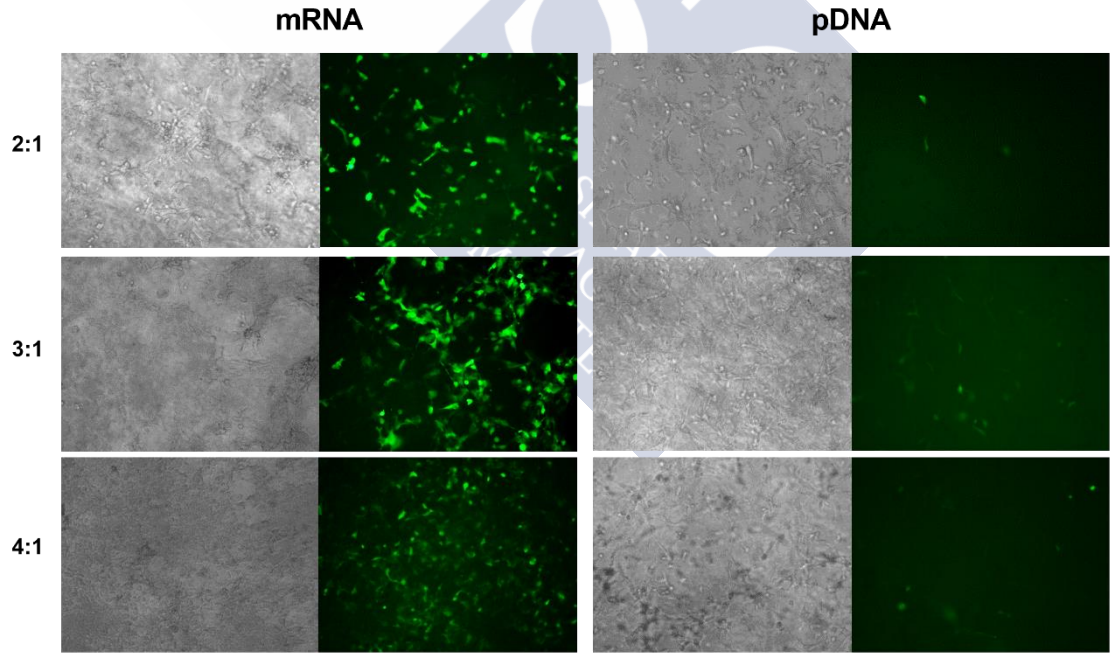

Fig. S5. 3DFectIN:mRNA/pDNA complexes at 3:1 ratio exhibit the best compromise between transfection efficiency and cytotoxicity. Screening of 3DFectIN:mRNA/pDNA ratios with YFP reporter sequence and U87MG cell line in 4 mg/mL fibrin gels. Representative fluorescence and optical micrographs corresponding to transfection experiments performed with 1 µg mRNA (left) and pDNA (right) complexed to 3DFectIN® reagent using 2:1 (top), 3:1 (middle) and 4:1 (bottom) 3DFectIN:mRNA/pDNA ratios (µL:µg).

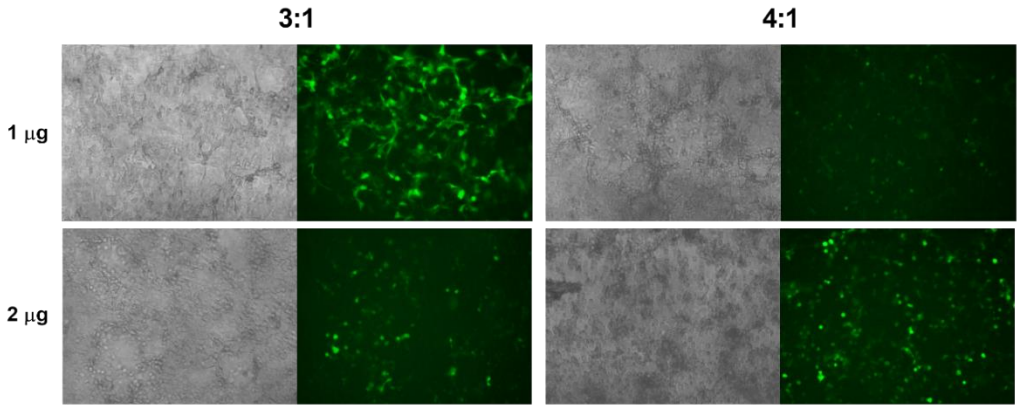

Fig. S6. A dose of 1 µg mRNA shows the best compromise between forced protein expression and cytotoxicity. Screening of mRNA dose with YFP reporter sequence in 4 mg/mL fibrin gels loaded with U87MG cells. Representative fluorescence and visible micrographs corresponding to transfection experiments performed with 1 and 2 µg of mRNA complexed with 3DFectIN® reagent using 3:1 (left) and 4:1 (right) 3DFectIN:mRNA ratios (µL:µg).

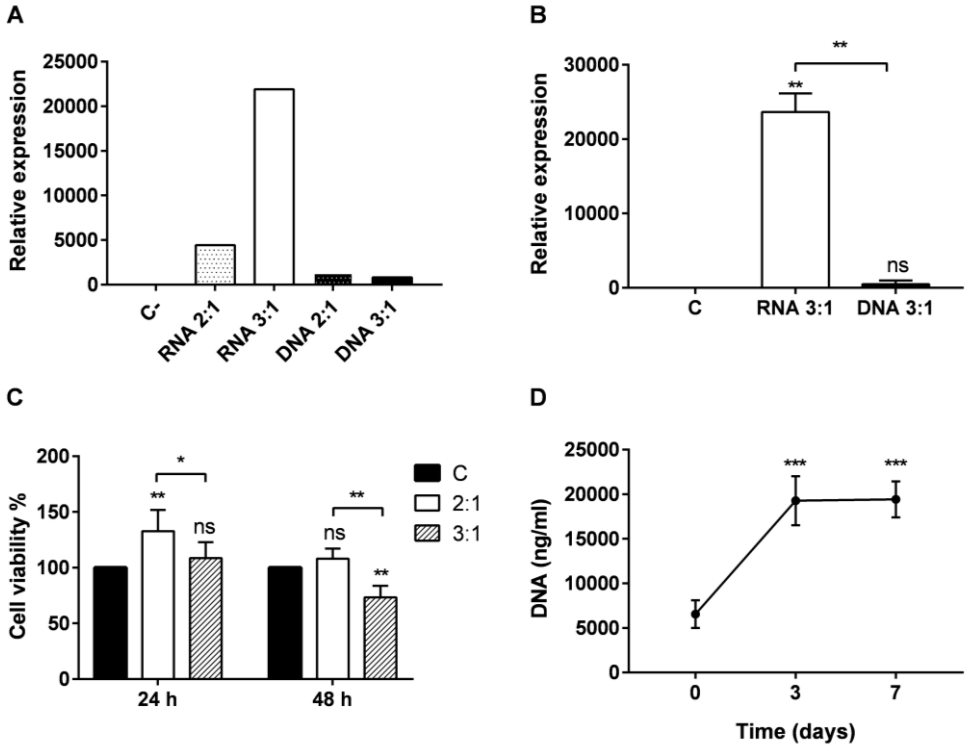

Fig. S7. qRT-PCR and cytotoxicity assays confirm that ratio 3:1 shows the best compromise between transfection efficiency and toxicity. Screening assay of transfection ratios and cytotoxicity of U87MG cells cultured within 4 mg/ml fibrin hydrogels. Non-activated gels were used as a control (labelled "C" in the graphs). Ratios 2:1 and 3:1 3DFectIN:mRNA/pDNA tested for SOX9 target gene expression (A) and the best condition (i.e. 3:1 ratio) was replicated to compare mRNA and pDNA transfection (One-way ANOVA, n=2, **P<0.01) (B). The cytotoxicity of the gels was measured by a MTT assay at 24 h and 48 h (Two-way ANOVA, n=3, *P<0.05, **P<0.01) (C) and the capacity of the control hydrogels to support cell proliferation was confirmed by analyzing DNA mass in the culture at 0, 3 and 7 days by a PicoGreen Assay (One-way ANOVA, n=3, ***P<0.01) (D). All statistical differences noted in the panel are vs. the control except explicitly noted.

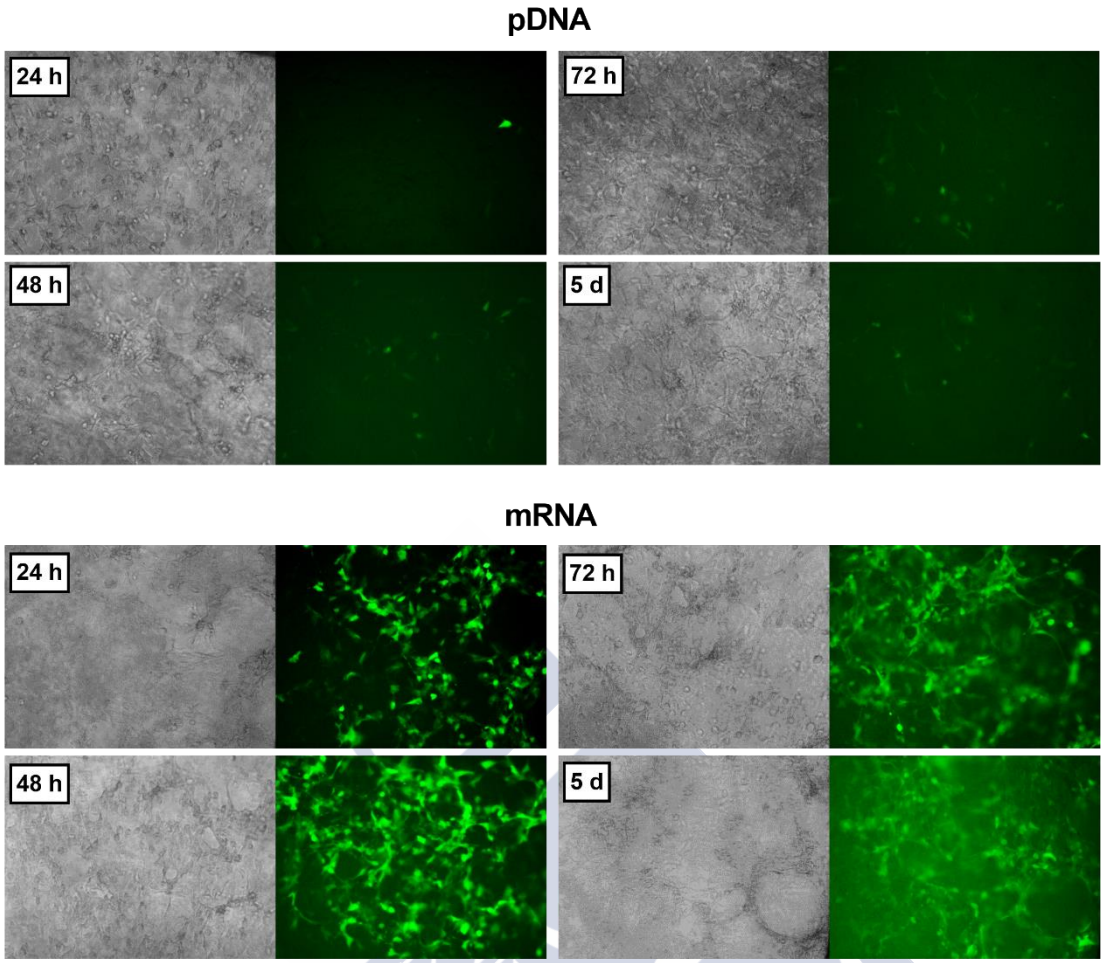

Fig. S8. Kinetics of YFP reporter protein expression in mRNA and pDNA activated matrices. Representative fluorescence and visible micrographs corresponding to transfection experiments performed with 1 µg of mRNA/pDNA and 3:1 3DFectIN:gene ratios (µL:µg). Fluorescence derived from YFP protein expression was monitored from 24 hours to 5 days post- cell encapsulation in 4 mg/mL fibrin gels.

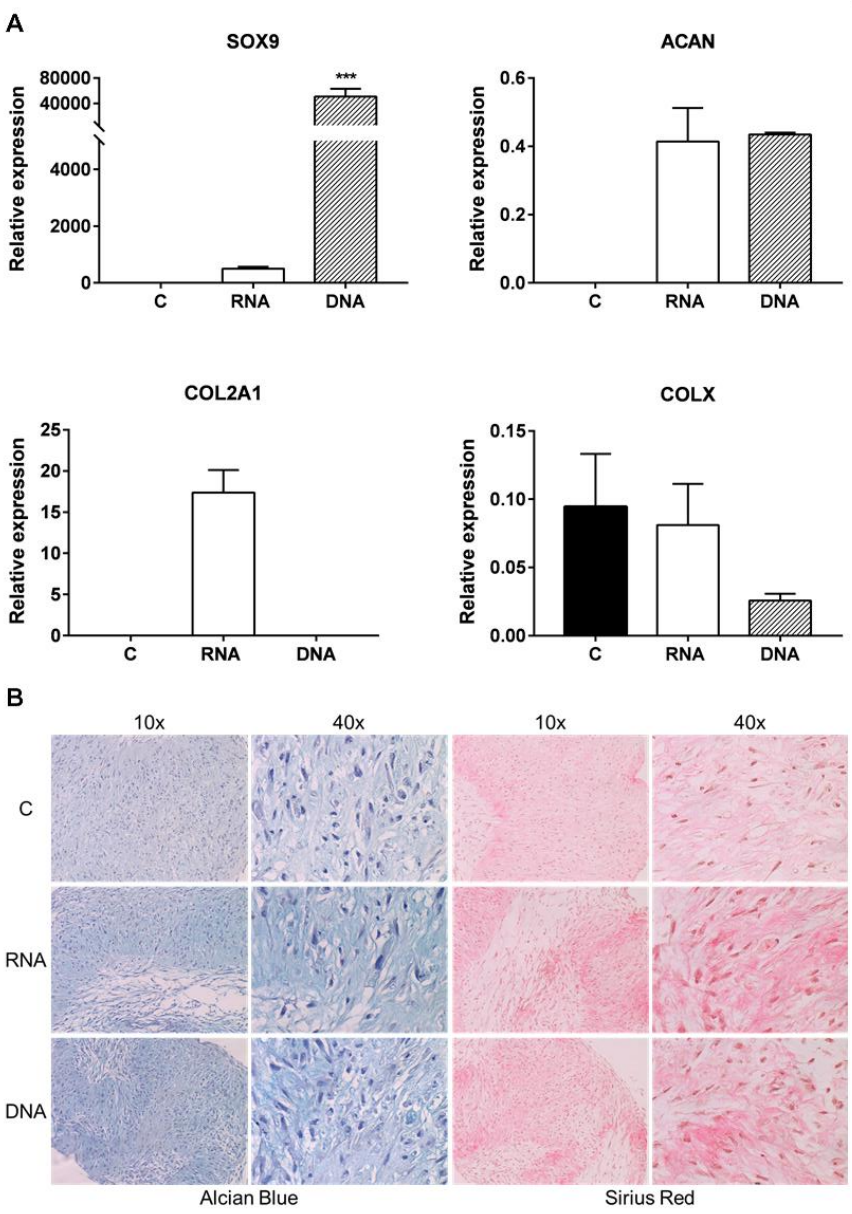

Fig. S9. Higher chondrogenic marker expression is observed in hMSCs encapsulated within 2 mg/ml SOX9-activated matrices as compared to control matrices in the absence of soluble TGF-β3. Hydrogels were cultured for 21 days in incomplete chondrogenic media. A) Gene expression levels of chondrogenic markers SOX9, aggrecan (ACAN), collagen type 2 (COL2A1) and collagen X (COLX) were measured by qRT-PCR, normalized to GAPDH expression and compared to the levels in hMSCs before encapsulation. Data are shown as mean and standard deviation of three replicates in one experiment at 3:1 3DFectIN:gene ratio. One-way ANOVA was performed to compare gene expression levels (***P<0.001). B) Histological examination of glycosaminoglycan and collagen deposition. Hydrogels were stained with alcian blue and Sirius red for sGAG and collagen staining, respectively.

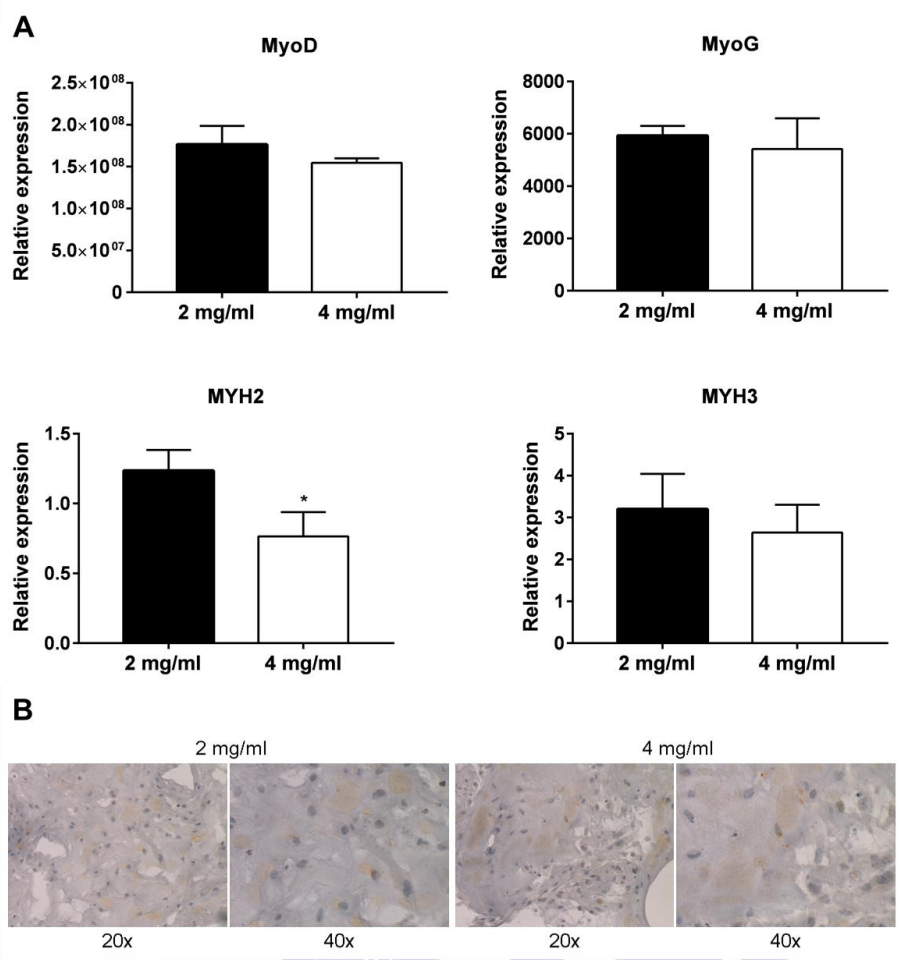

Fig. S10. Myogenic differentiation within MYOD matrices following the differentiation schedule. Hydrogels were cultured for 1 day in α-MEM supplemented with 10% FBS and 13 days in DMEM high glucose supplemented with 2% horse serum. (A-D) Gene expression levels of myogenic markers MYOD, myogenin (MYOG), myosin heavy chain 2 (MYH2) and myosin heavy chain 3 (MYH3) were measured by qRT-PCR, normalized to β actin expression and compared to the levels in hMSCs before encapsulation. Data are shown as mean and standard deviation of three replicates in one experiment. An unpaired T test was performed to compare gene expression levels (*P<0.05). (E) Immunohistochemistry examination of myosin heavy chain expression.

References

1. Zor, T. & Selinger, Z. Linearization of the Bradford Protein Assay Increases Its Sensitivity: Theoretical and Experimental Studies. *Anal. Biochem.* **236,** 302–308 (1996).

Chapter 3

USC
UNIVERSIDADE
DE SANTIAGO
DE COMPOSTELA

CHAPTER 3

Modulation of Gene Activated Matrix mechanics enhances the 3D transfection and SOX9-directed differentiation of Mesenchymal Stem Cells

This work has been done in collaboration with the Wyss Institute for Biologically Inspired Engineering and the John A. Paulson School of Engineering and Applied Sciences at Harvard University

ABSTRACT

Gene-activated matrices (GAMs) based on mRNA have been developed in order to overcome the low gene transfer efficiency of pDNA. However, even with the higher potency of mRNA-based GAMs, the process of 3D cell transfection remains to be completely understood to be able to design fully optimized GAMs. Here, we investigated whether GAM mechanical properties could be tuned to maximize cell transfection and phenotype specification for tissue engineering applications. We developed collagen-I-alginate interpenetrating polymer networks (IPNs) with tunable stiffness and adhesion, and we activated them with nanocomplexed SOX9 mRNA to direct mesenchymal stem cell (MSC) chondrogenic differentiation. We found that 3D transfection was enhanced by IPN stiffness and adhesion, which jointly promoted an increased cell proliferation and nanocomplex uptake. In differentiation experiments, IPN-mediated SOX9 transfection effectively induced MSCs chondrogenesis, reducing the levels of hypertrophy compared to non-transfected IPNs. More importantly, MSCs transfected within the IPNs showed a higher chondrogenic marker expression compared to MSCs transfected in 2D prior to encapsulation. These findings highlight matrix stiffness and adhesion as important design parameters in GAMs for use in regenerative medicine.

Key words: GAMs, IPNs, 3D transfection, mRNA, SOX9, tissue engineering

USC
UNIVERSIDADE
DE SANTIAGO
DE COMPOSTELA

1. Introduction

Stem Cell (SC) directed differentiation holds great promise in tissue engineering as a means to generate virtually any differentiated cell type to restore damaged or diseased tissue[1,2]. Studies in developmental biology have offered important insights into key growth factors (GFs) and, specifically, transcription factors (TFs) to direct SCs fate along specific pathways[3,4]. Based on this knowledge, several GFs have been included in polymer matrices to promote the differentiation of tissue resident SCs, and some devices based on this strategy have reached the market[5,6]. However, concerns have raised regarding the high doses of GF needed to compensate their short half-lives, and particularly the poor control over their release profiles, which in turn lead to side effects[7–9].

Gene Activated Matrices (GAMs) aim to overcome these limitations by delivery of polynucleotides encoding GFs and pivotal TFs in tissue development[10,11] to induce their stable expression. Although first GAMs were based on plasmid DNA (pDNA), recently it has been shown that mRNA-based GAMs may surpass the low gene transfer efficiency of pDNA. Indeed, Elangovan et al. first demonstrated the superior regenerative capacity of BMP-2 mRNA-GAMs compared to their pDNA counterparts[12], and subsequent work further showed the value of this strategy[13,14]. Nevertheless, even with the increased potency of mRNA-based GAMs, transfection efficiency should be maximized for these material systems to realize their full potential. Previous work has emphasized the role of the extracellular matrix (ECM) in gene transfer in 2D environments, identifying the positive effect of both stiffness[15] and adhesion[16] in bolus transfection. Other works performed in 2D have also investigated the influence of the nature of the ECM proteins to promote transfection[17,18]. However, due to the higher complexity of cell transfection in 3D environments[19,20], conclusions obtained from 2D studies do not always translate to 3D systems[21–24]. For this reason, there is a significant need for more systematic studies performed in 3D substrates. Moreover, in GAMs oriented to SC reprogramming, the adjustment of their mechanical properties may complement the effect of TF enforced expression, as mounting evidence has proved the modulation of SC fate by matrix stiffness, elasticity and stress-relaxation[25–29].

Here, we investigated whether 3D gene transfer could be enhanced by modulating the mechanical properties of the GAM environment, and whether GAM mechanics could be further exploited to stimulate tissue repair. To this end, we developed a set of interpenetrating polymer networks (IPNs) of collagen-I and alginate, and investigated their capacity to promote the transfection of SOX9 mRNA, a pivotal TF in chondrogenesis[30,31]. Previous works on mRNA GAMs have been focused on GF, and despite the success of mRNA for directing cell fate by enforced TF expression[32], to our knowledge, this approach has not been tested in a GAM yet. In addition, IPNs enable gel stiffness to be tuned independently of gel architecture, polymer concentration or

adhesion ligand density[33], and their composition resembles that of the native cartilaginous tissue[34,35], making them ideal platforms for this study. We fabricated IPNs with tunable stiffness and adhesion properties by modifying the concentration of the crosslinking agent[33] (i. e. calcium carbonate nanoparticles), and adjusting the ratios of the two polymers. We show that, for the same level of adhesion, IPNs of higher stiffness induced the highest transfection efficiency, and that this positive effect of stiffness was likely mediated by an increased cell proliferation and uptake of the mRNA condensates. In differentiation experiments, IPN-mediated SOX9 enforced expression induced the effective chondrogenesis of SCs, reducing the levels of hypertrophy compared to non-transfected IPNs. More importantly, SCs transfected within the IPNs showed an increased chondrogenic marker expression compared to SCs transfected in 2D prior to encapsulation. Taken together, these results provide insights to maximize non-viral mRNA delivery in synthetic ECMs in order to improve GAMs for use in regenerative medicine.

2. Materials and methods

2.1 Cell culture

Human adipose derived Mesenchymal Stem Cells (MSCs) and human bone marrow derived MSCs were acquired to ATCC and isolated from fresh unprocessed bone marrow (Lonza), respectively. Briefly, bone marrow samples were diluted in cold PBS pH 7.2 (Gibco) supplemented with 2% v/v heat inactivated fetal bovine serum (Gibco) and filtered (pore size 100 µm). Then, the diluted cell suspension was added over Lymphoprep (Stemcell Technologies) and centrifuged (800xg, 30 min, 20°C) yielding an interphase of mononuclear cells. CD14 microbeads (Miltenyi Biotech) were used for the depletion of CD14+ cells by magnetic separation and MSCs were allowed to adhere to tissue culture flasks. MSCs were cultured in α-MEM (Gibco) supplemented with 10 ng/ml rhFGF basic (Peprotech), 1% penicillin-streptomycin (Gibco) and 10% (adipose MSCs) or 20% (bone marrow MSCs) heat inactivated fetal bovine serum. Cells were detached from the plates using TrypLE enzyme solution (Gibco) and plated at 5000-7500 cells/cm^2. Media was changed every 2-3 days and cells were split at 70-80% confluency. For experiments involving ROCK inhibition, Y-27632 was added to cell culture media at 10 µM.

2.2 Preparation of 3DFectIN complexes

For 3D transfection experiments, 25 µl of transfection complexes were prepared per 150 µl of total IPN mix. Complexes were assembled in OptiMEM (Gibco) at 3:1 3DFectIN:mRNA/pDNA ratio (µl:µg), following the manufacturer's instructions. Briefly, a solution containing 1.5 µg of SOX9 mRNA/pDNA was added over a solution containing 4.5 µl of 3DFectIN reagent (OZ Biosciences) in a 1/1 v/v ratio, mixed by pipetting up-down and incubated for 20 min at room temperature. To investigate the distribution of

the complexes within the IPNs, SYBRGold-labeled pDNA complexes were prepared. A pDNA aqueous solution was labeled by mixing with a 50X DMSO solution of SYBR®Gold Nucleic Acid Gel Stain (Invitrogen) in a ratio 1:1 (µg:µl) and incubated for 5 min at room temperature before complex formation. Complexes were then encapsulated within the IPNs and visualized under fluorescence microscopy (EVOS FL Cell Imaging system).

2.3 IPNs preparation

Low viscosity, low MW sodium alginate was purchased from Pronova (UP VLVG). Before its use, alginate was dialyzed against deionized water for 2 days (3.5 kDa cutoff) and lyophilized. Dry alginate was then reconstituted at 8.0% w/v in Hank's Balanced Salt Solution (HBSS) without calcium and magnesium prior to IPN formation. Ice-cold bovine collagen type I (Advanced Biomatrix) was mixed with 1 M HEPES and 10X HBSS solutions at 1:50 and 1:10 v/v ratios to the amount of collagen needed, respectively, and pH was adjusted to 7.4 with NaOH 1 M. Calcium carbonate nanoparticles (nano-PCC, Multifex-MM, Specialty Minerals) were encapsulated within the IPNs to crosslink the alginate, and Ca^{2+} release was triggered by a media acidification induced by the addition of glucono delta-lactone (GDL). Before encapsulation, nanoparticles were suspended in RNAse free water (Invitrogen) at 1% w/v, sonicated for 15 s at 70% amplitude and 4°C (Branson Sonifier) and maintained under magnetic stirring to prevent sedimentation. GDL (Merck) was dissolved in HBSS (4% w/v) and incorporated to the IPN mix at a fourfold molar excess with respect to alginate, immediately before IPN molding. For transfection experiments, pDNA and mRNA complexes were prepared as previously described (2.2) and mixed with hMSCs prior to their encapsulation within the IPNs. hMSCs were suspended at 22.5 x 10^6 cells/ml in OptiMEM and added to the IPN at a density of 1.5 x 10^6 cells/ml.

All the different components were blended in 2 ml glass vials placed on an ice bath under magnetic stirring. HBSS supplemented with 20 mM HEPES and 37 mM NaOH was added first to reach the final volume of IPN mix. Ice-cold collagen solution was then included, and while it was stirring, transfection complexes were mixed with hMSCs by pipetting up-down and then added to the collagen solution. Once this mix was homogeneous, calcium carbonate nanoparticles were incorporated, followed by the addition of alginate. Finally, the solution of GDL was added and IPNs were casted in 96 or 48 well plates (Thermo Fisher Scientific). IPNs were then allowed to gel for 30 min at room temperature (alginate crosslinking) and 30 min at 37 °C (collagen crosslinking). Due to the drop in pH caused by the hydrolysis of GDL, pH was balanced by the addition of HBSS 20 mM HEPES during the first 4h after IPN crosslinking. Once pH was stabilized, culture media was added on top of the IPNs. Culture media was refreshed every 2-3 days.

2.4 Mechanical Characterization of IPNs

IPN mechanical properties were characterized with an AR-G2 stress controlled rheometer (TA Instruments). IPNs without cells and gene complexes were prepared as described above and placed onto the surface plate of the rheometer immediately before gelation. Right after, a 20 mm 2° aluminum cone was put into contact with the IPN creating a 20 mm gel disk. To prevent sample dehydration, the exposed gel surfaces within the rheometer geometry were surrounded with a wet Kimwipe, and 800 µl of HBSS were carefully added after the first step of IPN gelation. IPNs were allowed to gel at 25°C for 30 min (alginate crosslinking) followed by 30 min of collagen crosslinking at 37°C, and mechanical properties were measured over time as previously described[36]. The storage modulus at 0.5% strain and 1 Hz was recorded periodically until it reached its equilibrium value (30-60 min **Fig. S1**). Then, a strain sweep (0.1-20% strain) was performed to confirm this value was within the linear elastic regime, followed by a frequency sweep (0.1-10 Hz) (**Fig. S2**). No pre-stress was applied to the IPNs for these measurements. For stress-relaxation measurements, strain was raised during 1 s to 15% and then held constant, while the load was recorded as a function of time. Both the sweeps and stress-relaxation analysis were performed at 37°C.

2.5 Cell retrieval for gene expression and flow cytometry analysis

At the desired time points, cells were retrieved from the IPNs before RNA extraction and fluorocytometric analysis. Media was aspirated and IPNs were washed twice with PBS (Gibco). IPNs were then removed from the plates with a spatula and placed in 1.5 ml tubes before a two-step enzymatic digestion. Fresh enzyme solutions were prepared in Ca^{2+}, Mg^{2+} PBS (Gibco) supplemented with 1% bovine serum albumin (Sigma). In a first step, 350 µl of a solution containing 34 U/ml alginate lyase (Sigma) and 300 U/ml collagenase type I (Gibco) were added per 200 µl of IPNs and incubated for 15 min at 37°C under horizontal shaking (300 rpm, Heidolph Titramax platform shaker). Next, samples were centrifuged (5 min, 400xg) and the enzyme solution was removed. A second digestion was performed with 350 µl of a solution containing 300 U/ml collagenase and IPNs were further incubated for 15 min and centrifuged to discard the collagenase solution. For RNA extraction, the resulting pellet was mixed with 1 ml of 0.05M ice cold EDTA by pipetting up-down and then centrifuged again. This step was omitted for flow cytometry samples. Finally, the cell pellet was washed with 1 ml ice cold PBS and placed on ice until further analysis.

Total RNA was extracted with the SPEEDTOOLS total RNA extraction kit (Biotools) following the manufacturer's instructions. RNA concentration was quantified using a Nanodrop 2000 spectrophotometer (Thermo Fisher Scientific).

2.6 Uptake studies

Uptake of the transfection complexes within the IPNs was evaluated using a Cy5-labeled pDNA. For this, pcDNA3.1(+) (Addgene) was labeled with the Cy®5 *Label* IT® Tracker™

kit (Mirus) following the manufacturer's instructions and subsequently loaded in the transfection complexes. Complexes were then encapsulated within the IPNs together with MSCs and cultured for different lengths of time, after which cells were analyzed via flow cytometry and confocal microscopy. For flow cytometry analysis, MSCs were retrieved from the IPNs as previously described (section 2.5) and analyzed on a BD FACSCalibur. Cells were gated to eliminate interferences from remaining traces of polymers (**Fig. S3**) and the percentage of Cy5+ cells among the gated population was quantified. To evaluate the uptake via confocal microscopy, IPNs were cultured on glass coverslips. At the time of analysis, MSCs were fixed in 10% buffered formalin for 20 min at room temperature followed by permeabilization with Triton X-100 (0.2% v/v in PBS) for 10 min. Cells were then stained with DAPI (Sigma-Aldrich) and imaged on a Leica TCS SP5 confocal microscope.

2.7 cDNA synthesis and qRT-PCR

Reverse transcription was carried out using 100-500 ng of total RNA per sample in a 30 µl final reaction volume. First, total RNA was mixed with random primers and dNTPs (Invitrogen) and kept at 65 °C for 5 min. Samples were then incubated with a mix of RNAse OUT, 5x first strand buffer and DTT (Invitrogen) for 2 min at 37 °C and subsequently placed on ice. Finally, reverse transcriptase (M-MLV, Invitrogen) was included and the cycle was continued as follows: 10 min at 25 °C, 50 min at 37 °C and 15 min at 70 °C. The resulting cDNA (5-10 ng) was used to assemble qRT-PCR reactions in a final volume of 20 µl containing Universal PCR Mastermix and TaqMan assays (Applied Biosystems, **Table S1**). The thermal cycling was done in a StepOne Real Time PCR System (Applied Biosystems) performing a 10 min hold at 95 °C followed by 40 cycles of 15 sec at 95 °C and 1 min at 60 °C. Gene expression values were normalized to internal controls (Actin β and GAPDH) and presented either as the log2(ΔCt) or the fold change relative to cells plated in 2D before the experiments using the comparative $2^{-\Delta\Delta Ct}$ method[37].

2.8 Chondrogenic differentiation

Chondrogenesis experiments were performed with adipose hMSCs below passage 10. IPNs (200 µl) were casted in 48 well plates and cultured for 21 days in Complete Chondrogenic Medium (CCM) consisting of DMEM high-glucose 1 mM pyruvate (Gibco), 100 nM dexamethasone (Sigma-Aldrich), 50 µg/ml ascorbic acid 2-phosphate (Sigma-Aldrich), 40 µg/ml L-proline (Sigma-Aldrich), 1% ITS Premix supplement (Becton Dickinson), 1% penicillin/streptomycin (Gibco) and 10 ng/ml transforming growth factor-β3 (Peprotech). For experiments involving NF-κβ inhibition, CCM was supplemented with BMS-345541 at 5 µM. Media was replaced every 2 days in all experiments. IPNs were activated with two doses of SOX9 mRNA and pDNA, namely 2 and 0.5 µg per IPN, and their chondrogenic potential was compared to non-activated IPNs. At the end of the experiments, IPNs were retrieved for analysis. Gene expression of chondrogenic markers SOX9, aggrecan (ACAN), collagen type-II (COL2A1) and collagen

type-X (COLX) was assessed by qRT-PCR. SOX9, aggrecan and collagen type-X were also detected by immunohistochemistry (IHC).

2.9 Immunohistochemistry

IPNs were retrieved from tissue culture plates, washed with PBS twice and fixed with 10% buffered formalin at room temperature for less than 24 h. After fixation, samples were maintained in 70% ethanol until dehydration and paraffin sectioning. Sections of 4 µm thickness were cut and allowed to adhere to poly-L-lysine treated glass slides overnight at 55 °C. Before staining, sections were dewaxed in xylene and hydrated with graded ethanol, and antigens were retrieved in Tris-EDTA buffer during 20 min at 95 °C (PT Link, Agilent). Samples were pretreated with hydrogen peroxide and blocked with serum free protein block (Dako; Agilent) before incubation with primary antibodies against SOX9 (ab5535, Merck), aggrecan (ab3778, Abcam), and collagen type X (ab49945, Abcam). Primary antibodies were diluted in antibody diluent (Dako) at 1:500 (SOX9), 1:100 (aggrecan) and 1:1000 (collagen X) and incubated overnight at 4 °C. Then, samples were incubated with goat secondary antibodies labeled with HRP (Dako) at 1:100 for 1 h and stained with 3,3'-diaminobenzidine (DAB). Negative controls were obtained by omitting the primary antibodies (**Fig. S4**). All samples were observed using an Olympus BX43 microscope equipped with an Olympus XC50 camera. Samples were quantified with the IHC macro of the Fiji software[38].

2.10 Statistical Analysis

The statistical analysis was performed using GraphPad Prism. Where applicable, data are reported as the mean ±SD. Data were compared using One- or Two-way ANOVA and p-values less than 0.05 were considered to be statistically significant.

3. Results

3.1 Characterization of collagen-I-alginate interpenetrating networks (IPNs)

Collagen-I-alginate IPNs with tunable mechanical properties were fabricated to investigate the influence of stiffness and adhesion on the 3D transfection and chondrogenesis of human MSCs. To be able to elucidate the effect of each mechanical property, we designed an IPN set that would allow us to change both variables separately (**table 1**). We performed oscillatory rheology to tune IPN stiffness based on $CaCO_3$ concentration and fabricated four IPNs where the storage modulus (G') would vary from 150 to 1500 Pa at a fixed frequency of 1 Hz and across 60 min time periods (**Fig. 1A**). Within this range of stiffness, we modulated IPN adhesion by adjusting the collagen:alginate w:w ratio from 1:1 to 1:10. Compared to collagen, alginate presents no intrinsic integrin-binding domains for cells and hence higher collagen:alginate w:w ratios confer higher adhesion. The resulting IPN set can be divided in four groups: IPNs

of ↓stiffness and ↑↑adhesion (Soft 1:1), IPNs of ↓stiffness and ↑adhesion (Soft 1:2), IPNs of ↑stiffness and ↑adhesion (Stiff 1:2) and IPNs of ↑stiffness and ↓adhesion (Stiff 1:10). The paired comparison between the different groups enabled us to explore the effect of stiffness (Soft 1:2 vs Stiff 1:2) and adhesion (Soft 1:1 vs Soft 1:2 and Stiff 1:2 vs Stiff 1:10) on MSC behavior.

Table 1. Composition of the collagen-I-alginate IPNs.

IPN	Collagen (% w/v)	Alginate (% w/v)	Collagen:alginate w:w ratio	Calcium (% w/v)	Stiffness	Adhesion
Soft 1:1	0.5	0.5	1:1	0.300	↓	↑↑
Soft 1:2	0.5	1.0	1:2	0.135	↓	↑
Stiff 1:2	0.5	1.0	1:2	0.300	↑	↑
Stiff 1:10	0.1	1.0	1:10	0.300	↑	↓

Frequency dependent storage moduli on a frequency range of 0.1 to 1 Hz indicated that the IPNs exhibited some degree of viscoelasticity. This viscolastic behavior was higher for IPNs with low stiffness since they showed smaller differences between storage and loss moduli compared to IPNs of high stiffness. In addition, their storage modulus exhibited a greater dependence on the frequency compared to their stiff counterparts, which presented a predominantly elastic behavior (**Fig. S1**). Accordingly, IPNs of low stiffness and high collagen:alginate w:w ratio (Soft 1:1) showed the lowest stress relaxation half time ($\tau_{1/2} \approx 10$ s). Conversely, IPNs with the lowest collagen:alginate ratio (Stiff 1:10) exhibited the highest $\tau_{1/2}$ of about 300 s. At a fixed collagen:alginate ratio, IPNs presented half times of ≈100 s regardless of stiffness (**Fig. 1B**), suggesting that collagen:alginate w:w ratio is the main parameter affecting IPN stress relaxation. This half time of 100 s is in agreement with previous results for low viscosity, low MW alginate gels and has been identified as the optimum $\tau_{1/2}$ to allow cell-gel remodeling[39], a key process in tissue regeneration.

Due to the influence of fiber organization on long-range force transmission between cells[40–42], we next characterized the morphology of the collagen fibers within the IPN set (**Fig. 1C)**. As expected, IPNs with the lowest collagen concentration (Stiff 1:10) consequently showed the lowest density of collagen fibers. Interestingly, IPNs with collagen:alginate w:w ratios of 1:1 and 1:2 (Soft 1:1 and Stiff 1:2) exhibited a similar fibrillar pattern, suggesting that higher alginate concentrations do not impair collagen fiber formation. Soft 1:2 IPNs exhibited about the same density of collagen fibers as the

previous ones, but their fibers were thicker likely due to a larger lag in gelation time (**Fig. S2**).

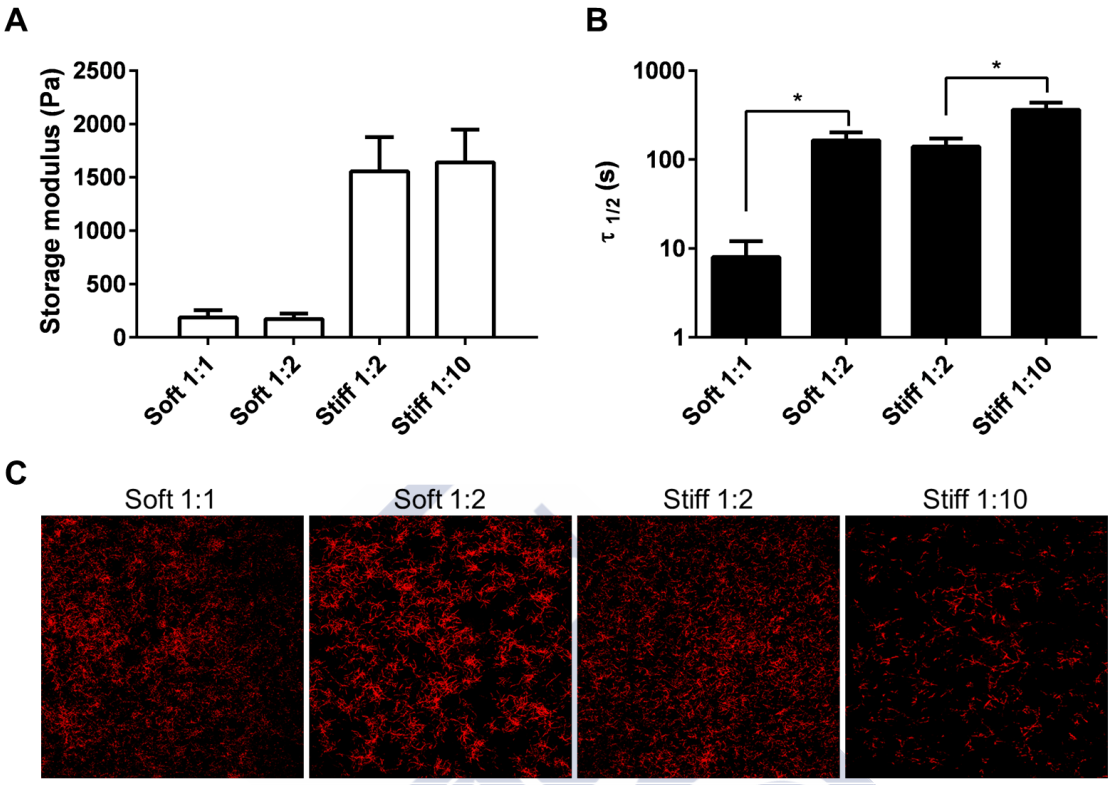

Figure 1. IPN stiffness and stress-relaxation can be modulated while maintaining collagen fiber morphology. A) Storage modulus at 1 Hz and 1% strain after 1 h of IPN crosslinking B) Quantification of timescale at which the stress is relaxed to half its original value, $\tau_{1/2}$, in stress-relaxation tests (shear stress 15% in 1 s) (One-way ANOVA, n=3, *P<0.05). C) Confocal reflectance micrographs of the different IPN compositions showing collagen fiber morphology.

3.2 Effect of stiffness and adhesion on IPN transfection efficiency

Once the IPN set was characterized in terms of microarchitecture and mechanical properties, human MSCs were encapsulated therein to examine the impact of these features on transfection efficiency. SOX9 mRNA and pDNA sequences were first nanocomplexed with 3DFectIN® reagent and subsequently loaded into the IPNs to prepare SOX9 GAMs. The encapsulation of MSCs within these GAMs promoted their 3D transfection and the consequent overexpression of SOX9, which was evaluated by qRT-PCR. Despite the high variability observed in net SOX9 expression values, probably due to the use of different mRNA and cell batches, qRT-PCR analysis showed the same trend in transfection efficiency: the higher SOX9 overexpression was achieved for Soft 1:1 and Stiff 1:2 IPNs and the lower for Soft 1:2 and Stiff 1:10 IPNs, regardless of the type of genetic material (pDNA or mRNA) (**Fig. 2A**). As commented previously, comparing the

two soft IPN conditions (Soft 1:1 and Soft 1:2) and the two stiff conditions (Stiff 1:2 and Stiff 1:10) can give us information about the influence of collagen:alginate w:w ratios, while comparing IPNs of opposite stiffness informs about the impact of the storage modulus on gene transfer efficacy. Accordingly, our gene expression results showed that lower collagen:alginate w:w ratios exerted a negative impact on transfection efficiency. In the case of stiff IPNs, where collagen:alginate ratio was modulated from 1:2 to 1:10, this negative impact was found to be related to an increased destabilization of the nanocomplexes with increasing alginate concentrations (**Fig. S5**). For soft IPNs, changing collagen:alginate ratio from 1:1 to 1:2 did not induce a notorious nanocomplex aggregation (**Fig. S5**) but it resulted in a dramatic decrease in SOX9 overexpression, suggesting an implication of IPN adhesion on transfection. Efficient cell attachment might be necessary for cytoskeletal organization, which in turn could modify the intracellular transport of the complexes. Indeed, for both Soft 1:1 and Stiff 1:2 IPNs, transfection proved to be affected by the state of cell cytoskeleton, as demonstrated by the drastic decrease in SOX9 overexpression after the addition of the ROCK inhibitor Y-27632 (**Fig. 2B**). Together with adhesion, gene transfer efficacy was also increased with stiffness, as evidenced by the differences between Soft 1:2 and Stiff 1:2 IPNs. Stiffness has been previously shown to promote transfection efficiency in 2D environments by increasing cell proliferation[15]. Considering that 3D transfection has also been linked to cell proliferation and matrix invasion[22,43], we checked whether IPN transfection was related to proliferation by determining the levels of two common genes implicated in cell cycle: c-Myc and Cyclin-D1. Although Cyclin-D1 levels were maintained across all the conditions, c-Myc levels varied significantly (**Fig. 2C**). We observed that, for soft IPNs, a higher collagen:alginate ratio resulted in a higher cell proliferation, that correlated with a higher transfection. At a fixed 1:2 collagen:alginate ratio, higher stiffness also resulted in higher cell division rates that were again linked to a more efficient transfection. Interestingly, lower collagen:alginate ratios did not reduce cell proliferation in stiff IPNs, suggesting that IPN stiffness partially compensates the negative impact of low adhesion on cell proliferation. This compensatory effect of stiffness was also evidenced by the lower decrease in SOX9 overexpression in Stiff 1:2 IPNs compared to Soft 1:1 IPNs after treatment with Y-27632, where disrupting cell adhesion diminished transfection in Soft 1:1 IPNs to the levels of the low adhesive Soft 1:2 IPNs (**Fig. 2B**).

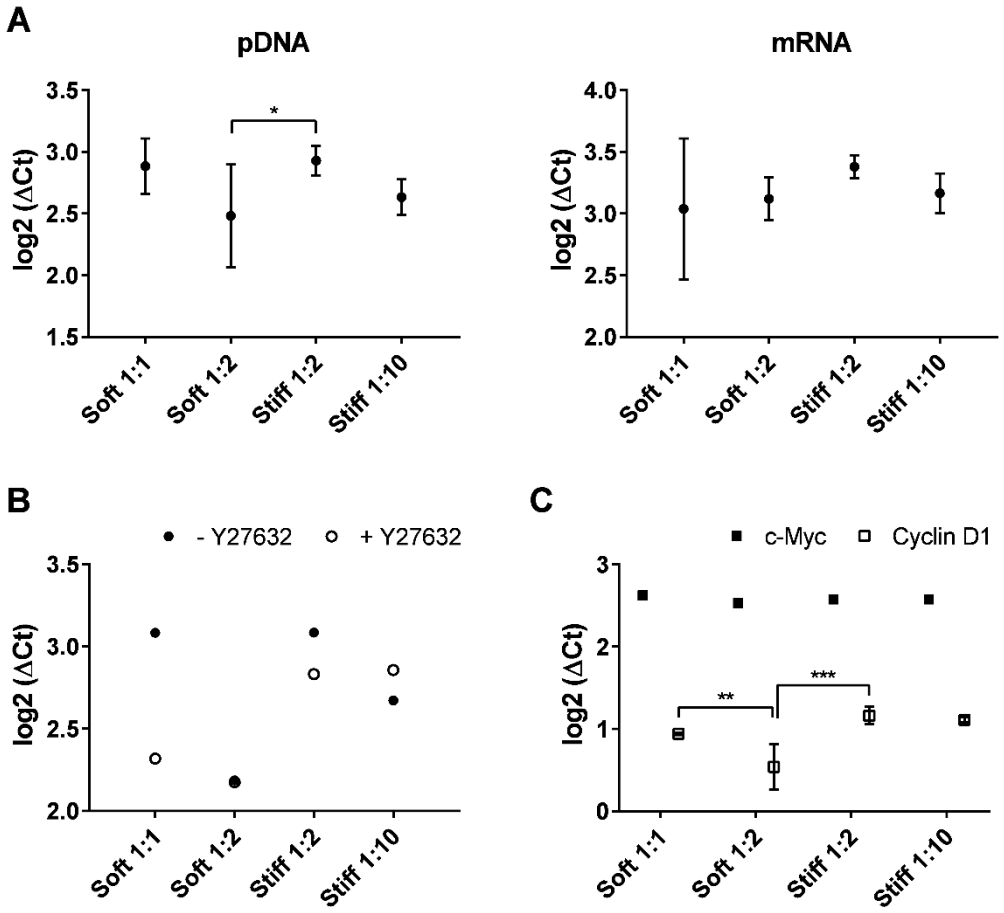

Figure 2. IPN stiffness and adhesion exert a positive effect on MSC 3D transfection likely mediated by an increased cell proliferation rate. A) SOX9 expression 48 h and 24 h after pDNA and mRNA transfection within the IPNs, respectively. One-way ANOVA was performed to compare gene expression levels (*P<0.05). B) Effect of ROCK inhibition on IPN transfection efficiency. hMSCs were transfected with SOX9 pDNA within the IPNs in the absence or presence of Y-27632. C) Cell proliferation rates in the different IPN conditions. qRT-PCR quantification of C-Myc and Cyclin D1 expression 48h after pDNA 3D transfection. Two-way ANOVA was performed to compare gene expression levels (*P<0.05; **P<0.01; ***P0.001). Gene expression levels are normalized to GAPDH and expressed as log2(ΔCts). A, C) Data represent the mean ± SD. B) Results from one representative experiment are shown.

Differences in transfection efficiency could be also related to a different cell internalization rate of the nanocomplexes among the different IPNs. In order to test this hypothesis, and to further investigate the positive effect of stiffness on transfection efficiency, we selected the two IPNs with the same collagen:alginate ratio and opposite stiffness: Soft 1:2 and Stiff 1:2 IPNs. We prepared the transfection complexes with a Cy5-labeled pDNA and we tracked their localization within the cells by confocal microscopy and quantified their association to the cells using flow cytometry. As observed in **Figure 3**, the nanocomplex uptake by MSCs was high for both IPNs. Based on the analysis of the FACS histogram (**Fig. 3C**), soft IPNs presented a higher proportion of Cy5 positive cells, suggesting that more Cy5-pDNA complexes were associated to the cells in these IPNs.

However, stiff IPNs induced a more homogeneous distribution of the complexes within the cells compared to soft IPNs, where complexes appeared to be attached to the cell membrane in a higher number of cells (**Fig. 3A-B**).

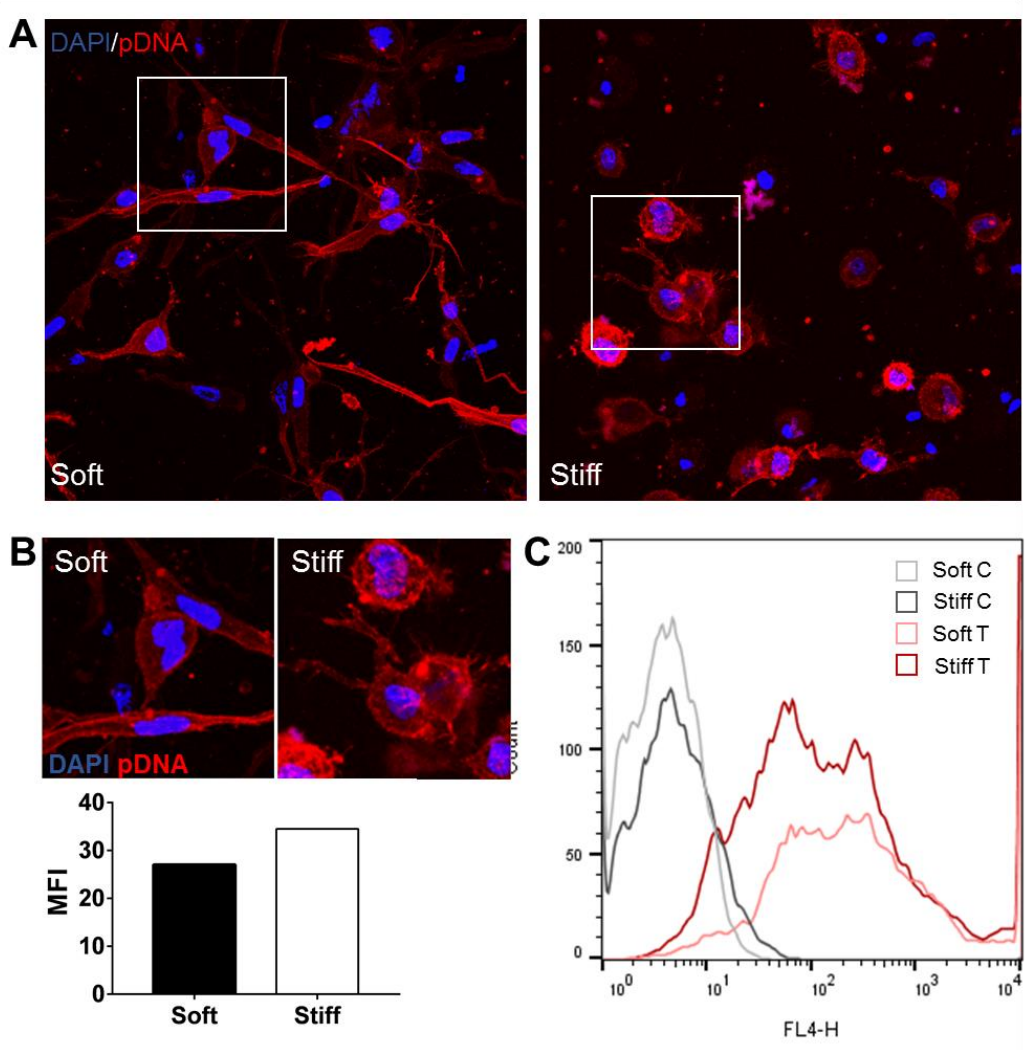

Figure 3. IPN stiffness increases the uptake of the pDNA condensates. A) Confocal images of hMSCs within IPNs showing the location of pDNA condensates. B) High-magnification image of A) (top) and the corresponding mean fluorescence quantification (bottom). C) Representative flow cytometry histogram showing the association of Cy5-labeled pDNA to cells encapsulated within soft and stiff IPNs.

With the aim to evaluate the interplay between SOX9 expression and IPN mechanics on MSC chondrogenesis, we performed a set of experiments transfecting MSCs in 2D before encapsulating them in the gels. Our hypothesis was that in this way we would eliminate the differences in SOX9 expression among the IPNs. However, for pDNA-activated IPNs, we found that 2D transfected cells showed a similar trend in SOX9 expression after their encapsulation within the IPNs as when transfection was directly performed in 3D (**Fig. 4A**). Even more, MSCs retrieved from the IPNs exhibited an increased SOX9 expression compared to transfected cells before encapsulation, pointing to some degree of cell transfection taking place within the gels. The most likely explanation for this increased

transfection was that some pDNA complexes used for 2D transfection were encapsulated with the cells in the IPNs. In order to check this hypothesis, we decided to track Cy5-pDNA Lipofectamine® complexes during the 2D transfection process using fluorescence microscopy. This allowed us to observe that pDNA complexes remained adhered to the cells for at least two days after transfection and one day after retrieving the cells from the plates by enzymatic separation (**Fig. 4B**), supporting the idea that some of the complexes were encapsulated within the IPNs together with the cells allowing their transfection in 3D. Conversely, in the case of pre-2D mRNA transfection, SOX9 expression was similar in MSCs before and after their encapsulation in IPNs, suggesting that there was no further transfection occurring within the IPNs (**Fig. 4A**). The different behavior of pDNA and mRNA complexes presumably arises from the fact that mRNA molecules are more prone to enzymatic degradation[32].

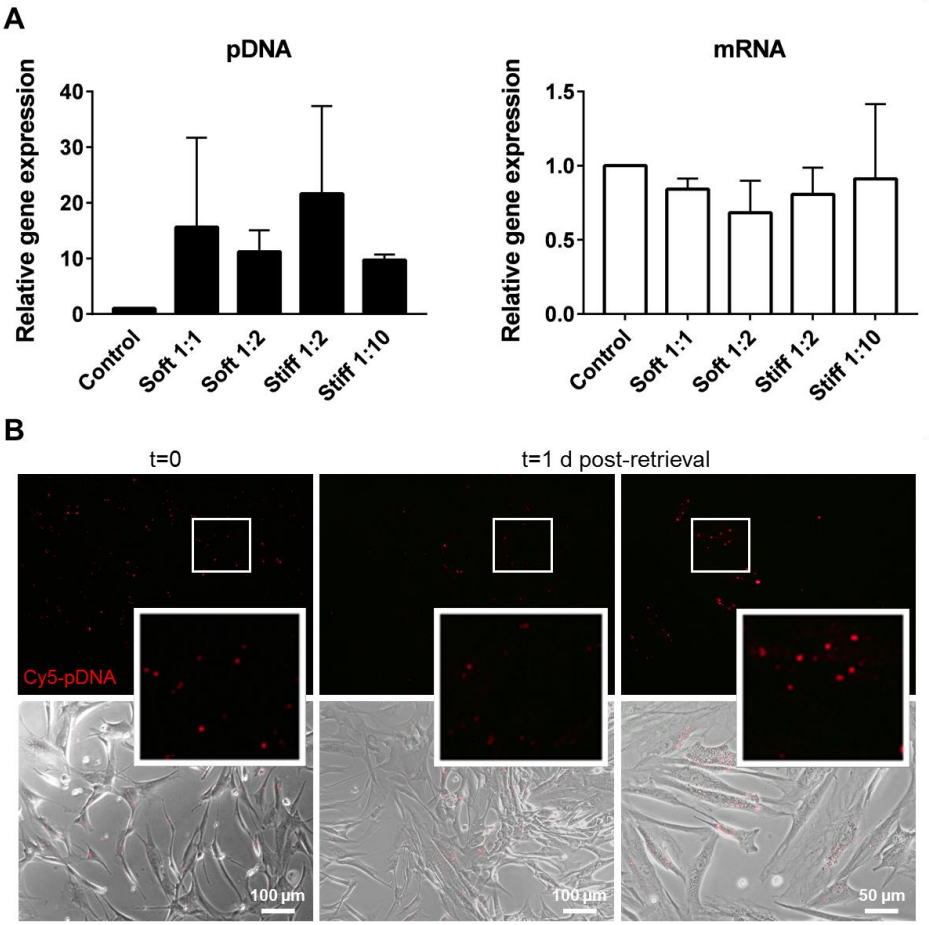

Figure 4. Matrix mechanics alters SOX9 overexpression levels of 2D transfected cells by further promoting their 3D transfection. A) SOX9 overexpression after encapsulation of pDNA and mRNA transfected cells within the IPNs (cells retrieved from tissue culture plates 72 and 24 h post transfection, respectively). Gene expression levels are normalized to GAPDH and presented as relative to SOX9 levels in 2D transfected cells before encapsulation (Control). B) Location of Cy5-labeled pDNA complexes in cells retrieved from tissue culture plates after 2D pDNA transfection. Transfection complexes were incubated with hMSCs for 4 h and media was changed afterwards (t=0). Cells were cultured for 72 h and then retrieved by enzymatic separation and transferred to a new plate. Images were taken one day after retrieval (t=1 d post-retrieval).

3.3 Effect of IPN mechanics on the chondrogenic differentiation of hMSCs

Considering the impact of IPN mechanical properties on MSC 3D transfection efficiency, we wanted to elucidate whether these properties could also influence MSC chondrogenic differentiation. Specifically, we sought to explore the synergy between IPN mechanics and SOX9 mRNA reprogramming in the design of GAMs for cartilage regeneration. First, we investigated the effect of IPN stiffness by comparing the behavior of Soft 1:2 and Stiff 1:2 IPNs that possess similar adhesion and stress-relaxation properties. With the aim to minimize the differences in SOX9 overexpression between the two IPNs, MSCs were transfected in 2D prior to their encapsulation. SOX9-transfected MSCs were then encapsulated within the IPNs and subjected to differentiation assays, after which cells were retrieved and the expression of chondrogenic markers was assessed. At the end of these experiments MSCs exhibited dramatic changes in cell morphology, with soft IPNs promoting elongated, spindle-like morphologies and stiff IPNs inducing spherical cell shapes, as previously observed[33] (**Fig. 5A**). As expected, SOX9-transfected MSCs showed higher levels of SOX9 mRNA expression compared to control (non-transfected) cells (**Fig. 5C**), but this higher mRNA expression did not translate into significant differences in SOX9 protein expression as assessed by immunohistochemistry (**Fig. 5D-E**). Whereas SOX9 mRNA levels were not significantly different between the two transfected IPNs, stiff IPNs induced a higher aggrecan (ACAN) mRNA expression. Interestingly, this aggrecan expression was increased in control IPNs compared to their SOX9-transfected counterparts, both at the mRNA and protein level (**Fig. 5C-E**). Importantly, levels of the hypertrophic marker collagen type-X (COLX), were lower in transfected IPNs, especially in the case of stiff IPNs, denoting a role of SOX9 overexpression in controlling MSC hypertrophy (**Fig. 5B-E**).

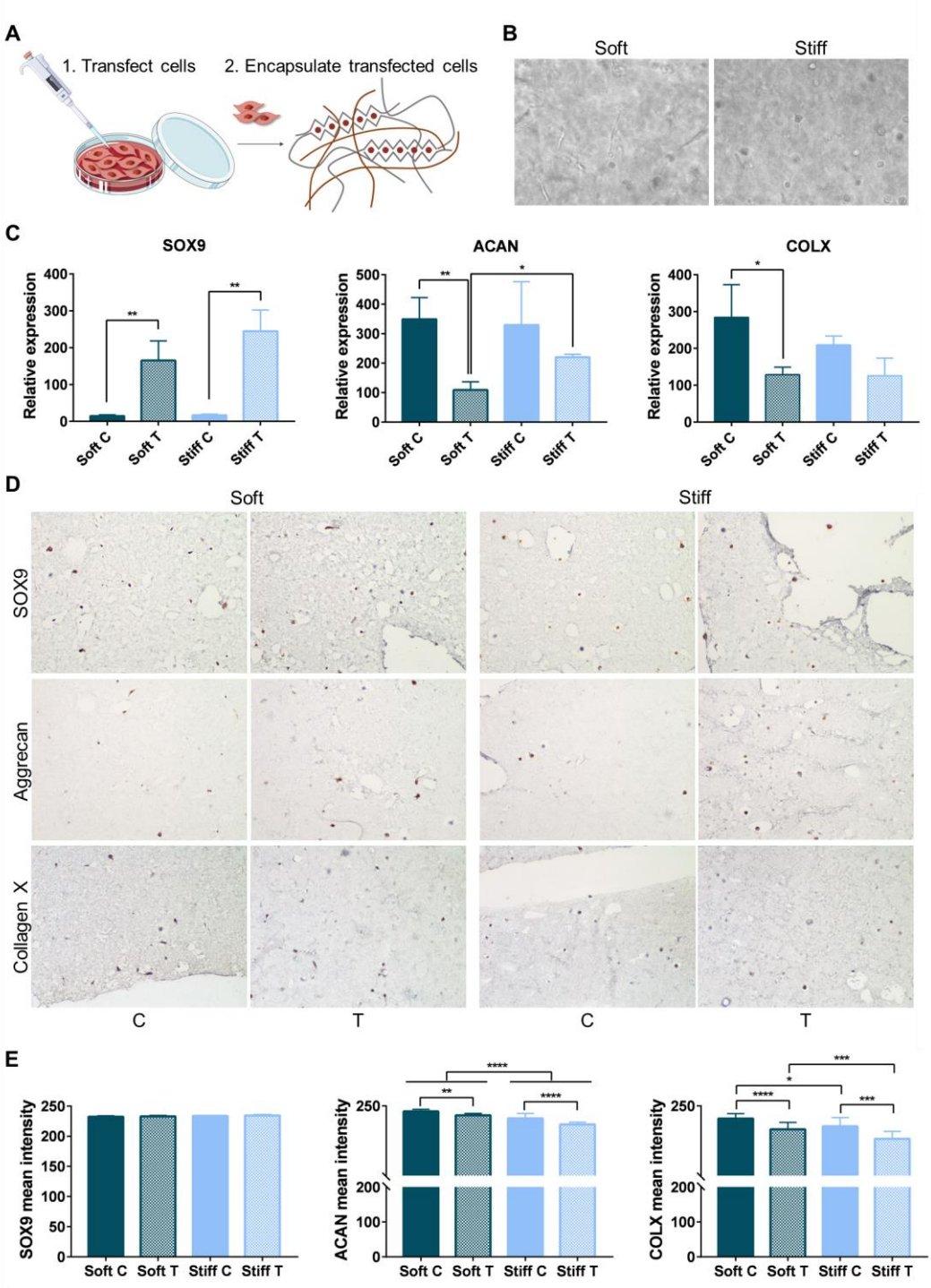

Figure 5. Stiff IPNs promote a higher chondrogenic marker expression in MSCs after SOX9 2D transfection. C: control (non-transfected) cells; T: SOX9-transfected cells. A) Schematic of the experimental setup. Cells are first transfected on tissue culture plates and then retrieved and encapsulated within the IPNs 24h later. The IPN is illustrated as brown collagen fibers and grey alginate polymer chains. The calcium ions crosslinking the G-blocks of the alginate network (zig-zag structures) are shown as red dots. Objects are not drawn to scale. B) Representative optical micrographs showing the morphology of hMSCs at the end of the chondrogenesis experiment. C) Gene expression of chondrogenic markers SOX9, aggrecan (ACAN), and collagen type-X (COLX) (One-way ANOVA, n =3, *P<0.05, **P<0.01). D) Immunostaining of SOX9, aggrecan and collagen type-X in IPN sections. E) Quantification of D) (One-way ANOVA, **P<0.01, ***P<0.001, ****P<0.0001). Data represent the mean ±SD.

Given the positive impact of SOX9 overexpression on MSC chondrogenic differentiation, we next wanted to test the effect of GAM-induced 3D transfection. We selected the Stiff 1:2 IPNs for further experiments since we found a higher expression of chondrogenic markers in these IPNs and they had shown a high transfection efficiency previously. In addition, the stiffness of Stiff 1:2 IPNs could fit better with the big loads bore by articular cartilage [34,35], further highlighting the suitability of this IPN. We tested two SOX9 mRNA doses in this set of experiments: 0.5 µg and 2 µg per 200 µl IPN, to tackle the effect of SOX9 overexpression on chondrogenic marker expression. In addition, we also investigated the use of the anti-inflammatory compound BMS-345541, since it has been described that inflammatory events linked to NF-κβ pathway can impair extracellular matrix (ECM) synthesis and chondrogenesis[44].

As expected, SOX9-activated IPNs promoted a higher SOX9 gene expression than non-activated IPNs at both SOX9 mRNA doses (**Fig.6A, Fig. S6A**). This SOX9 upregulation was higher in the IPNs with the high SOX9 mRNA dose, especially in the case of IPNs treated with the NF-κβ inhibitor **(Fig. 6A**). Although at the low SOX9 dose, gene expression of chondrogenic markers aggrecan and collagen type-II was lower compared to control IPNs (**Fig. S6A**), there was a notorious effect on collagen type II (COL2A1) mRNA expression after SOX9 transfection with the high dose (**Fig. S7**). Indeed, SOX9-GAMs induced a potent COL2A1 overexpression whereas this ECM protein was not detected in control and BMS-treated IPNs. Importantly, transfection with both SOX9 doses and treatment with the NF-κβ inhibitor resulted in mRNA downregulation of the hypertrophic marker collagen type-X. This mRNA downregulation correlated with a lower COLX protein expression as assessed by immunohistochemistry, suggesting that both, SOX9 transfection and treatment with BMS-345541 inhibitor, could be good strategies to improve the quality of the regenerated cartilage. Conversely, no notorious differences were found in SOX9 and aggrecan protein expression between control and transfected IPNs, even in the case of BMS-345541 treatment (**Fig. 6B, S6B**).

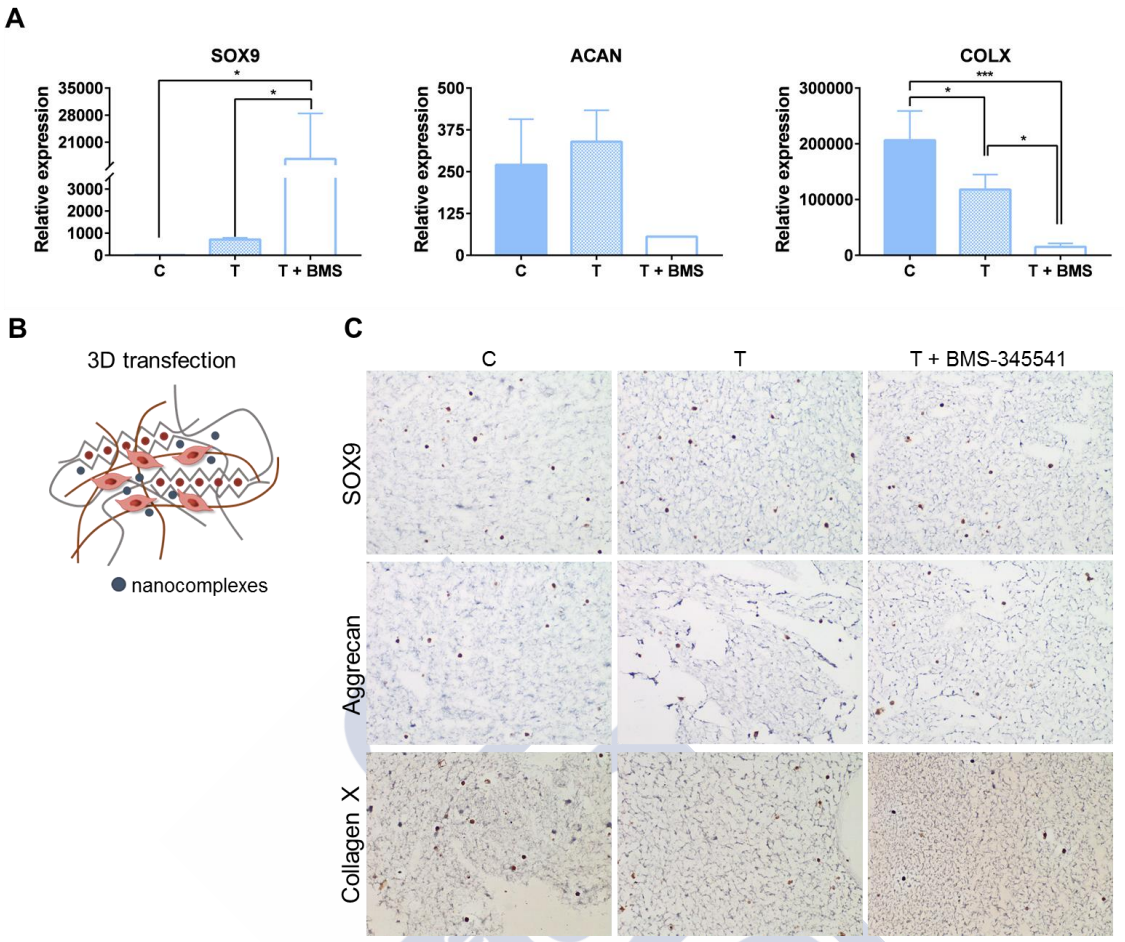

Figure 6. SOX9 3D transfection with a high mRNA dose promotes a higher chondrogenic marker expression in MSCs than pre-2D transfection. C: control (non-transfected) cells; T: SOX9-transfected cells; T + BMS: SOX9-transfected cells supplemented with the NF-κβ inhibitor BMS-345541 (5 μM). A) Gene expression of chondrogenic markers SOX9, aggrecan (ACAN) and collagen type-X (COLX) (One-way ANOVA, n =3, *P<0.05, ***P<0.001). B) Schematic of the experimental setup. Cells are encapsulated within the IPNs together with the nanocomplexes, promoting their 3D transfection. The IPN is illustrated as brown collagen fibers and grey alginate polymer chains. The calcium ions crosslinking the G-blocks of the alginate network (zig-zag structures) are shown as red dots. Objects are not drawn to scale. C) Immunostaining of SOX9, aggrecan and collagen type-X in IPN sections. Data represent the mean ±SD.

4. Discussion

IPNs of alginate and collagen-I were developed to investigate the effect of matrix mechanical properties on the 3D transfection and chondrogenesis of MSCs. IPNs enable gel stiffness and adhesion to be tuned independently, and hence represent an ideal platform to decouple the effect of these two parameters on MSC biology. In this work, IPN stiffness was modulated by changing the amount of the alginate crosslinking agent (i.e. calcium carbonate nanoparticles), while adhesion was tuned by modifying the weight ratio between alginate (lacking cell adhesion ligands) and collagen (with numerous integrin-binding domains). Characterization of IPN microarchitecture revealed that collagen fiber morphology was preserved regardless of stiffness, while

modulating collagen fiber density by changing collagen concentration did no alter the stiffness of the system. Likewise, for the same polymer composition, the stress-relaxation behavior of these IPNs was independent of stiffness. Previous work has highlighted the benefit of collagen-I-alginate IPNs over other IPN systems that modulate stiffness by changing polymer nature and concentration, which in turn may alter hydrogel architecture and porosity[33]. In addition, collagen-I-alginate IPNs could yield more realistic ECM models compared to biologically inert polymer hydrogels that present synthetic adhesion ligands[45,46], further supporting our selection of these systems.

A number of works have considered the impact of mechanical cues in 2D transfection efficiency of cells plated over substrates of different adhesion and stiffness[15,16,21,47]. Other studies have investigated the differences between 2D and 3D transfection in terms of endocytic pathways and cytoskeletal dynamics[23]. However, to day, the role of GAM mechanics on 3D gene transfer has not been well-established yet and more work is required to further understand the potential of these systems. To tackle this problem, we prepared SOX9 GAMs by loading SOX9 mRNA and pDNA nanocomplexes together with MSCs within collagen-I-alginate IPNs, and evaluated their transfection efficiency in 3D. Our results indicate that higher collagen:alginate w:w ratios and higher stiffness exert a positive effect on transgene expression within the IPNs. Besides, our data suggest that this positive effect of stiffness is mediated by cell adhesion ligands and cytoskeletal dynamics, since the addition of ROCK inhibitor Y-27632 dramatically reduced transfection efficiency in IPNs of high collagen:alginate w:w ratios. This positive effect of stiffness and adhesion is consistent with a similar trend observed for transfections performed in 2D and has been related to an increased cell proliferation rate[15] and a more efficient vesicular transport mediated by the microtubular network[23,48]. In agreement with these studies, we observed higher cell proliferation rates within IPNs of higher stiffness and adhesion. Interestingly, our results show that a high IPN stiffness may surpass the detrimental effect of low adhesion on cell proliferation. Indeed, stiff IPNs with collagen:alginate ratios of 1:2 and 1:10 exhibited similar cell proliferation rates. Similarly, Stiff 1:2 IPNs presented a lower reduction in transfection efficiency in the presence of the ROCK inhibitor Y-27632 compared to Soft 1:1 IPNs. In addition, our data suggest that the increased efficacy of stiff IPNs might be related to a higher cell uptake of the mRNA/pDNA condensates. Although more studies are required to elucidate the underlying mechanism, we anticipate that the endocytic pathway and subsequent intracellular trafficking followed by the condensates are responsible for this stiffness-mediated effect. Importantly, our transfection results are in contradiction with those recently reported for hyaluronic acid (HA)-based hydrogels, where soft gels induced higher cell proliferation and transgene expression levels than stiff gels[49]. Stiffness in these hydrogels was modulated by changing the ratio of thiols to acrylates (cross-linking by Michael addition chemistry) or the amount of HA. In

particular, in the range of stiffness where we found the differences in transfection efficiency (G'= 150-1500 Pa), their HA concentration ranged from 3 to 5%. This increase in HA concentration could change other parameters apart from stiffness, such as gel architecture or adhesion ligand density, which in turn may affect 3D transfection leading to the disparate results. As previously explained, collagen-I-alginate IPNs enable gel stiffness to be tuned independently of polymer concentration, allowing us to get more independent conclusions about the effects of stiffness.

To segregate the effects of mechanical properties on both SOX9 transfection efficiency and MSCs chondrogenic differentiation, we performed 2D transfections prior to the encapsulation of MSCs within the different IPNs. Contrary to our expectations, we found that transfection of 2D pre-transfected cells was further enhanced when they were encapsulated within the IPNs. We show that this increased transfection is due to the encapsulation of remaining pDNA complexes associated to MSCs, suggesting that these GAMs may represent an approach to boost the efficacy of traditional gene delivery systems. In addition, cells retrieved from the IPNs also showed the same trend in gene overexpression as when transfection was performed in 3D, highlighting the impact of GAM mechanical properties on gene transfer efficacy. Together, these results support our hypothesis that IPN stiffness induces a more efficient intracellular transport of the transfection complexes. This positive effect of stiffness likely stems from the generation of a tensional prestress in MSCs encapsulated within the IPNs, that translates in a stronger actin cytoskeleton and microtubular network that facilitates transfection[48,50–53]. The benefit of 3D over 2D gene transfer was further shown for SOX9 reprogramming in the chondrogenesis studies. Compared to the levels of chondrogenic markers obtained when cells were transfected in 2D before the encapsulation within the IPNs, IPN-mediated SOX9 transfection promoted a higher chondrogenic marker expression. This was especially relevant for the ECM related genes aggrecan and collagen type II, suggesting the generation of an improved cartilage-like tissue. Consistent with previous findings, SOX9 expression correlated with a reduction in the premature production of the hypertrophic marker collagen type-X[30]. This is particularly noteworthy since tissue engineered cartilage usually presents an impaired balance of collagen type-II and collagen type X, leading to a hypertrophic cartilage of poor mechanical properties[54]. The addition of the NF-κ-β inhibitor BMS-345541 also contributed to the interruption of premature hypertrophy, highlighting the utility of this inhibitor in cartilage tissue engineering.

Collectively, our observations suggest that more efficient tissue engineering GAMs can be designed by tuning GAM mechanical properties to boost their transfection efficiency and mimic the target native tissue. The fact that one can induce a potent enforced transcription factor expression through mRNA 3D transfection allows for in situ cell

reprogramming strategies that simplify their application in the clinical setting[32,55], since they circumvent tedious *in vitro* cell culture and modification procedures.

5. Conclusions

In this work, MSC 3D transfection and directed chondrogenic differentiation were efficiently modulated through the use of collagen-I-alginate IPNs of different mechanical properties. IPN stiffness and adhesion were identified as key factors promoting an increased 3D transfection, regardless of the genetic material used, mRNA or pDNA. This increased transfection was related to a higher cell proliferation and internalization rate of the mRNA/pDNA condensates, likely mediated by a more efficient intracellular trafficking in IPNs of high stiffness and adhesion. When these IPNs were used to induce SOX9-mRNA directed differentiation, they promoted MSC chondrogenesis with low hypertrophy levels. Importantly, IPN mediated SOX9 transfection resulted in the generation of an improved cartilage-like tissue compared to the IPN encapsulation of 2D transfected MSCs. These results indicate that matrix mechanics can be adjusted to design more efficient GAMs for *in situ* mRNA-based cell reprogramming in tissue engineering.

Acknowledgements

This work has been funded by Ministerio de Economía y Competitividad (MINECO-RETOS, Grant MAT2017-84361-R, Feder Funds), Fundación BBVA 2014-PO0110 and Xunta de Galicia (Grupos de Referencia Competitiva, Feder Funds; Convenio para fomentar a actividade investigadora do persoal investigador finalista nas convocatorias de axudas do ERC no marco da H2020). A. M. L. was supported by a FPU fellowship from the Spanish Ministry of Education. The authors thank Thomas Ferrante for assistance with confocal reflectance microscopy and Dr. J. Li, Dr. S. T. Koshy and Dr. A. S. Cheung for scientific discussions.

References

1. Merrell, A. J. & Stanger, B. Z. Adult cell plasticity in vivo: de-differentiation and transdifferentiation are back in style. *Nat. Rev. Mol. Cell Biol.* **17,** 413–425 (2016).

2. Jopling, C., Boue, S. & Belmonte, J. C. I. Dedifferentiation, transdifferentiation and reprogramming: three routes to regeneration. *Nat. Rev. Mol. Cell Biol.* **12,** 79–89 (2011).

3. Murry, C. E. & Keller, G. Differentiation of Embryonic Stem Cells to Clinically Relevant Populations: Lessons from Embryonic Development. *Cell* **132,** 661–680 (2008).

4. Yamamizu, K. *et al.* Identification of transcription factors for lineage-specific ESC differentiation. *Stem Cell Reports* **1,** 545–559 (2013).

5. Yannas, I. V, Lee, E., Orgill, D. P., Skrabut, E. M. & Murphy, G. F. Synthesis and characterization of a model extracellular matrix that induces partial regeneration of adult mammalian skin. *Proc. Natl. Acad. Sci. U. S. A.* **86,** 933–7 (1989).

6. Lo, K. W.-H., Ulery, B. D., Ashe, K. M. & Laurencin, C. T. Studies of bone morphogenetic protein-based surgical repair. *Adv. Drug Deliv. Rev.* **64,** 1277–91 (2012).

7. Kang, D. G., Hsu, W. K. & Lehman, R. A. Complications Associated With Bone Morphogenetic Protein in the Lumbar Spine. *Orthopedics* **40,** e229–e237 (2017).

8. Epstein, N. Complications due to the use of BMP/INFUSE in spine surgery: The evidence continues to mount. *Surg. Neurol. Int.* **4,** 343 (2013).

9. DeVine, J., Dettori, J., France, J., Brodt, E. & McGuire, R. The use of rhBMP in spine surgery: is there a cancer risk? *Evid. Based. Spine. Care. J.* **3,** 35–41 (2012).

10. Im, G. I., Kim, H. J. & Lee, J. H. Chondrogenesis of adipose stem cells in a porous PLGA scaffold impregnated with plasmid DNA containing SOX trio (SOX-5,-6 and -9) genes. *Biomaterials* **32,** 4385–4392 (2011).

11. Raisin, S., Belamie, E. & Morille, M. Non-viral gene activated matrices for mesenchymal stem cells based tissue engineering of bone and cartilage. *Biomaterials* **104,** 223–237 (2016).

12. Elangovan, S. *et al.* Chemically modified RNA activated matrices enhance bone regeneration. *J. Control. Release* **218,** 22–28 (2015).

13. Balmayor, E. R. *et al.* Modified mRNA for BMP-2 in Combination with Biomaterials Serves as a Transcript-Activated Matrix for Effectively Inducing Osteogenic Pathways in Stem Cells. *Stem Cells Dev.* **26,** 25–34 (2016).

14. Khorsand, B. *et al.* A Comparative Study of the Bone Regenerative Effect of Chemically Modified RNA Encoding BMP-2 or BMP-9. *AAPS J.* **19,** 438–446 (2017).

15. Kong, H. J. *et al.* Non-viral gene delivery regulated by stiffness of cell adhesion substrates. *Nat. Mater.* **4,** 460–464 (2005).

16. Wang, Y. A., Yu, X., Silverman, P. M., Harris, R. L. & Edward, H. Nanoscale Cell Adhesion Ligand Presentation Regulates Non- Viral Gene Delivery and Expression Hyun. *Nano Lett.* **7,** 161–166 (2007).

17. Dhaliwal, A., Maldonado, M., Han, Z. & Segura, T. Differential uptake of DNA-poly(ethylenimine) polyplexes in cells cultured on collagen and fibronectin surfaces. *Acta Biomater.* **6,** 3436–3447 (2010).

18. Perlstein, I. *et al.* DNA delivery from an intravascular stent with a denatured collagen-polylactic-polyglycolic acid-controlled release coating: Mechanisms of enhanced transfection. *Gene Ther.* **10,** 1420–1428 (2003).

19. Zhang, H., Lee, M. Y., Hogg, M. G., Dordick, J. S. & Sharfstein, S. T. High-throughput transfection of interfering RNA into a 3D cell-culture chip. *Small* **8,** 2091–2098 (2012).

20. Zhang, H., Lee, M., Hogg, M. G., Dordick, J. S. & Sharfstein, S. T. Gene Delivery in Three-Dimensional Nanoparticles. *ACS Nano* **4,** 4733–4743 (2010).

21. Chu, C. & Kong, H. Interplay of cell adhesion matrix stiffness and cell type for non-viral gene delivery. *Acta Biomater.* **8,** 2612–2619 (2012).

22. Shepard, J. A., Huang, A., Shikanov, A. & Shea, L. D. Balancing cell migration with matrix degradation enhances gene delivery to cells cultured three-dimensionally within hydrogels. *Journal of Controlled Release* **146,** 128–135 (2010).

23. Dhaliwal, A., Oshita, V. & Segura, T. Transfection in the third dimension. *Integr Biol* **5,** 1206–1216 (2013).

24. Lei, P., Padmashali, R. M. & Andreadis, S. T. Cell-controlled and spatially arrayed gene delivery from fibrin hydrogels. *Biomaterials* **30,** 3790–3799 (2009).

25. Engler, A. J., Sen, S., Sweeney, H. L. & Discher, D. E. Matrix Elasticity Directs Stem Cell Lineage Specification. *Cell* **126,** 677–689 (2006).

26. Guilak, F., Cohen, D. & Estes, B. Control of stem cell fate by physical interactions with the extracellular matrix. *Cell Stem Cell* **5,** 17–26 (2009).

27. Chaudhuri, O. *et al.* Substrate stress relaxation regulates cell spreading. *Nat. Commun.* **6,** 6365 (2015).

28. Huebsch, N. *et al.* Harnessing traction-mediated manipulation of the cell/matrix interface to control stem-cell fate. *Nat. Mater.* **9,** 518–526 (2010).

29. Vining, K. H. & Mooney, D. J. Mechanical forces direct stem cell behaviour in development and regeneration. *Nat. Rev. Mol. Cell Biol.* **18,** 728–742 (2017).

30. Dy, P. *et al.* Sox9 Directs Hypertrophic Maturation and Blocks Osteoblast Differentiation of Growth Plate Chondrocytes. *Dev. Cell* **22,** 597–609 (2012).

31. Bi, W., Deng, J. M., Zhang, Z., Behringer, R. R. & Crombrugghe, B. De. Sox9 is required for cartilage formation. *Nat. Genet.* **22,** 85–89 (1999).

32. Warren, L. *et al.* Highly efficient reprogramming to pluripotency and directed differentiation of human cells with synthetic modified mRNA. *Cell Stem Cell* **7,**

618–630 (2010).

33. Branco da Cunha, C. *et al.* Influence of the stiffness of three-dimensional alginate/collagen-I interpenetrating networks on fibroblast biology. *Biomaterials* **35,** 8927–8936 (2014).

34. Nathaniel, P., Mow, V. C. & Foster, R. J. Composition and Dynamics of Articular Cartilage : Structure, Function, and Maintaining a Healthy State. *J. Ortophaedic Sport. Phys. Ther.* **28,** 203–215 (1998).

35. Hardin, J. A., Cobelli, N. & Santambrogio, L. Consequences of metabolic and oxidative modifications of cartilage tissue. *Nat. Rev. Rheumatol.* **11,** 521–529 (2015).

36. Chaudhuri, O. *et al.* Extracellular matrix stiffness and composition jointly regulate the induction of malignant phenotypes in mammary epithelium. *Nat. Mater.* **13,** 970–978 (2014).

37. Pfaffl, M. W. A new mathematical model for relative quantification in real-time RT-PCR. *Nucleic Acids Res.* **29,** 45e–45 (2001).

38. Schindelin, J. *et al.* Fiji: An open-source platform for biological-image analysis. *Nat. Methods* **9,** 676–682 (2012).

39. Chaudhuri, O. *et al.* Hydrogels with tunable stress relaxation regulate stem cell fate and activity. *Nat. Mater.* **15,** 326–334 (2015).

40. Rudnicki, M. S. *et al.* Nonlinear strain stiffening is not sufficient to explain how far cells can feel on fibrous protein gels. *Biophys. J.* **105,** 11–20 (2013).

41. Wang, H., Abhilash, A. S., Chen, C. S., Wells, R. G. & Shenoy, V. B. Long-range force transmission in fibrous matrices enabled by tension-driven alignment of fibers. *Biophys. J.* **107,** 2592–2603 (2015).

42. Ma, X. *et al.* Fibers in the extracellular matrix enable long-range stress transmission between cells. *Biophys. J.* **104,** 1410–1418 (2013).

43. Gojgini, S., Tokatlian, T. & Segura, T. Utilizing cell-matrix interactions to modulate gene transfer to stem cells inside hyaluronic acid hydrogels. *Mol. Pharm.* **8,** 1582–1591 (2011).

44. Buhrmann, C., Busch, F., Shayan, P. & Shakibaei, M. Sirtuin-1 (SIRT1) is required for promoting chondrogenic differentiation of mesenchymal stem cells. *J. Biol. Chem.* **289,** 22048–22062 (2014).

45. Balakrishnan, B. & Banerjee, R. Biopolymer-based hydrogels for cartilage tissue engineering. *Chem. Rev.* **111,** 4453–4474 (2011).

46. Hinderer, S., Layland, S. L. & Schenke-Layland, K. ECM and ECM-like materials - Biomaterials for applications in regenerative medicine and cancer therapy. *Adv. Drug Deliv. Rev.* **97,** 260–269 (2016).

47. Kasputis, T. & Pannier, A. K. The role of surface chemistry-induced cell characteristics on nonviral gene delivery to mouse fibroblasts. *J. Biol. Eng.* **6,** 1

(2012).

48. Suh, J., Wirtz, D. & Hanes, J. Efficient active transport of gene nanocarriers to the cell nucleus. *Proc. Natl. Acad. Sci.* **100,** 3878–3882 (2003).

49. Shiva, G., Talar, T. & Segura, T. Utilizing Cell-matrix Interactions to Modulate Gene Transfer to Stem Cells Inside Hyaluronic Acid Hydrogels. *Mol. Pharm.* **8,** 1582–1591 (2011).

50. Geiger, R. C., Taylor, W., Glucksberg, M. R. & Dean, D. A. Cyclic stretch-induced reorganization of the cytoskeleton and its role in enhanced gene transfer. *Gene Ther.* **13,** 725–731 (2006).

51. Grosse, S., Aron, Y., Thévenot, G., Monsigny, M. & Fajac, I. Cytoskeletal involvement in the cellular trafficking of plasmid/PEI derivative complexes. *J. Control. Release* **122,** 111–117 (2007).

52. Guo, M. *et al.* Probing the stochastic, motor-driven properties of the cytoplasm using force spectrum microscopy. *Cell* **158,** 822–832 (2014).

53. Ding, X. *et al.* High-throughput nuclear delivery and rapid expression of DNA via mechanical and electrical cell-membrane disruption. *Nat. Biomed. Eng.* **1,** 1–7 (2017).

54. Huey, D. J., Hu, J. C. & Athanasiou, K. A. Unlike bone, cartilage regeneration remains elusive. *Science (80-.).* **338,** 917–921 (2012).

55. Mandal, P. K. & Rossi, D. J. Reprogramming human fibroblasts to pluripotency using modified mRNA. *Nat. Protoc.* **8,** 568–582 (2013).

USC
UNIVERSIDADE
DE SANTIAGO
DE COMPOSTELA

SUPPORTING INFORMATION

Supplementary methods

2D Lipofectamine® 2000 transfection

For 2D transfections, cells were plated in 96 well plates approximately 12 h prior to transfection at a density of 90000 (U87MG) or 75000 (hMSCs) cells/cm^2. Four hours before transfection, media was changed to OptiMEM reduced serum medium (Gibco). For transfections performed in the presence of alginate and $CaCl_2$, both compounds were diluted in OptiMEM at the desired final concentrations and added to the cells immediately before transfection. Then, 50 µl of Lipofectamine complexes (Gibco), at 0.5:1 Lipofectamine:DNA/RNA ratios (µl:µg), were prepared in OptiMEM following manufacturer's instructions. Briefly, a solution containing 1 µg of mRNA/pDNA was added over a solution containing 0.5 µl of Lipofectamine®2000 reagent in a 1/1 v/v ratio, mixed by pipetting up-down and incubated for 20 min at room temperature. Complexes were added over the cells drop-by-drop and incubated for 6 hours. Subsequently, complexes were aspirated and cells were maintained in regular growing media until analysis. The transfection reaction was escalated for plates of higher surface areas.

Supporting figures

Table S1. List of Taqman assays employed for qRT-PCR experiments.

TaqMan assays (Applied Biosystems)	
SOX9 (human)	Hs00165814_m1
ACAN (human)	Hs 00153936_m1
COL2A1 (human)	Hs00264051_m1
COL10A1 (human)	Hs00166657_m1
ACT B (human)	Hs99999903_m1
GAPDH (human)	Hs99999905_m1

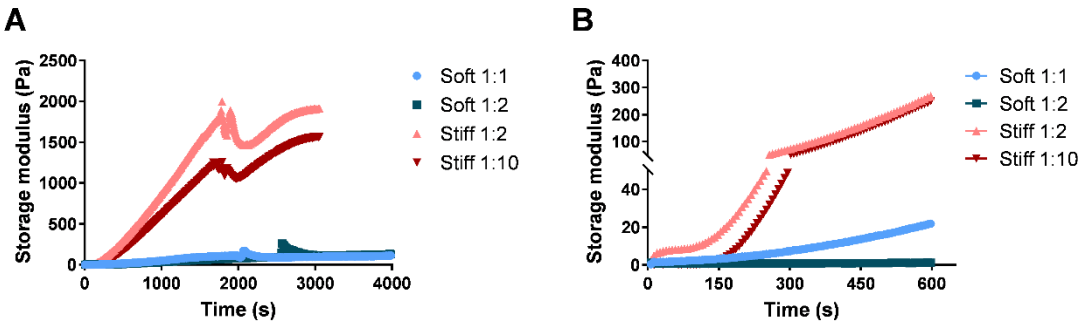

Figure S1. Evolution of the storage modulus with time. A) Storage modulus at 0.5% strain and 1 Hz was recorded periodically until it reached its equilibrium value. B) Inset of A) showing shorter gelation times. Data is representative of at least three measurements for each condition.

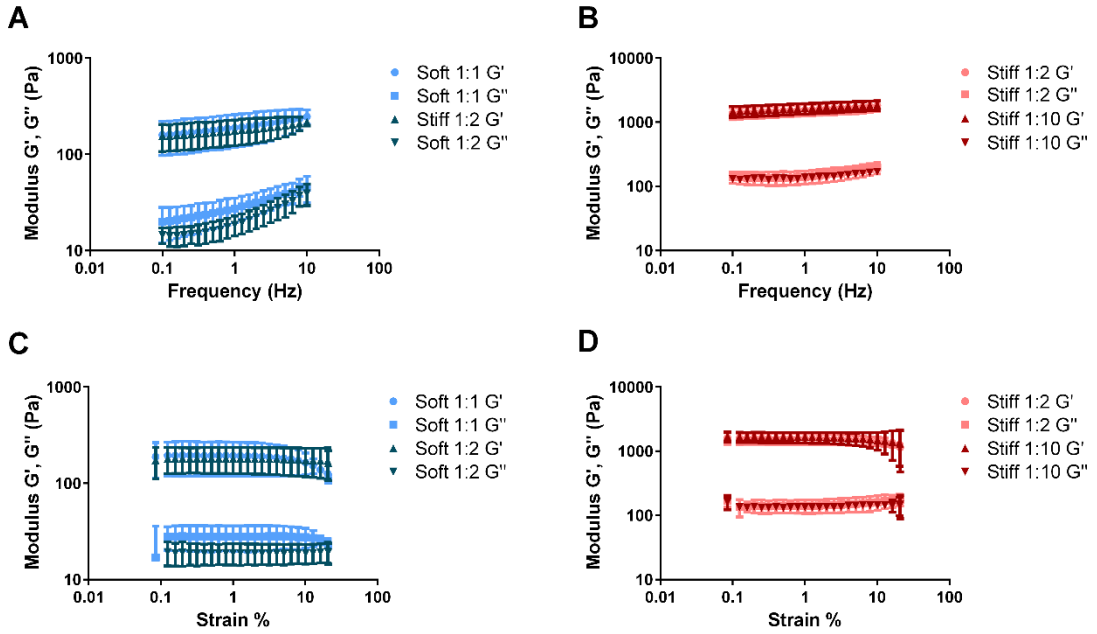

Figure S2. Strain and frequency sweeps of the IPN set. Frequency dependent rheology of soft (A) and stiff (B) IPNs performed at 1% strain after gelation was completed. Strain sweep (1 Hz) of soft (C) and stiff (D) IPNs. Data represent the mean ±SD.

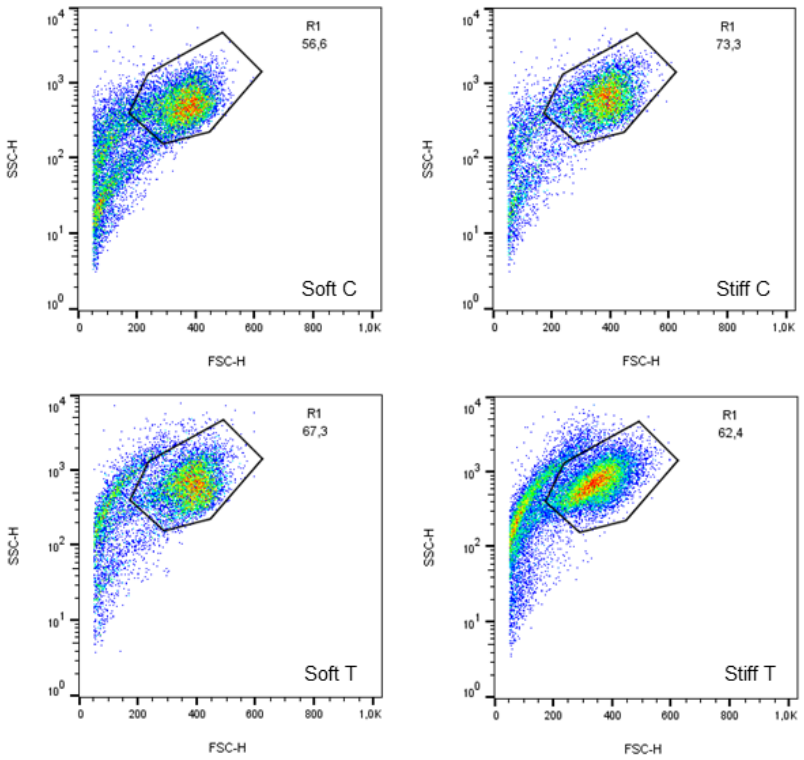

Figure S3. Gating scheme for the evaluation of Cy5-pDNA association to MSCs.

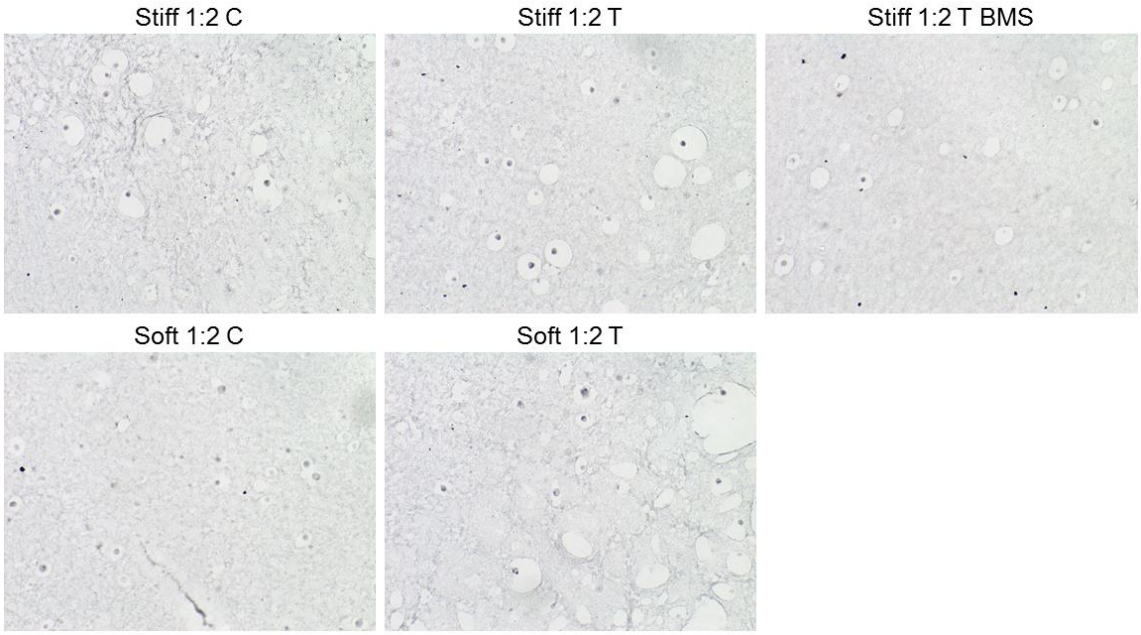

Figure S4. Negative controls in immunohistochemistry sections obtained by omitting the primary antibodies. C: control (non-transfected) cells; T: SOX9-transfected cells; T + BMS: SOX9-transfected cells in the presence of the NF-κβ inhibitor BMS-345541 (5 μM).

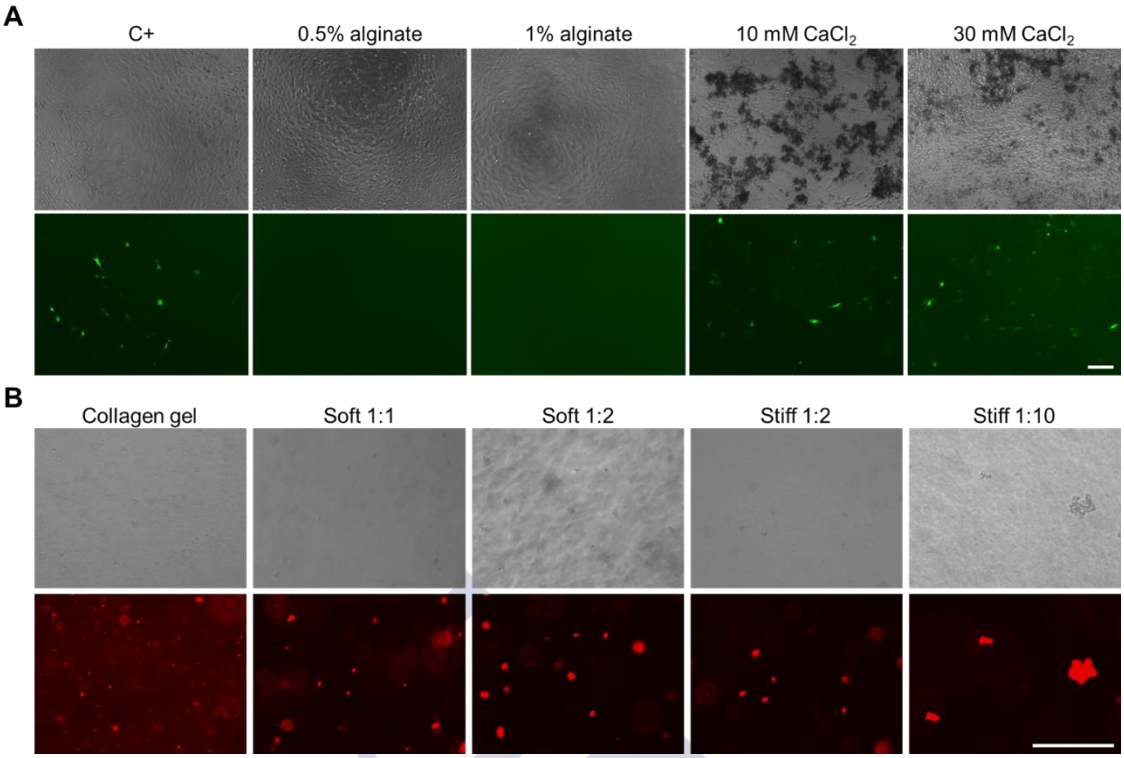

Figure S5. Alginate impairs 2D transfection and promotes the aggregation of the pDNA condensates within the IPNs. A) Effect of alginate and $CaCl_2$ on 2D transfection. Fluorescence micrographs of 3T3 fibroblasts 72 h after YFP DNA transfection with Lipofectamine 2000® reagent in the presence of increasing alginate and $CaCl_2$ concentrations. Scale bar = 100 µm for all the images. B) Distribution of labeled pDNA 3DFectIN® complexes within the IPNs and a control 0.5% w/v collagen gel. Optical (top) and fluorescence (bottom) micrographs. Scale bar = 200 µm for all the images.

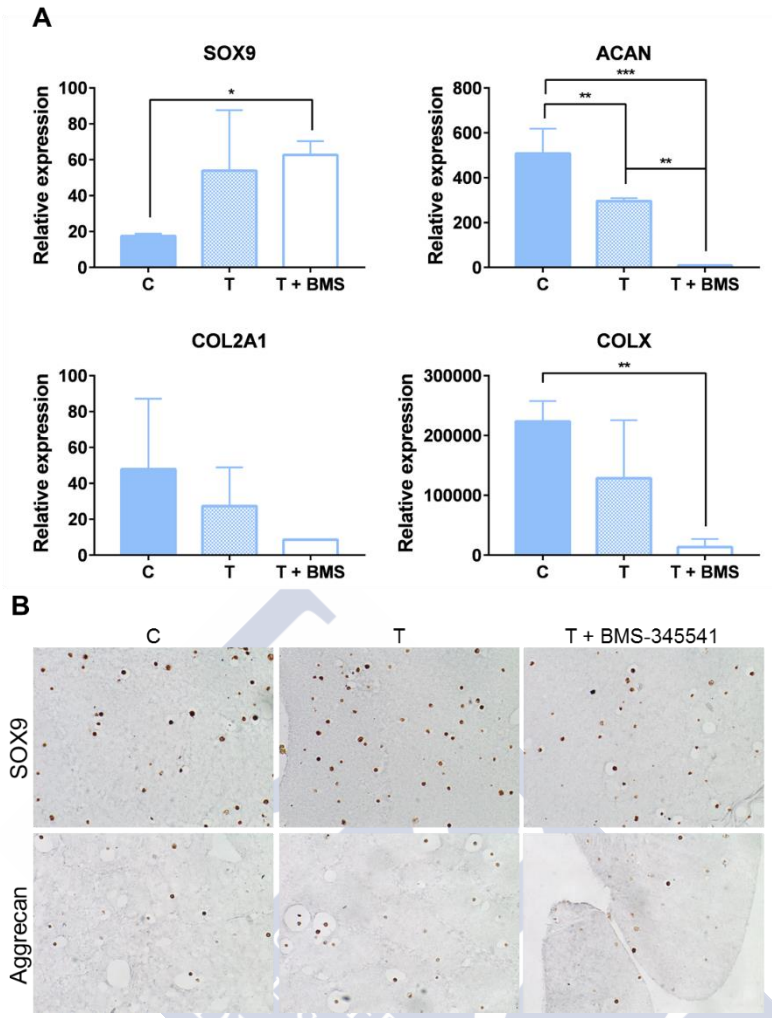

Figure S6. SOX9 3D transfection at low mRNA doses promotes a modest level of chondrogenic marker expression in MSCs. A) Gene expression of chondrogenic markers SOX9, aggrecan (ACAN), collagen type 2 (COL2A1) and collagen type 10 (COLX). B) Immunostaining of SOX9 and aggrecan in IPN sections. Data represent the mean ±SD. C: control (non-transfected) cells; T: SOX9-transfected cells; T + BMS: SOX9-transfected cells supplemented with the NF-κβ inhibitor BMS-345541 (5 µM).

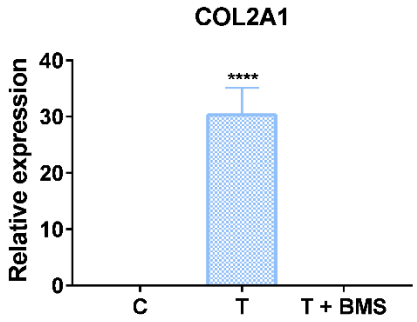

Figure S7. SOX9 3D transfection at high mRNA doses promotes a high overexpression of collagen type II mRNA. Gene expression of collagen type 2 (COL2A1). Data represent the mean ±SD. C: control (non-transfected) cells; T: SOX9-transfected cells; T + BMS: SOX9-transfected cells supplemented with the NF-κβ inhibitor BMS-345541 (5 µM).

USC
UNIVERSIDADE
DE SANTIAGO
DE COMPOSTELA

General discussion

USC
UNIVERSIDADE
DE SANTIAGO
DE COMPOSTELA

GENERAL DISCUSSION

RNA-based therapeutics can virtually target any gene or gene product responsible of a disease. Interference RNA (RNAi), such as small-interfering (siRNAs) and microRNAs (miRNAs), antisense oligonucleotides (ASOs), aptamers, synthetic mRNAs and CRISPR-Cas9 have the potential to be adapted to their target providing a global therapeutic strategy, leading to a new paradigm in medicine. Beyond this, RNA molecules have the ability to "pharmaco-evolve", being able to keep pace with cancer mutations or pandemic viral infections. Due to this high selectivity, over the past decade, RNA-based therapeutics have attracted a huge interest in research, resulting in a new range of therapeutic interventions that would never be possible with small-molecule inhibitors or antibodies.

However, for these therapies to reach their full potential, RNA should overcome the lipid bilayer of the cell membrane, a billion years barrier of evolutionary defenses that have kept RNAs outside of the cells. In the case of ASOs, of around 4-10 kDa, improved chemistries that increase their stability and hydrophobicity, have enabled them to reach specific diseased tissues resulting in a few clinical successes[1–4]. But chemical modifications are not enough for larger molecules such as miRNAs or mRNAs (≈14 and 600-10000 kDa, respectively), for which the "delivery problem" has led to the development of new drug delivery approaches able to direct the RNAs to the cytoplasm of the cells[5]. Although miRNAs could be conjugated to targeting molecules to improve their delivery, to date, the only feasible approach for mRNA systemic delivery consists of the use of nanotechnology. In addition, owing to the transient effect of RNA molecules, biomaterial-based technologies such as Gene Activated Matrices (GAMs) may be of interest for some applications by promoting a controlled release of the payload resulting in a sustained response (i. e. growth factor delivery)[6].

Within this frame, the work carried out in this PhD thesis has aimed to explore different alternatives of RNA delivery through different material systems of increasing complexity. Starting from the generation of a nanocarrier for the co-delivery of immunomodulatory RNAs and proteins, we moved to the investigation of a new concept of GAMs delivering mRNAs encoding pivotal transcription factors (TF) in musculoskeletal development. In line with the versatility of RNA-based therapies, the therapeutic scope of these systems has ranged from cancer immunotherapy to tissue engineering, but always with the common goal of using RNA delivery to achieve the therapeutic modulation of cell phenotypes. On the one hand, polyarginine nanocapsules were engineered to deliver RNAi polynucleotides targeting the C/EBPβ pathway, intended to re-educate the immunosuppressive population of MDSCs that promote tumor progression. On the other hand, mRNAs encoding the TFs SOX9 and MYOD were nanocomplexed and used to activate fibrin hydrogels to develop GAMs with the goal of directing stem cell specification towards cartilage and muscle, respectively. In a last step,

an improved generation of SOX9-GAMs based on collagen-I-alginate IPNs were fabricated to optimize GAM mechanical properties to enhance transfection and mimic the native cartilage tissue, further promoting cartilage repair.

Independently of the delivery system, the workflow followed for their development and in vitro testing was analogous. In a first step, the delivery platforms were characterized in terms of physicochemical, morphological and/or mechanical properties. A parallel step consisted on the optimization of their transfection efficiency in vitro, a process that was crucial for the improvement of the platforms and drove feedback changes in their design. Once their transfection efficiency was optimum, their ability for the modulation of the target cells was evaluated. As a last step, the co-delivery of complementary or synergistic drugs was also assessed.

1. RNA-delivery systems: development and optimization of their transfection properties

Despite of the different technological approaches for RNA-delivery explored in this PhD thesis, all of them had in common the use of nanotechnology to bring RNA molecules inside of the cytoplasm of the cells. As previously exposed, nanotechnology-based delivery systems have enabled the development of promising RNAs to clinical trials[7,8] and, to date, represent the only feasible strategy for the delivery of large RNA molecules such as mRNAs[9]. Several critical parameters need to be considered to optimize the complexation of RNA molecules in a particulate form. Whereas parameters such as particle size and polydispersity index, RNA stability and encapsulation efficiency have all been generally addressed, others such as RNA release at the target cells as well as endosomal escape still remain a major challenge[9]. In this work, we followed two main approaches to tackle these problems: 1) we developed polyarginine nanocapsules and loaded them with a chemoattractant protein (Chapter 1) and 2) we developed GAM-based cell gene therapies (Chapters 2 and 3).

Polyarginine presents a high biocompatibility compared to other synthetic polymers (e.g. PEI), and transcytotic ability for cell penetration and endosomal escape[10]. In addition, it has a high charge density, which enables a good interaction with RNA. Beyond this, previous research by our group has shown the potential of polyarginine for the development of multi-enveloped vaccines[11] and to facilitate intracellular drug delivery[12–14]. In agreement with our expectations, polyarginine nanocapsules allowed at least 2% w/w (RNA/NC) RNA loadings and promoted a high MDSC transfection efficiency, comparable to the reference commercial reagent (Chapter 1, pages 149-151). This high transfection efficiency suggests an adequate degree of endosomal escape, which is consistent with the buffering capacity of polyarginine already described in previous reports[10]. Polyarginine was also successfully used as a coating polymer to protect RNA from its degradation, following previously explored layer-by-layer approaches[15–17]. In addition, given the well-stablished interaction of hyaluronic acid with

CD44 receptors overexpressed in tumor cells [18], a double polymeric coating of polyarginine and hyaluronic acid was investigated for targeting purposes.

These nanocapsules were formulated by a novel self-emulsification method that avoids commonly used harsh procedures for Glycerol Monooleate (GMO) mesophase dispersion[19,20]. By employing this method, we were able to obtain monodisperse nanocapsules with inner aqueous domains of L2 inverse micellar phases suitable for protein encapsulation (Chapter 1, page 139). This is of particular relevance due to the increasing interest on GMO-based mesophases, specially L2 phases, for the encapsulation and slow release of various types of drugs[21–23]. These L2 phases were used to encapsulate the monocyte chemoattractant protein 1 (MCP-1), also known as CCL2. Previous work has explored the use of chemotactic signals to attract host immune cells to subcutaneously implanted drug delivery devices[24–26]. Building on this knowledge, and given the strong migration of monocytic- macrophagic MDSCs towards CCL2[27–30], the incorporation of this chemokine in our systems was intended to target the RNAi therapy to the most immunosuppressive MDSCs[31]. In agreement with previous research suggesting the role of polyarginine as a TLR4 agonist, in our work we found that blank polyarginine nanocapsules by themselves could induce a high macrophage chemoattraction, highlighting the potential of these vehicles for cancer immunotherapy and vaccination. Still, this migration was more pronounced for CCL2-loaded NCs as compared to blank NCs for the highest CCL2 concentration, suggesting their capacity to target monocytic-macrophagic MDSCs. When performing a Matrigel® invasion assay with a T cell line, strong differences appeared between blank and CCL2-loaded gels. Indeed, a much higher cell density was observed for CCL2-loaded gels, which promoted an increased T cell invasion compared to blank gels (Chapter 1, pages 147, 166). This is a particularly interesting result, considering that nitrated/nitrosilated CCL2 at the tumor site is unable to attract tumor-specific cytotoxic T cells (CTLs) but capable of recruiting immunosuppressive myeloid cells, further promoting the mechanism of tumor escape[32–34]. As a result, our NCs, with a natural tropism to the tumor[35], could be used as a means to restore native CCL2 levels within the tumor site and, hence, to favor CTL recruitment. Together with the tumor tropism, it was expected that the accumulation of the nanosystems in the spleen[36] of tumor-bearing mice, would help promoting a CCL2 release in the organs where MDSCs accumulate[37,38]. In addition, the Matrigel® system loaded with CCL2 could be used as the delivery system per se, loaded with tumor antigens for cancer vaccination schemes, or injected within the tumor to activate resident T cells. This strategy links this work to the GAM-based cell gene therapies also developed in the context of this PhD thesis.

GAM-based cell gene therapies were explored as another approach to target the RNA therapies to the desired cells. GAMs consist of polymer matrices loaded with DNA or RNA molecules and were initially developed to avoid the side effects of growth factor

protein delivery[39–41]. To get advantage of the 3D polymer matrix itself, a significant amount of the work related to GAMs was oriented to the application in tissue engineering, in particular to musculoskeletal regeneration. Here, we explored the use of mRNA encoding pivotal TFs SOX9[42,43] and MYOD[44] for cartilage and muscle specification and directed the therapy to MSCs, known for their plasticity to differentiate to multiple mesenchymal lineages[45,46]. MSCs were therefore loaded within the matrices, together with the nanocomplexed mRNA, in order to develop potential new cell gene therapies. 3D cell cultures represent more realistic models than 2D cell cultures and might help bridging the gap between in vitro and in vivo testing, eventually reducing in vivo experiments[47,48]. However, adding an extra dimension to the in vitro models usually implies a change in the protocols and parameters to consider. This is the case in transfection. Indeed, transfection in 3D environments is not only affected by the RNA nanocomplexes, but also by the matrix in which they are embedded and the interaction of this matrix and the cells to be transfected. Some works have explored the parameters affecting 3D transfection and highlighted its increased complexity compared to conventional 2D transfection experiments[49]. Trying to minimize this complexity, we selected fibrin gels as polymer matrices, as they had been used for reverse transfection and 3D transfection before[50–56]. Likewise, we employed the commercial transfection reagent 3DFectIN® (Oz Biosciences), optimized for 3D transfection[57], to complex the mRNA sequences. The use of such a system would allow us to develop our TF-mRNA GAMs and compare them with previously explored TF-pDNA GAMs while ensuring gel-gel inter-reproducibility.

To our knowledge, the first evidence related to the concept of mRNA GAMs dates from 2013, when Lui et al. used Matrigel® to deliver modified VEGF mRNA in vivo[58]. But it was only two years ago, when Elangovan et al. explicitly described the concept of mRNA GAM and showed their superior bone regeneration capacity compared to pDNA GAMs[59]. Subsequent work further showed the value of mRNA GAMs to deliver GFs, consolidating this approach over traditionally employed pDNA GAMs[60 61]. Compared to GFs, TFs have been shown to be more efficient in directing cell fate and reprogramming, and mRNA therapeutics has demonstrated to be a potent tool for TF delivery[62–69]. Building on this knowledge, we developed a new concept of mRNA GAMs encoding pivotal TFs in musculoskeletal development. In particular, we sought to explore whether mRNA GAMs induced a different kinetics of TF expression compared to pDNA GAMs, and if this potential situation could have an impact on tissue regeneration. Indeed, our results showed that, in the fibrin-based GAMs, SOX9 expression kinetics does not depend on the gel concentration but on the nature of the genetic material, either mRNA or pDNA. Consistent with previous studies performed in 2D, mRNA-GAMs showed a much higher transfection efficiency than pDNA GAMs, with about a 2-fold increase in relative gene expression values for non-modified mRNA sequences and a 1000-fold increase for RNase resistant sequences. In addition, SOX9 mRNA-GAMs induced a potent transgene

overexpression that peaked at short time points whereas pDNA-GAMs induced a SOX9 expression that increased over time[68,70]. Interestingly, RNase resistant MYOD-GAMs, exhibited a different expression kinetics compared with the previous GAMs. Whereas SOX9 expression in non-modified mRNA matrices decreased over time, MYOD expression was maintained for at least two days (Chapter 2, pages 185, 192). Taking into account the potential of mRNA, these results are of significant value as they bring insights on mRNA expression kinetics in 3D environments, and their importance in the processes of cell lineage priming. In addition, the different gene expression behavior found in our experiments highlights the nature of sequences (pDNA, mRNA, RNase-resistant mRNA) as an important parameter to consider in order to obtain the best gene expression profile depending on the desired application.

The observed potency of mRNA-GAMs, stimulated us to broaden the exploration of these systems. Apart from genetic or chemical control mechanisms of transcription, mounting evidence suggest that mechanical forces are equally important regulators of transcriptional control[71]. In fact, over the past few years, mechanostransduction has regained great attention as a means to regulate cell fate conversion[72–77]. In light of these observations, we decided to study the possibility to improve our mRNA-GAMs by further introducing mechanical cues to modulate cell fate. To this end, we chose to use collagen-I-alginate IPNs, developed at Prof. Mooney's Lab, and fabricated a set of IPNs with tunable stiffness and adhesion properties to maximize the chondrogenesis driven by SOX9 overexpression (Chapter 3, pages 221-222). IPNs enable gel stiffness to be tuned independently of gel architecture, polymer concentration or adhesion ligand density[78] and hence represent an ideal platform to study the effect of matrix mechanical properties on the 3D transfection and chondrogenesis of hMSCs. As commented before, some works have explored the differences between 2D and 3D transfection in terms of endocytic pathways and cytoskeletal dynamics[79]. Other authors have considered the impact of mechanical cues on 2D transfection efficiency of cells plated over substrates of different adhesion and stiffness[80–83]. However, up to date, the role of GAM mechanics on 3D gene transfer has not been well-established yet and more work is required to bring these promising systems further. Therefore, once the IPN set was characterized, we first used them to analyze the influence of stiffness and adhesion on 3D transfection efficiency. In contrast with the lack of differences on transfection efficiency found between the two fibrin gels previously assayed, we could observe different SOX9 overexpression values among the IPNs. Indeed, our results indicate that high collagen:alginate w:w ratios (high adhesion) and high stiffness exert a positive effect on gene transfer within the IPNs. Besides, our data suggest that this positive effect of stiffness is mediated by cell adhesion ligands, since the addition of ROCK inhibitor Y-27632 dramatically reduced transfection efficiency. This positive effect of stiffness and adhesion is consistent with a similar trend observed for transfections performed in 2D and has been related to an increased cell proliferation[80] and a more efficient vesicular

transport[79,84]. In agreement with these results, our experiments showed an increased cell proliferation in IPNs of high adhesion and stiffness. In addition, we observed that high stiffness exerted a positive effect on the internalization rate of the gene-condensates. Indeed, soft IPNs exhibited a higher number of Cy5-pDNA nanocomplexes attached to the cell membrane compared to stiff IPNs, where an increased number of complexes where found inside the cytoplasm of the cells. Although more experiments will be required to elucidate the underlying mechanism, we hypothesize that this increased uptake in stiff IPNs is related to a stronger actin cytoskeleton and microtubular network that facilitate the intracellular transport of the condensates. The fact that 2D transfected cells showed an increased transgene expression after their encapsulation within the IPNs, likely due to the transfection of remaining pDNA-complexes associated to the cells (Chapter 3, pages 224-226), further supports this hypothesis. Interestingly, our transfection results contradict a recent report for hyaluronic-acid (HA) based hydrogels, where softer gels achieved higher transgene expression levels compared to stiffer gels[85]. This discrepancy probably stems from how stiffness is tuned on both material systems. Stiffness in HA hydrogels was modulated by Michael-type crosslinking or the concentration of HA used. In particular, in the range of stiffness where we found the differences in transfection efficiency, their amount of HA ranged from 3 to 5%. This increase in HA concentration might change other parameters affecting 3D transfection, such as gel architecture or adhesion ligand density. Conversely, collagen-I-alginate IPNs enable gel stiffness to be tuned independently of these factors78, which allow us to get more independent conclusions about the effects of stiffness.

2. Cell phenotype priming

Once the three platforms were optimized, they were used to conduct in vitro differentiation studies to prove their functionality. In the case of polyarginine NCs, these experiments were intended to show the reversion of MDSCs immunosuppressive phenotype upon their transfection with RNAi-loaded NCs targeting the C/EBPβ pathway. C/EBPβ forms a feedback loop with miR-142-3p promoting myeloid cell differentiation towards immunosuppressive macrophages during tumor-induced myelopoiesis. In addition, it has been shown that miR-142-3p overexpression prevents the formation of the macrophagic fraction of MDSCs (CD11b+Gr-1low-neg), which is endowed with the strongest immunosuppressive activity[86]. Consequently, there is a need for delivery systems that enable these RNAi therapies for MDSC targeting to reach their full potential. Considering the good release and stability profiles of RNAi-loaded polyarginine NCs, and their high chemoattractant capacity, they appeared as ideal systems to re-educate MDSCs, controlling the immunosuppressive environment and reverting tumor-induced tolerance. Indeed, our data showed a potent downregulation of C/EBPβ by shC/EBPβ-loaded NCs and a dramatic reduction of the Gr-1 low negative after MDSCs transfection with miR 142-3p-loaded NCs (Chapter 1, pages 149-151). miR 142-3p and shC/EBPβ were previously reported to enhance the efficacy of adoptive cells

transfer and antitumoral DNA vaccination in vivo, respectively, when administered loaded in 4PD dendrimers[87]. Although our observations are mostly based on in vitro data, they suggest that the combination of both the RNAi and chemokine therapies could be a promising approach to boost adoptive cell transfer efficacy in cancer immunotherapy. In vivo data showing the downregulation of splenic and tumor C/EBPβ mRNA levels after administration of shC/EBPβ-loaded nanocapsules, and the subsequent prevention of monocyte differentiation into tumor-associated macrophages, further highlight the potential of these nanocarriers. In addition, the Matrigel® system, loaded with CCL2, could be an interesting strategy to deliver tumor antigens and activate T cells in situ.

In the case of the GAMs, studies were performed to assess their potential to direct MSC fate. Fibrin-based GAMs were activated with SOX9 and MYOD mRNA to promote chondrogenic and myogenic differentiation, respectively. Compared to previously explored SOX9 pDNA-GAMs, our mRNA-GAMs induced a more potent and faster gene upregulation of the condrogenic markers SOX9, aggrecan and collagen type II, suggesting a faster onset of the chondrogenic response. More importantly, this upregulation was translated in a higher matrix secretion as demonstrated by alcian blue staining and collagen type II immunohistochemistry. Accordingly, MYOD-GAMs also demonstrated a potent induction of the myogenic markers MYOD, myogenin and myosin heavy chains 2 and 3 that promoted myosin protein expression, further supporting the value of our mRNA-platforms (Chapter 2, pages 190-192, 209-210). Although mRNAs encoding TFs have been previously used for cell reprogramming showing very high efficiencies and potent responses[68,88], to our knowledge, this is the first evidence of TF-mRNA reprogramming induced in a GAM. As previously highlighted, GAM mechanical properties have an inherent effect of cell phenotype [75–77] that we sought to explore. In this regard, our observations also bring insights about the interplay between the matrix mechanical signals and mRNA-induced molecular cascades. Indeed, our results showed a better chondrogenic response in the less concentrated fibrin gels whereas the opposite was observed for myogenic differentiation. Given that matrix remodeling is faster in less concentrated gels, and that matrix degradation leads to cell condensation, our results are in agreement with previous literature describing mesenchymal condensation as a critical event to drive the onset of the chondrogenic program[89–92]. In the case of MYOD-GAMs, our results are also consistent with previous literature, since the higher myogenic response observed for the more concentrated matrices is likely related to a better cell alignment induced by the slowler degradation of this kind of matrices[93–95].

Trying to improve the synergy between matrix mechanics and mRNA-reprogramming, we next explored the use of collagen-I-alginate IPNs for chondrogenic differentiation. The tunable properties of these IPNs have been previously shown to influence fibroblast biology[78], so it was reasonable to hypothesize that they could help modulating the GAM-

mediated chondrogenic response. Besides, their composition resembles that of the ECM and their stiffness can be adjusted to reach values similar to the native cartilaginous tissue[96,97], further supporting our selection of these systems. Several works have studied the influence of matrix mechanics on the chondrogenesis of MSCs plated on 2D substrates[98,99]. However, conclusions obtained from 2D cultures do not always translate into the behavior of 3D systems due to their increased complexity[100], highlighting the need for more systematic 3D studies. Given that GAM mechanical properties have been previously shown to affect 3D gene transfer, in our first chondrogenesis experiments we transfected MSCs with mRNA in 2D prior to their encapsulation within the IPNs. We found that, compared to cells encapsulated within the Soft 1:2 IPNs (low stiffness, high adhesion), cells within the Stiff 1:2 IPNs (high stiffness, high adhesion) promoted a higher expression of chondrogenic markers. Stiff 1:2 IPNs (high stiffness, high adhesion) have previously shown the higher 3D transfection efficiency and therefore were selected for the next chondrogenesis experiments involving 3D transfection. As in the case of 2D SOX9 transfection, IPN-mediated SOX9 transfection induced a high expression of chondrogenic markers at both the mRNA and protein levels. However, for 3D transfection, the expression of chondrogenic markers was higher, especially in the case of collagen type-II mRNA expression, which was not upregulated in control IPNs. In agreement with previous literature[42], the levels of the hypertrophic marker collagen type-X were downregulated upon SOX9 transfection, both at the mRNA and protein level. This is especially noteworthy since tissue-engineered cartilage usually has an unfavorable balance between collagen type-II and collagen type-X expression, resulting in a cartilage-like tissue of poor mechanical properties[101]. Interestingly, the addition of the NF-kβ inhibitor BMS-345541 further reduced the expression of this hypertrophic marker, suggesting the potential of this inhibitor for use in regenerative medicine (Chapter 3, pages 230, 243).

Together with the impact of GAM mechanics on the differentiation output, our observations also bring insights on the significance of mRNA dose to induce TF-mediated MSC specification. In SOX9- and MYOD-fibrin GAMs, reducing the mRNA dose four and two times, respectively, did not alter significantly the mRNA expression of relevant tissue-specific markers, suggesting there is a plateau in TF-induced marker expression (Chapter 2, pages 188-192, 209-210). Given that high levels of master regulators have been shown to exert a negative feedback on target gene expression[102–104], these results highlight the importance of a careful optimization of TF mRNA dose in GAM development. The fact that one can tune both, GAM mechanics and mRNA dose, to induce a potent enforced TF expression, allows for in situ cell reprogramming strategies that simplify their application in the clinical setting since they circumvent tedious in vitro cell culture and modification procedures.[68,88]

References

1. Liang, X. H. *et al.* Hsp90 protein interacts with phosphorothioate oligonucleotides containing hydrophobic 2'-modifications and enhances antisense activity. *Nucleic Acids Res.* **44,** 3892–3907 (2016).

2. Eckstein, F. Phosphorothioates, Essential Components of Therapeutic Oligonucleotides. *Nucleic Acid Ther.* **24,** 374–387 (2014).

3. Beaudet, A. L. & Meng, L. Gene-targeting pharmaceuticals for single-gene disorders. *Hum. Mol. Genet.* **25,** R18–R26 (2016).

4. Crooke, S. T., Wang, S., Vickers, T. A., Shen, W. & Liang, X. H. Cellular uptake and trafficking of antisense oligonucleotides. *Nat. Biotechnol.* **35,** 230–237 (2017).

5. Dowdy, S. F. Overcoming cellular barriers for RNA therapeutics. *Nat. Biotechnol.* **35,** 222–229 (2017).

6. Raisin, S., Belamie, E. & Morille, M. Non-viral gene activated matrices for mesenchymal stem cells based tissue engineering of bone and cartilage. *Biomaterials* **104,** 223–237 (2016).

7. Rupaimoole, R. & Slack, F. J. MicroRNA therapeutics: Towards a new era for the management of cancer and other diseases. *Nat. Rev. Drug Discov.* **16,** 203–221 (2017).

8. Guan, S. & Rosenecker, J. Nanotechnologies in delivery of mRNA therapeutics using nonviral vector-based delivery systems. *Gene Ther.* 1–25 (2017).

9. Sahin, U., Karikó, K. & Türeci, Ö. mRNA-based therapeutics — developing a new class of drugs. *Nat. Rev. Drug Discov.* **13,** 759–780 (2014).

10. Szabo, F. K. & Hoffman, G. E. Cell transcytosing poly-arginine coated magnetic nanovector for safe and effective siRNA delivery. *Biomaterials* **32,** 5717–5725 (2011).

11. Correia-Pinto, J. F., Peleteiro, M., Csaba, N., González-Fernández, Á. & Alonso, M. J. Multi-enveloping of particulated antigens with biopolymers and immunostimulant polynucleotides. *J. Drug Deliv. Sci. Technol.* **30,** 424–434 (2015).

12. Lozano, M. V. *et al.* Polyarginine nanocapsules: A new platform for intracellular drug delivery. *J. Nanoparticle Res.* **15,** (2013).

13. Lollo, G. *et al.* Polyarginine Nanocapsules as a Potential Oral Peptide Delivery Carrier. *J. Pharm. Sci.* **106,** 611–618 (2017).

14. Niu, Z. *et al.* Rational design of polyarginine nanocapsules intended to help peptides overcoming intestinal barriers. *J. Control. Release* (2017).

15. Tan, Y. F. *et al.* Layer-by-layer nanoparticles as an efficient siRNA delivery vehicle for SPARC silencing. *Small* **10,** 1790–1798 (2014).

16. Elbakry, A. *et al.* Layer-by-layer coated gold nanoparticles: Size-dependent delivery of DNA into cells. *Small* **8,** 3847–3856 (2012).

17. Chen, Z., Zhang, L., He, Y., Shen, Y. & Li, Y. Enhanced shRNA delivery and ABCG2 silencing by charge-reversible layered nanocarriers. *Small* **11,** 952–962 (2015).

18. Virginia M, P. & Szoka Jr, F. C. Anticancer Therapeutics: Targeting Macromolecules and Nanocarriers to Hyaluronan or CD44, a Hyaluronan Receptor. *Mol. Pharm.* **5,** 474–486 (2008).

19. Chang, D. P., Jankunec, M., Barauskas, J., Tiberg, F. & Nylander, T. Adsorption of Lipid Liquid Crystalline Nanoparticles: Effects of Particle Composition, Internal Structure, and Phase Behavior. *Langmuir* **28,** 10688–10696 (2012).

20. Barauskas, J., Johnsson, M., Joabsson, F. & Tiberg, F. Cubic Phase Nanoparticles (Cubosome): Principles for Controlling Size, Structure, and Stability. *Langmuir* **21,** 2569–2577 (2005).

21. Drummond, C. J. & Fong, C. Surfactant self-assembly objects as novel drug delivery vehicles. *Curr. Opin. Colloid Interface Sci.* **4,** 449–456 (1999).

22. Clogston, J. & Caffrey, M. Controlling release from the lipidic cubic phase. Amino acids, peptides, proteins and nucleic acids. *J. Control. Release* **107,** 97–111 (2005).

23. Phan, S., Fong, W. K., Kirby, N., Hanley, T. & Boyd, B. J. Evaluating the link between self-assembled mesophase structure and drug release. *Int. J. Pharm.* **421,** 176–182 (2011).

24. Bencherif, S. A. *et al.* Injectable Cryogel-based Whole Cell Cancer Vaccines. *Nat. Commun.* **6,** 7556–7587 (2016).

25. Kim, J. *et al.* Injectable, spontaneously assembling, inorganic scaffolds modulate immune cells in vivo and increase vaccine efficacy. *Nat. Biotechnol.* **33,** 64–72 (2014).

26. Ali, O. A., Tayalia, P., Shvartsman, D., Lewin, S. & Mooney, D. J. Inflammatory cytokines presented from polymer matrices differentially generate and activate DCs in situ. *Adv. Funct. Mater.* **23,** 4621–4628 (2013).

27. Huang, B. *et al.* CCL2/CCR2 pathway mediates recruitment of myeloid suppressor cells to cancers. *Cancer Lett.* **252,** 86–92 (2007).

28. Qian, B.-Z. *et al.* CCL2 recruits inflammatory monocytes to facilitate breast-tumour metastasis. *Nature* **475,** 222–225 (2011).

29. Fang, W. Bin *et al.* Targeted gene silencing of CCL2 inhibits triple negative breast cancer progression by blocking cancer stem cell renewal and M2 macrophage recruitment. *Oncotarget* **7,** 49349–49367 (2014).

30. Sawanobori, Y. & Ueha, S. Chemokine-mediated rapid turnover of myeloid-derived suppressor cells in tumor-bearing mice. *Blood* **111,** 5457–5466 (2008).

31. Dolcetti, L. *et al.* Hierarchy of immunosuppressive strength among myeloid-derived suppressor cell subsets is determined by GM-CSF. *Eur. J. Immunol.* **40,** 22–35 (2010).

32. Molon, B. *et al.* Chemokine nitration prevents intratumoral infiltration of antigen-specific T cells. *J. Exp. Med.* **208,** 1949–1962 (2011).

33. Lesokhin, A. M. *et al.* Monocytic CCR2 + myeloid-derived suppressor cells promote immune escape by limiting activated CD8 T-cell infiltration into the tumor microenvironment. *Cancer Res.* **72,** 876–886 (2012).

34. Molon, B., Viola, A. & Bronte, V. Smoothing T cell roads to the tumor: Chemokine post-translational regulation. *Oncoimmunology* **1,** 390–392 (2012).

35. Nakamura, Y., Mochida, A., Choyke, P. L. & Kobayashi, H. Nanodrug Delivery: Is the Enhanced Permeability and Retention Effect Sufficient for Curing Cancer? *Bioconjug. Chem.* **27,** 2225–2238 (2016).

36. Kai, M. P. *et al.* Tumor Presence Induces Global Immune Changes and Enhances Nanoparticle Clearance. *ACS Nano* **10,** 861–870 (2016).

37. Gabrilovich, D. I., Ostrand-Rosenberg, S. & Bronte, V. Coordinated regulation of myeloid cells by tumours. *Nat. Rev. Immunol.* **12,** 253–268 (2012).

38. Bronte, V. & Pittet, M. J. The spleen in local and systemic regulation of immunity. *Immunity* **39,** 806–818 (2013).

39. Kang, D. G., Hsu, W. K. & Lehman, R. A. Complications Associated With Bone Morphogenetic Protein in the Lumbar Spine. *Orthopedics* **40,** e229–e237 (2017).

40. Epstein, N. Complications due to the use of BMP/INFUSE in spine surgery: The evidence continues to mount. *Surg. Neurol. Int.* **4,** 343 (2013).

41. DeVine, J., Dettori, J., France, J., Brodt, E. & McGuire, R. The use of rhBMP in spine surgery: is there a cancer risk? *Evid. Based. Spine. Care. J.* **3,** 35–41 (2012).

42. Dy, P. *et al.* Sox9 Directs Hypertrophic Maturation and Blocks Osteoblast Differentiation of Growth Plate Chondrocytes. *Dev. Cell* **22,** 597–609 (2012).

43. Bi, W., Deng, J. M., Zhang, Z., Behringer, R. R. & Crombrugghe, B. De. Sox9 is required for cartilage formation. *Nat. Genet.* **22,** 85–89 (1999).

44. Davis, R. L., Weintraub, H. & Lassar, A. B. Expression of a single transfected cDNA converts fibroblasts to myoblasts. *Cell* **51,** 987–1000 (1987).

45. Pittenger, M. F. Multilineage Potential of Adult Human Mesenchymal Stem Cells. *Science* **284,** 143–147 (1999).

46. Caplan, A. I. Adult mesenchymal stem cells for tissue engineering versus regenerative medicine. *J. Cell. Physiol.* **213,** 341–347 (2007).

47. Roth, A. & Singer, T. The application of 3D cell models to support drug safety

assessment: Opportunities & challenges. *Adv. Drug Deliv. Rev.* **69–70,** 179–189 (2014).

48. Thoma, C. R., Zimmermann, M., Agarkova, I., Kelm, J. M. & Krek, W. 3D cell culture systems modeling tumor growth determinants in cancer target discovery. *Adv. Drug Deliv. Rev.* **69–70,** 29–41 (2014).

49. Zhang, H., Lee, M. Y., Hogg, M. G., Dordick, J. S. & Sharfstein, S. T. High-throughput transfection of interfering RNA into a 3D cell-culture chip. *Small* **8,** 2091–2098 (2012).

50. Spotnitz, W. D. Fibrin sealant: Past, present, and future: A brief review. *World Journal of Surgery* **34,** 632–634 (2010).

51. Spotnitz, W. D. & Burks, S. Hemostats, sealants, and adhesives III: A new update as well as cost and regulatory considerations for components of the surgical toolbox. *Transfusion* **52,** 2243–2255 (2012).

52. Spotnitz, W. D. & Burks, S. State-of-the-art review: Hemostats, sealants, and adhesives II: Update as well as how and when to use the components of the surgical toolbox. *Clin. Appl. Thromb. Hemost.* **16,** 497–514 (2010).

53. Yanke, A. B. & Chubinskaya, S. The state of cartilage regeneration: current and future technologies. *Curr. Rev. Musculoskelet. Med.* **8,** 1–8 (2015).

54. Raut, S. D., Lei, P., Padmashali, R. M. & Andreadis, S. T. Fibrin-mediated lentivirus gene transfer: Implications for lentivirus microarrays. *J. Control. Release* **144,** 213–220 (2010).

55. Padmashali, R. M. & Andreadis, S. T. Engineering fibrinogen-binding VSV-G envelope for spatially- and cell-controlled lentivirus delivery through fibrin hydrogels. *Biomaterials* **32,** 3330–3339 (2011).

56. Lei, P., Padmashali, R. M. & Andreadis, S. T. Cell-controlled and spatially arrayed gene delivery from fibrin hydrogels. *Biomaterials* **30,** 3790–3799 (2009).

57. Sapet, C. *et al.* 3D-fection: cell transfection within 3D scaffolds and hydrogels. *Ther. Deliv.* **4,** 673–85 (2013).

58. Lui, K. O. *et al.* Driving vascular endothelial cell fate of human multipotent Isl1 + heart progenitors with VEGF modified mRNA. *Cell Res.* **23,** 1172–1186 (2013).

59. Elangovan, S. *et al.* Chemically modified RNA activated matrices enhance bone regeneration. *J. Control. Release* **218,** 22–28 (2015).

60. Balmayor, E. R. *et al.* Modified mRNA for BMP-2 in Combination with Biomaterials Serves as a Transcript-Activated Matrix for Effectively Inducing Osteogenic Pathways in Stem Cells. *Stem Cells Dev.* **26,** 25–34 (2016).

61. Khorsand, B. *et al.* A Comparative Study of the Bone Regenerative Effect of Chemically Modified RNA Encoding BMP-2 or BMP-9. *AAPS J.* **19,** 438–446 (2017).

62. Graf, T. Historical origins of transdifferentiation and reprogramming. *Cell Stem Cell* **9,** 504–516 (2011).

63. Rackham, O. J. L. *et al.* A predictive computational framework for direct reprogramming between human cell types. *Nat. Genet.* **48,** 331–335 (2016).

64. Merrell, A. J. & Stanger, B. Z. Adult cell plasticity in vivo: de-differentiation and transdifferentiation are back in style. *Nat. Rev. Mol. Cell Biol.* **17,** 413–425 (2016).

65. Takahashi, K. & Yamanaka, S. A decade of transcription factor-mediated reprogramming to pluripotency. *Nat. Rev. Mol. Cell Biol.* **17,** 183–193 (2016).

66. Makiko Iwafuchi-Doi and Kenneth S. Zaret. Pioneer transcription factors in cell reprogramming. *Genes Dev.* **28,** 2679–2692 (2014).

67. Buganim, Y., Faddah, D. A. & Jaenisch, R. Mechanisms and models of somatic cell reprogramming. *Nat. Rev. Genet.* **14,** 427–439 (2013).

68. Warren, L. *et al.* Highly efficient reprogramming to pluripotency and directed differentiation of human cells with synthetic modified mRNA. *Cell Stem Cell* **7,** 618–630 (2010).

69. Almalki, S. G. & Agrawal, D. K. Key transcription factors in the differentiation of mesenchymal stem cells. *Differentiation* **92,** 41–51 (2016).

70. Andries, O. *et al.* Comparison of the gene transfer efficiency of mRNA/GL67 and pDNA/GL67 complexes in respiratory cells. *Mol. Pharm.* **9,** 2136–2145 (2012).

71. Janmey, P. A. *et al.* From tissue mechanics to transcription factors. *Differenciation* **86,** 112–120 (2013).

72. Engler, A. J., Sen, S., Sweeney, H. L. & Discher, D. E. Matrix Elasticity Directs Stem Cell Lineage Specification. *Cell* **126,** 677–689 (2006).

73. Clause, K. C. . L. L. J. . T. K. Directed stem cell differentiation: the role of physical forces. **17,** 48–54 (2012).

74. Guilak, F., Cohen, D. & Estes, B. Control of stem cell fate by physical interactions with the extracellular matrix. *Cell Stem Cell* **5,** 17–26 (2009).

75. Huebsch, N. *et al.* Harnessing traction-mediated manipulation of the cell/matrix interface to control stem-cell fate. *Nat. Mater.* **9,** 518–526 (2010).

76. Chaudhuri, O. *et al.* Hydrogels with tunable stress relaxation regulate stem cell fate and activity. *Nat. Mater.* **15,** 326–334 (2015).

77. Mao, A. S., Shin, J. W. & Mooney, D. J. Effects of substrate stiffness and cell-cell contact on mesenchymal stem cell differentiation. *Biomaterials* **98,** 184–191 (2016).

78. Branco da Cunha, C. *et al.* Influence of the stiffness of three-dimensional alginate/collagen-I interpenetrating networks on fibroblast biology. *Biomaterials*

35, 8927–8936 (2014).

79. Dhaliwal, A., Oshita, V. & Segura, T. Transfection in the third dimension. *Integr Biol* **5,** 1206–1216 (2013).

80. Kong, H. J. *et al.* Non-viral gene delivery regulated by stiffness of cell adhesion substrates. *Nat. Mater.* **4,** 460–464 (2005).

81. Wang, Y. A., Yu, X., Silverman, P. M., Harris, R. L. & Edward, H. Nanoscale Cell Adhesion Ligand Presentation Regulates Non- Viral Gene Delivery and Expression Hyun. *Nano Lett.* **7,** 161–166 (2007).

82. Chu, C. & Kong, H. Interplay of cell adhesion matrix stiffness and cell type for non-viral gene delivery. *Acta Biomater.* **8,** 2612–2619 (2012).

83. Kasputis, T. & Pannier, A. K. The role of surface chemistry-induced cell characteristics on nonviral gene delivery to mouse fibroblasts. *J. Biol. Eng.* **6,** 1 (2012).

84. Suh, J., Wirtz, D. & Hanes, J. Efficient active transport of gene nanocarriers to the cell nucleus. *Proc. Natl. Acad. Sci.* **100,** 3878–3882 (2003).

85. Shiva, G., Talar, T. & Segura, T. Utilizing Cell-matrix Interactions to Modulate Gene Transfer to Stem Cells Inside Hyaluronic Acid Hydrogels. *Mol. Pharm.* **8,** 1582–1591 (2011).

86. Sonda, N. *et al.* miR-142-3p Prevents Macrophage Differentiation during Cancer-Induced Myelopoiesis. *Immunity* **38,** 1236–1249 (2013).

87. Zilio, S. *et al.* 4PD Functionalized Dendrimers: A Flexible Tool for In Vivo Gene Silencing of Tumor-Educated Myeloid Cells. *J. Immunol.* **198,** 4166–4177 (2017).

88. Mandal, P. K. & Rossi, D. J. Reprogramming human fibroblasts to pluripotency using modified mRNA. *Nat. Protoc.* **8,** 568–582 (2013).

89. Almalki, S. G. & Agrawal, D. K. Effects of matrix metalloproteinases on the fate of mesenchymal stem cells. *Stem Cell Res. Ther.* 1–12 (2016).

90. Ahmann, K. A. *et al.* Fibrin Degradation Enhances Vascular Smooth Muscle Cell Proliferation and Matrix Deposition in Fibrin-Based Tissue Constructs Fabricated In Vitro. *Tissue Eng. Part A* **16,** (2010).

91. Page-McCaw, A., Ewald, A. J. & Werb, Z. Matrix metalloproteinases and the regulation of tissue remodelling. *Nat Rev Mol Cell Biol.* **8,** 221–233 (2007).

92. Oh, J. *et al.* Mutations in two matrix metalloproteinase genes , MMP-2 and MT1-MMP , are synthetic lethal in mice. *Oncogene* **23,** 5041–5048 (2004).

93. Page, R. L. *et al.* Restoration of Skeletal Muscle Defects with Adult Human Cells Delivered on Fibrin Microthreads. *Tissue Eng. Part A* **17,** 2629–2640 (2011).

94. Heher, P. *et al.* A novel bioreactor for the generation of highly aligned 3D skeletal

muscle-like constructs through orientation of fibrin via application of static strain. *Acta Biomater.* **24,** 251–265 (2015).

95. Chen, S., Nakamoto, T., Kawazoe, N. & Chen, G. Engineering multi-layered skeletal muscle tissue by using 3D microgrooved collagen scaffolds. *Biomaterials* **73,** 23–31 (2015).

96. Nathaniel, P., Mow, V. C. & Foster, R. J. Composition and Dynamics of Articular Cartilage : Structure, Function, and Maintaining a Healthy State. *J. Ortophaedic Sport. Phys. Ther.* **28,** 203–215 (1998).

97. Hardin, J. A., Cobelli, N. & Santambrogio, L. Consequences of metabolic and oxidative modifications of cartilage tissue. *Nat. Rev. Rheumatol.* **11,** 521–529 (2015).

98. Goldshmid, R. *et al.* Steric Interference of Adhesion Supports In-Vitro Chondrogenesis of Mesenchymal Stem Cells on Hydrogels for Cartilage Repair. *Sci. Rep.* **5,** 1–13 (2015).

99. Park, J. S. *et al.* The Effect of Matrix Stiffness on the Differentiation of Mesenchymal Stem Cells in Response to TGF-β. *Biomaterials* **32,** 3921–3930 (2012).

100. Vega, L., Kwon, M., Soulas, E. M., Caliari, S. R. & Burdick, J. A. Dimensionality and spreading influence MSC YAP / TAZ signaling in hydrogel environments. *Biomaterials* **103,** 314–323 (2016).

101. Huey, D. J., Hu, J. C. & Athanasiou, K. A. Unlike bone, cartilage regeneration remains elusive. *Science (80-.).* **338,** 917–921 (2012).

102. Kypriotou, M. *et al.* SOX9 Exerts a Bifunctional Effect on Type II Collagen Gene (COL2A1) Expression in Chondrocytes Depending on the Differentiation State. *DNA Cell Biol.* **22,** 119–129 (2003).

103. Harada, A. *et al.* Spatial re-organization of myogenic regulatory sequences temporally controls gene expression. *Nucleic Acids Res.* **43,** 2008–2021 (2015).

104. Cho, H. C., Mallappa, C., Hernández-Hernández, J. M., Rivera-Pérez, J. A. & Imbalzano, A. N. Contrasting roles for MyoD in organizing structures during embryonic skeletal muscle development. *Dev. Dyn.* **244,** 43–55 (2015).

USC
UNIVERSIDADE
DE SANTIAGO
DE COMPOSTELA

Conclusions

USC
UNIVERSIDADE
DE SANTIAGO
DE COMPOSTELA

CONCLUSIONS

CHAPTER 1: Co-delivery of RNAi and Chemokine from Polyarginine Nanocapsules enables the modulation of Myeloid Derived Suppressor Cells

C1. Glycerol Monooleate-based nanoemulsions (GMO NEs) can be prepared by a mild self-emulsifying method that yields L2 inverse micellar phases suitable for CCL2 chemokine encapsulation. These oily cores can be surrounded by a polyarginine polymer shell yielding nanocapsules that can efficiently load various RNAi sequences by electrostatic interactions. Subsequent polyarginine and hyaluronic acid polymer layers can be assembled onto the RNA molecules creating "sandwich-like" structures that protect RNAi sequences from degradation.

C2. CCL2 and RNA-loaded NCs maintain their colloidal stability in biorelevant media. RNA-loaded NCs prevent the release of the cargo for at least 12 h and are able to protect the RNA molecules from plasma RNases.

C3. Both RNAi-loaded NCs induce a high transfection of Myeloid Derived Suppressor Cells (MDSCs). This transfection promotes the differentiation of MDSCs towards non-immunosuppressive phenotypes. CCL2-loaded NCs exert a potent chemoattraction on RAW264.7 macrophage cells, suggesting that CCL2 loading can be a good strategy to target the RNAi therapy to the most immunosuppressive monocytic-macrophagic MDSC subset.

CHAPTER 2: mRNA-Activated Matrices Encoding Transcription Factors as Primers of Cell Differentiation in Tissue Engineering

C1. Fibrin hydrogels can be effectively loaded with nanocomplexed mRNA to construct mRNA-activated matrices. These matrices are highly biocompatible and promote a more potent transfection of encapsulated human Mesenchymal Stem Cells (hMSCs) than similar systems with pDNA-activation.

C2. mRNA- and pDNA-activated matrices induced different gene expression kinetics in encapsulated hMSCs. mRNA matrices induced a rapid gene overexpression that decayed over time, while pDNA matrices increased gene expression over time. Matrices loaded with RNase-resistant mRNAs induced a very potent gene upregulation that was maintained over time.

C3. mRNA matrices loaded with Transcription Factor (TF) SOX9 promoted a faster onset of the chondrogenic differentiation program than pDNA-activated matrices. Likewise, MYOD mRNA matrices induced a rapid onset of the myogenic differentiation program in hMSCs. This high expression of chondrogenic and myogenic genes resulted in higher synthesis of tissue-specific proteins in mRNA matrices compared to pDNA and control matrices.

C4. The fibrinogen concentration of mRNA-GAMs affected the differentiation process: 2 mg/ml matrices promoted higher expression of chondrogenic markers, while 4 mg/ml matrices induced an improved myogenic response.

CHAPTER 3: Modulation of Gene Activated Matrix mechanics enhances the 3D transfection and SOX9-directed differentiation of Mesenchymal Stem Cells

C1. A set of collagen-I-alginate IPNs with tunable adhesion and stiffness was developed by adjusting collagen:alginate mass ratios and the concentration of the crosslinker, calcium carbonate nanoparticles. Within these IPNs, stiffness can be tuned independently of polymer concentration, adhesion ligand density and gel architecture.

C2. IPNs of various mechanical properties were successfully loaded with nanocomplexed SOX9 mRNA and pDNA sequences, and hMSCs were encapsulated therein. Regardless of the type of genetic material, the highest transfection efficiencies were achieved with IPNs of high collagen:alginate ratios (higher adhesion) and high stiffness.

C3. The positive effect of IPN stiffness on hMSCs transfection was found to be related to cell adhesion, an increased cell proliferation and a higher mRNA/pDNA cell uptake.

C4. SOX9-activated IPNs induced a more efficient chondrogenesis than that achieved with cells transfected in 2D and seeded in non-activated IPNs, indicating the interest of 3D reprogramming techniques. Compared to control IPNs, SOX9 IPNs induced lower levels of the hypertrophic marker COLX, suggesting the formation of an improved cartilage-like tissue. The use of the IKK inhibitor BMS-345541 further decreased COLX expression, making this inhibitor an attractive drug to consider in the design of biomaterials for cartilage repair.

USC
UNIVERSIDADE
DE SANTIAGO
DE COMPOSTELA

List of abbreviations

USC
UNIVERSIDADE
DE SANTIAGO
DE COMPOSTELA

LIST OF ABBREVIATIONS

2D Two dimensional

3D Three dimensional

ACAN Aggrecan

ACI Autologous Chondrocyte Implantation

ACT Adoptive Cell Transfer

ARCA Anti Reverse Cap Analog

BMP Bone Morphogenetic Protein

BSA Bovine Serum Albumin

°C Degrees Celsius

C/EBPβ CCAAT-enhancer-binding protein β

Ca^{2+} Calcium

CCL2 Chemokine (C-C motif) lingand 2. Also known as MCP-1 (Monocyte Chemoattractant Protein 1)

CCM Complete Chondrogenic Medium

CDH15 Cadherin 15

cDNA complementary Deoxyribonucleic Acid

CDS Coding Sequence

CD11b Cluster of differentiation molecule 11B

COL2A1 Collagen type II alpha 1 chain

COLX Collagen type X

CTL Cytotoxic T lymphocyte

DAB (3,3'-diaminobenzidine)

DMEN Dulbecco's Modified Eagle Medium

DMSO Dimetilsulfoxyde

DNA Deoxyribonucleic Acid

dNTPs Deoxynucleotides Triphosphate

dsDNA double stranded Deoxyribonucleic Acid

DTT Dithiothreitol

ECM Extracellular Matrix

FBS Fetal Bovine Serum

FDA US Food and Drug Administration

FGF Fibroblast Growth Factor

GAM Gene Activated Matrix

GAPDH Glyceraldehide-3-phosphate dehydrogenase

GF Growth Factor

GMO Glycerol Monooleate

h Hours

hMSC Human Mesenchymal Stem Cell

ICM Incomplete Chondrogenic Medium

IHC Immunohistochemistry

IPN Interpenetrating Polymer Network

IVT In Vitro Transcription

(M)-MDSCs monocytic MDSCs

MACI Matrix-assisted Autologous Chondrocyte Implantation

MDSCs Myeloid Derived Suppressor Cells

MEM Minimun Essential Medium

MFE Minimun Free Energy

mg Miligrams

Mg^2 Magnesium

min Minutes

miR, miRNA micro Ribonucleic Acid

ml Mililiters

M-MLV Moloney Murine Leukemia Virus

mRNA Messenger Ribonucleic Acid

MTT 3-(4,5-dimethylthiazol-2-yl)-2,5-diphenyltetrazolium bromide

MW Molecular Weight

MYH2 Myosin Heavy Chain 2

MYH3 Myosin Heavy Chain 3

MYOD Myogenic differentiation protein 1

MYOG Myogenin

NC nanocapsule

NE nanoemulsion

NF-κB nuclear factor kappa-light-chain-enhancer of activated B cells

nm Nanometers

ORF Open Reading Frame

OVA Ovalbumin

Pa Pascal

PBS Phosphate Buffered Saline

PDI Polidispersity Index

pDNA Plasmid Deoxyribonucleic Acid

(PMS)-MDSCs polymorphonuclear MDSCs

PVDF Polyvinylidine Fluoride

qRT-PCR Real-Time Quantitative Reverse Transcription PCR

RIPA buffer Radioimmunoprecipitation assay buffer

RNA Ribonucleic Acid

RNAi interference Ribonucleic Acid

ROCK Rho-associated protein kinase

SAXS Small Angle X-ray Scattering

SDS Sodium Dodecyl Sulfate

SEM Scanning Electron Microscopy

shR, shRNA short hairpin Ribonucleic Acid

SOX9 (Sex-determining region Y)-box 9

TEM Transmission Electron Microscopy

TF Transcription Factor

TGF-β3 Transforming Growth Factor β3

TLR4 Toll-like receptor 4

TNT buffer TRIS-NaCl-Tween 20 buffer

UTR Untranslated Region

UV Ultra Violet

YFP Yellow Fluorescent Protein

µg Micrograms

µl Microliters

µm Micrometers

Ethical considerations

USC
UNIVERSIDADE
DE SANTIAGO
DE COMPOSTELA

ETHICAL CONSIDERATIONS

Cell culture

Primary human Mesenchymal Stem cells were either acquired from commercially available resources (American Tissue Culture Collection, Tebu-bio) or obtained from commercial human bone marrow samples (Lonza). Donors were anonymous in both cases. Cells were cultured in the conditions recommended by the manufacturers and only used for the research purposes specifically described in this thesis.

Animal Studies

All animal experiments were done in Padova and approved by Ministero della Salute Italiano DECRETO 240/2012 and were executed in accordance with governing Italian law and EU directives and guidelines. Mice were monitored daily and euthanized when displaying excessive disconfort.

USC
UNIVERSIDADE
DE SANTIAGO
DE COMPOSTELA

Università degli Studi di Padova
Comitato Etico di Ateneo per la Sperimentazione Animale – CEASA.

UNIVERSITÀ DEGLI STUDI DI PADOVA

Allegato "B"

Dipartimento di Sc...
Anno 2012 Titolo 17
N. 458
UOR Sez QUC
9 1
21/3/2012

Data: 19/3/2012
Prot. n. 14931
Anno 2012 Tit. III Cl. 11 Fasc. 7

Al Resp. del Progetto di Ricerca
Prof. **Vincenzo Bronte**
Istituto Oncologico Veneto
Via Gattamelata n.64
35128 - Padova (PD)

Progetto Numero (*Project number*): **17/2012** Valutato il (*Evalueted on*): **15 febbraio 2012**

TITOLO DELLA RICERCA/ ***RESEARCH TITLE:***	**Approcci di terapia genica per il potenziamento dell'immunoterapia passiva anti-tumorale nel topo.**
RESPONSABILE del PROGETTO di RICERCA/ ***CHIEF OF RESEARCH PROJECT:***	Prof. **Vincenzo Bronte**
STABILIMENTO UTILIZZATORE/ ***ANIMAL FACILITY***	• Stabulario del dip.to di Scienze Chirurgiche, Oncologiche e Gastroenterologiche, via Gattamelata n.64 –Padova • Stabulario del Venetian Institute of Molecular Medicine (VIMM) via Orus n.2 - Padova
VETERINARIO RESPONSABILE/ ***VETERINARY CENTRAL SERVICES FOR THE PROTECTION OF ANIMALS USED FOR EXPERIMENTAL AND OTHER SCIENTIFIC PURPOSES***	Prof. *D. Bernardini*, Responsabile del Servizio Veterinario Centralizzato di Ateneo.
TIPO DI ANIMALI/*TYPE OF ANIMAL:* **TOPI C57Bl/6 anche transgenici**	**NUMERO DI ANIMALI/** ***NUMBERS OF ANIMALS*: 1077**

COMUNICAZIONE ☐ **AUTORIZZAZIONE IN DEROGA** ☒ **FUORI APPLICAZIONE D.Lgs 116/92** ☐

PARERE DEL COMITATO ETICO

FAVOREVOLE/ ***APPROVED*** ☒

Osservazioni:

Il progetto si inserisce nel filone di ricerca sulle MDSC e la risposta tumorale. In particolare, si cercherà di valutare se il silenziamento del gene c/EBPβ permetta di ottenere la regressione tumorale. Verrà inoltre valutata l'efficacia della terapia genica nel determinare resistenza alle metastasi e nel consentire l'eliminazione delle stesse mediante immunoterapia passiva. Alcuni animali saranno sottoposti ad irradiazione totale e successivo inoculo di cellule progenitrici in modo da indurre il chimerismo. Alcuni animali saranno sottoposti a inoculazione sottocutanea di cellule neoplastiche con una crescita della massa tumorale fino a 20 x 10 mm. Altri topi saranno inoculati con cellule di fibrosarcoma nel muscolo quadricipite della zampa anteriore destra e tenuti in vita per 3 settimane. Verranno eseguiti prelievi ematici anche retro orbitari. Il progetto è complesso, la sofferenza è legata alla crescita tumorale ed alle varie procedure di prelievi e di inoculi.

FIRMA/*SIGNATURE*: **Il Presidente CEASA/***The CEASA's President*
(prof. Massimo Riolfatti)
Massimo Riolfatti

16-17-18/2012
Dr Brovie

Ministero della Salute
DGSAF
0018568-P-12/10/2012

112015375

Ministero della Salute

Dipartimento della Sanità Pubblica Veterinaria, della Sicurezza Alimentare e degli Organi Collegiali per la tutela della Salute
Direzione Generale della Sanità Animale e dei Farmaci Veterinari
Ufficio VI (ex DGSA – Benessere Animale)

Università degli Studi di Padova
e-mail: unipd.ammcle@legalmail.it

Segreteria CEASA
c.a. Dott.ssa Vera CAVALLIN
e-mail: segreteria.ceasa@unipd.it

Servizio Veterinario Centralizzato
e-mail: servizio.veterinario@unipd.it

e p.c.

Regione Veneto
sanita.animale@regione.veneto.it

ASL n° 16 di Padova
Servizio Veterinario
sp.veterinaria_ulss16@sanita.padova.it

Prefettura di Padova
prefettura.padova@interno.it

Ufficio Veterinario per gli
Adempimenti Comunitari
sanvet-vr@postacert.sanita.it

OGGETTO:

D.lgs. 116/92 in materia di protezione degli animali utilizzati ai fini sperimentali e scientifici.
Trasmissione autorizzazioni ai sensi dell'art. 9.
Decreto n° 240/2012 – B
(Risp. DGSAF 6724- A del 03/04/2012)
(Risp. DGSAF 9219 – A del 14/05/2012)
Decreto n° 241/2012 – B
(Risp. DGSAF 11922 - A del 23/06/2012)
Decreto n° 242/2012 – B
(Risp. DGSA 23130 – A del 30/12/2011)

Si trasmettono i decreti ministeriali **n° 240/2012 –B, n° 241/2012 – B e n° 242/2012 – B** rilasciati in data **10/10/2012** che recano le autorizzazioni di cui all'oggetto.

Copia conforme delle predette autorizzazioni sono altresì trasmesse, per quanto di competenza, agli altri Enti in indirizzo.

p. IL DIRETTORE DELL'UFFICIO VI

USV Padova 10MMXII

Ministero della Salute

**DIPARTIMENTO DELLA SANITÀ PUBBLICA VETERINARIA,
DELLA SICUREZZA ALIMENTARE E DEGLI ORGANI COLLEGIALI PER LA TUTELA DELLA SALUTE
DIREZIONE GENERALE DELLA SANITÀ ANIMALE E DEI FARMACI**

DECRETO N° 240/2012 - B

IL DIRETTORE GENERALE

Visto l'articolo 9 del decreto legislativo 27 gennaio 1992 n°116, che demanda al Ministro della Sanità l'autorizzazione in deroga all'art. 4, comma 3 dello stesso decreto legislativo per gli esperimenti da effettuarsi senza anestesia;

Visti gli articoli 4 e 16 del Decreto Legislativo 30 marzo 2001, n°165, che demanda ai Dirigenti l'adozione degli atti che impegnano l'amministrazione verso l'esterno;

Visto l'articolo 7 secondo comma del decreto legislativo 27 gennaio 1992, n°116;

Viste le domande del **Dr. Vincenzo BRONTE del Dipartimento di Scienze Oncologiche e Chirurgiche, Sezione di Oncologia dell'Università degli Studi di Padova,** sede legale in **Padova,** Via VIII febbraio, 2, intese ad ottenere l'autorizzazione in deroga ai sensi dell'articolo 9 del decreto legislativo 27 gennaio 1992, n°116, concernente gli studi che saranno effettuati presso lo stabilimento utilizzatore **dell'Istituto Oncologico Veneto, sito in Padova,** Via Gattamelata, 64, e presso lo stabilimento utilizzatore del **Venetian Institute of Molecular Medicine, sito in Padova,** Via Orus, 2, sotto la diretta responsabilità del **Dr. Vincenzo BRONTE, laureato in Medicina e Chirurgia;**

Visti i progetti di ricerca allegati alla domanda;

Atteso che le finalità dei progetti sono comprese tra quelle di cui all'articolo 3, comma 1;

Ritenuto che l'anestesia è incompatibile con le finalità degli esperimenti stessi o più dannosa per gli animali che gli esperimenti stessi;

Visti i pareri favorevoli n. 26236 del 12/07/2012, n. 35035 del 02/10/2012 e n. 35043 del 02/10/2012, espressi dall'Istituto Superiore di Sanità;

Considerato che lo stabulario:

- dell'**Istituto Oncologico Veneto** è regolarmente autorizzato come stabilimento utilizzatore ai sensi dell'art.12 del D.lgs 27 gennaio 1992, n°116 con decreto **n°112/2003-A rilasciato in data 15/09/2003,** e che **il Dr. Antonio ROSATO, laureato in Medicina e Chirurgia** è responsabile dell'assistenza agli animali e del funzionamento delle attrezzature;
- del **Venetian Institute of Molecular Medicine** è regolarmente autorizzato come stabilimento utilizzatore ai sensi dell'art. 12 del D.lgs. 27 Gennaio 1992, n°116 con decreto **n°175/2002-A rilasciato in data 14/11/2002,** e che **il Dr. Marco MONGILLO, laureato in Medicina e Chirurgia** è responsabile dell'assistenza agli animali e del funzionamento delle attrezzature;

Preso atto che il **Medico Veterinario** responsabile del controllo della buona esecuzione delle procedure d'esperimento, ai sensi dell'art. 6, comma 4, sono **il Prof. Daniele BERNARDINI, il Dott. Ludovico SCENNA** e la **Dr.ssa Francesca PATRESE;**

DECRETA

Art 9 Uni Padova Bronte 10MMXII
G. Botta – 0659946754 – g.botta@sanita.it
C. di Vico – 0659942742 – c.divico@sanita.it

Il **Dr. Vincenzo BRONTE del Dipartimento di Scienze Oncologiche e Chirurgiche, Sezione di Oncologia dell'Università degli Studi di Padova,** sede legale in **Padova,** Via VIII febbraio, 2, è autorizzato, per la **durata massima di tre anni,** ad eseguire gli esperimenti di seguito riportati, ai sensi del primo comma dell'art. 9 del D.lgs. 27 Gennaio 1992, n°116:

- **"Studio dell'induzione della tolleranza immunitaria indotta da cellule di Origine Mieloide (MDSC) in modelli murini di carcinogenesi, nel topo"** 16/2012
- **"Approcci di terapia genica per il potenziamento dell'immunoterapia passiva anti-tumorale, nel topo"** 17/2012
- **"Studio della milza e dei fattori chemiotattici coinvolti nell'induzione di tolleranza verso antigeni tumorali mediata da MDSC nel topo"** 18/2012

Gli esperimenti saranno eseguiti sotto la diretta responsabilità del **Dr. Vincenzo BRONTE, laureato in Medicina e Chirurgia;**

Gli esperimenti saranno eseguiti presso:

- lo stabulario **dell'Istituto Oncologico Veneto** regolarmente autorizzato come stabilimento utilizzatore ai sensi dell'art. 12 del D.lgs. 27 Gennaio 1992, n°116 con decreto **n°112/2003 - A** rilasciato in data **15/09/2003;**
- lo stabulario del **Venetian Institute of Molecular Medicine** regolarmente autorizzato come stabilimento utilizzatore ai sensi dell'art. 12 del D.lgs. 27 Gennaio 1992, n°116 con decreto **n° 175/2002-A** rilasciato in data **14/11/2002.**

10 OTT. 2012

IL DIRETTORE GENERALE

Art 9 Uni Padova Bronte 10MMXII
G. Botta – 0659946754 – g.botta@sanita.it
C. di Vico – 0659942742 - c.divico@sanita.it

USC
UNIVERSIDADE
DE SANTIAGO
DE COMPOSTELA